# Image-guided surgery using invisible near-infrared fluorescent light : from pre-clinical studies to clinical validation

Hutteman, M.

# Image-Guided Surgery using Invisible Near-Infrared Fluorescent Light

From pre-clinical studies
to clinical validation

Merlijn Hutteman

Cover design: Matthijs Braamhaar


ISBN 978-94-6169-112-5

The research described in this thesis was financially supported by the Center for Translational Molecular Medicine (CTMM, DeCoDe and MUSIS projects), the Dutch Cancer Society, Foundation "De Drie Lichten" and the Leiden University Fund (LUF).

# Image-Guided Surgery using Invisible Near-Infrared Fluorescent Light

From pre-clinical studies to clinical validation

**Proefschrift**

ter verkrijging van
de graad van Doctor aan de Universiteit Leiden,
op gezag van Rector Magnificus prof.mr. P.F. van der Heijden,
volgens besluit van het College voor Promoties
te verdedigen op woensdag 1 september 2011
klokke 16.15 uur

door

**Merlijn Hutteman**

geboren te Rotterdam in 1983

**Promotiecommissie**

| | |
|---|---|
| Promotores: | Prof. dr. C.J.H. van de Velde |
| | Prof. dr. J.V. Frangioni (Harvard University) |
| Co-promotores: | Dr. A.L. Vahrmeijer |
| | Dr. P.J.K. Kuppen |
| Overige leden: | Prof. dr. B.P.F. Lelieveldt |
| | Prof. dr. C.W.G.M. Löwik |
| | Prof. dr. J.H.C. Reiber |
| | Dr. V.T.H.B.M. Smit |
| | Prof. dr. H.J. Tanke |

*To my family*

# CONTENTS

# Chapter 1

## General introduction and thesis outline

## INTRODUCTION

Despite many recent improvements in the medical treatment of cancer, surgical removal remains the single most important curative treatment option for solid tumors. For a curative resection, complete resection of the tumor, as confirmed by histopathological evaluation, is essential. To minimize comorbidity it is important to spare vital structures (e.g. nerves, ureters, bile ducts). While there are several imaging modalities available that can visualize tumor size, location and relation to vital structures up to a certain extent in the preoperative setting,[1] during surgery, other than incidental use of intraoperative ultrasonography, surgeons still mainly rely on visual inspection and palpation to determine what should be resected and what should be spared.

Unfortunately, it can be challenging to discriminate tumor tissue from normal tissue by visual inspection and palpation and as a result, irradical resections and damage to vital structures still occur relatively frequently.[2-4] Therefore, there is a need for an imaging modality that can provide the surgeon with real-time information during surgery on the exact location of tissues to be resected and tissues to be avoided.

## OPTICAL IMAGING

Optical imaging using near-infrared (NIR) fluorescence is a technique that has the potential to fulfill this need. Advantages of NIR fluorescent light (700-900 nm, Figure 1) include high tissue penetration (millimeters to centimeters deep) and low autofluorescence, thereby providing sufficient contrast.[5] Because the human eye is insensitive to NIR wavelengths, the use of NIR light does not alter the surgical field. Recently developed intraoperative imaging systems are able to provide simultaneous acquisition of surgical anatomy (white light, color video) and NIR fluorescence signal.[6-8] Furthermore, systems are available that can simultaneously acquire and display multiple separate fluorescence wavelengths, enabling labeling of tumors on one channel and vital structures on a second channel.[6] Therefore, the use of NIR fluorescence imaging could potentially be of great value in the intraoperative detection of critical anatomical structures and oncologic targets.

In addition to NIR fluorescence imaging systems, exogenous NIR fluorescent contrast agents are necessary to visualize specific tissues. Ideally, tumor cells are labeled by targeted contrast agents. However, the only NIR fluorescent contrast agents currently registered by the U.S. Food and Drug Administration (FDA) and European Medicines Agency (EMA) for clinical applications are the non-targeted indocyanine green (ICG; peak emission ≈ 820 nm) and methylene blue (peak emission ≈ 700 nm).

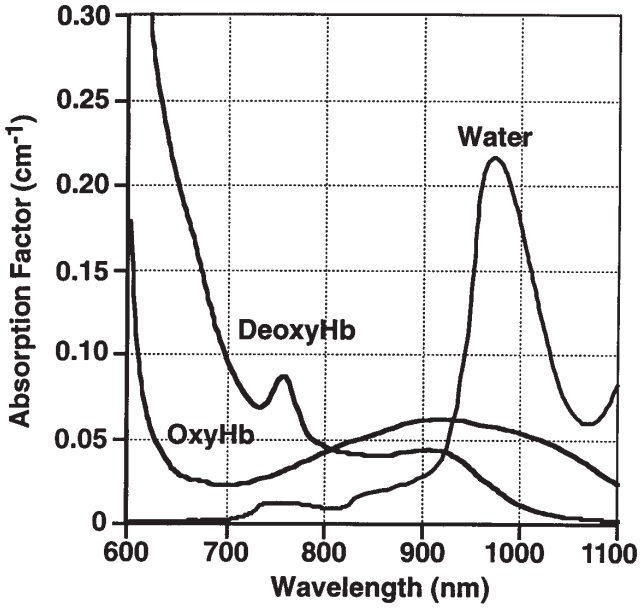


**Figure 1.** Absorption of light by various components varies over the wavelength spectrum, resulting in an optimal window for fluorescence imaging in the NIR light region between 650 and 900 nm. OxyHb, oxygenated hemoglobin; DeoxyHb, deoxygenated hemoglobin. Figure reprinted from Chance.[32] With permission, Copyright Clearance Center Rightslink.

## SENTINEL LYMPH NODE DETECTION

Sentinel lymph node (SLN) mapping, as introduced in the treatment of cutaneous melanoma by Donald Morton[9] is now considered part of the standard of care in cutaneous melanoma, breast cancer and vulvar cancer. The SLN is the lymph node that drains directly from the tumor and is therefore most likely to be the node to which tumor cells will first metastasize. By injecting a tracer around the primary tumor, the SLN can be identified and resected by following the drainage of that tracer. If the SLN contains no tumor cells, it is unlikely that the remaining lymph nodes contain metastases and the resection of these nodes and the associated comorbidity can be avoided.

Currently, SLN mapping typically involves the injection of a radiotracer preoperatively and injection of a blue dye shortly prior to surgery. Using this combined technique, high sensitivity and low false negative rates are achieved. However, these methods have their disadvantages. The use of a radiotracer exposes caregivers and patients to ionizing radiation and may not be possible in all clinics due to regulatory issues. Local injection of a blue dye stains the surgical field in an unnatural color that persists for several months after surgery and can not be visualized when it is covered by overlying tissue. The use of NIR fluorescence has the potential to overcome these limitations and simplify the use of SLN mapping in various cancer types. Indeed, the

first studies have been described that use the currently available ICG in combination with an intraoperative NIR fluorescence imaging system for SLN mapping in breast cancer,[6, 10] gynecologic cancer[7, 11] and gastrointestinal malignances[12].

## TUMOR MARGIN DETECTION AND IMAGE-GUIDED RESECTION

Different strategies can be followed to detect malignant cells or tissues during surgery. The various hallmarks of cancer can be used as a target for imaging strategies: increased growth and growth factor signaling receptors, limitless replicative potential, sustained angiogenesis, and increased proteolytic activity resulting in tissue invasion and metastasis.[13] Development of these probes is the focus of intensive research and many have been tested in a preclinical setting. Enzyme activatable probes allow detection of proteases that are relatively abundant in malignant tissue, which can be associated with specific characteristics of the tumor, e.g. invasive, aggressive or metastatic tendency. These agents are injected in a quenched (i.e. non-fluorescent) state, resulting in minimal fluorescence at the time of administration. After cleavage by the specific enzyme, the agent becomes dequenched (i.e., fluorescent), resulting in a high signal-to-background (SBR). Examples of activatable agents that have been used in animal cancer models are activatable polyarginine-based cell-penetrating peptides that detect matrix metalloproteinases,[14] activity-based probes that target cysteine cathepsins,[15] and several commercially available probes that have been developed by Weissleder et al., which are activated by cathepsins or matrix metalloproteinases (PerkinElmer, Waltham, USA).[16, 17]

Instead of detection of tumor-associated proteases, molecular-specific detection of cancer cells can be performed using a specific targeting ligand or monoclonal antibody conjugated to a fluorophore. Tumor detection by exploiting the increased growth factor receptor expression of tumors has been described in all kinds of different tumors. In these studies, fluorophores that were coupled to monoclonal antibodies targeting the epidermal growth factor receptor, Her2/neu receptor, or vascular endothelial growth factor receptor were used.[18-21] For imaging of tumor angiogenesis, targeting of alpha-v-beta-3 (αvβ3) integrin, a critically important adhesion molecule in the regulation of angiogenesis, is a widely used strategy. Targeting of αvβ3 integrin by cyclic arginine-glycine-aspartate conjugated to various non-quenched or quenched fluorophores has been reported.[22-24] Finally, in analogy with PET technology, increased glucose metabolism due to increased expression of membrane glucose transporter proteins in intracranial gliomas has been reported.[25]

## IDENTIFICATION OF VITAL STRUCTURES

In order to identify vital structures by using NIR fluorescence contrast agents, a distinction should be made between hollow and solid structures. Hollow structures, such as bile ducts, ureters and blood vessels can be visualized if contrast agents can be delivered intraluminally, whereas solid structures, as for example the nerves, can be visualized by targeting specific cellular markers, as membrane proteins.

Hollow structures can be visualized either by direct injection or by means of excretion from for example the liver or kidneys. ICG is excreted by the liver into the bile and has indeed been shown to identify bile ducts during surgery.[26-28] MB is cleared both hepatically and renally and has been shown to identify both ureters and bile ducts.[29]

The identification of nerves requires the development of novel contrast agents. Advances have been made in the development of nerve targeting probes, although many hurdles still exist as the probes are fluorescent in a lower wavelength than the NIR spectrum, thereby lowering tissue penetration and suffering from increased autofluorescence.[30] Another strategy is to use fluorescent peptides that target the nerve sheath, avoiding the need to cross the blood-nerve-barrier.[31]

## OUTLINE OF THE THESIS

This thesis is divided in two parts: in **Part I** focus lies on preclinical validation of NIR fluorescence image-guided surgery, **Part II** describes clinical translation of this technique and first-in-human studies.

**Part I, chapter 2** describes the intraoperative identification of colorectal liver metastases using NIR fluorescence and a novel integrin $\alpha_v\beta_3$ targeted probe in an experimental rat tumor model. **Chapter 3** explores the use of a protease activatable NIR fluorescent probe for intraoperative identification of tumor margins in a rat model of breast cancer and subsequent image-guided resection of breast tumors. In **chapter 4**, the clinically available probe indocyanine green (ICG) is used to intraoperatively identify colorectal liver metastases in an experimental rat tumor model.

In **part II, chapter 5**, NIR fluorescence imaging is used for *ex vivo* SLN mapping in colorectal cancer, to allow the use of novel probes that are not yet approved for clinical *in vivo* injections. First, this technique is validated in a swine model, where *in vivo* injections are compared to *ex vivo* injections. Subsequently, this technique is translated to the clinic in a pilot series of human colorectal cancer specimens. Chapters 6 and 7 are focused on the use of NIR fluorescence imaging for SLN mapping in breast cancer. In **chapter 6**, the development of an improved imaging system with reduced size and optimization of ICG:HSA dose are described. Whether premixing with HSA is indeed beneficial for SLN mapping in breast cancer patients is then studied in a

randomized trial in **chapter 7**. The use of intraoperative NIR fluorescence imaging for SLN mapping is reported in cervical cancer patients and vulvar cancer patients in **chapter 8** and **chapter 9**, respectively.

In breast reconstructive surgery using free skin flaps, good oxygenation of the transplanted tissue is essential for flap survival. Imaging of vascular anatomy may help the surgeon in choosing the vessels to be used for transplantation and has the potential to improve outcomes. **Chapter 10** describes intraoperative imaging of perforator vessels using NIR fluorescence in patients undergoing diep inferior epigastric perforator (DIEP) flap breast reconstruction after mastectomy.

As no tumor targeted NIR fluorescent probes are yet available for clinical application, the enhanced permeability and retention effect could potentially be used for tumor identification by non-targeted probes. In **chapter 11** it is attempted to visualize tumors intraoperatively after ICG injection in pancreatic cancer patients. Furthermore, visualization of bile ducts is studied using NIR fluorescence imaging. **Chapter 12** describes the use of NIR fluorescence imaging to intraoperatively visualize colorectal liver metastases in patients who were injected with ICG prior to surgery. In **chapter 13**, all results are then summarized and discussed and an outlook into the future is provided.

## REFERENCES


1. Frangioni JV. New technologies for human cancer imaging. J Clin Oncol 2008; 26:4012-4021.
2. Mai KT, Yazdi HM, Isotalo PA. Resection margin status in lumpectomy specimens of infiltrating lobular carcinoma. Breast Cancer Res Treat 2000; 60:29-33.
3. Chagpar AB, Martin RC, Hagendoorn LJ, et al. Lumpectomy margins are affected by tumor size and histologic subtype but not by biopsy technique. Am J Surg 2004; 188:399-402.
4. Smitt MC, Horst K. Association of clinical and pathologic variables with lumpectomy surgical margin status after preoperative diagnosis or excisional biopsy of invasive breast cancer. Ann Surg Oncol 2007; 14:1040-1044.
5. Frangioni JV. In vivo near-infrared fluorescence imaging. Curr Opin Chem Biol 2003; 7:626-634.
6. Troyan SL, Kianzad V, Gibbs-Strauss SL, et al. The FLARE intraoperative near-infrared fluorescence imaging system: a first-in-human clinical trial in breast cancer sentinel lymph node mapping. Ann Surg Oncol 2009; 16:2943-2952.
7. Crane LM, Themelis G, Pleijhuis RG, et al. Intraoperative Multispectral Fluorescence Imaging for the Detection of the Sentinel Lymph Node in Cervical Cancer: A Novel Concept. Mol Imaging Biol 2010.
8. Handa T, Katare RG, Nishimori H, et al. New device for intraoperative graft assessment: HyperEye charge-coupled device camera system. General thoracic and cardiovascular surgery 2010; 58:68-77.
9. Morton DL, Wen DR, Wong JH, et al. Technical details of intraoperative lymphatic mapping for early stage melanoma. Arch Surg 1992; 127:392-399.
10. Hojo T, Nagao T, Kikuyama M, et al. Evaluation of sentinel node biopsy by combined fluorescent and dye method and lymph flow for breast cancer. Breast 2010.
11. Crane LM, Themelis G, Arts HJ, et al. Intraoperative near-infrared fluorescence imaging for sentinel lymph node detection in vulvar cancer: First clinical results. Gynecol Oncol 2010.
12. Kusano M, Tajima Y, Yamazaki K, et al. Sentinel node mapping guided by indocyanine green fluorescence imaging: a new method for sentinel node navigation surgery in gastrointestinal cancer. Dig Surg 2008; 25:103-8.
13. Keereweer S, Kerrebijn JD, van Driel PB, et al. Optical Image-guided Surgery-Where Do We Stand? Mol Imaging Biol 2010.
14. Jiang T, Olson ES, Nguyen QT, et al. Tumor imaging by means of proteolytic activation of cell-penetrating peptides. Proc Natl Acad Sci U S A 2004; 101:17867-17872.
15. Blum G, von DG, Merchant MJ, et al. Noninvasive optical imaging of cysteine protease activity using fluorescently quenched activity-based probes. Nat Chem Biol 2007; 3:668-677.
16. Mahmood U, Weissleder R. Near-infrared optical imaging of proteases in cancer. Mol Cancer Ther 2003; 2:489-496.
17. Wunderbaldinger P, Turetschek K, Bremer C. Near-infrared fluorescence imaging of lymph nodes using a new enzyme sensing activatable macromolecular optical probe. Eur Radiol 2003; 13:2206-2211.
18. Gleysteen JP, Duncan RD, Magnuson JS, et al. Fluorescently labeled cetuximab to evaluate head and neck cancer response to treatment. Cancer Biol Ther 2007; 6:1181-1185.
19. Lee SB, Hassan M, Fisher R, et al. Affibody molecules for in vivo characterization of HER2-positive tumors by near-infrared imaging. Clin Cancer Res 2008; 14:3840-3849.
20. Withrow KP, Newman JR, Skipper JB, et al. Assessment of bevacizumab conjugated to Cy5.5 for detection of head and neck cancer xenografts. Technol Cancer Res Treat 2008; 7:61-66.
21. Ogawa M, Kosaka N, Longmire MR, et al. Fluorophore-Quencher Based Activatable Targeted Optical Probes for Detecting in Vivo Cancer Metastases. Mol Pharm 2009.
22. Chen K, Xie J, Chen X. RGD-human serum albumin conjugates as efficient tumor targeting probes. Mol Imaging 2009; 8:65-73.
23. Jin ZH, Razkin J, Josserand V, et al. In vivo noninvasive optical imaging of receptor-mediated RGD internalization using self-quenched Cy5-labeled RAFT-c(-RGDfK-)(4). Mol Imaging 2007; 6:43-55.

24. Kossodo S, Pickarski M, Lin SA, et al. Dual In Vivo Quantification of Integrin-targeted and Protease-activated Agents in Cancer Using Fluorescence Molecular Tomography (FMT). Mol Imaging Biol 2009.
25. Zhou H, Luby-Phelps K, Mickey BE, et al. Dynamic near-infrared optical imaging of 2-deoxyglucose uptake by intracranial glioma of athymic mice. PLoS ONE 2009; 4:e8051.
26. Matsui A, Tanaka E, Choi HS, et al. Real-time intra-operative near-infrared fluorescence identification of the extrahepatic bile ducts using clinically available contrast agents. Surgery 2010; 148:87-95.
27. Aoki T, Murakami M, Yasuda D, et al. Intraoperative fluorescent imaging using indocyanine green for liver mapping and cholangiography. J Hepatobiliary Pancreat Surg 2009; 17:590-594.
28. Ishizawa T, Bandai Y, Ijichi M, et al. Fluorescent cholangiography illuminating the biliary tree during laparoscopic cholecystectomy. Br J Surg 2010; 97:1369-1377.
29. Matsui A, Tanaka E, Choi HS, et al. Real-time, near-infrared, fluorescence-guided identification of the ureters using methylene blue. Surgery 2010; 148:78-86.
30. Gibbs-Strauss SL, Nasr K, Fish KM, et al. Nerve-Highlighting Fluorescent Contrast Agents for Image-Guided Surgery. Mol Imaging 2011; In press.
31. Whitney MA, Crisp JL, Nguyen LT, et al. Fluorescent peptides highlight peripheral nerves during surgery in mice. Nat Biotechnol 2011.
32. Chance B. Near-infrared images using continuous, phase-modulated, and pulsed light with quantitation of blood and blood oxygenation. Ann N Y Acad Sci 1998; 838:29-45.

# Part I

## Pre-clinical validation of near-infrared fluorescence image-guided surgery

# Chapter 2

# Intraoperative near-infrared fluorescence imaging of colorectal metastases targeting integrin $\alpha_v\beta_3$ expression in a syngeneic rat model

Hutteman M[1], Mieog JSD[1], van der Vorst JR, Dijkstra J, Kuppen PJK, van der Laan AMA, Tanke HJ, Kaijzel EL, Que I, van de Velde CJ, Löwik CWGM, Vahrmeijer AL

[1] Shared first authorship.

*Eur J Surg Oncol 2011; 37:252-257.*

# ABSTRACT

## Aim

Near-infrared (NIR) fluorescence optical imaging is a promising technique to assess the extent of colorectal metastases during curative-intended surgery. However, NIR fluorescence imaging of liver metastases is highly challenging due to hepatic uptake and clearance of many fluorescent dyes. In the current study, the biodistribution and the ability to demarcate liver and peritoneal metastases were assessed during surgery in a syngeneic rat model of colorectal cancer using an integrin $\alpha_v\beta_3$-directed NIR fluorescence probe.

## Methods

Liver tumors and peritoneal metastases were induced in 7 male WAG/Rij rats by subcapsular inoculation of 0.5 x$10^6$ CC531 colorectal cancer rat cells into three distinct liver lobes. Intraoperative and ex vivo fluorescence measurements were performed 24 (N = 3 rats, 7 tumors) and 48 h (N = 4 rats, 9 tumors) after intravenous administration of the integrin $\alpha_v\beta_3$-directed NIR fluorescence probe.

## Results

Colorectal metastases had a minimal two-fold higher NIR fluorescence signal than healthy liver tissue and other abdominal organs ($p < 0.001$). The tumor-to-background ratio was independent of time of imaging (24 h vs. 48 h post-injection; $p = 0.31$), which facilitates flexible operation planning in future clinical applications. Total fluorescence intensity was significantly correlated with the size of metastases ($R^2 = 0.92$ for the 24 h group, $R^2 = 0.96$ for the 48 h group).

## Conclusion

These results demonstrate that colorectal intra-abdominal metastases can be clearly demarcated during surgery using an integrin $\alpha_v\beta_3$ targeting NIR fluorescence probe. Translating these findings to the clinic will have an excellent potential to substantially improve the quality of cancer surgery.

# INTRODUCTION

Survival of colorectal cancer patients is largely restricted by the occurrence of metastases, predominantly in the liver. In the course of the disease, up to 50% of patients will eventually develop liver metastases.[1] If confined to the liver, surgery offers a possible curative treatment option with 5-year survival rates of 35-40%.[2] However, at the time of surgery, adequate assessment of the extent of the disease is still limited, resulting in a 40-50% recurrence rate.[3] Clearly, innovative visualization techniques are needed to facilitate intraoperative assessment of the extent of the cancer tissue and to guide the subsequent surgical removal of these tumors with adequate margins in an attempt to increase the complete resection rate.

Real-time visualization of cancer cells using near-infrared (NIR) fluorescence optical imaging is a promising technique to assess the extent of colorectal metastases during curative-intended surgery.[4-6] However, optical imaging of liver metastases is highly challenging due to the high absorptivity of liver tissue for visble light and hepatic uptake and clearance of many fluorescent dyes.[7, 8] Recent studies demonstrated successful identification of breast, lung and glioblastoma cancers by targeting a member of the integrin family, integrin $\alpha_v\beta_3$.[9-13] Integrins are cell-surface transmembrane heterodimeric glycoproteins that are involved in cell adhesion, matrix interaction and cell signaling pathways. Integrin $\alpha_v\beta_3$ plays a key role in the early phase of tumor angiogenesis, tumor cell migration and is overexpressed in various cancer types, including colorectal cancer.[14-17] Because hepatocytes show little expression of integrin $\alpha_v\beta_3$,[16, 18] it is expected that NIR fluorescence probes targeting integrin $\alpha_v\beta_3$ result in little background in the liver.[9] Therefore, the aim of this study was to investigate the biodistribution and the ability to clearly demarcate liver and peritoneal metastases during surgery in a syngeneic rat model of colorectal cancer using an integrin $\alpha_v\beta_3$-directed NIR fluorescence probe.

# MATERIALS AND METHODS

## Animal model

Rat CC531 colorectal cancer cells were cultured in RPMI 1640 supplemented with 2 mM L-glutamine (Gibco, Invitrogen Ltd, Carlsbad, USA), 10% heat-inactivated fetal calf serum, 100 U/ml penicillin and 0.1 mg/ml streptomycin sulphate.[19] In order to induce liver and peritoneal metastases, CC531-syngeneic male WAG/Rij rats (Charles River, Maastricht, the Netherlands) weighing 300-350 g underwent median laparotomy and the liver was exposed. Subsequently, 500,000 CC531 cells (50 µl) were subcapsularly inoculated into the left and right main liver lobes, and the right accessory liver lobe.[19] To prevent tumor spill, puncture sites were covered with a small sponge, directly after

tumor cell injection. Four weeks after inoculation, metastases of approximately 5 mm in diameter had originated in the liver. The Animal Welfare Committee of the Leiden University Medical Center approved the experiments.

**NIR fluorescence probe**

The NIR fluorescence probe IntegriSense®680 (PerkinElmer, Waltham, USA) with peak absorbance at 680 nm was used for fluorescence imaging. IntegriSense680 consists of a small non-peptide integrin $\alpha_v\beta_3$ antagonist,[20] which is conjugated to the NIR fluorescence probe VivoTag®-S680 (PerkinElmer).

**Intraoperative NIR fluorescence camera system**

The Fluobeam® system (Fluoptics, Grenoble, France) was used for these experiments and has been described previously.[21] In short, the Fluobeam system is composed of a 100 mW laser emitting at 690 nm with an illumination power of 2.6 mW/cm$^2$ and a 12-bit CCD camera. The animal is placed under the laser and illuminated by white light filtered with a band-pass filter (350-650 nm) providing an irradiance of 7x10$^3$ lx at the animal level.

**Animal experiments**

All animals were housed in the animal facility of the Leiden University Medical Center. Pellet food and fresh tap water were provided ad libitum. The weight of the animals was followed throughout the experiment to monitor their general health state. Throughout tumor inoculation, imaging and surgical procedures, the animals were anesthetized with 5% isoflurane for induction and 2% isoflurane for maintenance in oxygen with a flow of 0.8 L/min and placed on an animal bed with an integrated nose mask. Rats (N = 7) were injected intravenously into the penile vein with IntegriSense680 (12 nmol per animal) 24 h (3 rats, N = 7 tumors) or 48 h (4 rats, N = 9 tumors) before imaging. These time points were chosen based on the blood pharmacokinetics of IntegriSense680 (PerkinElmer website: www.perkinelmer.com). Before injection, the level of autofluorescence was determined of metastases, surrounding tissue and abdominal organs. During intraoperative NIR fluorescence imaging of metastases a median laparotomy was performed followed by a systematic exploration of the peritoneal cavity. After intraoperative imaging, livers containing metastases were completely excised for additional *ex vivo* fluorescence measurements. Peritoneal metastases identified clinically or by fluorescence were carefully excised. Fluorescence intensity of metastases and abdominal organs was determined in vivo and ex vivo using the Fluobeam system. After resection, tumors were imaged ex vivo using the IVIS Spectrum (Caliper LifeSciences, Hopkinton, USA), which allowed

isolation of the IntegriSense680 signal from the background fluorescence by means of spectral unmixing.[22]

**Microscopy**

Excised tumors were fixed in 10% buffered formalin overnight and washed in 70% ethanol. Following paraffin embedding and mounting, tissue sections specimens of 4 μm were air-dried and stained with standard hematoxylin-eosin. In parallel, freshly excised liver lobes containing tumors were processed for fluorescence microscopy. Fresh tumors and surrounding liver tissue blocks of approximately 2 cm in diameter were incubated with 0.5 ml phalloidin-Alexa Fluor 488 (0.5 μM) and Hoechst 33342 (48 μM; both from Invitrogen) for 1 hr at room temperature to stain the F-actin filaments in particular those of the cell membrane of hepatocytes,[23] and the dsDNA at the cell nucleus, respectively. Tumors were placed in glass-bottom Petri dish (P35G-1.5-14-C , Mattek Corporation, Ashland, USA) and analyzed using the Leica TCS SP5 inverted confocal microscope (Leica Microsystems, Wetzlar, Germany; HCX PL APO 40x; N.A. 1.25 oil immersion objective). Hoechst, phalloidin-AlexaFluor488 and IntegriSense680 were excited by a 405 nm diode, a 488 nm Argon laser and a 633 HeNe nm laser, respectively. The 12-bit images were analyzed using the Leica LAS AF software and the three signals were pseudo-colored with blue for Hoechst, green for phalloidin-AlexaFluor488, and red for IntegriSense680.

**Statistical analysis**

Fluobeam derived NIR fluorescence data were analyzed using the open-source software ImageJ[24] by drawing regions of interest at the tumor and at the surrounding tissue within a range of 2 mm of the demarcation line of the tumor and the surrounding tissue by visual interpretation and measuring the fluorescent intensity of the 12-bit images. Merged images of visible light images and NIR fluorescence light images generated by the Fluobeam system were created using Adobe Photoshop CS3 Software (version 10.0.1, Adobe Systems Inc., San Jose, USA). IVIS Spectrum derived NIR fluorescence data were analyzed using LivingImage software (version 3.2, Caliper LifeSciences, Hopkinton, USA) using the methods described above. Statistical analysis and generation of graphs were performed using GraphPad Prism Software (version 5.01, La Jolla, USA). Mean fluorescence intensity and associated standard deviations were reported. Unpaired and paired t-tests were used for testing differences of fluorescence intensity between groups. Pearson's correlation coefficients were calculated for the analysis of the size of tumors and the total fluorescence intensity. Statistical tests were two-tailed and $p < 0.05$ was considered significant.

# RESULTS

## Intraoperative detection of colorectal liver metastases

In a total of 7 rats, all colorectal liver metastases (N = 16) were identified during surgery with the intraoperative Fluobeam camera system after targeting of integrin $\alpha_v\beta_3$ expression with IntegriSense680 (Fig. 1A). Quantification of the NIR fluorescence signal was performed using spectral unmixing with the IVIS Spectrum, enabling separation of true IntegriSense680 signal from background fluorescence. The NIR fluorescence signal was significantly higher in the colorectal metastases in comparison to healthy liver tissue, regardless of the rats were imaged 24 hours after injection (N = 7, paired $t$ = 10.8, $p < 0.0001$) or 48 hours after injection (N = 9, paired $t$ = 6.59, p = 0.0002; Fig. 1B). The NIR fluorescence signal of the colorectal metastases was on average two-fold higher than that of the healthy liver and the tumor-to-background ratio was not significantly different when comparing the 24 hours (mean TBR = 2.04) and 48 hours group (mean TBR = 1.81, unpaired $t$ = 1.06, p = 0.31; Fig. 1C). Total fluorescence intensity was significantly correlated with the size of metastases ($R^2 = 0.92$ for the 24 h group, $R^2 = 0.96$ for the 48 h group). Measurements on the IVIS Spectrum were in concordance with the visual information provided by the Fluobeam system (data not shown). Sectioning of tumor and liver tissue showed a clear demarcation of fluorescence signal at the tumor border, which was confirmed by fluorescence microscopy (Fig. 2).

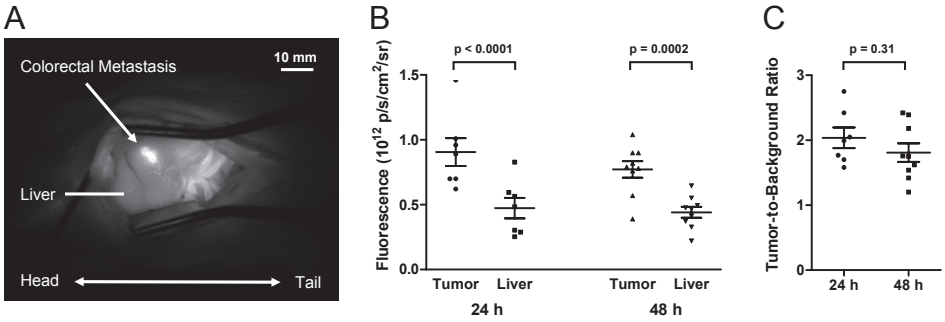


**Figure 1. NIR fluorescence detection of colorectal liver metastases using IntegriSense680: A.** Intraoperative NIR fluorescence detection of a 1.2 * 5 mm CC531 colorectal liver metastasis in a male rat 24 h after injection of 12 nmol IntegriSense680. Camera exposure time was 15 ms. **B.** The NIR fluorescence signal of colorectal liver metastases and healthy liver tissue is plotted for rats injected with IntegriSense680 after 24 h (N = 3 rats, 7 tumors) and 48 h (N = 4 rats, 9 tumors). P values represent paired t-test comparisons. **C.** Tumor-to-background ratio is plotted for rats injected with IntegriSense680 after 24 h and 48 h. There was no significant difference between the groups (unpaired t-test, t = 1.06, p = 0.31).

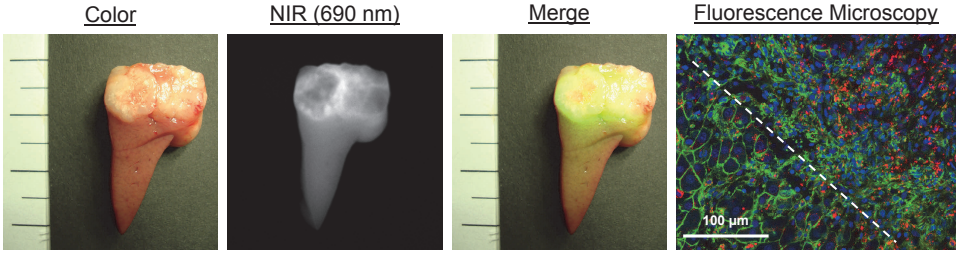


**Figure 2. Ex vivo NIR fluorescence imaging of a colorectal liver metastasis:** Shown are a color image (left), a NIR fluorescence image (middle left), and a pseudocolored green merge (middle right) of a 0.9 * 1.8 cm CC531 colorectal liver metastasis within an excised liver lobe. Imaging was performed 48 h after injection of 12 nmol IntegriSense680. Camera exposure time was 10 ms. The distance between two major ruler ticks is 1 cm. Ex vivo fluorescence microscopy (right) of a freshly resected liver lobe containing a CC531 colorectal liver metastasis after incubation with Hoechst (dsDNA, pseudo-colored blue) and phalloidin-AlexaFluor488 (F-actin filaments, pseudo-colored green). The IntegriSense680 signal is pseudo-colored red. The dashed line indicates the transition zone between the normal liver (left bottom corner) and the liver tumor (right upper corner).

## Biodistribution of IntegriSense680

To assess the potential use of IntegriSense680 in intraoperative identification of colorectal metastases in close proximity to other organs in the peritoneal cavity, the NIR fluorescence intensity of abdominal organs was quantified 24 and 48 hours after injection of IntegriSense680 using the Fluobeam system (Fig. 3). All abdominal organs showed fluorescence intensity levels comparable to or lower than the liver. No difference was observed between measurements at 24 and 48 hours after injection.

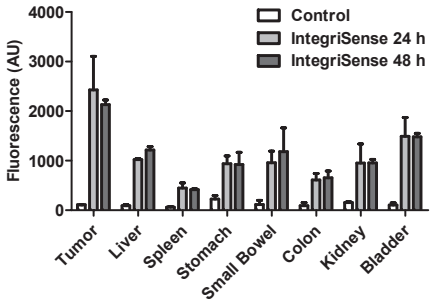


**Figure 3. In vivo biodistribution of IntegriSense680:** Fluorescence intensity of colorectal CC531 liver tumors and abdominal organs was measured using the Fluobeam camera system in two rats before (level of autofluorescence), 24 h and 48 h after administration of 12 nmol IntegriSense680. Camera exposure time was 10 ms. Bars represent mean ± SD.

## Intraoperative detection of intra-peritoneal metastases

The sufficiently low fluorescence levels of abdominal organs suggest a potential use of IntegriSense680 for identification of peritoneal colorectal metastases. In all animals, the peritoneal cavity was carefully inspected for tumor deposits. In several animals, several suspected tumors were found in the mesentery (Fig. 4). These nodules were

fluorescent and were confirmed as malignancies by histological analyses. Total fluorescence was significantly correlated with the size of mesenterial metastases ($R^2$ = 0.99). No clinically evident intra-abdominal tumor deposits without fluorescence were observed.

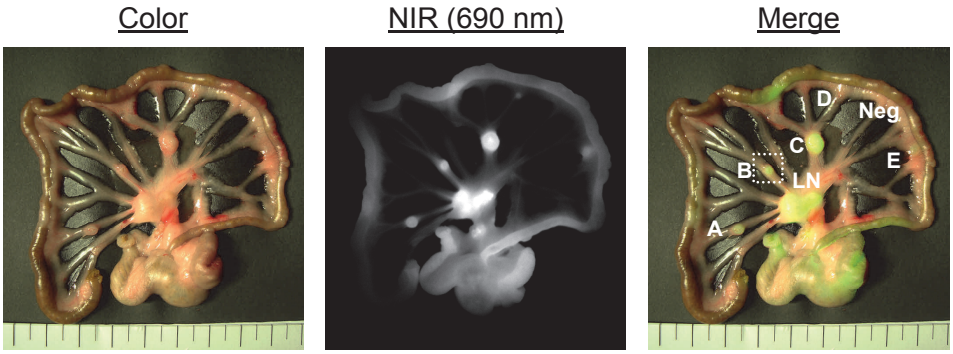


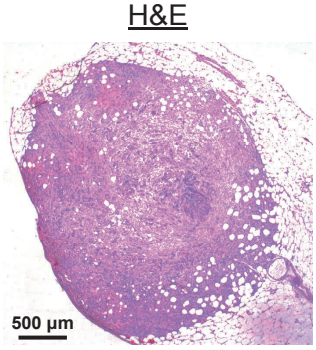


| | Size (mm) | Total NIRF (x10$^3$) | Average NIRF | Tumor |
|---|---|---|---|---|
| **A** | 3.4 x 2.5 | 199.4 | 779.0 | + |
| **B** | 2.3 x 2.0 | 163.1 | 1101.7 | + |
| **C** | 5.0 x 4.8 | 1024.8 | 1362.8 | + |
| **D** | 0.8 x 0.8 | 24.2 | 302.5 | + |
| **E** | 1.7 x 1.3 | 137.2 | 581.4 | + |
| **LN** | 10.6 x 6.0 | 3504.4 | 1633.8 | + |
| **Neg** | 0.9 x 0.9 | 10.6 | 173.7 | - |

**Figure 4. NIR fluorescence imaging of colorectal CC531 mesenterial metastases using IntegriSense680 and the intraoperative camera system:** Shown are a color image (top left), a NIR fluorescence image (top middle), and a pseudocolored green merge of the two images (top right) of a part of the jejunum and accompanied mesentery of a rat bearing multiple CC531 mesenterial metastases. A – E indicate suspected metastases, LN indicates mesenteric lymph nodes, Neg indicates area selected as negative control). Imaging was performed 24 h after injection of 12 nmol IntegriSense680. Camera exposure time was 20 ms. The distance between two major ruler ticks is 1 cm. H&E staining (bottom left) of a 4 µm formalin-fixed, paraffin-embedded tissue section of the metastasis indicated by B (dashed square, top right). The size, NIR fluorescence measurements and presence of tumor cells of the indicated regions (top right) are tabulated at the bottom right panel. Total NIRF is the total NIR fluorescence signal of the region-of-interest. Average NIRF is the total NIR fluorescence signal of the region-of-interest divided by the area. Total NIR fluorescence was significantly correlated with the size of the metastases (R2 = 0.99).

# DISCUSSION

## NIR fluorescence imaging

We have demonstrated the potential use of the NIR fluorescence probe IntegriSense680 for intraoperative tumor identification in both colorectal metastases confined to the

liver and metastases elsewhere in the peritoneal cavity. To our knowledge, the current study is the first study on targeting liver metastases using a targeted NIR fluorophore. NIR fluorescence imaging within the peritoneal cavity is often hampered by high levels of background fluorescence. Despite these difficulties, IntegriSense680 provided an adequate tumor-to-background ratio to identify tumors in the vicinity of abdominal organs. The targeting ligand of IntegriSense680 is a non-peptide integrin $\alpha_v\beta_3$ antagonist that is derived from the full-length RGD tripeptide.[20] This non-peptide molecule has a significantly improved affinity in comparison with the full-length RGD peptides, which have been used in imaging studies.[10, 25-27] No difference was observed between imaging 24 hours post administration and imaging 48 hours post administration. This broad window of intraoperative imaging facilitates flexible operation planning in future clinical applications.

**Peritoneal metastases**

In the current study, we were able to detect both liver and peritoneal metastases. Although the model is set up as a liver tumor model, some rats also developed peritoneal metastases, particularly those bearing larger liver tumors. Peritoneal spreading of tumor cells could have derived from tumor spill during the inoculation procedure or "real" metastases from large liver tumors.[28] Although, this may be a biologically relevant difference, it possesses no alteration for the purpose of the current study. During the experiments, no clinically evident intra-abdominal or lung metastases were found that were not NIR fluorescent.

It is well known that small metastases can easily be missed on preoperative imaging studies, as CT or MRI. Previously, a minimal detectable number of tumor cells of approximately 13,000 was reported with the CC531 colorectal cancer cell line and NIR fluorescence imaging,[21] reflecting submillimeter tumor depositions. NIR fluorescence imaging could therefore potentially be used in the clinic as an adjunct to preoperative staging, for intraoperative detection of metastases that were not observed on preoperative tumor dissemination imaging.

**Clinical implications**

Integrin $\alpha_v\beta_3$ as a targeting ligand has been studied extensively in a preclinical setting.[18, 29, 30] Several clinical studies have been performed using integrin $\alpha_v\beta_3$ as a target for radioimmunotherapy in breast cancer and glioblastoma patients.[11, 25] Although radiotracers are potentially useful for diagnosis and treatment by means of radioimmunotherapy, their applicability during surgery is limited due to a lack of intraoperative visualization of the tracer. Nonetheless, these studies suggest a successful introduction of integrin $\alpha_v\beta_3$ as a targeting ligand for NIR fluorescence image-guided surgery in the clinic, which will enable real-time, intraoperative visualization of tumor

cells. A major hurdle to be taken is clinical approval of novel NIR fluorophores. Currently, indocyanine green and methylene blue are the sole NIR fluorophores available for clinical applications. Both compounds have suboptimal properties for intraoperative applications and both are not easily conjugated to a targeting ligand. Ishizawa and colleagues have demonstrated the possibility of intraoperative identification of colorectal liver metastases after intravenous injection of indocyanine green.[31] In this study, colorectal liver metastases displayed a fluorescence pattern described as "rim fluorescence", where the tumor itself is not fluorescent, but the surrounding liver tissue is. Ishizawa et al suggest that this is caused by decreased biliary excretion of indocyanine green around the tumor. Whereas this is an interesting observation for the detection of hepatic colorectal metastases, the mechanism exploited for this purpose (biliary excretion) prevents this from being used for extra-hepatic intra-abdominal colorectal metastases. This is of particular importance, as the detection of extra-hepatic metastases is a determining factor for clinical decision making. Furthermore, the efficacy of this probe for tumor imaging is strongly dependent on biliary excretion and liver function, limiting its applicability in some patients. Many research groups are working on advancing novel NIR fluorescence fluorophores to the clinic. When these agents become available for clinical testing, NIR fluorescence image-guided surgery will have the potential to greatly improve surgical practice and patient outcome.

## CONCLUSION

NIR fluorescence image-guided surgery has the potential to improve surgical oncology by addressing one of its most fundamental challenges, the complete and en bloc resection of tumors. The current study demonstrates the feasibility of employing a novel NIR fluorescence contrast agent, IntegriSense680, for the intraoperative detection of colorectal metastases in a syngeneic rat model. Clinical translation of NIR fluorescence agents such as IntegriSense680 is pivotal for improving the quality of cancer surgery.

## ACKNOWLEDGEMENTS

We want to thank Fluoptics (Grenoble, France) for providing us with the Fluobeam system to perform the above described experiments and Gabi van Pelt and Karien de Rooij for technical assistance.

This study was performed within the framework of CTMM, the Center for Translational Molecular Medicine (DeCoDe project, grant 03O-101). This study was supported by the Sacha Swarttouw-Hijmans Foundation. J.S.D. Mieog is a MD-medical research trainee funded by The Netherlands Organisation for Health Research and Development (grant nr. 92003526).

# REFERENCES


1. McMillan DC, McArdle CS. Epidemiology of colorectal liver metastases. Surg Oncol 2007; 16:3-5.
2. Ruers T, Bleichrodt RP. Treatment of liver metastases, an update on the possibilities and results. Eur J Cancer 2002; 38:1023-1033.
3. Finch RJ, Malik HZ, Hamady ZZ, et al. Effect of type of resection on outcome of hepatic resection for colorectal metastases. Br J Surg 2007; 94:1242-1248.
4. Frangioni JV. New technologies for human cancer imaging. J Clin Oncol 2008; 26:4012-4021.
5. Weissleder R, Pittet MJ. Imaging in the era of molecular oncology. Nature 2008; 452:580-589.
6. Te Velde EA, Veerman T, Subramaniam V, et al. The use of fluorescent dyes and probes in surgical oncology. Eur J Surg Oncol 2010; 36:6-15.
7. Blum G, Weimer RM, Edgington LE, et al. Comparative assessment of substrates and activity based probes as tools for non-invasive optical imaging of cysteine protease activity. PLoS ONE 2009; 4:e6374.
8. Frangioni JV. The problem is background, not signal. Mol Imaging 2009; 8:303-304.
9. Axelsson R, Bach-Gansmo T, Castell-Conesa J, et al. An open-label, multicenter, phase 2a study to assess the feasibility of imaging metastases in late-stage cancer patients with the alpha(v) beta(3)-selective angiogenesis imaging agent (99m)Tc-NC100692. Acta Radiol 2010; 51:40-46.
10. Edwards WB, Akers WJ, Ye Y, et al. Multimodal imaging of integrin receptor-positive tumors by bioluminescence, fluorescence, gamma scintigraphy, and single-photon emission computed tomography using a cyclic RGD peptide labeled with a near-infrared fluorescent dye and a radionuclide. Mol Imaging 2009; 8:101-110.
11. Beer AJ, Niemeyer M, Carlsen J, et al. Patterns of alphavbeta3 expression in primary and metastatic human breast cancer as shown by 18F-Galacto-RGD PET. J Nucl Med 2008; 49:255-259.
12. Wu Y, Cai W, Chen X. Near-infrared fluorescence imaging of tumor integrin alpha v beta 3 expression with Cy7-labeled RGD multimers. Mol Imaging Biol 2006; 8:226-236.
13. Chen X, Hou Y, Tohme M, et al. Pegylated Arg-Gly-Asp peptide: 64Cu labeling and PET imaging of brain tumor alphavbeta3-integrin expression. J Nucl Med 2004; 45:1776-1783.
14. Hood JD, Cheresh DA. Role of integrins in cell invasion and migration. Nat Rev Cancer 2002; 2:91-100.
15. Vonlaufen A, Wiedle G, Borisch B, et al. Integrin alpha(v)beta(3) expression in colon carcinoma correlates with survival. Mod Pathol 2001; 14:1126-1132.
16. Merono A, Lucena C, Lopez A, et al. Immunohistochemical analysis of beta3 integrin (CD61): expression in pig tissues and human tumors. Histol Histopathol 2002; 17:347-352.
17. Le Tourneau C, Faivre S, Raymond E. The role of integrins in colorectal cancer. Oncology (WillistonPark) 2007; 21:21-24.
18. Dijkgraaf I, Beer AJ, Wester HJ. Application of RGD-containing peptides as imaging probes for alphavbeta3 expression. Front Biosci 2009; 14:887-899.
19. Vahrmeijer AL, van Dierendonck JH, Schutrups J, et al. Potentiation of the cytostatic effect of melphalan on colorectal cancer hepatic metastases by infusion of buthionine sulfoximine (BSO) in the rat: enhanced tumor glutathione depletion by infusion of BSO in the hepatic artery. Cancer Chemother Pharmacol 1999; 44:111-116.
20. Coleman PJ, Brashear KM, Askew BC, et al. Nonpeptide alphavbeta3 antagonists. Part 11: discovery and preclinical evaluation of potent alphavbeta3 antagonists for the prevention and treatment of osteoporosis. J Med Chem 2004; 47:4829-4837.
21. Mieog JS, Vahrmeijer AL, Hutteman M, et al. Novel Intraoperative Near-infrared Fluorescence Camera System For Optical Image-guided Cancer Surgery. Mol Imaging 2010; 9:223-231.
22. Mansfield JR, Hoyt C, Levenson RM. Visualization of microscopy-based spectral imaging data from multi-label tissue sections. Curr Protoc Mol Biol 2008; Chapter 14:Unit.
23. Wieland T, Faulstich H. Amatoxins, phallotoxins, phallolysin, and antamanide: the biologically active components of poisonous Amanita mushrooms. CRC Crit Rev Biochem 1978; 5:185-260.
24. Rasband WS. ImageJ, U. S. National Institutes of Health, Bethesda, Maryland, USA, http://rsb.info.nih.gov/ij. 2009.

25. Beer AJ, Haubner R, Sarbia M, et al. Positron emission tomography using [18F]Galacto-RGD identifies the level of integrin alpha(v)beta3 expression in man. Clin Cancer Res 2006; 12:3942-3949.
26. Chen X, Conti PS, Moats RA. In vivo near-infrared fluorescence imaging of integrin alphavbeta3 in brain tumor xenografts. Cancer Res 2004; 64:8009-8014.
27. Schnell O, Krebs B, Carlsen J, et al. Imaging of integrin alpha(v)beta(3) expression in patients with malignant glioma by [18F] Galacto-RGD positron emission tomography. Neuro Oncol 2009; 11:861-870.
28. Kollmar O, Schilling MK, Menger MD. Experimental liver metastasis: standards for local cell implantation to study isolated tumor growth in mice. Clin Exp Metastasis 2004; 21:453-460.
29. Mulder WJ, Castermans K, van Beijnum JR, et al. Molecular imaging of tumor angiogenesis using alphavbeta3-integrin targeted multimodal quantum dots. Angiogenesis 2009; 12:17-24.
30. Sancey L, Garanger E, Foillard S, et al. Clustering and internalization of integrin alphavbeta3 with a tetrameric RGD-synthetic peptide. Mol Ther 2009; 17:837-843.
31. Ishizawa T, Fukushima N, Shibahara J, et al. Real-time identification of liver cancers by using indocyanine green fluorescent imaging. Cancer 2009; 115:2491-2504.

# Chapter 3

# Image-guided tumor resection using real-time near-infrared fluorescence in a syngeneic rat model of primary breast cancer

Mieog JSD, Hutteman M, van der Vorst JR, Kuppen PJK, Que I, Dijkstra J, Kaijzel EL, Prins F, Löwik CWGM, Smit VTHBM, van de Velde CJ, Vahrmeijer AL

*Breast Cancer Res Treat; In press.*

## ABSTRACT

Tumor involvement of resection margins is found in a large proportion of patients who undergo breast-conserving surgery. Near-infrared (NIR) fluorescence imaging is an experimental technique to visualize cancer cells during surgery. To determine the accuracy of real-time NIR fluorescence imaging in obtaining tumor-free resection margins, a protease-activatable NIR fluorescence probe and an intraoperative camera system were used in the EMR86 orthotopic syngeneic breast cancer rat model. Influence of concentration, timing and number of tumor cells were tested in the MCR86 rat breast cancer cell line. These variables were significantly associated with NIR fluorescence probe activation. Dosing and tumor size were also significantly associated with fluorescence intensity in the EMR86 rat model, whereas time of imaging was not. Real-time NIR fluorescence guidance of tumor resection resulted in a complete resection of 17 out of 17 tumors with minimal excision of normal healthy tissue (mean minimum and a mean maximum tumor-free margin of 0.2 ± 0.2 mm and 1.3 ± 0.6 mm, respectively). Moreover, the technique enabled identification of remnant tumor tissue in the surgical cavity. Histological analysis revealed that the NIR fluorescence signal was highest at the invasive tumor border and in the stromal compartment of the tumor. In conclusion, NIR fluorescence detection of breast tumor margins was successful in a rat model. The present study suggests that clinical introduction of intraoperative NIR fluorescence imaging has the potential to increase the number of complete tumor resections in breast cancer patients undergoing breast-conserving surgery.

# INTRODUCTION

Incomplete tumor resections are an important clinical problem in breast cancer surgery. Tumor involvement of resection margins is found in 5-40% of patients who undergo breast-conserving surgery and these patients require additional surgery or intensified radiotherapy.[1-4] Furthermore, additional biopsies of the surgical cavity after primary resection have been shown to contain residual disease in 10% of patients with tumor-free specimen margins.[5] As a result, 5-year isolated local recurrences rates of 6.7-11% are reported in patients with tumor-free specimen margins treated with breast-conserving surgery and radiotherapy.[6] The occurrence of local relapse reduces the 15-year breast cancer specific and overall survival.[6] Consequently, increase of the radical resection rate will likely improve breast cancer outcome. Intraoperative real-time visualization of cancer cells is a promising method to achieve that goal.[7]

Near-infrared (NIR) fluorescence imaging is an experimental technique that can be used to visualize cancer cells during surgery. In current surgical practice, surgeons can only rely on palpation and visual inspection. Therefore, the use of NIR fluorescence imaging can be of great value, as already demonstrated in patients with glioma and liver cancer.[8-10] Advantages of NIR fluorescence light (700-900nm) include high tissue penetration (up to several centimeters deep) and low autofluorescence providing sufficient signal-to-background ratio.[11] Moreover, as the human eye is insensitive to NIR wavelengths, the use of NIR light will not interfere with the surgical field.

NIR fluorescence probes can target tumor cells through several mechanisms. For example, fluorophores can be conjugated to a tumor-specific antibody (e.g. directed to the Her-2/neu receptor), labeled to glucose derivates in order to visualize elevated metabolic rate, or autoquenched fluorophores can be activated by enzymatic cleavage in order to become fluorescent. The latter is of particular interest as certain enzyme systems are upregulated by a wide variety of cancer types, thus providing a more universally applicable NIR fluorescence probe. Proteolytic enzymes and in particular cathepsins from the cysteine protease family are a good candidate as they play essential roles in tumor growth, angiogenesis, resistance to apoptosis, and invasion.[12, 13] A member of this family, cathepsin B, is commonly active in the tumor microenvironment in various human cancers including breast cancer.[12, 14-16] Upregulated expression of cathepsin B is found in tumor, endothelial and immune cells, in particular macrophages.[13] Cathepsin B overexpression in human breast carcinomas is associated with poor differentiation, lymph node involvement, absence of estrogen receptor expression and impaired overall survival.[17, 18]

The protease-activatable NIR fluorescence probe ProSense (PerkinElmer, Waltham, USA) has been shown to detect a variety of tumors in nude or transgenic mice.[19-31] However, as tumor progression and metastasis are regulated by the surrounding microenvironment, it is important to use syngeneic animal models

that allow appropriate crosstalk at the invasive tumor border to study probes that are activated by proteolytic activity. Moreover, the use of a larger animal model such as the rat offers more challenges in terms of tissue penetration of NIR fluorescence probes.

Therefore, the aim of this study was to assess the technique of NIR fluorescence imaging in a syngeneic breast cancer rat model using ProSense and to determine the accuracy of intraoperative tumor detection to obtain an adequate tumor-free resection margin.

## MATERIALS AND METHODS

### Breast cancer cell line and culture conditions

The MCR86 cell line is a rapidly growing, syngeneic breast cancer cell line derived after subcutaneous transplantation of macroscopic lung tumors, which developed in a female WAG/Rij rat after intravenous inoculation of MCR83 breast cancer cells.[32] Tumor cells were cultured in RPMI 1640 supplemented with 2 mM L-glutamine (Gibco, Invitrogen Ltd, Carlsbad, USA), 10% heat-inactivated fetal calf serum, 100 U/ml penicillin and 0.1 mg/ml streptomycin sulphate.

### Breast cancer model and tumor induction

The related EMR86 model is a transplantable, hormone-dependent, metastasizing mammary carcinoma that originated in a female WAG/Rij rat bearing a subcutaneously implanted estrogen pellet and is developed by our research group (Fig. 1a).[33] Tumors are only induced and maintained in rats carrying estrogen pellets, whereas tumors transplanted into non-estrogenized animals do not grow out. Removal of the estrogen pellet induces apoptosis and tumor regression (Fig. 1b). EMR86 tumors are histologically classified as high-grade invasive ductaltype adenocarcinomas, with both a cribiform and a solid growth pattern. In large tumors areas, comedo type necrosis can be appreciated. Tumors have a stromal compartment of approximately 30% depending on tumor size (Fig. 1c). EMR86 tumor cells show strong nuclear expression of the estrogen and progesterone receptor in more than 90% of cells, but stain negative for HER2/neu receptor (Fig. 1d-f). Therefore, EMR86 tumors closely resemble the luminal A molecular subtype – the most prevalent subtype of human breast cancer.[34, 35]

For tumor induction, fresh EMR86 tumor fragments of 0.5-1 $mm^3$ were implanted in the mammary fat pad at four sites of female WAG/Rij rats (Charles River, Maastricht, the Netherlands) aging 4-6 months. (A stable cell line from EMR86 tumor has not yet been established successfully, therefore, tumor transplantation is used.) During the same session, an estrogen pellet was implanted subcutaneously in the intrascapular region of the neck. The in-house generated pellets consist of 2 mm

by 3 mm silicone tubes containing 1.5 mg 17 β-estradiol on a 1:3 cholesterol/paraffin basis. Tumor volumes were estimated twice weekly using digital calipers by measuring three orthogonal diameters of the tumor and multiplying this product by π/6. All rats were housed in the animal facility of the Leiden University Medical Center. Pellet food and fresh tap water were provided ad libitum. The weight of the animals was followed throughout the experiment to monitor their general health state. The Animal Welfare Committee of the Leiden University Medical Center approved the study. The study was conducted in concordance with the "Guidelines for the Welfare of Animals in Experimental Neoplasia" (Second Edition, 1997) available online at http://www.ncrn.org.uk/csg/animal_guides_text.pdf.

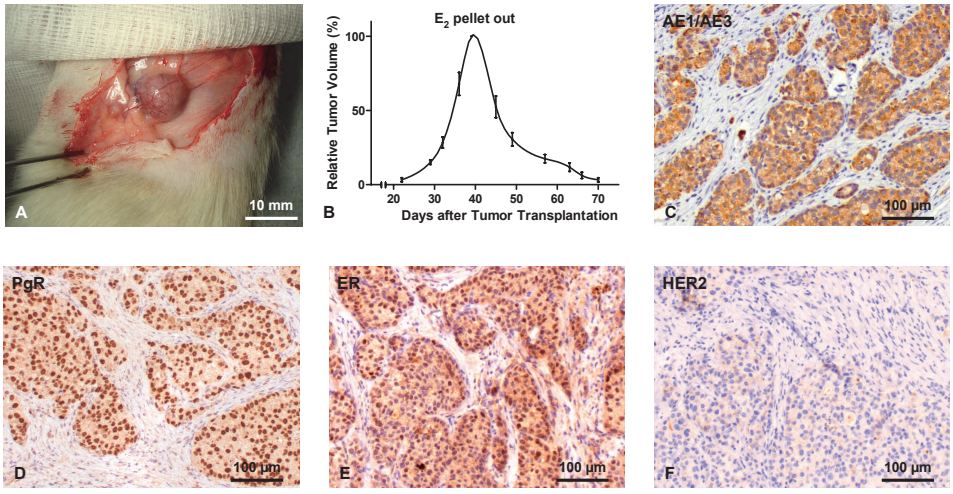


**Figure 1. Description of a syngeneic rat model of hormone-dependent breast cancer: A.** EMR86 breast tumors originate after transplantation of 0.5 mm3 fresh tumor fragments at the mammary fat path of female Wag/Rij rats. Shown is a tumor four weeks after transplantation. **B.** EMR86 tumors are only induced and maintained in rats carrying estrogen pellets. Removal of the estrogen pellet induces apoptosis and tumor regression (N = 16 tumors, 4 rats). **C.** EMR86 tumors are histologically classified as high-grade invasive ductal carcinomas, with both a cribiform and a solid growth pattern. Tumors have a stromal compartment of approximately 30% depending on tumor size. **D-F.** EMR86 tumor cells show strong nuclear expression of the estrogen and progesterone receptor in more than 90% of cells, but stain negative for HER2/neu receptor. Therefore, EMR86 tumors closely resemble the luminal A molecular subtype.

## NIR fluorescence probe

The commercially available, protease-activatable NIR fluorescence probes ProSense680 and ProSense750 were used (PerkinElmer). The probes consist of a synthetic graft polymer composed of poly-L-lysine that is sterically protected by multiple methoxypolyethylene glycol side chains and to which multiple fluorophores are attached.[19] In this non-activated state, the fluorophores are positioned in close proximity to one another, which results in mutual energy transfer and thus inhibition of fluorescence emission. After enzymatic cleavage of the backbone, the fluorophores

are released and regain their fluorescent characteristics. A number of cysteine proteases are involved in this process. Cathepsin B, and to a lesser degree cathepsin K, L, and S, has been demonstrated to be a major contributor to cleavage and activation of ProSense.[19] ProSense680 and ProSense750 have peak absorption of 680 nm and 750 nm, respectively. ProSense680 was selected for intraoperative studies and fluorescence microscopy because of the better matching of the laser of the intraoperative camera system with the peak excitation of ProSense680. ProSense750 was used for cell line experiments and non-invasive animal experiments because of the better spectral separation of autofluorescence signal.

**Intraoperative NIR fluorescence camera system**

The Fluobeam intraoperative NIR fluorescence camera system (Fluoptics, Grenoble, France) used in this study has been described previously by our group.[36, 37] Briefly, the system is composed of a class 3B laser (100mW) emitting at 690 nm resulting in an illumination power of 2.6 mW/cm$^2$. Filtered white light (350-650 nm) provides an irradiance of 7x10$^3$ lx at the focus level. The emitted fluorescence is collected through a high pass filter (> 700 nm) by a 12 bits CCD camera resulting in a system spatial resolution of 0.17 mm/pixel.

**Experimental design**

*Cell line experiments*

For fluorescence measurements, tumor cells were harvested with a solution of 0.25% (w/v) EDTA and 0.25% (w/v) trypsin in Hanks' Buffered Salt Solution (Sigma-Aldrich, St. Louis, USA), washed three times in 0.9% phosphate buffered saline and 200 µL complete medium suspensions were made and transferred on a 96-well acrylate plate (Greiner Bio-one, Alphen aan de Rijn, the Netherlands, #655090; suitable for fluorescence measurements) and kept at 37°C and 5% $CO_2$. At day 2, cells were washed and autoquenched ProSense750 (22.5 to 180 nM, 200 µl) was added. At day 3, cells were washed and 200 µl complete medium was added. Also, time-dependent studies were performed, during which ProSense750 was added at the indicated time-points (8 to 48 h). Fluorescence intensity was measured using the Odyssey NIR fluorescence scanning device (LI-COR Biosciences, Lincoln, USA). Overlying grids were drawn and fluorescence intensity was measured for each well using the Odyssey software (Version 2.1).

*Animal experiments*

Throughout injection, imaging and surgical procedures, rats were anaesthetized with inhalation of 2% mixture of isoflurane in oxygen. The rats were constantly monitored for the rate of the respiration and depth of anesthesia. Before imaging, rats were shaved to reduce absorption of the optical signal. A total of 20 rats bearing 77 primary mammary tumors varying in size from 0.01 to 1.8 $cm^3$ were used in this study.

In a dose-dependent and time-dependent experiment, tumor-bearing rats (N = 9) were randomly assigned over three ProSense750 dose groups and intravenously injected with 2.5, 5 or 10 nmol ProSense750 (150 µl). Whole-body fluorescence was measured 24 h and 48 h after administration of ProSense750 using the IVIS Spectrum (Caliper LifeSciences, Hopkinton, USA), which allowed separation of the ProSense750 signal from the background fluorescence by means of spectral unmixing.[38] Acquisition settings were kept constant for the different dose groups and on the two consecutive days. Total photon counts per second were measured for each tumor using the Living Image software (Version 3.0, Caliper LifeSciences) and divided by the tumor volume as assessed by digital caliper measurement.

In an intra-operative experiment, tumor-bearing rats (N = 7) were operated under direct fluorescence guidance 24 h after intravenous administration of 10 nmol ProSense680 (150 µl). NIR fluorescence intensity of exposed tumors and surrounding tissues was measured with the Fluobeam intraoperative camera system. Tumor-to-background ratios were calculated by drawing regions of interest at the tumor and at the surrounding tissue by visual interpretation and subsequent measurement of fluorescent intensity using the open-source software ImageJ.[39] Merged visible light and NIR fluorescence light images were created using Adobe Photoshop CS3 Software (Version 10.0.1, Adobe Systems Inc., San Jose, USA). In order to determine sensitivity and specificity of the intraoperative NIR fluorescence technique, an attempt was made to completely remove all tumor tissue while removing as little as possible of the normal surrounding mammary fat pad tissue strictly based on the fluorescence signal in 5 of these 7 rats. Tumors were removed by sharp dissection. Excised tumors were inked with India ink, sliced in two or three parts depending on the size of the tumor and fixed overnight in 4% buffered formalin and embedded in paraffin (FFPE) blocks, mimicking the standard clinical workflow. After resection of the primary tumor, the surgical cavity was inspected with the Fluobeam to detect any remnant fluorescent tissue. After resection of all remnant fluorescent spots, random biopsies were taken of the surgical cavity from every quadrant in order to determine specificity of the technique. In one additional rat an irradical resection was performed intentionally to test the Fluobeam's ability to detect remnant tumor tissue. All specimens were fixed in formalin as described above. FFPE tumor sections of 4 µm were air-dried and stained with hematoxylin and eosin (H&E). The tumor size, the minimum and maximum

tumor-free margin and the presence of tumor in the random biopsies were determined by an experienced breast pathologist (V.T.H.B.M.S.).

**Fluorescence microscopy**

*Cell line experiments*

Time-dependent microscopic analysis of ProSense680 activation by cultured MCR86 cancer cells was performed using the LSM510 Zeiss confocal microscope (Jena, Germany, 40x/0,75w Ph2 ACHROPLAN objective). A 633 nm laser was used for fluorescence excitation and a 650 nm Long Pass for emission. Cells were cultured in 3.5 cm petri dishes incubated with 33.3 nM ProSense680 in 3 ml medium. Cells were kept at 37°C and imaged for 4.5 hours.

*Ex vivo tumor imaging*

Freshly excised tumors with a wide rim of surrounding normal mammary tissue of rats injected with 10 nmol ProSense680 (N = 3) were halved. From one half, a 2 mm section was analyzed using the Odyssey scanning device at 21 μm resolution. Tumor border was defined as the outer rim of the tumor and its width was approximately 15% of the tumor diameter. The other half was snap-frozen on dry ice and stored at -80°C. Unfixed 20 μm sections were measured for fluorescence using the Odyssey scanning device at 21 μm resolution. Processing of sections was performed under reduced light conditions to prevent photobleaching. Subsequently, the tissue sections were stained with H&E. The fluorescence image and the H&E image were merged using Adobe Photoshop enabling detailed analysis of the NIR fluorescence distribution along with the histological context.

**Statistical analysis**

Statistical analyses and generation of graphs were performed using GraphPad Prism software (Version 5.01, La Jolla, USA). Continuous variables were analyzed using the (paired) t-test for comparison of two groups and one-way analysis of variance (ANOVA) for comparison of more than two groups. To test the effect of two independent variables two-way ANOVA was used. Trend analysis and one-tailed planned comparisons between adjacent groups were conducted. When the assumption of homogeneity of variance was violated (Levene's test), the Brown-Forsythe *F*-ratio was reported. Pearson's correlation coefficients R were calculated for correlation analyses. All statistical tests were two-tailed and $P < 0.050$ was considered significant.

# RESULTS

## *In vitro* activation of ProSense by breast cancer rat cell line

The autoquenched NIR fluorescence probe ProSense680 was activated by MCR86 breast cancer cells within two hours. Microscopic analysis revealed an intracellular localization of activated ProSense680 (Fig. 2a-b). Both incubation time ($F(3, 36)=1615$, $P < 0.0001$) and concentration of ProSense750 ($F(3, 36)=3704$, $P < 0.0001$) significantly influenced ProSense750 activation as measured by fluorescence intensity (two-way ANOVA, Fig. 2c). Also, there was an interaction between incubation time and ProSense750 concentration ($F(9, 36)=230.4$, $P < 0.0001$), indicating that the difference in incubation time within ProSense750 concentration groups influenced ProSense750 activation. Furthermore, fluorescence intensity was highly correlated with number of MCR86 cells ($F(4, 10.97) = 39.13$, $P < 0.0001$, $R = 0.904$; Fig. 2d).

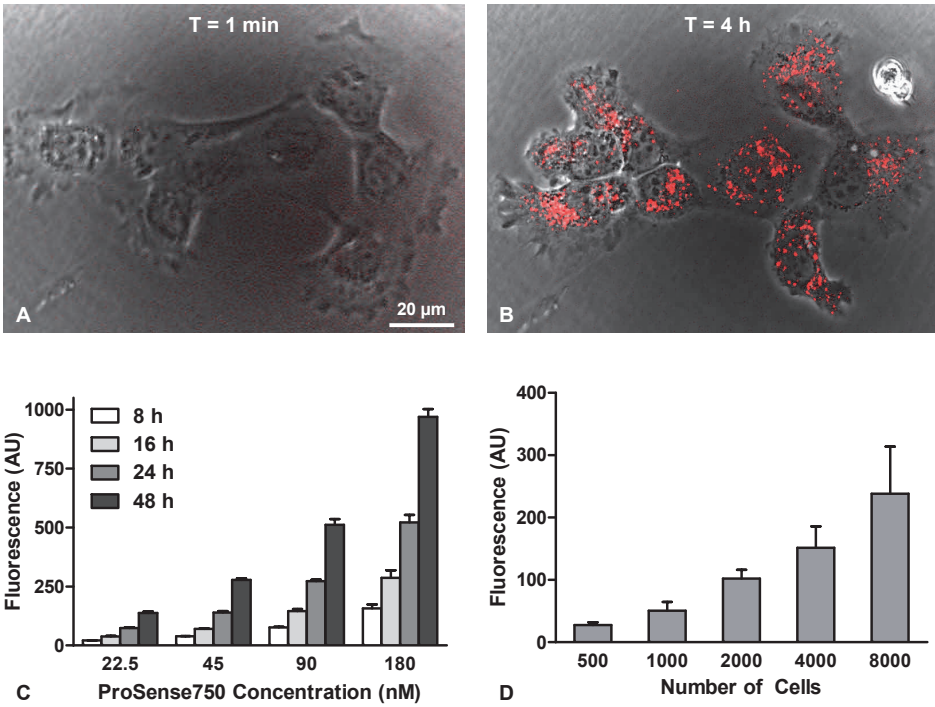


**Figure 2. In vitro activation of ProSense by syngeneic breast cancer rat cell line: A,B.** Fluorescence microscopy (LSM510 Zeiss confocal microscope, 40x objective) of a cluster of MCR86 cells, 1 minute (left panel) and 4.5 h (right panel) after incubation with ProSense680 (33.3 nM). **C.** ProSense750 concentration and incubation time both significantly influence NIR fluorescence intensity (4.000 MCR86 cells per well, two-way ANOVA, Odyssey scanner). Bars represent mean ± SEM (N = 4). **D.** NIR fluorescence intensity is positively correlated with number of MCR86 cells (45 nM ProSense750, 24 h incubation, $R = 0.890$, $P < 0.0001$, Odyssey scanner). Bars represent mean ± SEM (N = 8).

**In vivo activation of ProSense by syngeneic rat model of primary breast cancer**

EMR86 breast tumors were successfully imaged percutaneously using the IVIS Spectrum after intravenous administration of ProSense750 (Fig. 3a-b). To test the effect of ProSense750 dose and time of imaging on fluorescence intensity, nine rats (N = 35 mammary tumors, mean volume = 0.38 ± 0.36 $cm^3$) were randomly assigned to three ProSense750 dose groups and were imaged 24 h and 48 h post-injection. In concordance with the *in vitro* data, ProSense750 dose significantly influenced fluorescence intensity ($F(2,32) = 3.56$, P = 0.04, two-way ANOVA, Fig. 3c). Of note, a substantial part of the tumors could not be identified in the 2.5 nmol dose group (24 h: 4 of 11 tumors, 48 h: 7 of 11 tumors) and the 5 nmol dose group (24 h: 2 of 12 tumors, 48 h: 3 of 12 tumors), whereas in the 10 nmol dose group all tumors were identified. In contrast to the *in vitro* data, time of imaging did not influence fluorescence intensity ($F(2,32) = 2.47$, P = 0.13, two-way ANOVA, Fig. 3c). Furthermore, there was no interaction between time of imaging and ProSense750 dose ($F(2,32) = 1.06$, P = 0.36), indicating that the difference in time of imaging within dose groups did not influence fluorescence intensity. Based on these results, a dose of 10 nmol was selected for further *in vivo* testing. Imaging 24 h after administration of ProSense was selected for practical purposes. With these settings, fluorescence intensity was significantly correlated with tumor volume (R = 0.934, P < 0.0001; Fig. 3d), which was in concordance with the *in vitro* data.

**Intraoperative NIR fluorescence-guided resection of primary breast cancer**

Using the Fluobeam intraoperative camera system, all primary breast tumors (N = 26 tumors, 7 rats) were successfully identified 24 h after intravenous administration of 10 nmol ProSense680 (Fig. 4a). The technique provided a clear demarcation of tumor and surrounding mammary fat pad tissue with a mean tumor-to-background ratio of 2.35 ± 0.37 (paired t-test, $t = 14.95$, P < 0.0001, Fig. 4b). To determine the accuracy of tumor margin detection of the intraoperative NIR fluorescence technique, 17 tumors (N = 5 rats) were resected completely under direct, real-time NIR fluorescence guidance, while removing as little as possible of the normal surrounding mammary fat pad tissue and processed for histopathological analysis (Fig. 4c). All 17 tumors were completely excised with a mean minimum and a mean maximum tumor-free margin of 0.2 ± 0.2 mm and 1.3 ± 0.6 mm, respectively (Table 1). Mean pathological tumor size was 5.0 ± 2.1 mm. In two cases, after resection of the primary tumor, remnant fluorescent tissue was detected in the surgical cavity with Fluobeam (Table 1). One specimen contained a lymph node with metastatic involvement and the other contained a reactive lymph node with abundant macrophage influx but no tumor involvement. This false-positive finding can be explained by the fact that macrophages show high cathepsin B expression.[13] After resection of all fluorescent spots, random biopsies were taken of

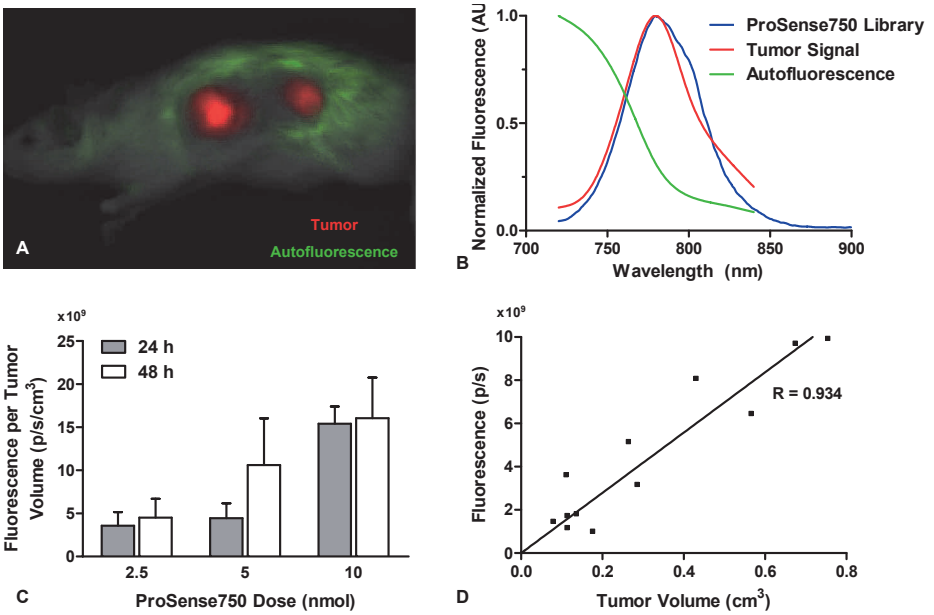


**Figure 3. In vivo activation of ProSense by syngeneic rat model of primary breast cancer:** A. Typical example of a spectral unmixed image of an EMR86 tumor-bearing female WAG/Rij rat, acquired 24 h after intravenous administration of 10 nmol ProSense750. Shown is the separation of the autofluorescence signal (pseudocolored green) and the ProSense750 signal (pseudocolored red; IVIS Spectrum). **B.** Emission curve plot of the spectrally unmixed fluorescence signals from a. demonstrates matching of the tumor signal (red line) with the predefined ProSense750 emission curve (blue line), confirming the localization of activated ProSense750 at the tumors. **C.** In a dose-dependent and time-dependent experiment, nine tumor-bearing rats (N = 35 tumors) were randomized to three ProSense750 dose groups and imaged 24 h (grey bars) and 48 h (open bars) after intravenous administration of ProSense750 using the IVIS Spectrum. Bars represent mean ± SEM. **D.** Scatter plot of fluorescence intensity and tumor volume of the 10 nmol dose group imaged 24 h after intravenous administration of ProSense750 ($R = 0.934$, $P < 0.0001$, N = 12 tumors from 3 rats).

the surgical cavity from every quadrant. None of the random biopsies (N = 64, 5 rats) contained histologically any tumor cells. These results indicate an excellent accuracy of the technique.

In one additional rat, an irradical resection was performed intentionally in order to show the Fluobeam's ability to detect remnant tumor tissue. Remnant tumor tissue could be detected and subsequently resected under direct NIR fluorescence guidance.

## Ex vivo NIR fluorescence microscopy

In order to determine the histological localization of ProSense680, tumors were excised with a wide rim of normal mammary tissue 24 h after intravenous administration of 10 nmol ProSense680 (N = 12 tumors, 3 rats; Fig. 5a). Fluorescence imaging of 2 mm thick, fresh tumor slices revealed that the NIR fluorescence intensity was 1.6 ± 0.3 times higher at the border of the tumor than at its center (paired t-test, $t = 4.99$, $P = 0.0005$, N = 12 tumors; Fig. 5b). In order to obtain more detail about the histological

**Table 1.** Pathological assessment of inked resection margins after NIR fluorescence guided excision of primary breast cancer

| Rat | Tumor ID | Maximum ø Specimen (mm) | Maximum ø Tumor (mm) | Radical resection? | Minimum margin (mm) | Maximum margin (mm) | Remnant fluorescence tumor-positive? | Random non-fluorescence biopsies tumor-positive? |
|---|---|---|---|---|---|---|---|---|
| A | 1 | 7.4 | 3.8 | yes | <0.1 | 1.3 | 0 | 0/4 |
| | 2 | 2.8 | 0.8 | yes | <0.1 | 0.9 | 1/1[a] | 0/4 |
| | 3 | 8.8 | 4.8 | yes | 0.7 | 2.4 | 0 | 0/3 |
| B | 4 | 7.5 | 5.1 | yes | <0.1 | 1.4 | 0 | 0/4 |
| | 5 | 4.9 | 3.1 | yes | <0.1 | 1.0 | 0 | 0/4 |
| | 6 | 5.4 | 4.2 | yes | 0.1 | 1.0 | 0 | 0/4 |
| | 7 | 9.2 | 8.0 | yes | <0.1 | 1.0 | 0 | 0/4 |
| C | 8 | 9.1 | 7.9 | yes | <0.1 | 1.1 | 0 | 0/4 |
| | 9 | 8.9 | 5.7 | yes | 0.2 | 2.5 | 0 | 0/4 |
| | 10 | 9.7 | 7.7 | yes | <0.1 | 1.8 | 0 | 0/4 |
| D | 11 | 5.3 | 2.4 | yes | 0.4 | 1.6 | 0 | 0/3 |
| | 12 | 6.1 | 4.3 | yes | 0.2 | 1.0 | 0 | 0/4 |
| | 13 | 5.7 | 4.4 | yes | 0.2 | 1.5 | 0 | 0/4 |
| E | 14 | 8.2 | 6.9 | yes | <0.1 | 0.8 | 0 | 0/4 |
| | 15 | 8.3 | 7.3 | yes | <0.1 | 0.6 | 0 | 0/4 |
| | 16 | 7.3 | 5.6 | yes | 0.3 | 0.7 | 0 | 0/4 |
| | 17 | 6.6 | 3.0 | yes | <0.1 | 1.9 | 0/1[b] | 0/4 |
| **Mean ± SD** | | **7.1 ± 1.9** | **5.0 ± 2.1** | | 0.2 ± 0.2 | 1.3 ± 0.6 | 1/2 | 0/64 |

[a] Macrometastasis in lymph node
[b] Reactive lymph node with abundant macrophage influx

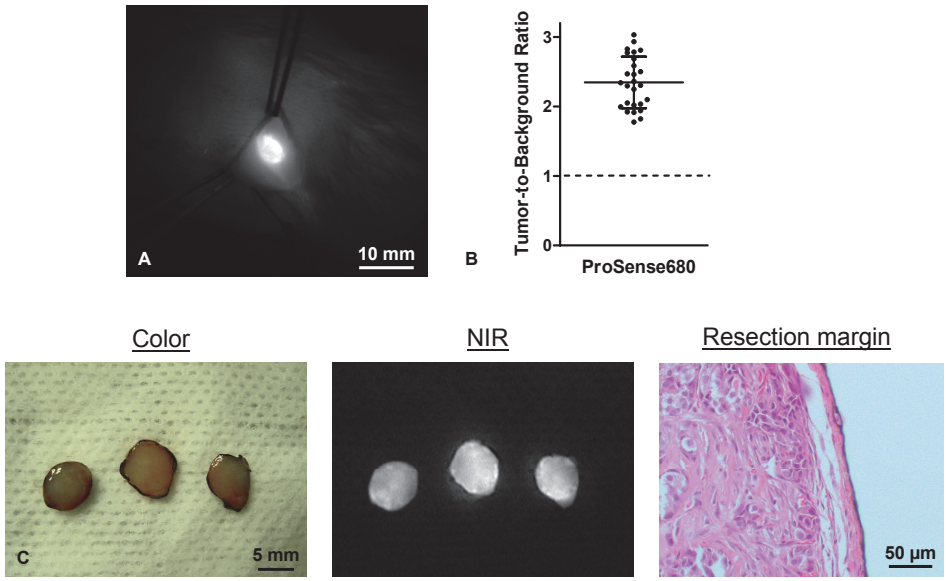


**Figure 4. Intraoperative NIR fluorescence-guided resection of primary breast cancer and pathological assessment: A.** Intraoperative NIR fluorescence image showing a 6-mm EMR86 breast tumor in a female WAG/Rij rat 24 h after intravenous administration of 10 nmol ProSense680 (Fluobeam camera system). Camera exposure time was 10 ms. **B.** Tumor-to-background ratios were determined in vivo in rats 24 h after intravenous administration of 10 nmol ProSense680 (N = 26 tumors, 7 rats). Fluobeam camera exposure time was 10 ms. Horizontal lines represent mean ± SD. Mean tumor-to-background ratio was 2.35 ± 0.37. **C.** Ex vivo color image (left panel), NIR fluorescence image (Fluobeam, middle panel) of 3 slices of an EMR86 tumor after resection and inking using India ink. The tumor was excised from a rat 24 h after intravenous administration of 10 nmol ProSense680. Camera exposure time was 10 ms. Resection margin of the tumor is shown after H&E staining of a 4 µm FFPE tissue section (right panel).

localization of ProSense680, unfixed 20 µm frozen tissue sections were measured for fluorescence using the Odyssey and subsequently stained with H&E (Fig. 5c). These results showed that NIR fluorescence is mainly located in the stromal compartment of the breast tumors and in particular at the tumor border.

## DISCUSSION

In the current study, we demonstrated the feasibility of real-time intraoperative NIR fluorescence identification of breast tumors in a syngeneic orthotopic breast cancer rat model using the protease-activatable probe ProSense. In both the cell line and animal experiments, fluorescence intensity was strongly correlated with number of tumor cells, tumor size and ProSense dose. In contrast to the *in vitro* data, time of imaging (24 h vs. 48 h after administration of ProSense) did not significantly influence fluorescence intensity of breast tumors. This is likely a result of the relatively long blood half-life of ProSense (half-life in mice 18 h, PerkinElmer website) and may provide flexible operation planning in future clinical applications. Histological analysis demonstrated

that NIR fluorescence intensity of tumors was highest at the invasive tumor border. Resection of tumors under real-time NIR fluorescence guidance showed excellent accuracy of the technique in the intraoperative detection of tumor margins. These results suggest that clinical introduction of intraoperative NIR fluorescence imaging using a protease-activatable probe such as ProSense has the potential to increase the number of complete tumor resections in breast cancer patients undergoing breast-conserving surgery.

Previous studies in which NIR fluorescent and protease-activatable probes were tested have utilized xenograft or transgenic mouse models.[19-31] A limitation of many animal models of breast cancer is that, compared to the human situation, less normal mammary tissue is present in relation to tumor size. Therefore, these tumors are easily resected by removing all breast tissue. However, this approach does not resemble the principles underlying breast-conserving surgery. This study was performed using an orthotopic breast cancer model that is syngeneic to immunocompetent female WAG/Rij rats. In syngeneic models, tumors are grown in homologous species and in the strain in which the tumor has originated. Therefore, these models are more representative of the natural tumor-host interaction. Although no preclinical tumor model will contain all features of the complex biology of human cancer, this syngeneic model has several strengths, including its hormone-sensitivity, cribiform growth pattern and its ability to induce regression by estrogen pellet removal. Moreover, this model captures several important features of luminal A hormone-dependent, HER2/neu negative human breast cancer, which is the most predominant subtype of breast cancer.[34, 35] Another intrinsic limitation of animal models of surgical interventions is the potential occurrence of performance bias, because researchers carrying out the intervention can not be blinded to the allocated treatment. This form of bias may lead to flawed results.[40] To surpass these limitations in our study, a one-arm study design was chosen using small breast tumors (5.0 ± 2.1 mm). Tumors were excised based on the NIR fluorescence signal and examined by a breast pathologist using standard clinical methodology. Using this approach, all tumors were completely resected with a mean maximum tumor-free resection margin of 1.3 ± 0.6 mm, indicating that a minimal amount of normal mammary tissue was resected. Although syngeneic models provide a relevant tumor-host interaction, their major drawback is that the tumor cells are rodent, and therefore express the rodent homologues of the desired targets. However, the main target of ProSense, the cysteine protease family (most particular cathepsin B) is strongly conserved amongst mammals.[12] Upregulation of cathepsin B has been confirmed extensively in human breast cancer.[12, 14, 15, 41] It is therefore expected that this kind of protease-activated NIR fluorescence probes will be applicable for intraoperative NIR fluorescence imaging in a large proportion of breast cancer patients.

Analysis of the histological localization of activated ProSense demonstrated that the invasive tumor border exhibited the most intense NIR fluorescence signal.

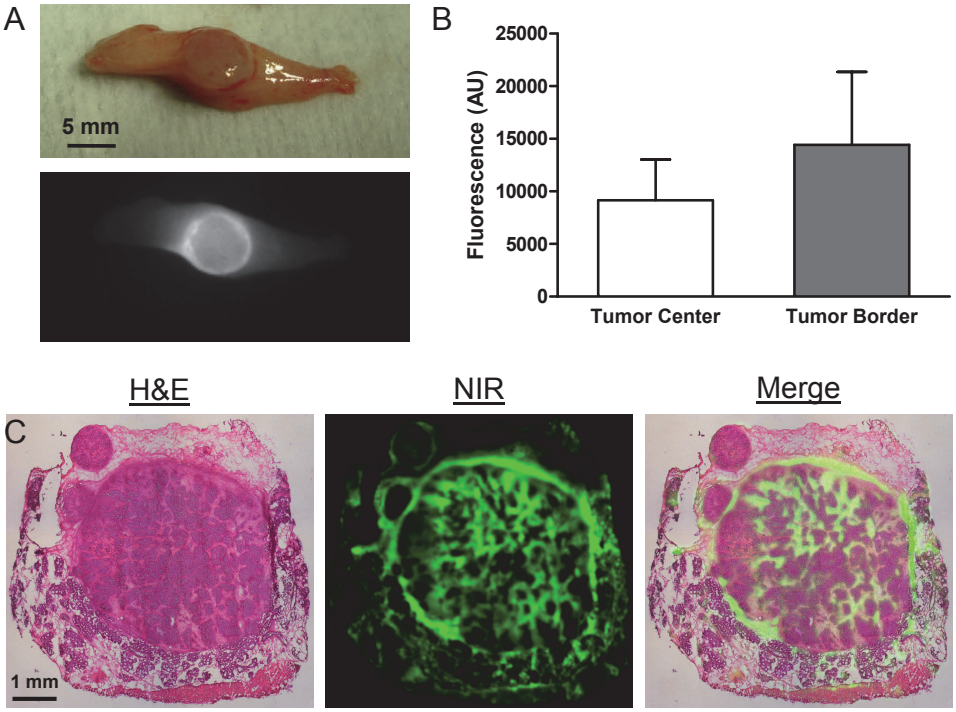


**Figure 5. Ex vivo NIR fluorescence microscopy of resected breast cancer: A.** Ex vivo color image (top panel) and NIR fluorescence image (Fluobeam, bottom panel) of an excised EMR86 tumor with surrounding normal mammary fat pad. Fluobeam camera exposure time was 10 ms. The tumor was excised from a rat 24 h after administration of 10 nmol ProSense680. **B.** Quantification of NIR fluorescence measurements of tumor tissue slices showed that the fluorescence signal was 1.6 ± 0.3 times higher at the border of the tumor than at its center (Odyssey scanner, paired t-test, t = 4.99, P = 0.0005, N = 12 tumors). **C.** Shown are a color image of H&E staining (left panel), a pseudocolored green NIR fluorescence image (middle panel; Odyssey scanner), and a merge of the two images (right panel) of a 20 µm frozen section of a 4-mm EMR86 breast tumor with surrounding mammary fat pad. The tumor was excised from a rat 24 h after administration of 10 nmol ProSense680.

This observation is in concordance with immunohistological analysis of cathepsin B reported by others[14, 24] and is in line with the pathophysiological role of cathepsins as reviewed by Gocheva.[42] Cathepsins promote tumor invasion through several possible mechanisms. First, they can directly cleave components of the extracellular matrix and basement membrane, essentially clearing a path for the migration of tumor cells away from the primary tumor. Second, at the cell membrane, cathepsins can direct a proteolytic cascade in which they activate other proteases such as matrix metalloproteinases and urokinase plasminogen activator, which in turn promotes tumor invasion. Third, cleavage of the cell adhesion protein, E-cadherin, at the cell surface can disrupt adherens junctions and thus facilitate cancer cell migration and invasion.[42] Apart from tumor border, NIR fluorescence was higher in the stromal compartment of the tumors. This finding is in concordance with Gounaris et al., who demonstrated that $CD11^+$ tumor-infiltrating macrophages accounted for 75% of the

ProSense signal at FACS analysis.[29] In summary, as complete resection of breast tumors requires adequate visualization of tumor margins, the increased activity of proteolytic enzymes at the invasive tumor border provides an excellent target for intraoperative NIR fluorescence-guided surgery.

Future clinical studies will have to provide proof-of-principle of intraoperative NIR fluorescence tumor detection. Currently, a number of intraoperative NIR fluorescence imaging systems are clinically available and have already been used for sentinel lymph node mapping.[43-45] It is expected that several tumor-targeting NIR fluorescent probes (such as ProSense) will receive regulatory approval within the next few years.

A therapeutic challenge of any new breast cancer imaging technology is the detection of occult tumor deposits in the breast. These tumor deposits could influence surgical decision making, but do not necessarily have a prognostic relevance, because in the vast majority of cases postoperative radiation will eradicate these microscopic deposits. For instance, in preoperative MR imaging, the identification of additional tumor deposits is two to three times higher than the incidence of local recurrence, resulting in mastectomies that may not be beneficial to the patient.[46] Consequently, detection of tumor at the margins would be beneficial, detection of tumor deposits beyond the margins, below the cut edge of the lumpectomy cavity, could have the potential to increase surgical resection volume (or even mastectomy rates) without a benefit in survival. Since the maximum penetration depth for NIR fluorescence imaging is currently around 1 cm,[47] it is unlikely that intraoperative NIR fluorescence imaging will detect occult lesions at several centimeters distance from the primary tumor.

Sensitivity of NIR fluorescence is mostly dependent on photon absorption of the tissue, fluorescence excitation power of the light source and concentration of the NIR fluorophore in tissue. Required camera exposure times are inversely correlated with the amount of fluorescence signal. In the current study, camera exposure times of 2-20 ms were used. The field-of-view of the Fluobeam camera system is 7 cm of diameter. Therefore, the time needed to evaluate tumor margins and excision cavities is at most several seconds. Consequently, this real-time intraoperative technique is unlikely to prolong surgical time significantly.

In conclusion, this study provides preclinical validation of an innovative technique in which NIR fluorescence light is used to visualize breast tumors and to provide real-time guidance during subsequent resection. Clinical translation of these results might be very promising because of high accuracy of the technique, flexible surgical planning, increased proteolytic activity at the tumor border and upregulation of cathepsin B in a large proportion of breast cancer patients. Therefore, this study warrants clinical validation of this technique, once NIR fluorescence probes become

available for clinical testing, with the ultimate goal to increase the radical resection rate of patients undergoing breast-conserving surgery.

## ACKNOWLEDGEMENTS

We want to thank Rob Keyzer and Anita Sajet for technical assistance and Fluoptics (Grenoble, France) for use of the Fluobeam® system. J.S.D. Mieog is a MD-medical research trainee funded by The Netherlands Organisation for Health Research and Development (grant nr. 92003526).

## REFERENCES


1. Mai KT, Yazdi HM, Isotalo PA. Resection margin status in lumpectomy specimens of infiltrating lobular carcinoma. Breast Cancer Res Treat 2000; 60:29-33.
2. Chagpar AB, Martin RC, Hagendoorn LJ, et al. Lumpectomy margins are affected by tumor size and histologic subtype but not by biopsy technique. Am J Surg 2004; 188:399-402.
3. Smitt MC, Horst K. Association of clinical and pathologic variables with lumpectomy surgical margin status after preoperative diagnosis or excisional biopsy of invasive breast cancer. Ann Surg Oncol 2007; 14:1040-1044.
4. Rizzo M, Iyengar R, Gabram SG, et al. The effects of additional tumor cavity sampling at the time of breast-conserving surgery on final margin status, volume of resection, and pathologist workload. Ann Surg Oncol 2010; 17:228-234.
5. Hewes JC, Imkampe A, Haji A, et al. Importance of routine cavity sampling in breast conservation surgery. Br J Surg 2009; 96:47-53.
6. Clarke M, Collins R, Darby S, et al. Effects of radiotherapy and of differences in the extent of surgery for early breast cancer on local recurrence and 15-year survival: an overview of the randomised trials. Lancet 2005; 366:2087-2106.
7. Nyirenda N, Farkas DL, Ramanujan VK. Preclinical evaluation of nuclear morphometry and tissue topology for breast carcinoma detection and margin assessment. Breast Cancer Res Treat 2010.
8. Stepp H, Beck T, Pongratz T, et al. ALA and malignant glioma: fluorescence-guided resection and photodynamic treatment. J Environ Pathol Toxicol Oncol 2007; 26:157-164.
9. Ishizawa T, Fukushima N, Shibahara J, et al. Real-time identification of liver cancers by using indocyanine green fluorescent imaging. Cancer 2009; 115:2491-2504.
10. Nguyen NQ, Biankin AV, Leong RW, et al. Real time intraoperative confocal laser microscopy-guided surgery. Ann Surg 2009; 249:735-737.
11. Frangioni JV. New technologies for human cancer imaging. J Clin Oncol 2008; 26:4012-4021.
12. Mohamed MM, Sloane BF. Cysteine cathepsins: multifunctional enzymes in cancer. Nat.Rev. Cancer 2006; 6:764-775.
13. Gocheva V, Zeng W, Ke D, et al. Distinct roles for cysteine cathepsin genes in multistage tumorigenesis. Genes Dev 2006; 20:543-556.
14. Parker BS, Ciocca DR, Bidwell BN, et al. Primary tumour expression of the cysteine cathepsin inhibitor Stefin A inhibits distant metastasis in breast cancer. J Pathol 2008; 214:337-346.
15. Harbeck N, Alt U, Berger U, et al. Prognostic impact of proteolytic factors (urokinase-type plasminogen activator, plasminogen activator inhibitor 1, and cathepsins B, D, and L) in primary breast cancer reflects effects of adjuvant systemic therapy. Clin Cancer Res 2001; 7:2757-2764.
16. Lah TT, Kokalj-Kunovar M, Strukelj B, et al. Stefins and lysosomal cathepsins B, L and D in human breast carcinoma. Int J Cancer 1992; 50:36-44.
17. Lah TT, Kos J, Blejec A, et al. The Expression of Lysosomal Proteinases and Their Inhibitors in Breast Cancer: Possible Relationship to Prognosis of the Disease. Pathol Oncol Res 1997; 3:89-99.
18. Foekens JA, Kos J, Peters HA, et al. Prognostic significance of cathepsins B and L in primary human breast cancer. J Clin Oncol 1998; 16:1013-1021.
19. Weissleder R, Tung CH, Mahmood U, et al. In vivo imaging of tumors with protease-activated near-infrared fluorescent probes. Nat Biotechnol 1999; 17:375-378.
20. Kirsch DG, Dinulescu DM, Miller JB, et al. A spatially and temporally restricted mouse model of soft tissue sarcoma. Nat Med 2007; 13:992-997.
21. Bremer C, Tung CH, Bogdanov A, Jr., et al. Imaging of differential protease expression in breast cancers for detection of aggressive tumor phenotypes. Radiology 2002; 222:814-818.
22. von Burstin J, Eser S, Seidler B, et al. Highly sensitive detection of early-stage pancreatic cancer by multimodal near-infrared molecular imaging in living mice. Int J Cancer 2008; 123:2138-2147.
23. Sheth RA, Upadhyay R, Stangenberg L, et al. Improved detection of ovarian cancer metastases by intraoperative quantitative fluorescence protease imaging in a pre-clinical model. Gynecol Oncol 2009; 112:616-622.

24. Alencar H, Funovics MA, Figueiredo J, et al. Colonic adenocarcinomas: near-infrared microcatheter imaging of smart probes for early detection--study in mice. Radiology 2007; 244:232-238.
25. Bogdanov AA, Jr., Lin CP, Simonova M, et al. Cellular activation of the self-quenched fluorescent reporter probe in tumor microenvironment. Neoplasia. 2002; 4:228-236.
26. Niedre MJ, de Kleine RH, Aikawa E, et al. Early photon tomography allows fluorescence detection of lung carcinomas and disease progression in mice in vivo. Proc.Natl.Acad.Sci.U.S.A 2008; 105:19126-19131.
27. Ntziachristos V, Tung CH, Bremer C, et al. Fluorescence molecular tomography resolves protease activity in vivo. Nat Med 2002; 8:757-760.
28. Bremer C, Ntziachristos V, Weitkamp B, et al. Optical imaging of spontaneous breast tumors using protease sensing 'smart' optical probes. Invest Radiol. 2005; 40:321-327.
29. Gounaris E, Tung CH, Restaino C, et al. Live imaging of cysteine-cathepsin activity reveals dynamics of focal inflammation, angiogenesis, and polyp growth. PLoS.One. 2008; 3:e2916.
30. Grimm J, Kirsch DG, Windsor SD, et al. Use of gene expression profiling to direct in vivo molecular imaging of lung cancer. Proc.Natl.Acad.Sci.U.S.A 2005; 102:14404-14409.
31. Nguyen QT, Olson ES, Aguilera TA, et al. Surgery with molecular fluorescence imaging using activatable cell-penetrating peptides decreases residual cancer and improves survival. Proc. Natl.Acad.Sci.U.S.A 2010; 107:4317-4322.
32. van Dierendonck JH, Keijzer R, Cornelisse CJ, et al. Surgically induced cytokinetic responses in experimental rat mammary tumor models. Cancer 1991; 68:759-767.
33. Wijsman JH, Cornelisse CJ, Keijzer R, et al. A prolactin-dependent, metastasising rat mammary carcinoma as a model for endocrine-related tumour dormancy. Br J Cancer 1991; 64:463-468.
34. Sorlie T, Tibshirani R, Parker J, et al. Repeated observation of breast tumor subtypes in independent gene expression data sets. Proc.Natl.Acad.Sci.U.S.A 2003; 100:8418-8423.
35. Sihto H, Lundin J, Lehtimaki T, et al. Molecular subtypes of breast cancers detected in mammography screening and outside of screening. Clin Cancer Res 2008; 14:4103-4110.
36. Mieog JS, Vahrmeijer AL, Hutteman M, et al. Novel Intraoperative Near-infrared Fluorescence Camera System For Optical Image-guided Cancer Surgery. Mol.Imaging 2010; 9:223-231.
37. Keramidas M, Josserand V, Righini CA, et al. Intraoperative near-infrared image-guided surgery for peritoneal carcinomatosis in a preclinical experimental model. Br J Surg 2010; 97:737-743.
38. Mansfield JR, Hoyt C, Levenson RM. Visualization of microscopy-based spectral imaging data from multi-label tissue sections. Curr.Protoc.Mol.Biol. 2008; Chapter 14:Unit.
39. Rasband WS. ImageJ, U. S. National Institutes of Health, Bethesda, Maryland, USA, http://rsb.info.nih.gov/ij. 2009.
40. Juni P, Altman DG, Egger M. Systematic reviews in health care: Assessing the quality of controlled clinical trials. BMJ 2001; 323:42-46.
41. Kuester D, Lippert H, Roessner A, et al. The cathepsin family and their role in colorectal cancer. Pathol Res Pract 2008; 204:491-500.
42. Gocheva V, Joyce JA. Cysteine cathepsins and the cutting edge of cancer invasion. Cell Cycle 2007; 6:60-64.
43. Troyan SL, Kianzad V, Gibbs-Strauss SL, et al. The FLARE intraoperative near-infrared fluorescence imaging system: a first-in-human clinical trial in breast cancer sentinel lymph node mapping. Ann Surg Oncol 2009; 16:2943-2952.
44. Hirche C, Murawa D, Mohr Z, et al. ICG fluorescence-guided sentinel node biopsy for axillary nodal staging in breast cancer. Breast Cancer Res Treat 2010.
45. Kitai T, Inomoto T, Miwa M, et al. Fluorescence navigation with indocyanine green for detecting sentinel lymph nodes in breast cancer. Breast Cancer 2005; 12:211-215.
46. Bloom S, Morrow M. A clinical oncologic perspective on breast magnetic resonance imaging. Magn Reson.Imaging Clin.N.Am. 2010; 18:277-94, ix.
47. De Grand AM, Lomnes SJ, Lee DS, et al. Tissue-like phantoms for near-infrared fluorescence imaging system assessment and the training of surgeons. J.Biomed.Opt. 2006; 11:014007.

# Chapter 4

## Near-infrared fluorescence imaging of liver metastases in rats using indocyanine green

van der Vorst JR, Hutteman M, Mieog JSD, de Rooij KE, Kaijzel EL, Löwik CWGM, Putter H, Kuppen PJK, Frangioni JV, van de Velde CJ, Vahrmeijer AL

*J Surg Res; In press.*

# ABSTRACT

## Background

Near-infrared (NIR) fluorescence imaging using indocyanine green (ICG) is a promising technique to obtain real-time assessment of the extent and number of colorectal liver metastases during surgery. The current study aims to optimize dosage and timing of ICG administration.

## Materials and methods

Liver tumors were induced in 18 male WAG/Rij rats by subcapsular inoculation of CC531 rat colorectal cancer cells into three distinct liver lobes. Rats were divided in 2 groups: imaging after 24 and 48 hours or 72 and 96 hours after intravenous ICG administration. In each time group, rats were allocated to three dose groups: 0.04, 0.08, or 0.16 mg ICG. Intraoperative imaging and *ex vivo* measurements were performed using Mini-FLARE™ and confirmed by fluorescence microscopy. Fluorescence intensity was quantified using the Mini-FLARE software and the difference between tumor signal and liver signal (tumor-to-liver ratio; TLR) was calculated.

## Results

In all 18 rats, all colorectal liver metastases (N = 34), some as small as 1.2 mm, were identified using ICG and the Mini-FLARE™ imaging system. Average tumor-to-liver ratio (TLR) over all groups was 3.0 ± 1.2. TLR was significantly higher in the 72 h time group compared to other time points. ICG dose did not significantly influence TLR, but a trend was found favoring the 0.08 mg dose group. Fluorescence microscopy demonstrated a clear fluorescent rim around the tumor.

## Conclusions

This study demonstrates that colorectal cancer liver metastases can be clearly identified during surgery using ICG and the Mini-FLARE™ imaging system, with optimal timing of 72 h post-injection and an optimal dose of 0.08 mg (0.25 mg/kg) ICG. NIR fluorescence imaging has the potential to improve intraoperative detection of micrometastases and thus the completeness of resection.

## INTRODUCTION

With a worldwide annual incidence of approximately 1 million cases and an annual mortality of over 500.000 cases, colorectal cancer is the second cause of cancer death worldwide.[1] The survival of patients with colorectal carcinoma is mostly determined by the occurrence of distance metastases. Approximately 30% of patients with CRC eventually develop liver metastases.[2, 3] When metastases are confined to the liver and are resectable, surgical resection can offer a 5-year survival rate of 35-40%.[3, 4] Despite improved surgical techniques, preoperative imaging modalities and improved chemotherapy regimens, intrahepatic recurrence rates vary from 11-26%.[5-8] This is possibly due to an inadequate assessment of the extent of disease before and during liver surgery. Currently, the most frequently used imaging modalities to make this assessment are computed tomography (CT) and intraoperative ultrasonography (IOUS). However, even with the combined use of these modalities, 6-20 % of liver metastases can not be identified.[9-11] In particular, the detection of small (< 5 mm) liver metastases and superficially located liver metastases appears to be difficult.[11] New imaging modalities are necessary to facilitate a more complete assessment of the extent of disease.

Near-infrared (NIR) fluorescence imaging is a promising technique to intraoperatively assess the extent of colorectal liver metastases. Recently, Ishizawa and colleagues[12] have shown that primary hepatocellular carcinoma and colorectal liver metastases could be identified using NIR fluorescence imaging and the NIR fluorescent agent indocyanine green (ICG). Colorectal liver metastases could be identified by a fluorescent rim around the metastases. They hypothesized that this distinct fluorescent pattern is probably based on biliary excretion disorders in the surrounding normal liver tissue that is compressed by expanding pressure of the tumor. In their study of 49 patients, a fixed dose of 0.5 mg/kg ICG was administered preoperatively as part of a routine ICG clearance test, which is commonly used in Asia to plan the safe extent of hepatectomy. The interval between administration of ICG and surgery varied between 1 to 7 days. Consequently, the optimal dose of ICG and time of administration before surgery remain unclear.

The goal of our study was to determine the optimal ICG dose and administration time before surgery, using a syngeneic rat model of colorectal cancer metastases in conjunction with the Mini-FLARE™ image-guided surgery system.

# MATERIALS AND METHODS

## Animal model

The colorectal cancer rat CC531 cell line was used for this study. The cell line and the induction of liver metastases have been described previously.[13] In short, cells were cultured in RPMI 1640 supplemented with 2 mM L-glutamine (Gibco, Invitrogen Ltd, Carlsbad, USA), 10% heat-inactivated fetal calf serum, 100 U/ml penicillin and 0.1 mg/ml streptomycin sulphate. In order to induce liver metastases, CC531-syngeneic male WAG/Rij rats (Harlan, Horst, the Netherlands) weighing approximately 300-350 g underwent median laparotomy and the liver was mobilized and exposed. Subsequently, 125,000 CC531 cells (in 50 µl PBS) were subcapsularly inoculated into the left and right main liver lobes and the right accessory liver lobe.[13] Four weeks after inoculation, metastases ranging from 1.2 to 13.4 mm in size had originated in the liver.

The weight of the animals was followed throughout the experiment to monitor their general health state. Throughout tumor inoculation, injection of ICG and imaging, the animals were anesthetized with 5% isoflurane for induction and 2% isoflurane for maintenance in oxygen with a flow of 0.8 L/min. During anesthesia, the respiration rate was constantly monitored. For postoperative analgesia, the analgesic buprenorphine (0.1 mg / kg) was used. The Animal Welfare Committee of the Leiden University Medical Center approved the experiments. All animals were housed in the animal facility of the Leiden University Medical Center. Pellet food and fresh tap water were provided *ad libitum*.

## NIR fluorescent contrast agent

The clinically available NIR fluorescent contrast agent ICG (Pulsion Medical Systems, Munich, Germany) was used. Three ICG dose groups were tested: 0.04, 0.08 and 0.16 mg. Before injection, ICG powder was resuspended in 200 µL sterile water.

## Intraoperative NIR fluorescence imaging system

Imaging of liver metastases was performed using the Mini-FLARE™ imaging system (described in detail in Chapter 6), which is a miniaturized version of the FLARE™ imaging system.[14] Briefly, the system consists of two wavelength-isolated light sources: a "white" light source, generating 26,600 lx of 400-650 nm light and a "near infrared" light source, generating 7.7 mW/cm$^2$ of 760 nm light. Color video and NIR fluorescence images are simultaneously acquired and displayed in real-time using custom optics and software that separate the color video and NIR fluorescence images. A pseudo-colored (lime green) merged image of the color video and NIR fluorescence images is also displayed. The imaging head is attached to a flexible gooseneck arm, which

permits positioning of the imaging head virtually anywhere over the surgical field, and at extreme angles.

**Experimental design**

In a time-dependent and dose-dependent experiment, NIR fluorescence imaging was performed in 18 tumor-bearing rats. To minimize surgery-related trauma and distress, rats were divided in two groups: imaging after 24 and 48 hours, and imaging after 72 and 96 hours of ICG administration. In each time group, rats were allocated to three dose groups of 0.04, 0.08, or 0.16 mg ICG, which was administered intravenously in the penile vein. Each dose group contained 3 rats. ICG dose levels were chosen based on clinically relevant doses using human body weight and correspond to doses of 10, 20 and 40 mg of ICG. The imaging time-points were chosen based on Ishizawa et al.[12] who reported NIR fluorescence imaging is preferably performed at least 24 hours after ICG administration. Furthermore, for clinical translation, these time-points must be logistically acceptable to use in a clinical setting. For intraoperative imaging, the liver and other intra-abdominal organs were exposed after median laparotomy. After the first intraoperative imaging session (24 or 72 hours after ICG administration), the abdomen was closed in two layers and the animal was imaged again 24 hours later. At all time-points, tumor fluorescence and fluorescence of abdominal organs was measured.

**Data analysis**

NIR fluorescence data generated with the Mini-FLARE™ system were analyzed using the Mini-FLARE™ software package. Regions-of-interest were drawn on the outline of the tumor, liver, kidney, spleen, stomach, small bowel, colon and bladder as traced manually by visual interpretation on the white light image. Subsequently, fluorescence intensity was automatically calculated and exported to statistical analysis software.

**Fluorescence microscopy**

After intraoperative imaging experiments at 48 or 96 hours, the liver was excised completely for *ex vivo* fluorescence measurements. Subsequently, liver tumors were sliced in two to examine internal fluorescent patterns using the Mini-FLARE™ system. Excised tumor slices were snap-frozen on dry ice and stored at -80°C or were fixed in 10% buffered formalin overnight, washed in 70% ethanol and subsequently embedded in paraffin. Frozen tissue sections were measured for fluorescence using the Nuance multispectral imager (CRi, Woburn, USA) mounted on a Leica DM IRE2 inverted microscope (Leica, Wetzlar, Germany) and subsequently stained with hematoxylin and eosin. White light images where created using the same microscope and subsequently merged with fluorescence images.

### Statistical analysis

Statistical analysis and generation of graphs were performed using GraphPad Prism Software (version 5.01, La Jolla, USA) and SPSS (version 17.0). Fluorescence intensity and tumor size were reported as mean and standard deviation. To test differences between dose groups and time groups, repeated measures ANOVA was used with rat as random factor and dose, time, and dose by time interaction as fixed effects. When the dose by time interaction was not significant, it was subsequently removed from the model. Comparisons between doses and between time points were performed using least square difference (LSD) adjustment for multiple testing. Statistical tests were two-tailed and $p < 0.05$ was considered significant.

## RESULTS

### Intraoperative detection of colorectal liver metastases

In 18 rats, syngeneic colorectal liver metastases were induced using the colorectal cancer rat cell line CC531. The mean number of metastases per rat was 1.8 ± 0.8 (range 1 – 3). The mean size of the liver metastases was 5.2 ± 0.3 mm (range 1.2 – 13.4 mm). In all 18 rats, all colorectal liver metastases (N = 34) were identified using ICG and the Mini-FLARE™ imaging system (Fig. 1).

### Dose of ICG and time of intraoperative imaging

To determine the influence of ICG dosage and time of imaging, rats were allocated to three dose groups and imaged at four time points and tumor-to-liver ratios (TLRs) were calculated. At all time-points (24, 48, 72 and 96 hours) and in all dose groups (0.04, 0.08 and 0.16 mg), fluorescence intensity of liver metastases was significantly higher than the fluorescent intensity of normal liver tissue ($P < 0.001$). Average TLR over all groups was 3.0 ± 1.2. The highest average TLR (4.3 ± 1.8) was reached in the 0.08 mg dose group and 72 h after intravenous administration (Fig. 2C).

Repeated measures ANOVA was used to test for differences in TLR between dose and time groups. There was a significant effect of time ($P < 0.001$), but the effects of dose ($P = 0.12$) and dose by time interaction ($P = 0.91$) were not significant. Dose by time interaction was therefore removed from the model. Consequently, the model included rat as random factor and dose and time as fixed effects. This model showed that the TLR was significantly higher in the 72 h time group compared to the 24 h ($P < 0.001$), 48 h ($P = 0.001$) and 96 h ($P = 0.004$) time groups (Fig. 2D). Also, the TLR was significantly higher in the 96 h time group compared to the 24 h group ($P = 0.049$).

ICG dose did not significantly influence TLRs, but a trend was found favoring the 0.08 mg dose group (0.08 vs. 0.04, P = 0.06; 0.08 vs. 0.16, P = 0.09).

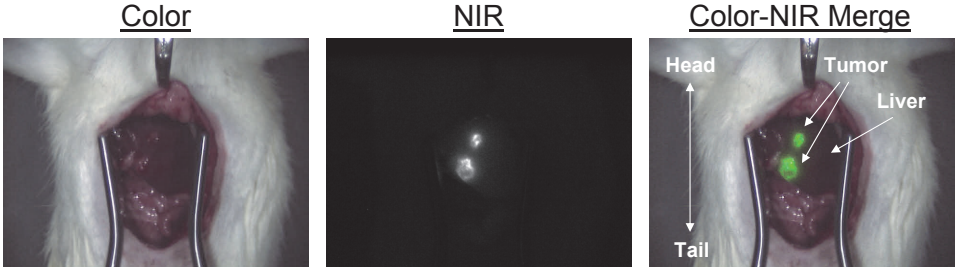


**Figure 1. Intraoperative detection of colorectal liver metastases using NIR fluorescence:** Shown are a color image (left), a NIR fluorescence image (middle) and a pseudo-colored green merge (right) of two CC531 colorectal liver metastases intraoperatively detected using NIR fluorescence in a male rat 72 h after injection of 0.08 mg indocyanine green.

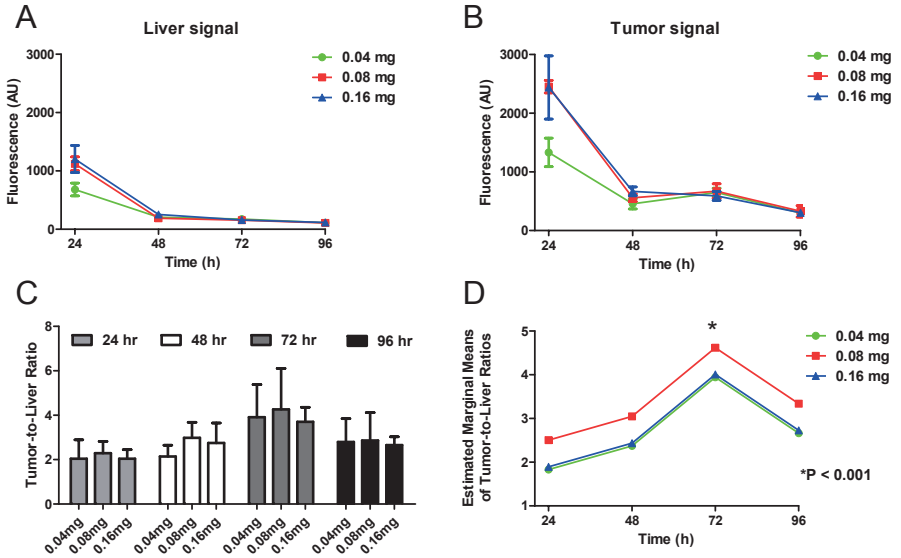


**Figure 2 - Dose of ICG and timing of intraoperative imaging: A.** Fluorescent intensity of the liver in 18 rats injected with 0.04, 0.08 or 0.16 after 24, 48, 72 and 96 h. **B.** Fluorescent intensity of all liver tumors (N = 34) in 18 rats injected with 0.04, 0.08 or 0.16 mg ICG after 24, 48, 72 and 96 h. **C.** Average tumor-to-liver ratios and standard deviations are plotted for all liver metastases (N = 34) in 18 rats injected with 0.04, 0.08 or 0.16 mg ICG after 24, 48, 72 and 96 h. **D.** Estimated marginal means of tumor-to-liver ratio for rats injected with 0.04, 0.08 or 0.16 mg ICG after 24, 48, 72 and 96 h using the repeated measures ANOVA and least square difference (LSD) adjustment for multiple testing. This model showed that the tumor-to-liver ratio was significantly higher in the 72 h time group compared to the 24 h (P < 0.001), 48 h (P = 0.001) and 96 h (P = 0.004) time groups. ICG dose did not significantly influence tumor-to-liver ratios, but a trend was found favoring the 0.08 mg dose group (0.08 vs. 0.04, P = 0.06; 0.08 vs. 0.16, P = 0.09).

### Biodistribution of indocyanine green

Fluorescent intensity of the metastases, liver, kidney, stomach, spleen, small bowel, colon and bladder was measured at all time points and in all dose groups (data not shown).

Repeated measures ANOVA was used to test for differences in fluorescent intensity of the liver (Fig. 2A) and liver metastases (Fig. 2B) between dose and time groups. Dose by time interaction did not significantly effect liver signal ($P = 0.1$) and metastases signal ($P = 0.125$) and was therefore removed from the model. There was a significant effect of time on both liver signal ($P < 0.001$) and liver metastases signal ($P < 0.001$). No significant effect of dose was found on liver signal ($P = 0.061$) and metastases signal ($P = 0.152$). This model showed that liver signal and metastases signal were both significantly higher in the 24 h group compared to all other time-points ($P < 0.001$).

NIR fluorescence intensity of all organs except for the stomach, colon and the small bowel, was lower or equal to the liver signal. Fluorescence intensity of the stomach, colon and small bowel was significantly higher compared to other organs and had a maximum at 48 and 72 hours.

### Microscopic distribution of ICG in liver metastases

To determine the precise location of ICG in the vicinity of the tumor, sliced liver metastases were examined for internal fluorescent patterns using the Mini-FLARE™ system. In all liver metastases a clear fluorescent rim around the tumor was found. Frozen tissue sections were examined using the Nuance multispectral imager (CRi, Woburn, MA) mounted on a Leica DM IRE2 inverted microscope (Leica, Wetzlar, Germany). A clear fluorescent rim was found in stromal tissue in the transition area between tumor and normal liver tissue in all liver metastases. In this area, multiple cell types that are involved in tissue inflammation (e.g. granulocytes, lymphocytes) were found (Fig 3).

## DISCUSSION

In the present study, significant differences in TLR were shown between four different time points after ICG administration, with an optimal time of imaging of 72 h after ICG administration. No significant effects were found with regard to dose level; however, a trend was shown favoring 0.08 mg. Moreover, all liver metastases, even as small as 1.2 mm, could be clearly identified during liver surgery using clinically available ICG and the Mini-FLARE™ system in this syngeneic rat model.

Highest TLRs were reached 72 h after ICG administration. Fluorescence intensity of the liver and the liver metastases were also examined separately. Fluorescent

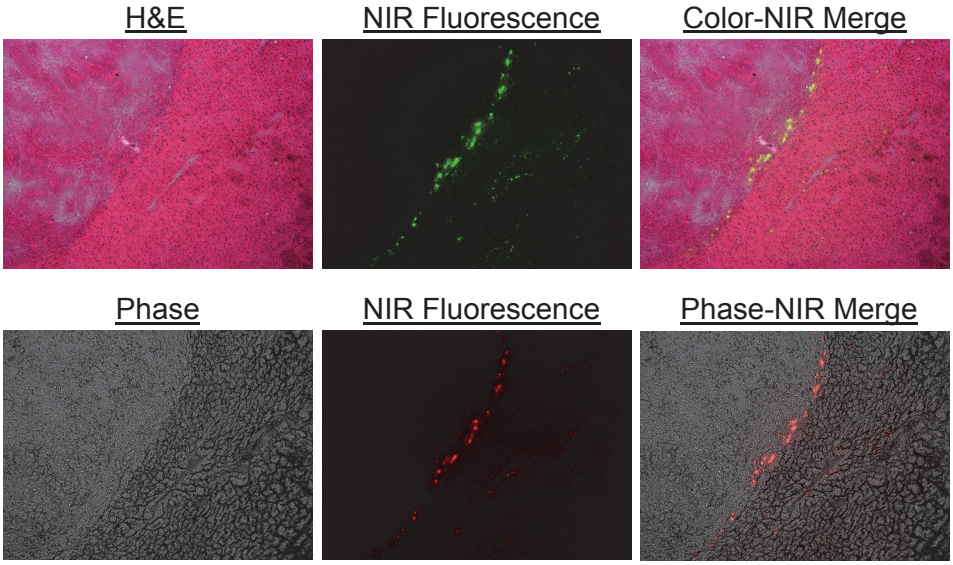


**Figure 3 – Fluorescent microscopy of a colorectal liver metastasis:** Shown are a hematoxylin and eosin staining (top left), a pseudo-colored green NIR fluorescence image (top middle) and pseudo-colored green merge (top right) of a 20 µm frozen tissue section of a colorectal liver metastasis. Furthermore, a phase image (bottom left), a pseudo-colored red NIR fluorescence image (bottom middle) and a pseudo-colored red merge (bottom right) of a 20 µm frozen tissue section of a colorectal liver metastasis is shown. The fluorescent rim in stromal tissue in the transition area between tumor and normal liver tissue can be clearly identified.

intensity of the liver decreased strongly after 24 h and was not dose dependent. Fluorescent intensity of the liver metastases also decreased strongly at 48 h, but a small, non-significant peak was found at 72 h. This small peak can be explained by the re-uptake of ICG in the small bowel as part of the enterohepatic circulation and subsequent passage through the bowel tract, hence the highest TLR at 72 h.

Regarding ICG dosage, a trend was found favoring the 0.08 mg ICG group. Extrapolating to human body weight, this dose corresponds to a dose of 20 mg ICG, which is frequently used in a clinical setting. To optimize this technique in clinical practice, a dose-finding study is imperative. As ICG is already clinically available and FDA-approved, a straightforward translation of our results to the clinic can be made.

It is known that a substantial part of liver metastases, mainly the small (< 5 mm) and superficially located, can not be identified using conventional imaging modalities such as CT or IOUS. Size of metastases in the present study varied from 1.2 to 13.4 mm of which 50 % were smaller than 5 mm. This emphasizes that ICG fluorescence in liver surgery might be of great value in detecting small colorectal liver metastases. As the currently used preclinical animal model only generated colorectal liver metastases, future clinical studies will have to determine the ability of this technique to discriminate between malignant and benign lesions of the liver.

Since maximum penetration depth of NIR fluorescence is currently up to 1 cm, identification of non-superficially situated liver metastases will be more challenging.

Therefore, intraoperative ICG fluorescence must be regarded as a complement on currently used conventional imaging modalities as IOUS and CT. Improvements in imaging systems, NIR fluorescence contrast agents and software and reduction in background fluorescence may facilitate NIR fluorescence imaging of deeper located metastases.

The currently used technique to detect liver metastases using NIR fluorescence and ICG is based on the clearance capacity of the liver. It has been described that in patients with a cirrhotic liver, or in patients pretreated with chemotherapy, the liver function and clearing capacity can be reduced. A reduced liver function could also affect the clearance of ICG, which can result in a higher background signal and therefore lower contrast. However, it has been shown that even cirrhotic livers have an extensive clearance capacity.[15] This implies that the currently used technique can probably be used in subjects with a reduced liver function. Though, in these patients, the optimal time interval between ICG administration and imaging could be longer. Future clinical studies have to elaborate on this topic.

A recent development in liver surgery is the introduction of laparoscopic surgery. NIR fluorescence can be of great value, also in laparoscopic surgery, since palpation of the liver is not possible and the surgeon can only rely on visual inspection and preoperative imaging. To anticipate on this potential new application, laparoscopic NIR fluorescence camera systems are presently being developed and tested.[16, 17]

In summary, this study demonstrates clear identification of colorectal liver metastases during surgery using the clinically available NIR fluorescent agent ICG and the Mini-FLARE™ system. Imaging 72 h after administration of 0.08 mg ICG provided the highest TLRs. In particular, the ability to detect small (< 5 mm) and superficially located metastases can be of great value during liver surgery. When the current intraoperative identification of colorectal liver metastases can be improved using this technique, the resection can potentially be performed more accurately and preoperatively missed metastases can be involved in surgical decision making.

## ACKNOWLEDGEMENTS

This study was performed within the framework of CTMM, the Center for Translational Molecular Medicine (DeCoDe project, grant 03O-101). This study was supported by the Sacha Swarttouw-Hijmans Foundation .

# REFERENCES


1. Parkin DM, Bray F, Ferlay J, et al. Global cancer statistics, 2002. CA Cancer J.Clin. 2005; 55:74-108.
2. Manfredi S, Lepage C, Hatem C, et al. Epidemiology and management of liver metastases from colorectal cancer. Ann Surg 2006; 244:254-259.
3. Ruers T, Bleichrodt RP. Treatment of liver metastases, an update on the possibilities and results. Eur J Cancer 2002; 38:1023-1033.
4. Simmonds PC, Primrose JN, Colquitt JL, et al. Surgical resection of hepatic metastases from colorectal cancer: a systematic review of published studies. Br J Cancer 2006; 94:982-999.
5. Wei AC, Greig PD, Grant D, et al. Survival after hepatic resection for colorectal metastases: a 10-year experience. Ann Surg Oncol 2006; 13:668-676.
6. Pawlik TM, Scoggins CR, Zorzi D, et al. Effect of surgical margin status on survival and site of recurrence after hepatic resection for colorectal metastases. Ann Surg 2005; 241:715-22, discussion.
7. Abdalla EK, Vauthey JN, Ellis LM, et al. Recurrence and outcomes following hepatic resection, radiofrequency ablation, and combined resection/ablation for colorectal liver metastases. Ann Surg 2004; 239:818-825.
8. Karanjia ND, Lordan JT, Fawcett WJ, et al. Survival and recurrence after neo-adjuvant chemotherapy and liver resection for colorectal metastases: a ten year study. Eur J Surg Oncol 2009; 35:838-843.
9. Leen E, Ceccotti P, Moug SJ, et al. Potential value of contrast-enhanced intraoperative ultrasonography during partial hepatectomy for metastases: an essential investigation before resection? Ann Surg 2006; 243:236-240.
10. Sahani DV, Kalva SP, Tanabe KK, et al. Intraoperative US in patients undergoing surgery for liver neoplasms: comparison with MR imaging. Radiology 2004; 232:810-814.
11. Nomura K, Kadoya M, Ueda K, et al. Detection of hepatic metastases from colorectal carcinoma: comparison of histopathologic features of anatomically resected liver with results of preoperative imaging. J Clin Gastroenterol 2007; 41:789-795.
12. Ishizawa T, Fukushima N, Shibahara J, et al. Real-time identification of liver cancers by using indocyanine green fluorescent imaging. Cancer 2009; 115:2491-2504.
13. Vahrmeijer AL, van Dierendonck JH, Schutrups J, et al. Potentiation of the cytostatic effect of melphalan on colorectal cancer hepatic metastases by infusion of buthionine sulfoximine (BSO) in the rat: enhanced tumor glutathione depletion by infusion of BSO in the hepatic artery. Cancer Chemother Pharmacol 1999; 44:111-116.
14. Troyan SL, Kianzad V, Gibbs-Strauss SL, et al. The FLARE intraoperative near-infrared fluorescence imaging system: a first-in-human clinical trial in breast cancer sentinel lymph node mapping. Ann Surg Oncol 2009; 16:2943-2952.
15. Bloemen JG, Olde Damink SW, Venema K, et al. Short chain fatty acids exchange: Is the cirrhotic, dysfunctional liver still able to clear them? Clin Nutr 2010; 29:365-369.
16. Matsui A, Tanaka E, Choi HS, et al. Real-time intra-operative near-infrared fluorescence identification of the extrahepatic bile ducts using clinically available contrast agents. Surgery 2010; 148:87-95.
17. van der Pas MH, van Dongen GA, Cailler F, et al. Sentinel node procedure of the sigmoid using indocyanine green: feasibility study in a goat model. Surg Endosc 2010; 24:2182-2187.

# Part II

## Clinical translation

# Chapter 5

# Clinical translation of ex vivo sentinel lymph node mapping for colorectal cancer using invisible near-infrared fluorescence light

Hutteman M, Choi HS, Mieog JSD, van der Vorst JR, Ashitate Y, Kuppen PJK, van Groningen MC, Löwik CWGM, Smit VTHBM, van de Velde CJ, Frangioni JV, Vahrmeijer AL

*Ann Surg Oncol 2011; 18:1006-14.*

## ABSTRACT

### Background

Sentinel lymph node (SLN) mapping in colorectal cancer may have prognostic and therapeutic significance, however, currently available techniques are not optimal. We hypothesized that the combination of invisible near-infrared (NIR) fluorescent light and *ex vivo* injection could solve remaining problems of SLN mapping in colorectal cancer.

### Methods

The FLARE™ imaging system was used for real-time identification of SLNs after injection of the NIR lymphatic tracer HSA800 in the colon and rectum of (n = 4) pigs. A total of 32 SLN mappings were performed *in vivo* and *ex vivo* after oncologic resection using an identical injection technique. Guided by these results, SLN mappings were performed in *ex vivo* tissue specimens of 24 consecutive colorectal cancer patients undergoing resection.

### Results

Lymph flow could be followed in real-time from the injection site to the SLN using NIR fluorescence. In pigs, the SLN was identified in 32/32 (100%) of SLN mappings under both *in vivo* and *ex vivo* conditions. Clinically, SLNs were identified in all patients (n = 24) using the *ex vivo* strategy within 5 minutes after injection of fluorescent tracer. Nine patients showed lymph node involvement (N1-disease). In one patient, a 3 mm mesenteric metastasis was found adjacent to a tumor-negative SLN.

### Conclusions

The current pilot study shows proof of principle that *ex vivo* NIR fluorescence-guided SLN mapping can provide high-sensitivity, rapid, and accurate identification of SLNs in colon and rectum. This creates an experimental platform to test optimized, non-FDA-approved NIR fluorescent lymphatic tracers in a clinical setting.

## INTRODUCTION

The prognosis and quality of life for patients suffering from colorectal cancer (CRC) depends on the extent and quality of surgical treatment. Apart from tumor characteristics (i.e. stage, differentiation grade), complete surgical removal with en bloc regional lymphadenectomy is pivotal for patient prognosis. Metastatic spread to regional lymph nodes is one of the most important prognostic factors and determines the need for adjuvant chemotherapy. The sentinel lymph node (SLN) is the first lymph node that receives lymphatic drainage from a tumor, and identification of the SLN and analysis for tumor involvement should predict the status of the remaining lymph nodes. The SLN procedure is regarded standard of care in the treatment of breast cancer[1, 2] and melanoma.[3] However, its added value in colorectal cancer has not yet been established.

Retrospective studies on micrometastatic disease in CRC and the risk of recurrence are conflicting.[4-6] Our group has previously shown that ultra-staging of lymph nodes with RT-PCR identifies a subgroup of pN0 patients with an inferior prognosis.[7] However, this methodology is labor intensive and not used routinely. Identifying the SLN in the surgical specimen provides the pathologist with an opportunity to optimally stage the lymphatic basin beyond standard H&E analysis of the regional nodes.[8] Published results on identifying SLN in CRC show variable success rates ranging from 58 to 100 percent.[9-17] Consequently, there is ample room for improvement of mapping methodology.

In the majority of published studies of CRC patients, subserosal, circumferential, and peri-tumoral injection of the visible dye isosulfan blue has been used, both *in vivo* and *ex vivo*.[11, 12, 14, 18] Isosulfan blue is distributed rapidly through the afferent lymphatic channels, however, due to its small size, the dye particles can readily diffuse through the true SLN to second and third tier nodes (a total of up to 21 "sentinel" nodes are reported). [15] Isosulfan blue also stains tissue in an unnatural color and provides poor overall contrast.

Dyes that emit fluorescence in the invisible, near-infrared (NIR) portion of the electromagnetic spectrum (700 to 900 nm) have several advantages for SLN mapping. NIR light penetrates relatively deep into living tissue, and tissue itself has low autofluorescence in the NIR, resulting in a high signal-to-background ratio.[19] Since NIR light is not visible to the human eye, there is no change to the look of the surgical field. Several clinical studies have been published on SLN mapping in breast cancer, gastric cancer and colon cancer, using the clinically available NIR probe indocyanine green.[20-24] However, these studies were performed using imaging systems that display the NIR signal without the visible image as a surgical anatomical reference. Our group has developed a system (FLARE™) that is capable of displaying NIR signal and visible image (captured by a color video camera) simultaneously and can superimpose the NIR signal over the color image.[25, 26]

Previously, our group reported the use of NIR light for real-time intraoperative SLN mapping of the gastrointestinal tract.[27, 28] These and earlier studies show clear advantages of NIR imaging over the conventional blue dyes.[29] Of published organic molecules, the NIR fluorophore HSA800 emerged as the molecule with the best overall performance with respect to entry to the lymphatics, flow to the SLN, retention in the SLN, fluorescence yield, and reproducibility. Since HSA800 cannot be translated to the clinic without a long and costly regulatory process, we hypothesized that *ex vivo* SLN mapping in colon and rectal cancer could provide all of the benefits of NIR fluorescence imaging over visible blue dyes, without the need for regulatory approval, and without risk to the patient.

## MATERIALS AND METHODS

### Lymphatic tracers

The preparation of HSA800 (IRDye 800CW conjugated to human serum albumin) has been described in detail previously.[27] The ratio of fluorophore (IRDye 800CW; LI-COR, Lincoln, USA) to albumin (HSA) was 3:1, estimated using the extinction coefficients of HSA ($\varepsilon_{280nm}$ = 32,900 $M^{-1}cm^{-1}$) and CW800 ($\varepsilon_{778nm}$ = 240,000 $M^{-1}cm^{-1}$) in PBS. Peak absorbance and emission of HSA800 were 778 nm and 795 nm, respectively. A stock solution of 10 μM (in pig) or 50 μM (in human) HSA800 in phosphate-buffered saline (PBS), pH 7.4 was used for all injections.

### Real-time NIR fluorescence imaging

Preclinical SLN mapping was performed using the FLARE™ image-guided surgery system as described in detail previously.[26] The system is shown schematically in Figure 1. It consists of two wavelength isolated light sources: a "white" light source, generating 40,000 lx of 400-650 nm light and a "near infrared" light source, generating 12.5 $mW/cm^2$ 760 nm light over a 15 cm field of view. Color video and NIR fluorescence images are simultaneously acquired and displayed in real-time using custom optics and software that separate the color video and NIR fluorescence images.[26] A pseudo-colored (lime green) merged image of the color video and NIR fluorescence images is also displayed. Clinical SLN mapping was performed using a miniaturized version of FLARE™ (Mini-FLARE™), which is described in detail in Chapter 6, with settings of 20,000 lx of 400-650 nm "white" light and 7 $mW/cm^2$ of 760 nm NIR light.

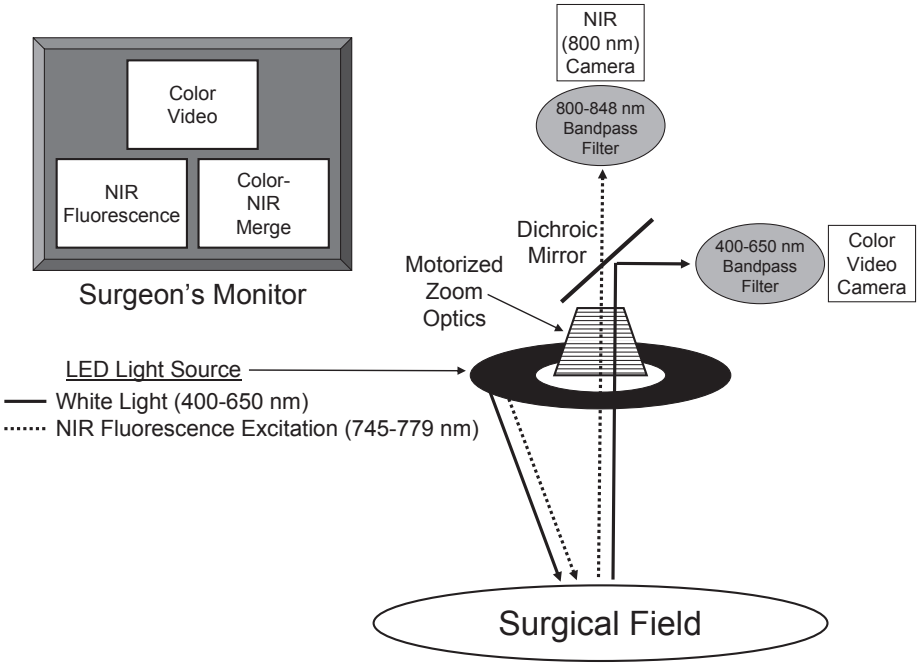


**Figure 1. Schematic of the FLARE™ Image-Guided Surgery System:** The dichroic mirror directs light below and above 650 nm to a color video camera and NIR fluorescence camera, respectively, permitting simultaneous acquisition of color video and NIR fluorescence images. The surgeon's monitor includes a pseudo-colored (lime green) merge of the two images.

## Animal model systems

Animals were housed in an AAALAC-certified facility staffed by full-time veterinarians and were studied under the supervision of an approved institutional protocol. This protocol adhered to the "Guide for the Care and Use of Laboratory Animals", NRC 1996. 4 female Yorkshire pigs were purchased at 35 kg from E.M. Parsons and Sons (Hadley, USA). All animals acclimated to the animal facility for at least 48 hr prior to experimentation. Anesthesia was induced with 4.4 mg/kg intramuscular Telazol (Fort Dodge Labs, Fort Dodge, USA). The animal was then intubated and anesthesia was maintained with 2% isoflurane (Baxter Healthcare Corporation, Deerfield, USA). ECG, heart rate, oxygen saturation and body temperature were monitored throughout the experiment. At the end of each experiment, euthanasia was induced by rapid intravenous injection of 10 mL of Fatal-Plus (Vortech Pharmaceuticals, Dearborn, USA), a method consistent with the recommendation of the Panel on Euthanasia of the American Veterinary Medical Association.

**Preclinical sentinel lymph node mapping *in vivo* vs. *ex vivo***

SLN mapping was performed using a 1 cc syringe equipped with a 27-gauge, ½" needle. Each injection consisted of 0.1 cc of HSA800 solution injected subserosally, with the needle bevel facing upwards. The injection site was then gently massaged to stimulate lymphatic flow through increased hydrostatic pressure.

All animals received multiple injections at separate locations in the colon and rectum. For each condition (*in vivo* and *ex vivo*) 8 injections were performed in colon and 8 injections were performed in the rectum, for a total of 32 injections. The NIR fluorescence signal was monitored using the FLARE™ system and the SLN identified by watching uninterrupted lymphatic flow reach the first lymph node in real-time. After successful identification, the suspected lymph node was resected under fluorescence guidance, fixed in 2% paraformaldehyde for 12 hours, frozen in $LN_2$ using Tissue-Tek OCT, cryo-sectioned at 10 μm, and analyzed by hematoxylin and eosin (H&E) staining.

After the *in vivo* injections, a subtotal colectomy and a total mesorectal excision (TME) were performed. The resected bowel specimens were placed on a table and at locations that were not injected *in vivo*, 0.1 cc of HSA800 was injected subserosally, identical to the technique used for *in vivo* injections. Tissue samples were also collected and processed for histology as described above.

Time needed to identify the SLN was compared between *in vivo* and *ex vivo* conditions using an unpaired t-test. Assumption of equal variances was confirmed by Levene's test. Statistical analyses, performed using SPSS software version 17.0 (SPSS Inc., Chicago, USA), were two-tailed and $p < 0.05$ was considered significant.

**Translation to the clinic**

Twenty-four consecutive patients undergoing curative intended surgery for colorectal cancer were included. This study was approved by the Leiden University Medical Center Medical Ethics Committee and performed in accordance with the ethical standards of the Helsinki Declaration of 1975. All patients underwent a standard oncological resection including lymphadenectomy. In case of colon cancer, a segmental colonic resection was performed; in case of rectal cancer, a resection following the principles of the total mesorectal excision (TME) was performed. Directly following resection, bowel segments were delivered fresh to the department of pathology, where the specimen was opened anti-mesenterically by the pathologist. In rectal cancer, surgical quality audit protocol prohibits altering the perirectal fat in any way. Consequently, in rectal cancer, the specimen was opened no further than the rectosigmoid junction. 1 cc of 50 μM HSA800 was injected submucosally circumferentially with a 5 mm margin around the tumor and the injection site was massaged for 5 minutes. After 5 minutes, the specimen was inspected using Mini-FLARE™. Any fluorescent

hotspots were either marked with a suture or directly resected for separate fixation in 2% buffered formalin. The specimen was fixed using 2% buffered formalin for 24 h (colon) or 48 h (rectum). After fixation, fluorescent nodes were identified under direct NIR fluorescence guidance with the Mini-FLARE™ and the specimen was processed following the standard clinical protocol. For rectal cancer, the specimen was processed using the slicing technique as described by Quirke.[30] All lymph nodes (sentinel and non-sentinel) were paraffin embedded and 4 μm sections were H&E stained and subsequently analyzed by microscope for the presence of tumor cells.

## RESULTS

### Preclinical NIR fluorescence-guided SLN identification and resection

In both *in vivo* and *ex vivo* conditions, all injections led to a successful identification of a SLN (Table 1). Shortly after massaging the injection site, lymphatic flow was visualized on the NIR fluorescence image (Figure 2). In all cases, lymphatic flow terminated, without interruption, in one or more lymph nodes.

In colon, we found no difference (Table 1) in the time needed to identify the SLN between *in vivo* (56.4 sec on average) and *ex vivo* (58.8 sec on average) conditions ($t = -0.111$, $p = 0.913$). In the rectum, however, *ex vivo* injection lead to a significantly faster identification time for the SLN (26.8 sec on average) compared to *in vivo* (54.1 sec; $t = 2.942$, $p = 0.011$). Mean time between resection of the bowel and *ex vivo* injection was 25 min (range 10 to 57 min). All resected specimens (n = 32) were analyzed by H&E histology and confirmed to be lymph node tissue (Figure 2B).

**Table 1.** Preclinical In Vivo and Ex Vivo Identification Rates for SLN Mapping of Pig Colon and Rectum with HSA800

| Organ | Number of Injections (n) | Successful Identifications (n, %) | Number of SLNs Identified (n) | Average Identification Time (sec) |
|---|---|---|---|---|
| *Colon* | | | | |
| In vivo | 8 | 8 (100%) | 9 | 56.4 ± 48.3 |
| Ex vivo | 8 | 8 (100%) | 8 | 58.8 ± 36.2 |
| Rectum | | | | |
| In vivo | 8 | 8 (100%) | 10 | 54.1 ± 16.3 |
| Ex vivo | 8 | 8 (100%) | 9 | 26.8 ± 21.3 |

### Clinical *ex vivo* NIR fluorescence-guided SLN mapping in colorectal cancer patients

Patient and tumor characteristics are listed in Table 2.

In a preliminary set of experiments on n = 6 clinical specimens, it was found that the subserosal injection technique that worked so well with normal pig specimens

did not provide reliable results with human tumor specimens (data not shown). Injecting subserosally and circumferentially around human tumors resulted in a larger injection site, which outshined lymph nodes close to the tumor. To overcome this problem, a submucosal injection technique was used.[15, 31] It was also found that due to the thickness of human specimens versus normal pig specimens, a high concentration (50 μM) of HSA800 was optimal.

Using this optimized strategy, in all 24 consecutive patients, the procedure led to a successful detection of SLNs. An example of the NIR fluorescence images of the procedure in colon cancer is shown in Figure 3A. In rectal cancer, quality control dictates that the specimen is not altered prior to inking, fixation and slicing. As shown in Figure 3B, in rectal cancer, nodes were harvested successfully after mesorectal slicing. Based on pre- and post-fixation images, the formalin fixation process did not appear to alter NIR fluorescence of HSA800. On average, per specimen, 3.0 (range 1 – 5) SLNs were identified by NIR fluorescence (Table 2). On average, a total of 15.9 (range 8 – 31) lymph nodes were harvested per specimen. Histological analysis showed that 9 of 24 patients had lymph node metastases. In all but one of those cases, at least one of the SLNs contained tumor cells. In one patient, however, a small tumor deposit (3 mm) was found in the mesentery whereas the SLN was tumor-negative. Although no clear lymphatic tissue could be identified (Figure 4), pathological guidelines (WHO-classification sixth edition) require that this lesion be classified as a lymph node metastasis.

## DISCUSSION

The presence of lymph node metastases in CRC patients is the most important prognostic factor and an indication for adjuvant chemotherapy. The presence of nodal involvement decreases 5-year survival rates by 25 to 35%. Long-term follow-up of adjuvant chemotherapy for patients with stage III colon cancer showed a survival benefit with a 22 to 33% relative reduction in mortality.[32, 33] Therefore, adequate staging in order to select patients who may benefit from adjuvant chemotherapy treatment is a necessity. Moreover, patients without nodal disease (stage I/II) still develop recurrent tumors in up to 25% of the cases within 5 years after surgical resection of the primary tumor. This could be due to pathological understaging of the tissue specimen at the time of primary treatment. SLN mapping would be a useful method to circumvent this problem.[11]

Contradicting studies have also been published, showing a high false negative rate of SLN mapping in colon cancer.[34, 35] These so called skip metastases, a tumor negative SLN combined with a positive non-SLN, are an important limiting factor to the validity of the SLN procedure. In colorectal cancer, skip metastases rates of 3% - 60% are reported.[11, 36] It has been suggested that these variable rates are caused by the

applied SLN identification technique, which could be overcome by a more reliable method of identifying the SLN.

The current study shows proof of principle that by using invisible NIR fluorescent light and an optimal contrast agent, identification of the lymphatic channels and the

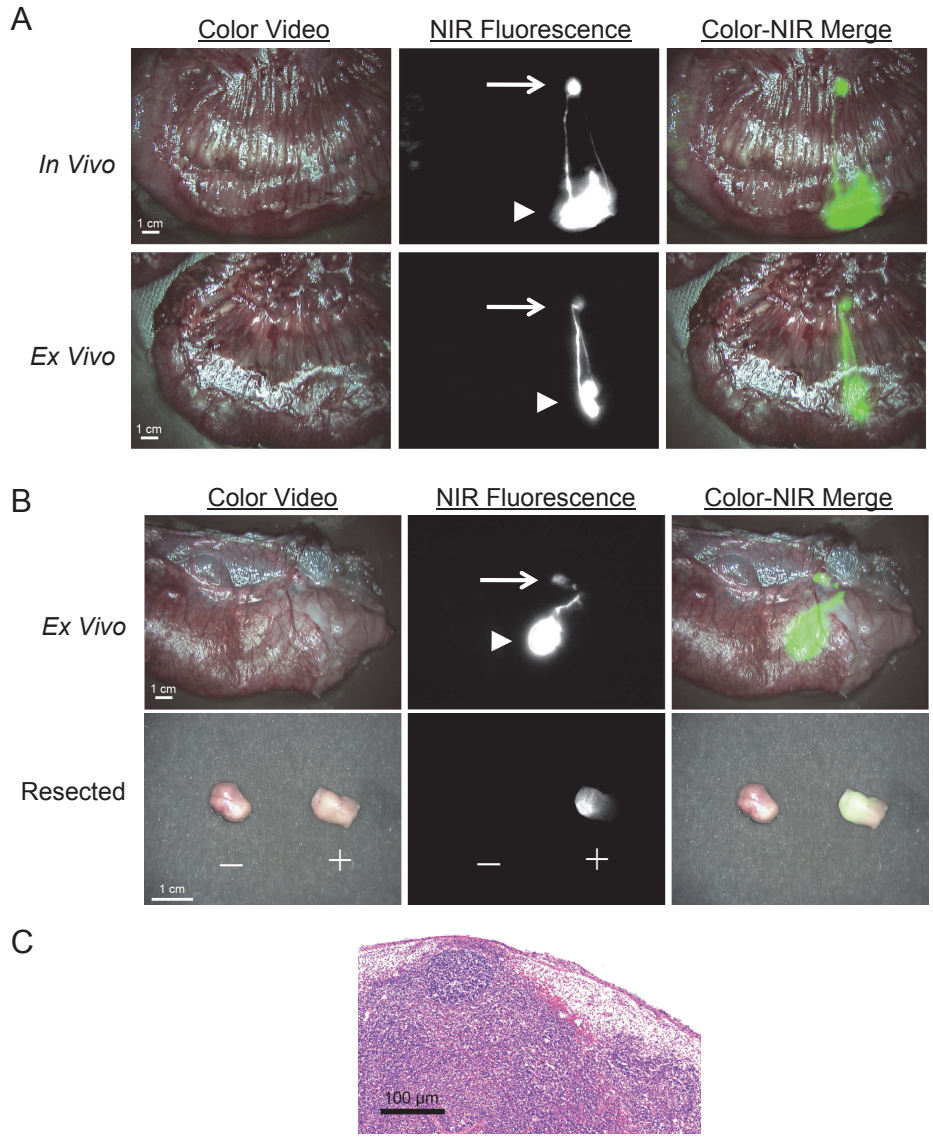


**Figure 2. In Vivo and Ex Vivo SLN Mapping in Colon and Rectum: A.** Identification of the SLN (arrows) in pig colon after in vivo (top row) or ex vivo (bottom row) injection (arrowheads) of 0.1 cc of 10 mM HSA800. Shown are the color video (left), NIR fluorescence (middle), and pseudo-colored (lime green) merge of the two (right). **B.** Ex vivo identification of the SLN (arrow) after injection (arrowhead) of 0.1 cc of 10 mM HSA800 (top row). Resected negative (-) and positive (+) nodes in rectum (bottom row). Shown are the color video (left), NIR fluorescence (middle), and pseudo-colored (lime green) merge of the two (right). Note accumulation of the dye at the sinus entry site. **C.** H&E histological staining of the (+) tissue section (100X magnification) from Figure 3A.

SLN is rapid and accurate. In the presented preclinical experiments in pigs, both *ex vivo* NIR fluorescence imaging of the SLN as well as *in vivo* imaging showed similar results. These preclinical results were successfully translated into a pilot clinical study in which the SLN was identified *ex vivo* in all patients. Whereas the NIR fluorescent signal of subserosal injections outshined lymph nodes located close to the tumor, submucosal injections showed superior results in patient specimens.

In one patient with three tumor-negative SLNs, a small tumor metastasis was found in the mesenteric fat, without any remnants of pre-existent lymphatic tissue (Figure 4). According to the WHO-classification, sixth edition, such tumor deposits are regarded as lymph node involvement. This is supported by the configuration of the lesion, being encapsulated and round. Since the lesion was completely effaced by tumor cells and lymphatic tissue was not observable, it is plausible that no lymphatic drainage could reach this node and in fact the NIR lymphatic tracer had bypassed this

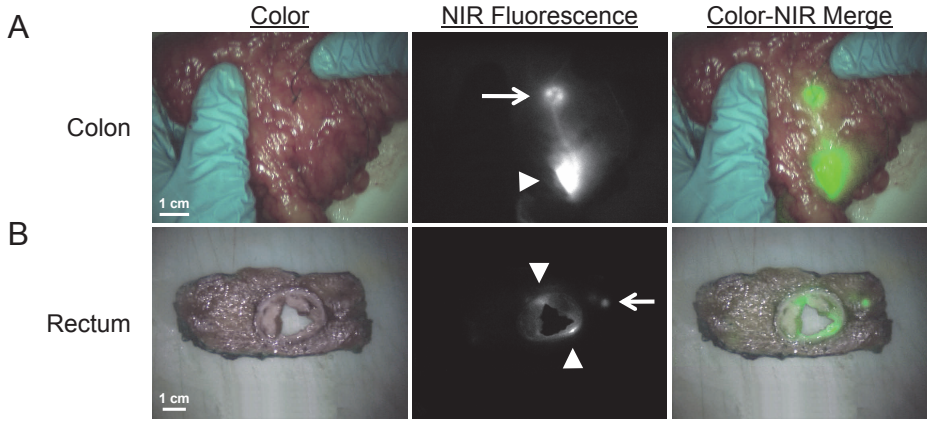


**Figure 3. NIR Fluorescence-Guided SLN Mapping in Patients with Colorectal Cancer: A.** Ex vivo identification of a SLN (arrow) in the mesentery of the right hemicolon of a patient with a cecal adenocarcinoma after submucosal peritumoral injection (arrowhead) of 1 cc of 50 mM HSA800. Shown are the color video (left), NIR fluorescence (middle), and pseudo-colored (lime green) merge of the two (right). **B.** Ex vivo identification of a SLN (arrow) in the mesorectum of a patient with a rectal adenocarcinoma after submucosal peritumoral injection (arrowhead) of 1 cc of 50 mM HSA800. After 48 hours fixation in 2% buffered formalin, tissue specimen was sliced and imaged. Shown are the color video (left), NIR fluorescence (middle), and pseudo-colored (lime green) merge of the two (right).

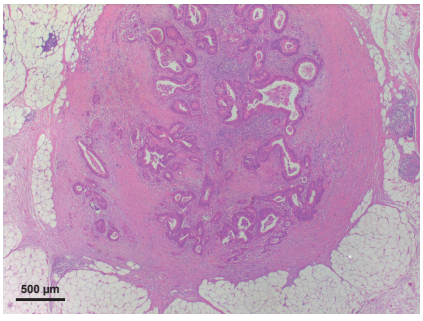


**Figure 4. Palpable Metastatic Lesion Identified in the Mesenteric Fat:** H&E histological staining of a mesenteric metastasis (25X magnification) not identified as a SLN. No nodal tissue was observed.

**Table 2.** Patient Characteristics and Results of Sentinel Lymph Node Mapping

| Patient | Age (yr) | Body Mass Index | Tumor Location | Tumor Differentiation | Tumor Size (cm) | Tumor Stage | NIR-Identified SLNs | Tumor Positive SLNs | Total LN | Total LN+ | False Negative |
|---|---|---|---|---|---|---|---|---|---|---|---|
| 1 | 80 | 24 | Cecum | Moderate | 6.0 | T3 | 2 | 0 | 16 | 0 | No |
| 2 | 69 | 29 | Cecum | Moderate | 5.5 | T3 | 3 | 0 | 20 | 0 | No |
| 3 | 66 | 21 | Cecum | Moderate | 6.7 | T3 | 3 | 0 | 18 | 0 | No |
| 4 | 38 | 39 | Cecum | Moderate | 3.5 | T4 | 2 | 0 | 20 | 0 | No |
| 5 | 92 | 27 | Cecum | Moderate | 4 | T3 | 4 | 2 | 12 | 3 | No |
| 6 | 65 | 16 | Cecum | Moderate | 1.3 | T2 | 5 | 0 | 12 | 0 | No |
| 7 | 68 | 21 | Asc. Colon | Moderate | 5 | T4 | 5 | 1 | 24 | 5 | No |
| 8 | 67 | 35 | Asc. Colon | Moderate | 4 | T3 | 3 | 0 | 31 | 0 | No |
| 9 | 75 | 26 | Asc. Colon | Moderate | 4 | T3 | 3 | 0 | 11 | 0 | No |
| 10 | 67 | 37 | Asc. Colon | Moderate | 2.3 | T2 | 2 | 0 | 11 | 0 | No |
| 11 | 67 | 26 | Asc. Colon | Moderate | 5 | T2 | 3 | 0 | 11 | 1 | Yes |
| 12 | 77 | 24 | Hepatic Flexure | Poor | 4.7 | T3 | 2 | 1 | 16 | 1 | No |
| 13 | 91 | 29 | Hepatic Flexure | Moderate | 3.8 | T4 | 4 | 2 | 18 | 9 | No |
| 14 | 43 | 38 | Hepatic Flexure | Moderate | 4 | T3 | 3 | 0 | 11 | 0 | No |
| 15 | 75 | 26 | Hepatic Flexure | Moderate | 4.5 | T3 | 2 | 0 | 19 | 0 | No |
| 16 | 68 | 28 | Transv. Colon | Moderate | 2.5 | T1 | 3 | 2 | 16 | 6 | No |
| 17 | 48 | 28 | Sigmoid | Well | 3 | T2 | 5 | 1 | 10 | 2 | No |
| 18 | 33 | 21 | Sigmoid | Moderate | 4 | T3 | 3 | 0 | 18 | 0 | No |
| 19 | 46 | 28 | Sigmoid | Moderate | 4.5 | T3 | 3 | 0 | 14 | 0 | No |
| 20 | 71 | 27 | Rectum | Poor | 2.6 | T1 | 2 | 0 | 8 | 0 | No |
| 21 | 25 | 22 | Rectum | Moderate | 5.5 | T3 | 2 | 2 | 24 | 5 | No |
| 22 | 76 | 21 | Rectum | Min. Resid. Foci* | n/a* | T2 | 1 | 0 | 14 | 0 | No |
| 23 | 52 | 24 | Rectum | Moderate | 3 | T2 | 5 | 0 | 17 | 0 | No |
| 24 | 46 | 29 | Rectum | Moderate | 2 | T3 | 2 | 1 | 10 | 1 | No |
| Mean | 62.7 | 26.9 | | | 4.0 | | 3.0 | | 15.9 | | |

SLN = Sentinel Lymph Node, NIR = Near-Infrared, LN = Lymph Node, LN+ = Lymph Node with histologically proven metastases. Tumor Stage was determined by TNM classification. * Patient received neoadjuvant radiation and chemotherapy with a near complete pathological response.

mass. This phenomenon of lymph node effacement is well known for breast cancer patients. The fact that no fluorescence could be measured in the paraffin block of the lesion supports this hypothesis.

The great advantage of NIR fluorescence imaging is that the lymphatic channels traveling to the SLN are clearly visualized in real-time, even deep within the bowel mesentery. NIR fluorescence imaging also permits the use of small volumes (1 cc) of a colorless dye, and does not alter the appearance of the surgical field. Furthermore, the timing constraints of the technique we describe are very flexible, with successful identification of the SLN up to 1 hour after resection of the bowel.

These results and earlier findings[27, 28] suggest that NIR imaging has the potential to simplify the SLN procedure in colorectal cancer, when compared to the use of visible contrast agents like isosulfan blue. Therefore, larger studies comparing both techniques should be performed. The *ex vivo* approach[10] has certain advantages, such as the use of contrast agents that are not yet approved for *in vivo* administration. The agent used in our study, HSA800, has previously been compared to clinically available agents like indocyanine green and methylene blue and has clear advantages over them.[27] Due to conjugation of fluorophore IRDye 800CW to human serum albumin (HSA800), the hydrodynamic diameter of the probe increases from less than 1 to 7.4 nm, thereby facilitating a better retention in the first (sentinel) node as compared to blue dyes.

Because the agent is not injected into the patient, adverse reactions and patient safety are non-issues. Also, because the injection is performed after resection, it is not necessary that the surgeon performs the injection. Therefore, this technique does not add any time to the surgery, which is beneficial for the patient and could improve acceptance of the technique. In our hospital, the fluorescent dye is injected immediately after surgery at the department of pathology, thereby eliminating any interference with the surgical procedure. Using this technology, it should now be possible to design even more effective lymphatic tracers having higher fluorescence intensity and better lymph node retention.

The current NIR fluorescence imaging technique does not interfere with routine gross pathology and makes it possible to detect the SLN in sliced sections of rectal cancer specimens. Although neoadjuvant radiotherapy is known to affect lymphatic channels, even in rectal cancer patients that were treated with radiotherapy, SLNs were identified. A possible explanation is that only small amounts of HSA800 need to accumulate in the lymph node to be detected by the Mini-FLARE imaging system. As the mesorectum was not altered in any way, no lymphatic channels were disrupted. Furthermore, because lymph flow is induced by massaging the *ex vivo* specimen, decreased lymphatic flow can be overcome.

Compared to published clinical studies on SLN imaging using blue dyes, an important difference with the current study is the condition of the injection site. The current preclinical study was performed in healthy pigs, whereas the clinical application

of this technique was performed in cancer patients. Large tumors are especially known to alter and disrupt lymphatic channels. Since earlier studies show that there is still sufficient lymphatic flow to identify lymph nodes,[12, 37] we did not expect this to be a major problem. Viehl and colleagues showed that with larger tumors, a larger amount of blue dye (0.5 cc per cm tumor diameter) should be used to identify the SLN.[37] This observation suggests an advantage for NIR fluorescence imaging, since in our pilot clinical study in which the mean diameter of the tumors was 4.5 cm, a smaller amount of dye (1 cc) was sufficient to be able to identify a fluorescent signal in the SLN.

In conclusion, our study suggests that *ex vivo* SLN mapping using an optimal lymphatic tracer and invisible NIR fluorescent light permits real-time imaging of lymph flow and identification of the SLN in colon and rectal cancer specimens.

## ACKNOWLEDGEMENTS

We thank Rita G. Laurence for assistance with animal anesthesia, Summer L. Gibbs-Strauss for cryo-sectioning, Lorissa A. Moffitt and Eugenia Trabucchi for administrative assistance and Daan J. Lips for technical assistance. This work was supported in part by NIH grant R01-CA-115296 (JVF), the Michäel van Vloten fund (AV), Foundation "De Drie Lichten" (MH), the Dutch Cancer Society (MH), Leiden University Fund (MH), Nuts Ohra Fund, Foundation "Maurits and Anna de Kock" and the Center for Translational Molecular Medicine (DeCoDe project, grant 03O-101).

## REFERENCES


1. Giuliano AE, Dale PS, Turner RR, et al. Improved axillary staging of breast cancer with sentinel lymphadenectomy. Ann Surg 1995; 222:394-401.
2. Giuliano AE, Kirgan DM, Guenther JM, et al. Lymphatic mapping and sentinel lymphadenectomy for breast cancer. Ann Surg 1994; 220:391-398.
3. Morton DL, Thompson JF, Essner R, et al. Validation of the accuracy of intraoperative lymphatic mapping and sentinel lymphadenectomy for early-stage melanoma: a multicenter trial. Multicenter Selective Lymphadenectomy Trial Group. Ann Surg 1999; 230:453-5.
4. Adell G, Boeryd B, Frånlund B, et al. Occurrence and prognostic importance of micrometastases in regional lymph nodes in Dukes' B colorectal carcinoma: an immunohistochemical study. Eur J Surg 1996; 162:637-42.
5. Noura S, Yamamoto H, Ohnishi T, et al. Comparative detection of lymph node micrometastases of stage II colorectal cancer by reverse transcriptase polymerase chain reaction and immunohistochemistry. J Clin Oncol 2002; 20:4232-41.
6. Palma RT, Waisberg J, Bromberg SH, et al. Micrometastasis in regional lymph nodes of extirpated colorectal carcinoma: immunohistochemical study using anti-cytokeratin antibodies AE1/AE3. Colorectal Dis 2003; 5:164-8.
7. Liefers GJ, Cleton-Jansen AM, van de Velde CJ, et al. Micrometastases and survival in stage II colorectal cancer. N Engl J Med 1998; 339:223-228.
8. Bilchik AJ, Hoon DS, Saha S, et al. Prognostic impact of micrometastases in colon cancer: interim results of a prospective multicenter trial. Ann Surg 2007; 246:568-575.
9. Iddings D, Bilchik A. The biologic significance of micrometastatic disease and sentinel lymph node technology on colorectal cancer. J Surg Oncol 2007; 96:671-7.
10. Nordgård O, Oltedal S, Kørner H, et al. Quantitative RT-PCR detection of tumor cells in sentinel lymph nodes isolated from colon cancer patients with an ex vivo approach. Ann Surg 2009; 249:602-7.
11. Saha S, Seghal R, Patel M, et al. A multicenter trial of sentinel lymph node mapping in colorectal cancer: prognostic implications for nodal staging and recurrence. Am J Surg 2006; 191:305-10.
12. Stojadinovic A, Allen PJ, Protic M, et al. Colon sentinel lymph node mapping: practical surgical applications. J Am Coll Surg 2005; 201:297-313.
13. van der Zaag ES, Buskens CJ, Kooij N, et al. Improving staging accuracy in colon and rectal cancer by sentinel lymph node mapping: A comparative study. Eur J Surg Oncol 2009:Epub ahead of print.
14. Wiese D, Saha S, Yestrepsky B, et al. A Prospective Study of False-Positive Diagnosis of Micrometastatic Cells in the Sentinel Lymph Nodes in Colorectal Cancer. Ann Surg Oncol 2009; 8:2166-9.
15. Wong JH, Johnson DS, Namiki T, et al. Validation of ex vivo lymphatic mapping in hematoxylin-eosin node-negative carcinoma of the colon and rectum. Ann Surg Oncol 2004; 11:772-7.
16. Wong JH, Steineman S, Calderia C, et al. Ex vivo sentinel node mapping in carcinoma of the colon and rectum. Ann Surg 2001; 233:515-21.
17. Doekhie FS, Peeters KC, Kuppen PJ, et al. The feasibility and reliability of sentinel node mapping in colorectal cancer. Eur J Surg Oncol 2005; 31:854-62.
18. Stojadinovic A, Nissan A, Protic M, et al. Prospective randomized study comparing sentinel lymph node evaluation with standard pathologic evaluation for the staging of colon carcinoma: results from the United States Military Cancer Institute Clinical Trials Group Study GI-01. Ann Surg 2007; 245:846-57.
19. Frangioni JV. In vivo near-infrared fluorescence imaging. Curr Opin Chem Biol 2003; 7:626-634.
20. Kitai T, Inomoto T, Miwa M, et al. Fluorescence navigation with indocyanine green for detecting sentinel lymph nodes in breast cancer. Breast Cancer 2005; 12:211-215.
21. Kusano M, Tajima Y, Yamazaki K, et al. Sentinel node mapping guided by indocyanine green fluorescence imaging: a new method for sentinel node navigation surgery in gastrointestinal cancer. Dig Surg 2008; 25:103-8.

22. Miyashiro I, Miyoshi N, Hiratsuka M, et al. Detection of sentinel node in gastric cancer surgery by indocyanine green fluorescence imaging: comparison with infrared imaging. Ann Surg Oncol 2008; 15:1640-3.
23. Ogasawara Y, Ikeda H, Takahashi M, et al. Evaluation of breast lymphatic pathways with indocyanine green fluorescence imaging in patients with breast cancer. World J Surg 2008; 32:1924-9.
24. Sevick-Muraca EM, Sharma R, Rasmussen JC, et al. Imaging of lymph flow in breast cancer patients after microdose administration of a near-infrared fluorophore: feasibility study. Radiology 2008; 246:734-741.
25. Tanaka E, Choi HS, Fujii H, et al. Image-guided oncologic surgery using invisible light: completed pre-clinical development for sentinel lymph node mapping. Ann Surg Oncol 2006; 13:1671-1681.
26. Troyan SL, Kianzad V, Gibbs-Strauss SL, et al. The FLARE intraoperative near-infrared fluorescence imaging system: a first-in-human clinical trial in breast cancer sentinel lymph node mapping. Ann Surg Oncol 2009; 16:2943-2952.
27. Ohnishi S, Lomnes SJ, Laurence RG, et al. Organic alternatives to quantum dots for intraoperative near-infrared fluorescent sentinel lymph node mapping. Mol.Imaging 2005; 4:172-181.
28. Soltesz EG, Kim S, Kim SW, et al. Sentinel lymph node mapping of the gastrointestinal tract by using invisible light. Ann Surg Oncol 2006; 13:386-396.
29. Coleman PJ, Brashear KM, Askew BC, et al. Nonpeptide alphavbeta3 antagonists. Part 11: discovery and preclinical evaluation of potent alphavbeta3 antagonists for the prevention and treatment of osteoporosis. J Med Chem 2004; 47:4829-4837.
30. Quirke P, Durdey P, Dixon MF, et al. Local recurrence of rectal adenocarcinoma due to inadequate surgical resection. Histopathological study of lateral tumour spread and surgical excision. Lancet 1986; 2:996-9.
31. van Schaik PM, van der Linden JC, Ernst MF, et al. Ex vivo sentinel lymph node "mapping" in colorectal cancer. Eur J Surg Oncol 2007; 33:1177-82.
32. Efficacy of adjuvant fluorouracil and folinic acid in colon cancer. International Multicentre Pooled Analysis of Colon Cancer Trials (IMPACT) investigators. Lancet 1995; 345:939-44.
33. Wolmark N, Rockette H, Fisher B, et al. The benefit of leucovorin-modulated fluorouracil as postoperative adjuvant therapy for primary colon cancer: results from National Surgical Adjuvant Breast and Bowel Project protocol C-03. J Clin Oncol 1993; 11:1879-87.
34. Bertagnolli M, Miedema B, Redston M, et al. Sentinel node staging of resectable colon cancer: results of a multicenter study. Ann Surg 2004; 240:624-30.
35. Redston M, Compton CC, Miedema BW, et al. Analysis of micrometastatic disease in sentinel lymph nodes from resectable colon cancer: results of Cancer and Leukemia Group B Trial 80001. J Clin Oncol 2006; 24:878-83.
36. Bembenek AE, Rosenberg R, Wagler E, et al. Sentinel lymph node biopsy in colon cancer: a prospective multicenter trial. Ann Surg 2007; 245:858-63.
37. Viehl CT, Hamel CT, Marti WR, et al. Identification of sentinel lymph nodes in colon cancer depends on the amount of dye injected relative to tumor size. World J Surg 2003; 27:1285-90.

# Chapter 6

# Towards optimization of imaging system and lymphatic tracer for near-infrared fluorescent sentinel lymph node mapping in breast cancer

Mieog JSD[1], Troyan SL[1], Hutteman M[1], Donohue KJ, van der Vorst JR, Stockdale A, Liefers GJ, Choi HS, Gibbs-Strauss SL, Putter H, Gioux S, Kuppen PJK, Ashitate Y, Löwik CWGM, Smit VTHBM, Oketokoun R, Ngo LH, van de Velde CJH, Frangioni JV, Vahrmeijer AL

[1] Shared first authorship

*Ann Surg Oncol; In press.*

# ABSTRACT

## Background

Near-infrared (NIR) fluorescent sentinel lymph node (SLN) mapping in breast cancer requires optimized imaging systems and lymphatic tracers.

## Methods

A small, portable version of the FLARE™ imaging system, termed Mini-FLARE™, was developed for capturing color video and two semi-independent channels of NIR fluorescence (700 nm and 800 nm) in real-time. Initial optimization of lymphatic tracer dose was performed using 35-kg Yorkshire pigs and a 6-patient pilot clinical trial. More refined optimization was performed in twenty-four consecutive breast cancer patients. All patients received the standard of care using $^{99m}$Technetium-nanocolloid and patent blue. In addition, 1.6 mL of indocyanine green adsorbed to human serum albumin (ICG:HSA) was injected directly after patent blue at the same location. Patients were allocated to one of eight escalating ICG:HSA concentration groups from 50 to 1000 μM.

## Results

The Mini-FLARE™ system was positioned easily in the operating room and could be used up to 13" from the patient. Mini-FLARE™ enabled visualization of lymphatic channels and SLNs in all patients. A total of 35 SLNs (mean = 1.45, range 1-3) were detected: 35 radioactive (100%), 30 blue (86%), and 35 NIR fluorescent (100%). Contrast agent quenching at the injection site and dilution within lymphatic channels were major contributors to signal strength of the SLN. Optimal injection dose of ICG:HSA ranged between 400 and 800 μM. No adverse reactions were observed.

## Conclusions

We describe the clinical translation of a new NIR fluorescence imaging system and define the optimal ICG:HSA dose range for SLN mapping in breast cancer.

# INTRODUCTION

Sentinel lymph node (SLN) mapping, as introduced for the management of breast cancer by Giuliano et al,[1] is currently regarded as the standard of care for staging of the axilla.[2] In general, a combination of radioactive colloid and blue dye is used. However, this exposes patients and caregivers to ionizing radiation, and blue dyes cannot be seen through skin and fatty tissue. Nonetheless, in recent trials, SLN identification rates of 95-97% are achieved when using this combination, and use of only one agent results in significantly lower identification rates.[3-6]

Recent preclinical and clinical data have demonstrated that near-infrared (NIR) fluorescence imaging using the NIR fluorescence agent indocyanine green (ICG) enables real-time transcutaneous and intraoperative visualization of lymphatic channels and detection of the SLN.[7-14] Therefore, NIR fluorescence imaging could provide an alternative for, or an addition to, conventional techniques used for SLN mapping. However, to date, clinical data are lacking a direct comparison of NIR fluorescence to the combination of radioactive tracer and blue dye. Also, even though ICG is the only fluorescent agent currently available in the clinic, it is not an optimal lymphatic tracer. Previous preclinical work has demonstrated that adsorption of ICG to human serum albumin (HSA, complex is ICG:HSA) increases the fluorescence intensity and the hydrodynamic diameter, thereby providing improved detection and better retention in the SLN.[15]

Recently, first-in-human clinical testing of ICG:HSA was performed.[14] The Fluorescence-Assisted Resection and Exploration (FLARE™) imaging system, developed by our group[14, 16] and used in the trial, is a general-purpose optical imaging platform that provides the surgeon with two independent NIR fluorescence channels (centered at 700 nm and 800 nm) to see otherwise invisible structures within the surgical field. The first generation of FLARE™ was large, expensive to build, and had a heavy imaging head that required a specially-designed articulated arm.[14] This prevented shipment of FLARE™ to researchers around the world, and therefore impeded efficient scientific investigation. During the first-in-human clinical testing of FLARE™, it also became apparent that contrast agents for SLN mapping were not yet optimal. The goals of the present study were to develop a miniaturized version of FLARE™, termed Mini-FLARE™, and to determine optimal lymphatic tracer dosing for SLN mapping in breast cancer.

## MATERIALS AND METHODS

### Mini-FLARE™ Imaging System

A detailed description of the Mini-FLARE™ imaging system and *in vitro* characterization is provided in Supplementary Data (available online at http://www.springerlink.com/content/r4712247933613tv/). For sterile usage in the operating room, a 0.118" thick acrylic splash shield having 95% optical transmission at 800 nm was hermetically bonded to a clear plastic drape and sterilized (Medical Technique, Inc., Tucson, USA).

### Preparation of Indocyanine Green adsorbed to Human Serum Albumin

ICG (25-mg vials) was purchased from Pulsion Medical Systems (Munich, Germany) and was resuspended in 10 cc of sterile water for injection to yield a 2.5 mg/ml (3.2 mM) stock solution. Various amounts of this stock solution were transferred to a 50 cc vial of Cealb (20% human serum albumin (HSA) solution; Sanquin, Amsterdam, The Netherlands) to yield ICG in HSA (ICG:HSA) at a final concentration of 50 μM, 100 μM, 200 μM, 400 μM, 500 μM, 600 μM, 800 μM, or 1000 μM. To obtain a final concentration of 800 μM and 1000 μM, ICG was resuspended in 5 cc of sterile water, to yield a 6.4-mM stock solution prior to dilution.

### Pre-Clinical Characterization

Animals were studied under the supervision of approved institutional protocol. Female Yorkshire pigs (E. M. Parsons and Sons, Hadley, USA) averaging 35 kg were induced with 4.4-mg/kg intramuscular Telazol (Fort Dodge Labs, Fort Dodge, USA), intubated, and maintained with 2% isoflurane (Baxter Healthcare, Deerfield, USA). Vital signs were monitored continuously. Excitation fluence rate for white light and 800-nm excitation light were 26,600 lux and 7.7 mW/cm$^2$, respectively. One hundred microliters of the specified ICG:HSA solution was injected intradermally. ICG concentration of the ICG:HSA complex was systematically increased from 10 μM to 500 μM to explore the counteracting effects of NIR fluorophore quenching at the injection site and NIR fluorophore dilution within the lymphatic channels.

### Dose-Optimization Clinical Trial

A 24-patient dose-escalation clinical trial was approved by the Medical Ethics Committee of the Leiden University Medical Center and was performed in accordance with the ethical standards of the Helsinki Declaration of 1975. All patients that had planned to undergo a SLN procedure for invasive breast cancer or extensive high-risk carcinoma *in situ* were eligible for participation in the study. Patients had clinically

negative axillary nodes as assessed by palpation and ultrasonography. Exclusion criteria were pregnancy, lactation or an allergy to iodine, shellfish, or indocyanine green.

Twenty-four consecutive patients were included. All patients gave informed consent and were anonymized. Patients received the standard-of-care SLN procedure. For our institution, this implies one periareolar injection of approximately 100 MBq $^{99m}$Technetium-nanocolloid (mean ± S.D. = 99.6 ± 5.8 MBq) the day before surgery. Before the start of the operation, one mL of patent blue V was injected peritumorally or periareolarly. Choice of the injection site was left to the surgeon. Directly after patent blue injection, 1.6-mL ICG:HSA was administered as four injections at the same location as the patent blue injections. After surgical scrub and sterile covering of the operation field, NIR fluorescence imaging was performed with the imaging head of the Mini-FLARE™ at approximately 30 cm distance to the surgical field.

The surgical technique consisted of percutaneous assessment of NIR fluorescent signal in the breast and the axilla prior to skin incision. The location and length of the axillary skin incision was determined by the surgeon. Assessment of the surgical field using NIR fluorescence was applied continuously throughout the SLN procedure and surgical exploration. If the SLN was not easily detected by NIR fluorescence, the gamma probe was used to provide direction for surgical exploration. Camera exposure was between 5 to 250 msec as indicated. A SLN exhibiting a signal-to-background ratio (SBR) ≥ 1.1 *in situ* was considered positive by NIR fluorescence. Background was chosen as an area within the surgical field, directly adjacent (within 1-2 cm) to the SLN.

Routine histopathological frozen analysis of SLNs was performed during surgery. If the patient participated in the After Mapping of the Axilla Radiotherapy or Surgery (AMAROS) trial and was randomized to the radiotherapy arm, no intraoperative frozen analysis was performed. SLNs were fixed in formalin and embedded in paraffin for routine hematoxylin, eosin, and immunohistopathological staining for AE1/AE3 at three levels, with an interval of 150-250 μm, according to the Dutch guidelines for SLN analysis. Patients underwent an axillary lymph node dissection if the SLN was found to contain metastases, except for those patients who participated in the radiotherapy arm of the AMAROS trial. If isolated tumor cells (ITCs) were found (< 0.2 mm), no axillary lymph node dissection was performed.

**Statistical Analysis**

For statistical analysis, SPSS statistical software package (Version 16.0, Chicago, USA) was used. Graphs were generated using GraphPad Prism Software (Version 5.01, La Jolla, USA). To compare the SBR between concentration groups, a one-way analysis of variance (ANOVA) was performed with pairwise comparison with

least square difference (LSD) adjustment for multiple testing. When the assumption of homogeneity of variance was violated (Levene's test), a log10 transformation was applied. All statistical tests were two-tailed and $P < 0.05$ was considered significant.

## RESULTS

### Design of the Mini-FLARE™ Imaging System and *In Vitro* Characterization

The Mini-FLARE™ imaging system (Figure 1A) is composed of a small portable electronics cart and a counter-weighted pole stand that supports the imaging head. Unlike FLARE™, Mini-FLARE™ utilizes a flexible gooseneck arm, which permits positioning of the imaging head at extreme angles virtually anywhere over the surgical field. The only consumable for Mini-FLARE™ is a specially designed acrylic splash plate that is hermetically sealed to a plastic drape. Using sterile technique, the shield/drape is inserted into the imaging head, locked into place, and the drape is unfolded to encase the imaging head and imaging system pole stand (Figure 1B). Optical light paths for white light (i.e., color video images) and the two semi-independent NIR fluorescence channels, one centered at 700 nm emission and the other at 800 nm emission, are shown in Figure 1C.

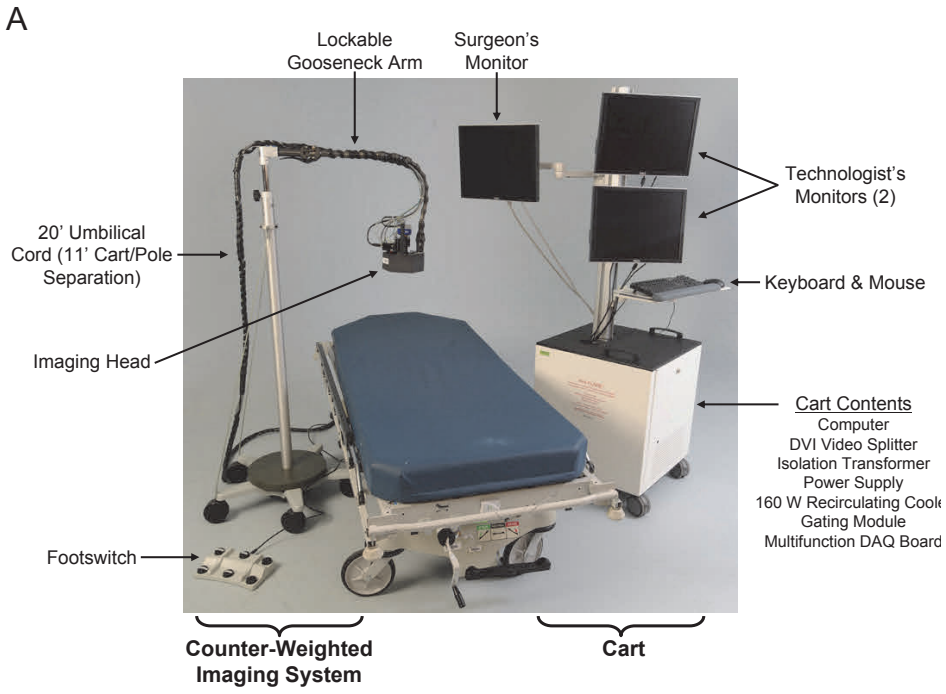

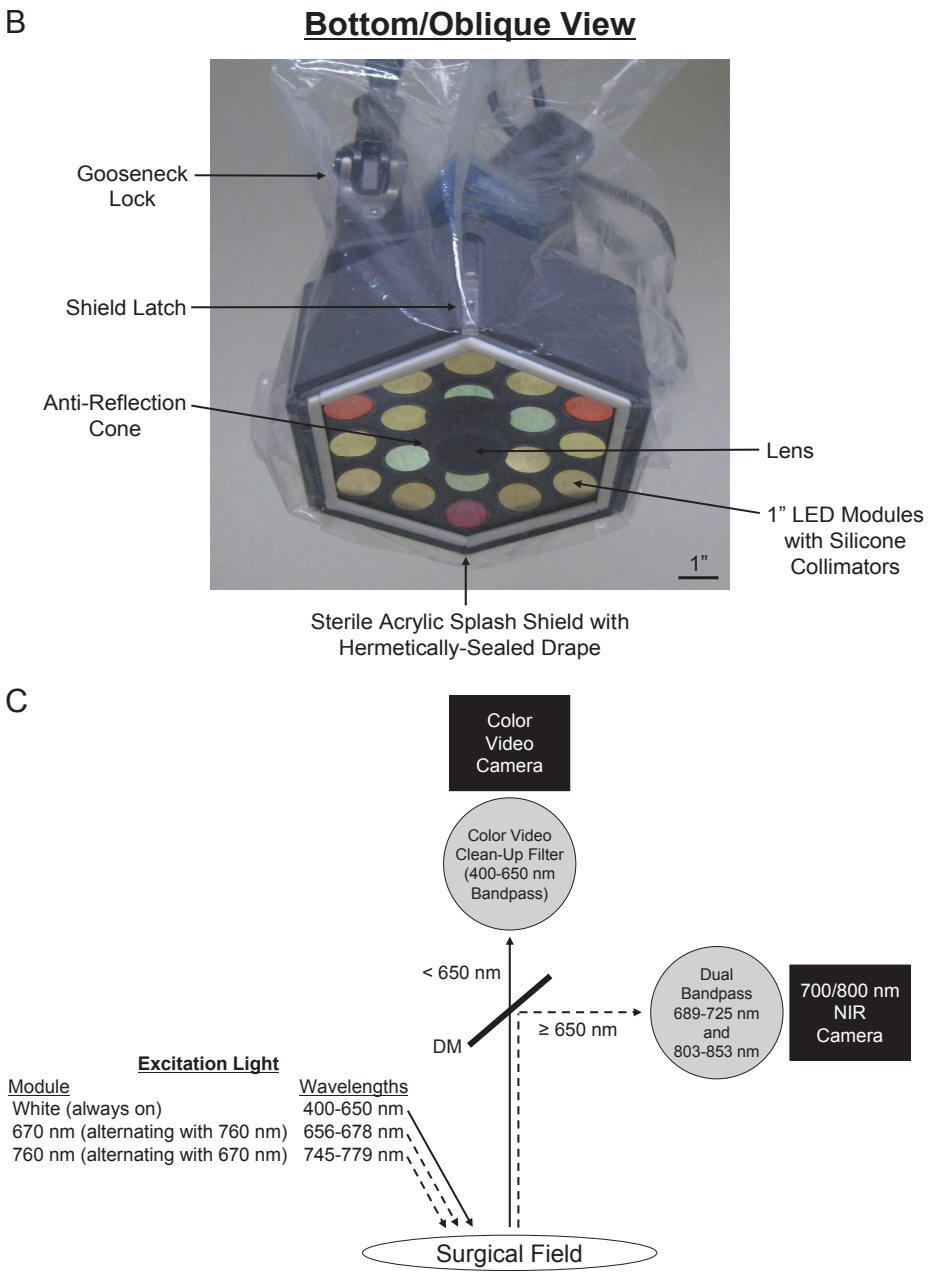


**Figure 1.** The Mini-FLARE™ Portable Near-Infrared Fluorescence Imaging System: **A.** Imaging system, composed of electronics/monitor cart and counter-weighted imaging system pole. **B.** Sterile drape/shield attached to the imaging head with other major parts identified. **C.** Excitation and emission light paths, and filtration for the Mini-FLARE™ imaging system. DM = 650 nm dichroic mirror.

Technical specifications of Mini-FLARE™ are detailed in Table 1. Of note, the working distance is up to 13" away from the patient, with field-of-view adjustable from 4.7" (12 cm) to 2" (5 cm) simply by moving the device toward or away from the surgical field. The cart occupies a volume of only 9.7 cu ft, and weighs only 272 lbs. A 6-pedal footswitch and autofocus circuit permit hands-free operation. The cost of all parts is ≈ $40,000.

**Table 1.** Mini-FLARE™ Imaging System Specifications

| Category | Specification | Description |
|---|---|---|
| Physical | Size | Mobile Cart: 24" W x 24" D x 29" H; Mast Height: 76.5" |
| | Weights | Cart: 272 lbs, including all electronics<br>Arm: 95 lbs, including, stand, gooseneck, and imaging head<br>Imaging Head: 8.8 lbs. |
| | Arm and Stand | Flexible Arm; Reach: 27" – 64" from floor, 42" from center of stand. Center of stand up to 11 linear feet from cart |
| Electrical | Voltage and Plug | 120 V AC, 60 Hz; single NEMA 5-15 120 V/15 A AC plug |
| | Current | 5 A max |
| | Grounding | Isolation transformer for all components; redundant chassis grounding |
| | Leakage Current | < 300 μA (per AAMI/IEC #60601) |
| Sterility | Shield | Disposable acrylic shield with ≥95% transmission |
| | Drape | Disposable, custom-fit plastic drape bonded to shield |
| Light Source | Housing | Anodized aluminum with integrated liquid cooling |
| | Elements | Custom 25 mm circular LED arrays w/ integrated linear drivers |
| | Electronics | Custom control board with embedded microcontroller |
| | Fluence Rates | 26,600 lux white light (400-650 nm), 1.08 mW/cm$^2$ of 700 nm (656-678 nm) excitation light, 7.70 mW/cm$^2$ of 800 nm (745-779 nm) excitation light |
| Optics | Working Distance | 4" (10 cm) to 13" (32 cm) from patient (reverse telephoto) |
| | Field-of-View | 12 cm W x 9 cm H at 13" working distance |
| | Emission/ Reflectance Channels | Color Video (400-650 nm), 700 nm fluorescence (689-725 nm), 800 nm fluorescence (800-848 nm), all with simultaneous acquisition |
| | Pixel Resolution | 640 x 480 for each camera |
| | System Resolution | 320 x 320 μm (x,y) |
| | Display Refresh | Up to 15 Hz simultaneous acquisition on both cameras |
| | NIR Exposure Time | Adjustable from 100 μsec to 8 sec |
| Hands-Free | Optics | Automatic focus |
| | Control | 6-pedal footswitch |
| Monitors | Number | 3 cart-mounted 20": 2 for operator and 1 for surgeon |

## Pre-Clinical Optimization of NIR Fluorescent Lymphatic Tracers

Our group has previously reported that ICG (and ICG:HSA) exhibits intense quenching (i.e., reduction of fluorescence emission) as its concentration is increased.[15] That is, increasing concentration actually decreases fluorescence, so there would theoretically be no benefit to injecting high concentration for SLN mapping. This effect is demonstrated vividly in Figure 2A (left), where the injection site becomes dramatically less fluorescent as concentration increases. As a general rule, if the

concentration is high enough to see green color at the injection site, ICG fluorescence is severely quenched.

Importantly, we have recently discovered that dilution of the injected NIR fluorophore as it travels through the lymphatic system and mixes with lymph counteracts the effect of quenching and results in signal in the SLN that increases with concentration, even when the injection site is barely fluorescent (Figure 2A, right). This suggests that there will be an "optimal" concentration of injected NIR fluorophore such that final signal in the SLN is as high as possible.

**Optimization of ICG:HSA Dose in Women undergoing SLN Mapping for Breast Cancer**

This study aimed to test the feasibility of NIR fluorescence in SLN detection, using ICG:HSA and the Mini-FLARE™, in direct comparison with the conventional lymphatic tracers radiocolloid and patent blue. Twenty-four consecutive breast cancer patients underwent standard-of-care SLN mapping with the addition of preoperative ICG:HSA injection and subsequent intraoperative NIR fluorescence imaging. Patient and tumor characteristics are provided in Table 2. Use of the Mini-FLARE™ during surgery did not interfere with the standard of care. Average time between ICG:HSA injection and skin incision was 16 ± 3 minutes (Table 3). In all patients (N = 24), NIR fluorescence imaging enabled visualization of the SLN (Figure 3). A total of 35 SLNs were identified, which were all radioactive and NIR fluorescent (Table 3). Five SLNs from four patients did not have blue staining from patent blue. In all patients, the NIR fluorescence signal in the SLN was detected before patent blue. Average time between skin incision and resection of the first SLN was 17 ± 5 minutes. After all nodes detected using NIR fluorescence were resected, the axilla was systematically inspected for any remaining radioactivity. No additional radioactive nodes were identified that were not detected by NIR fluorescence. No adverse reactions associated with the use of ICG:HSA or the Mini-FLARE™ occurred. Two patients experienced a wound infection requiring antibiotics and one patient underwent surgical re-exploration because of an expanding hematoma following axillary lymph node dissection (Table 3).

A second objective of this trial was to determine the optimal concentration of injected ICG:HSA for NIR fluorescence SLN mapping, i.e. which concentration provides the highest SBR in the SLN. Because ICG and ICG:HSA exhibit intense quenching as their concentrations are increased (typically above 50 μM), there would be theoretically no advantage of injecting higher doses of ICG:HSA. However, dilution of the lymphatic tracer occurs upon injection in the breast and uptake by the lymphatic system counteracting the quenching effect. To assess the relationship between the concentration of injected NIR fluorescent lymphatic tracer and final SBR in the SLN, patients were allocated to 8 ICG:HSA concentration groups ranging from 50 μM to 1000 μM. The concentration of ICG:HSA influenced the SBR and showed a normal

distribution (Figure 2B). The variances of the concentration groups were not equal (Levene's test, $P = 0.02$). A log10 transformation of the data could account for part of the unequal variances (Levene's test, $P = 0.05$). A one-way ANOVA with pairwise comparison with LSD adjustment for multiple comparison showed that the SBRs of the 400, 500, 600, and 800 μM concentration groups were significantly higher than of the 50, 100, 200, and 1000 μM concentration groups (200 vs. 400, $P = 0.001$; 200 vs. 500, $P = 0.001$; 200 vs. 600, $P < 0.0001$; 200 vs. 800, $P = 0.001$; 1000 vs. 400, $P < 0.0001$; 1000 vs. 500, $P < 0.0001$; 1000 vs. 600, $P < 0.0001$; 1000 vs. 800, $P < 0.0001$). The SBRs of the 400, 500, 600, and 800 μM concentration groups were not significantly different, although a trend was found favoring the 600 μM concentration group (500 vs. 600, $P = 0.06$). The decline of the SBR in the 1000 μM concentration group was caused by decreased NIR fluorescence signal of the SLN (800 vs. 1000, $P = 0.001$), which suggests that quenching of ICG indeed occurred in the SLN.

## DISCUSSION

Near-infrared (NIR) fluorescent light in the wavelength range of 700 to 900 nm is invisible to the human eye. It is also capable of penetrating millimeters into living tissue and is not obscured by autofluorescence. For these reasons, NIR fluorescent light is ideal for image-guided surgery. Indeed, several NIR fluorescence surgical imaging systems are already FDA-approved or are in the process of obtaining approval (reviewed in [17]). The Mini-FLARE™ camera system used in this study is capable of displaying NIR fluorescence signal in relation to the surgical anatomy and illuminates the surgical field with white light. This enabled the surgeon to perform surgery under direct image guidance.

NIR fluorescence optical imaging using Mini-FLARE™ offers the advantages of real-time, continuous, high-resolution, and high sensitivity detection of SLNs, without the need for ionizing radiation. Because NIR light is invisible, there is no staining of the surgical field as with blue dyes, and the class of chemicals in which ICG belongs has a remarkable safety record in humans. ICG:HSA adds approximately $150 to the cost of a case, but if future studies show that the blue dye and/or Tc-99m sulfur colloid can be eliminated when using NIR fluorescence, a much larger savings will offset this cost. And, the surgeon can perform the injection procedure only minutes before SLN identification and resection. Although a technologist was used in this first-in-human study, Mini-FLARE™ is equipped with hand-free operation and there is virtually no learning curve because unlike other SLN techniques, the lymphatic tracer can be visualized in real-time throughout the procedure.

An important objective of the study was to optimize NIR fluorescent contrast agent dose for breast cancer SLN mapping. The only clinically available NIR fluorescent lymphatic tracer, albeit approved for other indications, is ICG.[7, 11, 13, 18, 19] We have

**Table 2.** Patient and Tumor Characteristics

| Characteristic | N | % |
|---|---|---|
| Age (Median, Range) | 59.5 (33-81) | |
| Menopausal State | | |
| - Premenopausal | 5 | 21 |
| - Postmenopausal | 19 | 79 |
| Body Mass Index (Median, Range) | 25 (18-38) | |
| Skin Type | | |
| - II | 4 | 17 |
| - III | 20 | 83 |
| Previous Breast Surgery [a] | 3 | 13 |
| Multifocality | 4 | 17 |
| Tumor Side | | |
| - Left | 14 | 58 |
| - Right | 10 | 42 |
| Tumor Localization | | |
| - Central | 5 | 21 |
| - Lower Inner | 1 | 4 |
| - Lower Outer | 1 | 4 |
| - Upper Inner | 6 | 25 |
| - Upper Outer | 11 | 46 |
| Type of Operation | | |
| - Ablation | 9 | 38 |
| - Wide Local Excision | 15 | 63 |
| Pathological Tumor Size (Median, Range) | 15 (3-35) | |
| Histological Type | | |
| - Infiltrating Ductal Adenocarcinoma | 18 | 75 |
| - Infiltrating Lobular Adenocarcinoma | 2 | 8 |
| - Ductal Carcinoma *In Situ* | 4 | 17 |
| Histological Grade | | |
| - I | 3 | 13 |
| - II | 13 | 54 |
| - III | 8 | 33 |
| Receptor Status [b] | | |
| - ER+ HER2- | 16 | 67 |
| - ER+ HER2+ | 3 | 13 |
| - ER- HER2- | 1 | 4 |
| - Missing [c] | 4 | 17 |

[a] Previous breast surgery: silicone breast implantation, breast reduction and re-excision.
[b] HER2 status was determined using the chromogenic *in situ* hybridization (CISH) kit of Zymed (Invitrogen, Carlsbad, CA)
[c] Not applicable in four patients with ductal carcinoma *in situ*.

previously proposed simple mixing of ICG and HSA (ICG:HSA) prior to injection[14, 15] because ICG is a small molecule and like blue dyes can pass through SLNs, and exhibit a relatively low quantum yield in aqueous environments.[15] Indeed, the product insert for ICG notes that it rapidly binds albumin when injected intravenously, so pre-mixing merely improves kinetics. Importantly, though, pre-mixing increases quantum yield

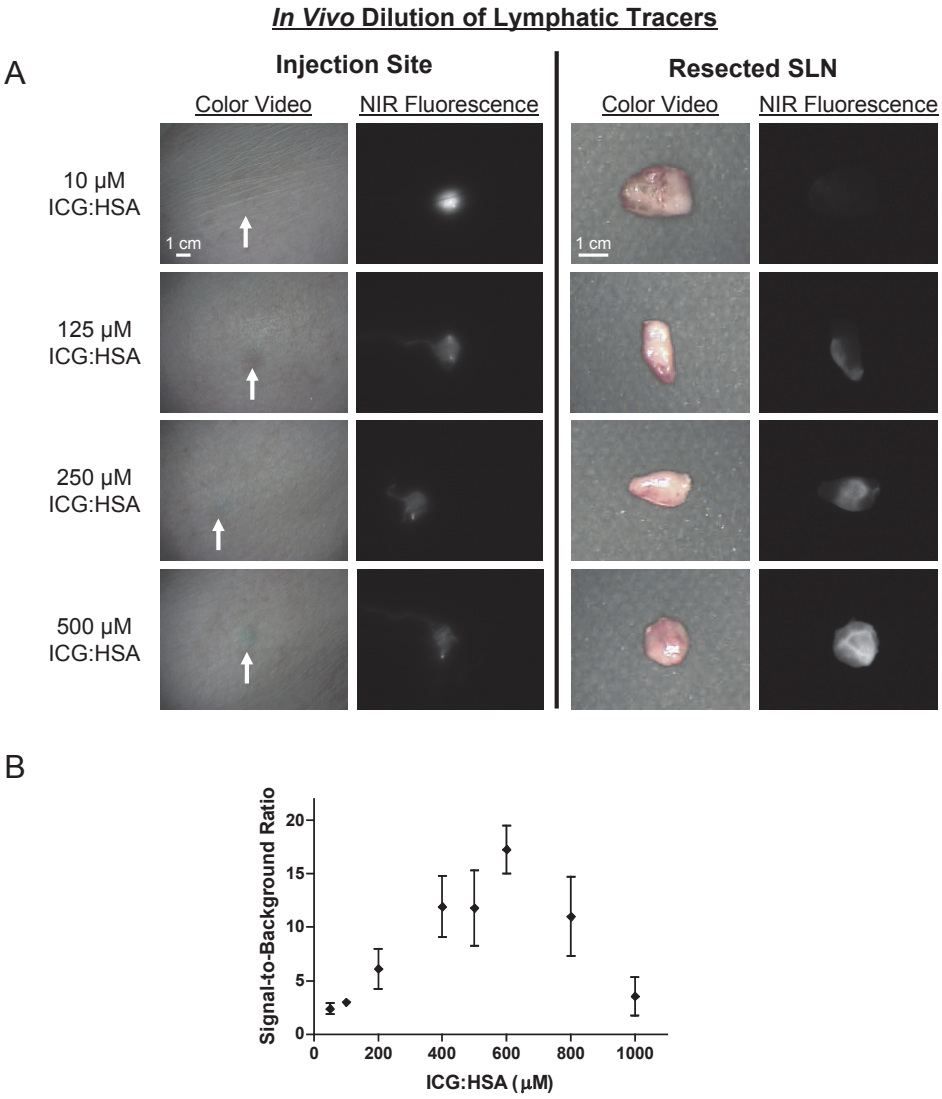


**Figure 2.** Optimization of ICG:HSA Dose as a Function of the Complex Tradeoff Between Fluorescence Quenching at the Injection Site and Dilution of Fluorophore in Lymphatic Channels: **A.** Pre-clinical studies in Yorkshire pigs. Subcutaneous injection sites (left; white arrows) showing quenching and resected SLNs (right) showing NIR fluorophore dilution for increasing concentrations of ICG:HSA. For each are displayed color video (left columns) and 800 nm NIR fluorescence (right columns) images obtained using 760 nm excitation light at 7.7 mW/cm2. All camera exposure times were 45 msec. Data are representative of n = 3 pigs. **B.** Optimization of ICG:HSA dose for breast cancer SLN mapping: Signal-to-background ratio (mean ± S.D) of the SLNs (ordinate) as a function of injected dose of ICG:HSA (abscissa) in women undergoing SLN mapping for breast cancer. Statistical comparisons are as follows: 200 μM vs. 400 μM, P = 0.001; 200 μM vs. 500 μM, P = 0.001; 200 μM vs. 600 μM, P < 0.0001; 200 μM vs. 800 μM, P = 0.001; 1000 μM vs. 400 μM, P < 0.0001; 1000 μM vs. 500 μM, P < 0.0001; 1000 μM vs. 600 μM, P < 0.0001; 1000 μM vs. 800 μM, P < 0.0001). The SBRs of the 400, 500, 600 and 800 μM concentration groups were not significantly different, although a trend was found favoring the 600 μM concentration group (500 vs. 600, P = 0.06).

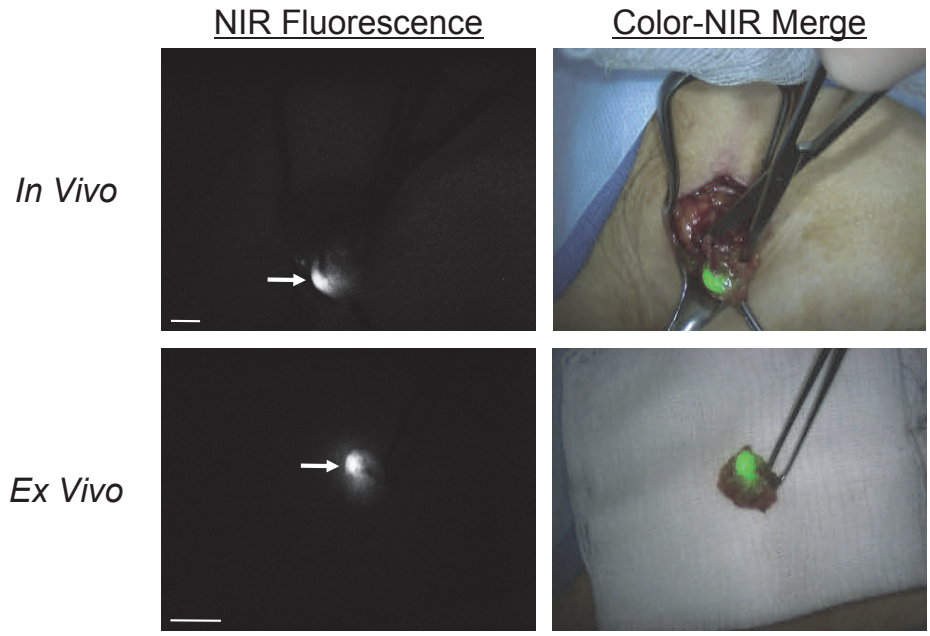


**Figure 3.** Real-Time NIR Fluorescence Imaging during Sentinel Lymph Node Mapping in Women with Breast Cancer: Shown are typical in vivo (top row) and ex vivo (bottom row; post-resection) results from a subject injected with 500 μM ICG:HSA. White arrow identifies the SLN. NIR fluorescence (left) and pseudo-colored (lime green) merge with the color video image (right). Exposure times were 50 msec for in vivo images and 30 msec for ex vivo images. 760 nm excitation fluence rate was ≈ 7.7 mW/cm2 for all images. Scale bars indicate 1 cm.

(i.e., brightness) 3-fold and also results in a final hydrodynamic diameter (≈ 7 nm) that is better retained in the SLN.[15]

NIR fluorescent signal in the SLN is a complex function of the concentration of the injected NIR lymphatic tracer, the distance between the injection site and the SLN, the volume of ultra-filtrate within the lymphatic channels encountered by the NIR fluorophore, and retention of the NIR fluorophore by the SLN. Of these, only the injection concentration can be controlled. Our study suggested that an optimal ICG:HSA concentration is in the range 400 μM and 800 μM. In the 1000 μM concentration group, the fluorescence intensity of the SLN and the SBR decreased rapidly, most likely due to quenching. Furthermore, since lymphatic vessels could be visualized percutaneously and directly after incision, particularly in the optimal dose range groups, a more efficient identification of SLNs was facilitated. This is of particular benefit for lymph nodes located deeper in the axilla, which exceed the 1-2 cm depth limit of the technology. These nodes could often be located by following the NIR fluorescent signal of the afferent lymphatic tract.

The accuracy of SLN identification using ICG fluorescence was similar to that using conventional radioisotope scanning, as both techniques identified all

**Table 3.** SLN Identification Results

| Characteristic | N | % |
|---|---|---|
| Injection Site Patent Blue and ICG:HSA | | |
| - Periareolar | 20 | 83 |
| - Peritumoral | 4 | 17 |
| | | |
| SLN Detection | | |
| - Number of SLNs Identified | 35 | |
| - Average Number of SLNs Identified (range) | 1.45 (1-3) | |
| Method of Detection | | |
| - Radioactive | 35 | 100 |
| - Blue | 30 | 86 |
| - Near-Infrared Fluorescence | 35 | 100 |
| | | |
| Average Time between Injection of ICG:HSA and Skin Incision (S.D.) | 16 minutes ± 3 | |
| Average Time between Skin Incision and SLN Resection (S.D.) | 17 minutes ± 5 | |
| | | |
| Histology | | |
| - Negative | 26 | 74 |
| - Isolated Tumor Cells | 3 | 9 |
| - Micrometastases | 0 | 0 |
| - Macrometastases | 6 | 17 |
| | | |
| Axillary Treatment | | |
| - None | 16 | 67 |
| - Axillary Lymph Node Dissection | 5 | 21 |
| - Axillary Radiotherapy | 3 | 13 |
| Complications | | |
| - No | 21 | 87 |
| - Yes | 3 [a] | 13 |

Abbreviations: ICG:HSA = indocyanine green adsorbed to human serum albumin, SLN = sentinel lymph node, S.D. = standard deviation

[a] Two patients experienced postoperative wound infection requiring treatment with antibiotics and one patient underwent surgical re-exploration because of an expanding hematoma following axillary lymph node dissection.

SLNs and no additional fluorescent lymph nodes were identified. However, blue dye identification was not successful in 5 of 35 (14%) SLNs. These results suggest that patent blue staining can be replaced by NIR fluorescence using ICG:HSA. Replacing patent blue has the additional advantage of absent tattooing of the breast and visual alteration of the surgical field. Moreover, the intrinsic dark color of patent blue dye can obscure the fluorescence intensity of any fluorescent lymphatic tracer. Indeed, *in vitro* tests using a fixed ICG:HSA concentration showed that addition of patent blue dye decreased NIR fluorescence of ICG:HSA (data not shown). An as yet unanswered question is whether radioisotope scanning can be omitted from the SLN procedure. A larger trial to address whether NIR fluorescence imaging alone can replace blue dyes and/or radiocolloids is ongoing.

In summary, this study demonstrated feasibility and accuracy of NIR fluorescence imaging using ICG:HSA and the Mini-FLARE™ imaging system for SLN mapping in breast cancer patients. The optimal dose of injected ICG:HSA lies between 400 μM and 800 μM and can be chosen based on local preparation preferences. For example, in the United States, a dose of 500 μM is most convenient since it requires minimal manipulation of albumin volumes.

## ACKNOWLEDGEMENTS

The BIDMC study team thanks Barbara L. Clough and Mireille Rosenberg for clinical trial preparation, Keith V. Belken from the BIDMC Investigational Pharmacy, Judith Hirshfield-Bartek for assistance with patient medical histories, Sunil Gupta for technical assistance with the imaging system, Lorissa A. Moffitt and Lindsey Gendall for editing, and Eugenia Trabucchi for administrative support. The Leiden study team thanks Gemma Ranke, Elly Krol-Warmerdam, Annemarie Voet-van den Brink, Gerlinda van Gent-de Bruijn (Breast Cancer Unit) and Linda van der Hulst (Central Pharmacy). Part of the study protocol was written during the 10th ECCO-AACR-ASCO Workshop on Methods in Clinical Cancer Research (Flims, Switzerland). We thank the following individuals and companies for their contributions to this project: Gordon Row (Yankee Modern Engineering), Kelly Stockwell and Paul Millman (Chroma Technology), David Comeau and Robert Waitt (Albright Technologies), Bob Zinter, Gary Avery, Phil Dillon, Will Barker, Craig Shaffer, and Ed Schultz (Qioptiq), Jeffrey Thumm (Duke River Engineering), Colin Johnson (LAE Technologies), Robert Eastlund (Graftek Imaging), John Fortini (Lauzon Manufacturing), Steve Huchro (Solid State Cooling), Clay Sakewitz, Johnny Fraga, and Will Richards (Design and Assembly Concepts), Ken Thomas and Fernando Irizarry (Sure Design), Paul Bistline and Phil Bonnette (Medical Technique, Inc.), Amy King (Civco), and Jim Cuthbertson (Nashua Circuits).

This study was supported in part by the following grants from the National Institutes of Health (National Cancer Institute) to JVF: NIH Bioengineering Research Partnership grant #R01-CA-115296 (JVF), Quick Trials for Imaging grant #R21-CA-130297 (JVF), Nuts Ohra Fund (ALV), the Maurits and Anna de Kock Foundation (ALV), and the American Women's Club of The Hague. JSDM is a MD-medical research trainee funded by The Netherlands Organisation for Health Research and Development (grant nr. 92003526).

## REFERENCES


1. Giuliano AE, Kirgan DM, Guenther JM, et al. Lymphatic mapping and sentinel lymphadenectomy for breast cancer. Ann Surg 1994; 220:391-398.
2. Cox CE, Pendas S, Cox JM, et al. Guidelines for sentinel node biopsy and lymphatic mapping of patients with breast cancer. Ann Surg 1998; 227:645-651.
3. Goyal A, Newcombe RG, Chhabra A, et al. Factors affecting failed localisation and false-negative rates of sentinel node biopsy in breast cancer--results of the ALMANAC validation phase. Breast Cancer Res Treat 2006; 99:203-208.
4. Krag DN, Anderson SJ, Julian TB, et al. Technical outcomes of sentinel-lymph-node resection and conventional axillary-lymph-node dissection in patients with clinically node-negative breast cancer: results from the NSABP B-32 randomised phase III trial. Lancet Oncol. 2007; 8:881-888.
5. Straver ME, Meijnen P, van Tienhoven G, et al. Sentinel Node Identification Rate and Nodal Involvement in the EORTC 10981-22023 AMAROS Trial. Ann Surg Oncol 2010.
6. Zavagno G, De Salvo GL, Scalco G, et al. A Randomized clinical trial on sentinel lymph node biopsy versus axillary lymph node dissection in breast cancer: results of the Sentinella/GIVOM trial. Ann Surg 2008; 247:207-213.
7. Hirche C, Murawa D, Mohr Z, et al. ICG fluorescence-guided sentinel node biopsy for axillary nodal staging in breast cancer. Breast Cancer Res Treat 2010.
8. Hojo T, Nagao T, Kikuyama M, et al. Evaluation of sentinel node biopsy by combined fluorescent and dye method and lymph flow for breast cancer. Breast 2010.
9. Kitai T, Inomoto T, Miwa M, et al. Fluorescence navigation with indocyanine green for detecting sentinel lymph nodes in breast cancer. Breast Cancer 2005; 12:211-215.
10. Murawa D, Hirche C, Dresel S, et al. Sentinel lymph node biopsy in breast cancer guided by indocyanine green fluorescence. Br J Surg 2009; 96:1289-1294.
11. Sevick-Muraca EM, Sharma R, Rasmussen JC, et al. Imaging of lymph flow in breast cancer patients after microdose administration of a near-infrared fluorophore: feasibility study. Radiology 2008; 246:734-741.
12. Tagaya N, Yamazaki R, Nakagawa A, et al. Intraoperative identification of sentinel lymph nodes by near-infrared fluorescence imaging in patients with breast cancer. Am J Surg 2008; 195:850-853.
13. Tanaka E, Chen FY, Flaumenhaft R, et al. Real-time assessment of cardiac perfusion, coronary angiography, and acute intravascular thrombi using dual-channel near-infrared fluorescence imaging. J Thorac Cardiovasc Surg 2009; 138:133-140.
14. Troyan SL, Kianzad V, Gibbs-Strauss SL, et al. The FLARE intraoperative near-infrared fluorescence imaging system: a first-in-human clinical trial in breast cancer sentinel lymph node mapping. Ann Surg Oncol 2009; 16:2943-2952.
15. Ohnishi S, Lomnes SJ, Laurence RG, et al. Organic alternatives to quantum dots for intraoperative near-infrared fluorescent sentinel lymph node mapping. Mol.Imaging 2005; 4:172-181.
16. Gioux S, Kianzad V, Ciocan R, et al. High-power, computer-controlled, light-emitting diode-based light sources for fluorescence imaging and image-guided surgery. Mol Imaging 2009; 8:156-65.
17. Gioux S, Choi HS, Frangioni JV. Image-guided surgery using invisible near-infrared light: fundamentals of clinical translation. Mol.Imaging 2010; 9:237-255.
18. Kusano M, Tajima Y, Yamazaki K, et al. Sentinel node mapping guided by indocyanine green fluorescence imaging: a new method for sentinel node navigation surgery in gastrointestinal cancer. Dig Surg 2008; 25:103-8.
19. Yamashita S, Tokuishi K, Anami K, et al. Video-assisted thoracoscopic indocyanine green fluorescence imaging system shows sentinel lymph nodes in non-small-cell lung cancer. J Thorac Cardiovasc Surg 2011; 141:141-4.

# Chapter 7

# Randomized, double-blind comparison of indocyanine green with or without albumin premixing for near-infrared fluorescence imaging of sentinel lymph nodes in breast cancer patients

Hutteman M[1], Mieog JSD[1], van der Vorst JR, Liefers GJ, Putter H, Löwik CWGM, Frangioni JV, van de Velde CJH, Vahrmeijer AL

[1] Shared first authorship

*Breast Cancer Res Treat 2011; 127:163-70.*

## ABSTRACT

Near-infrared (NIR) fluorescence imaging has the potential to improve sentinel lymph node (SLN) mapping in breast cancer. Indocyanine green (ICG) is currently the only clinically available fluorophore that can be used for SLN mapping. Preclinically, ICG adsorbed to human serum albumin (ICG:HSA) improves its performance as a lymphatic tracer in some anatomical sites. The benefit of ICG:HSA for SLN mapping of breast cancer has not yet been assessed in a clinical trial. We performed a double-blind, randomized study to determine if ICG:HSA has advantages over ICG alone. The primary endpoint was the fluorescence brightness, defined as the signal-to-background ratio (SBR), of identified SLNs. Clinical trial subjects were 18 consecutive breast cancer patients scheduled to undergo SLN biopsy. All patients received standard of care using $^{99m}$Technetium-nanocolloid and patent blue. Patients were randomly assigned to receive 1.6 mL of 500 μM ICG:HSA or ICG that was injected periareolarly directly after patent blue. The Mini-Fluorescence-Assisted Resection and Exploration (Mini-FLARE) imaging system was used for NIR fluorescence detection and quantitation. SLN mapping was successful in all patients. Patient, tumor and treatment characteristics were equally distributed over the treatment groups. No significant difference was found in SBR between the ICG:HSA group and the ICG alone group (8.4 vs. 11.3, respectively, $P = 0.18$). In both groups, the average number of detected SLNs was 1.4 ± 0.5 SLNs per patient ($P = 0.74$). This study shows that there is no direct benefit of premixing ICG with HSA prior to injection for SLN mapping in breast cancer patients, thereby reducing the cost and complexity of the procedure. With these optimized parameters that eliminate the necessity of HSA, larger trials can now be performed to determine patient benefit.

## INTRODUCTION

Sentinel lymph node (SLN) mapping is currently regarded as standard of care in staging of the axilla in breast cancer patients with clinically negative axillary lymph nodes.[1] In general, a combination of radioactive colloid and blue dye is used for SLN mapping. Using this combination, identification rates of 95% to 97% are achieved.[2-5] The use of only one of these two detection methods results in significantly lower identification rates.[2-5] Both detection methods possess certain disadvantages. Radioactive colloids require involvement of a nuclear medicine physician, can be difficult to localize with a handheld gamma probe, and the time-window for SLN identification is limited due to the short half-life (6 hours) of $^{99m}$Technetium. Blue dyes cannot be seen through skin and fatty tissue, and permit only limited visualization of afferent lymphatic vessels and the SLN.

Optical imaging using the near-infrared (NIR) fluorescence lymphatic tracer indocyanine green (ICG) enables real-time transcutaneous and intraoperative visualization of lymphatic channels and SLNs.[6-13] Therefore, NIR fluorescence imaging could provide an alternative for, or an addition to, conventional techniques used for SLN mapping. Recently, our group has demonstrated that NIR fluorescence performed equally well as the combination of radioactive colloid and blue dye in SLN mapping of breast cancer patients.[14]

ICG is currently the only clinically available NIR lymphatic tracer. However, due to its relatively low fluorescence brightness and its small hydrodynamic diameter, which permits flow through the SLN to higher tier nodes, it is not an optimal lymphatic tracer. Preclinical work has demonstrated that adsorption of ICG to human serum albumin (HSA, complex is ICG:HSA), by simply mixing it, increases the fluorescence intensity and the hydrodynamic diameter, thereby providing improved detection and better retention in the SLN in certain anatomical sites, such as the intestine.[15] Another parameter that must be considered when using ICG or ICG:HSA is the effect of fluorescence quenching, which results in a decrease in fluorescence intensity as the concentration of ICG (or ICG:HSA) is increased above 50 μM. The use of 50 μM ICG for SLN imaging, however, is suboptimal, because ICG will be diluted once taken up by the lymphatic system. To assess the magnitude of this *in vivo* dilution effect, our group has conducted a dose-finding study to demonstrate that the optimal concentration of ICG:HSA for NIR-based SLN mapping in breast cancer patients lies between 400 μM and 800 μM.[14]

A theoretical disadvantage of the use of ICG alone is poor retention of the lymphatic tracer in the SLN, which as a consequence results in fluorescent staining of higher tier nodes and background staining of the axilla. Although not compared directly, studies using ICG alone reported a higher average number of identified SLNs (range = 1.8-5.4; aggregate average = 3.4),[6-10] than with the use of ICG:HSA (aggregate: 1.5).[11, 14] However, comparison of these data is difficult because the concentration of

ICG used was significantly higher (typically 6.4 mM) than in the trials using ICG:HSA (10 μM to 1000 μM).

Although we have obtained good results with the use of ICG:HSA for SLN mapping in breast cancer patients, the use of albumin adds cost and complexity to the procedure. Moreover, the use of human blood products, such as HSA, poses regulatory hurdles in certain countries, such as the United States. Therefore, the use of ICG alone would be favorable. After intravenous administration, ICG binds rapidly and completely to plasma proteins.[16] Lymph fluid has a similar protein constitution as serum, albeit in a lower concentration (20.6 g/L for lymph fluid versus 73.7 g/L for plasma).[17] After intradermal or subcutaneous injection, ICG could theoretically bind to these proteins, eliminating the need for premixing ICG and HSA. We therefore hypothesized that ICG alone could render the same fluorescence intensity in SLNs as ICG:HSA, and tested this hypothesis in a double-blind randomized trial.

## MATERIALS AND METHODS

### Preparation of Indocyanine Green adsorbed to Human Serum Albumin

ICG (25 mg vials) was purchased from Pulsion Medical Systems (Munich, Germany) and was resuspended in 10 cc of sterile water for injection to yield a 2.5 mg/ml (3.2 mM) stock solution. To obtain a 500 μM dilution, 7.8 mL of the 3.2 mM ICG solution was diluted in 50 cc vial of sterile water for injection or 50 cc vial of Cealb (20% human serum albumin, Sanquin, Amsterdam, The Netherlands) for the preparation of ICG alone or ICG:HSA, respectively. Prior to the addition of ICG, 7.8 mL was drawn from the 50 cc vials. In a previous study, we determined that the optimal dose of ICG:HSA lies between 400 μM and 800 μM.[14] A dose of 500 μM was chosen because it requires minimal manipulation of ICG and albumin volumes.

### Intraoperative Near-Infrared Imaging System (Mini-FLARE)

SLN mapping was performed using the Mini-Fluorescence-Assisted Resection and Exploration (Mini-FLARE) image-guided surgery system as in Chapter 6. Briefly, the system consists of two wavelength isolated light sources: a "white" light source, generating 26,600 lx of 400-650 nm light, and a "near-infrared" light source, generating 7.7 mW/cm$^2$ of 760 nm light. Color video and NIR fluorescence images are simultaneously acquired and displayed in real-time using custom optics and software that separate the color video and NIR fluorescence images. A pseudo-colored (lime green) merged image of the color video and NIR fluorescence images is also displayed. The imaging head is attached to a flexible gooseneck arm, which permits positioning

of the imaging head at extreme angles virtually anywhere over the surgical field. For intraoperative use, the imaging head and imaging system pole stand are wrapped in a sterile shield and drape (Medical Technique Inc., Tucson, USA).

**Clinical Trial**

The double-blind, randomized, single-institution, non-inferiority trial comparing ICG:HSA with ICG alone was approved by the Medical Ethics Committee of the Leiden University Medical Center and was performed in accordance with the ethical standards of the Helsinki Declaration of 1975. All patients planning to undergo a sentinel lymph node procedure whether for invasive breast cancer or for high-risk carcinoma *in situ* were eligible for participation in the study. Patients had clinically negative axillary nodes as assessed by palpation and ultrasonography. Exclusion criteria were pregnancy, lactation or an allergy to iodine, shellfish, or indocyanine green.

All patients gave informed consent and were anonymized. Patients were randomized by the Department of Clinical Pharmacy. Treatment allocation was performed by block randomization. Patients received the standard-of-care sentinel lymph node procedure. For our institution, this implies one periareolar injection of approximately 100 MBq $^{99m}$Technetium-nanocolloid (mean ± S.D. = 96.6 ± 14.7 MBq, no difference between treatment groups [$P$ = 0.47]) the day before surgery. Before the start of the operation, one mL of patent blue V was injected. Directly after patent blue injection, the surgeon injected a total of 1.6 mL of 500 μM ICG:HSA or ICG alone. Both dyes were injected intradermally and periareolarly at four sites. Gentle pumping pressure was applied to the injection site for 1 min. After surgical scrub and sterile covering of the operation field, NIR fluorescence imaging was performed with the imaging head of the Mini-FLARE at approximately 30 cm distance to the surgical field. Camera exposure times were between 5 to 200 msec. A SLN exhibiting a signal-to-background ratio (SBR) ≥ 1.1 *in situ* was considered positive by NIR fluorescence. Both the surgeon and the Mini-FLARE operator, who was responsible for analyzing the data, were blinded to the treatment allocation.

Routine histopathological frozen analysis of SLNs was performed during surgery. SLNs were fixed in formalin and embedded in paraffin for routine hematoxylin and eosin staining and immunohistopathological staining for AE1/AE3 at three levels, with an interval of 150 to 250 μm, according to the Dutch guidelines for SLN analysis. Patients underwent an axillary lymph node dissection if the SLN was found to contain metastases. If isolated tumor cells were found (< 0.2 mm), no axillary lymph node dissection was performed.

### Power Calculation and Statistical Analysis

A power calculation based on data from our previous study[14] revealed that 18 patients are needed to achieve 91% power to detect non-inferiority using a one-sided, two-sample t-test ($\alpha = 0.025$) with a margin of equivalence of 5.0 while assuming no difference between the SBRs of ICG:HSA and ICG alone. For statistical analysis, SPSS statistical software package (Version 16.0, Chicago, USA) was used. Graphs were generated using GraphPad Prism Software (Version 5.01, La Jolla, USA). To compare the SBR and the number of SLNs identified between ICG:HSA and ICG alone, a one-sided, two-sample t-test was performed. $P < 0.05$ was considered significant.

## RESULTS

Eighteen consecutive breast cancer patients undergoing standard-of-care SLN mapping were randomized to ICG:HSA or ICG alone for the NIR-based SLN imaging. Patient, tumor, and treatment characteristics were equally distributed over the treatment groups (Table 1). Use of the Mini-FLARE during surgery did not interfere with the standard of care. Average time between lymphatic tracer injection and skin incision was 15.6 ± 2.2 minutes (Table 2). In all patients (N = 18), NIR fluorescence imaging enabled visualization of one or more SLNs (Figure 1). In the ICG:HSA group (N = 8 subjects), a total of 11 SLNs were identified (average per patient = 1.4 ± 0.5); 9 (82%) were radioactive, 8 (73%) were blue and 11 (100%) were NIR fluorescent. In the ICG alone group (N = 10 subjects), a total of 14 SLNs were identified (average per patient = 1.4 ± 0.5); 14 (100%) were radioactive, 10 (71%) were blue and 14 (100%) were NIR fluorescent. The average number of SLNs identified was not significantly different between both groups ($P = 0.74$).

The primary endpoint of this study was the average brightness of the SLN in both groups, expressed in signal-to-background ratio (SBR). The results are presented in Table 2. The average SBR of ICG:HSA (8.4 ± 3.6) and ICG alone (11.3 ± 4.8) was not significantly different ($P = 0.18$). However, in the ICG alone group, the afferent lymphatics were significantly better visualized percutaneously compared to the ICG:HSA group ($P = 0.004$; Table 2 and Figure 1).

In all patients, the NIR fluorescence signal in the SLN was detected earlier in the procedure before patent blue was visualized. Average time between skin incision and resection of the first SLN was 11.0 ± 4.1 minutes and was not different between both groups (t-test, $P = 0.74$). No adverse reactions associated with the use of ICG, ICG:HSA, or Mini-FLARE occurred.

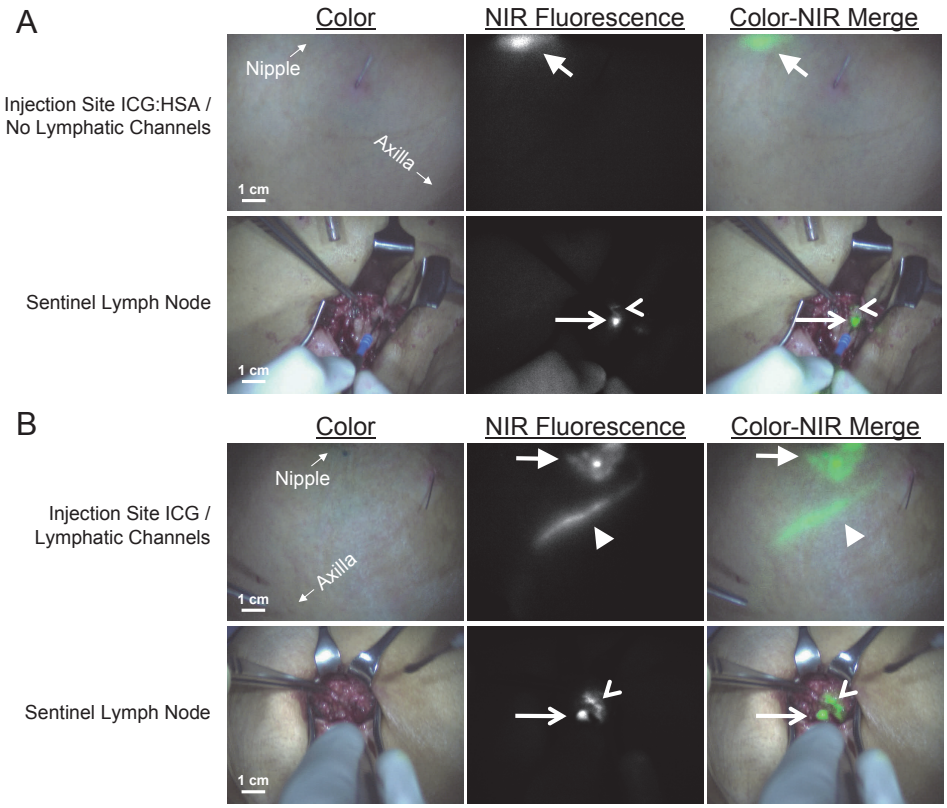


**Figure 1. NIR fluorescence imaging during sentinel lymph node mapping in breast cancer patients: A.** ICG:HSA. In the upper panel, the periareolar injection site (arrow) is shown, but percutaneously, no lymphatic channel can be visualized. In the lower panel, identification of the SLN (arrow) and an afferent lymphatic channel (open arrowhead) with NIR fluorescence imaging is demonstrated 27 min after injection of 1.6 mL of 500 μM ICG:HSA. Camera exposure times were 60 msec (top row) and 150 msec (bottom row). Scale bars represent 1 cm. **B.** ICG alone. In the upper panel, the periareolar injection site (arrow) and a lymphatic channel (arrowhead) are clearly visualized. In the lower panel, identification of the SLN (arrow) and an afferent lymphatic channel (open arrowhead) with NIR fluorescence imaging is demonstrated 28 min after injection of 1.6 mL of 500 μM ICG. Camera exposure times were 30 msec (top row) and 100 msec (bottom row). Scale bars represent 1 cm.

## DISCUSSION

The use of NIR fluorescence for SLN mapping has several advantages over conventional methods, such as better tissue penetration when compared to blue dyes, and lack of ionizing radiation and real-time visualization when compared to radiotracers. A number of clinical studies have been published on the use of NIR fluorescence in the SLN procedure in breast cancer, all of which use ICG, which is currently clinically available.[6, 9, 11, 12, 14] Preclinical studies indicated that adsorption of ICG to human serum albumin (HSA, complex is ICG:HSA), by simply mixing it, increases the fluorescence intensity and the hydrodynamic diameter, thereby providing improved detection and better retention in the SLN.[15] Our group has subsequently conducted a dose-finding

**Table 1.** Patient and Tumor Characteristics

| | ICG:HSA (N = 8) | | ICG alone (N = 10) | | |
|---|---|---|---|---|---|
| **Characteristic** | **N** | **%** | **N** | **%** | **P** |
| Age (Median, Range) | 59.5 (38-72) | | 57.5 (40-73) | | 0.99 |
| Menopausal State | | | | | 0.74 |
| - Premenopausal | 3 | 37.5 | 3 | 30 | |
| - Postmenopausal | 5 | 62.5 | 7 | 70 | |
| Body Mass Index (median, range) | 26 (20-41) | | 23.5 (21-30) | | 0.26 |
| Skin Type | | | | | 0.40 |
| - II | 2 | 25 | 1 | 10 | |
| - III | 6 | 75 | 9 | 90 | |
| Previous Procedure of Breast | | | | | 0.12 |
| - Breast Implants | 1 | | 0 | | |
| - Breast Reduction | 0 | | 1 | | |
| - Lumpectomy | 2 | | 0 | | |
| - Radiotherapy | 0 | | 1 | | |
| - Neoadjuvant Chemotherapy | 1 | | 0 | | |
| Multifocality | 0 | | 0 | | 1.00 |
| Tumor side | | | | | 0.81 |
| - Left | 2 | 25 | 3 | 30 | |
| - Right | 6 | 75 | 7 | 70 | |
| Tumor localization | | | | | 0.23 |
| - Upper Outer | 6 | 75 | 4 | 40 | |
| - Lower Outer | 0 | 0 | 1 | 10 | |
| - Lower Medial | 1 | 12.5 | 2 | 20 | |
| - Upper Medial | 0 | 0 | 3 | 30 | |
| - Central | 1 | 12.5 | 0 | 0 | |
| Type of Operation | | | | | 0.15 |
| - Mastectomy | 3 | 37.5 | 1 | 10 | |
| - Wide Local Excision | 4 | 50 | 9 | 90 | |
| - SNB Only | 1 | 12.5 | 0 | 0 | |
| Pathological Tumor Size (Median, Range) | 7 (5-11) | | 12 (8-15) | | 0.13 |
| Histological Type | | | | | 0.62 |
| - Infiltrating Ductal Adenocarcinoma | 7 | 87.5 | 7 | 70 | |
| - Infiltrating Lobular Adenocarcinoma | 0 | 0 | 1 | 10 | |
| - Ductal Carcinoma In Situ | 1 | 12.5 | 1 | 10 | |
| - Other | 0 | 0 | 1 | 10 | |
| Histological Grade | | | | | 0.15 |
| - I | 1 | 16.7 | 3 | 33.3 | |
| - II | 2 | 33.3 | 5 | 55.6 | |
| - III | 3 | 50 | 1 | 11.1 | |

Abbreviations: ICG:HSA = indocyanine green adsorbed to human serum albumin Skin type = American Academy of Dermatology Skin Types I-VI:
I. Pale, white skin: always burns easily; never tans (Celtic, Scandinavian, and infants)
II. White: usually burns easily; tans minimally (Northern European)
III. White (average): sometimes burns; tans gradually to light brown (Central European)
IV. Beige or lightly tanned: burns minimally; always tans to moderately brown (Mediterranean, Asian)
V. Moderate brown or tanned: rarely burns; tans well (South American, Indian, Native American)
VI. Dark brown or black: never burns; deeply pigmented (African, African-American, Aborigine)

**Table 2.** SLN Identification Results

| Characteristic | Total (18 Subjects) N | % | ICG:HSA (8 Subjects) N | % | ICG alone (10 Subjects) N | % | P |
|---|---|---|---|---|---|---|---|
| Number of SLNs Identified | 25 | | 11 | | 14 | | |
| Number of SLNs Identified per Patient | | | | | | | 0.91 |
| - One SLN | 11 | 61 | 5 | 63 | 6 | 60 | |
| - Two SLNs | 7 | 39 | 3 | 37 | 4 | 40 | |
| Average Number of SLNs Identified ± S.D. | 1.4 ± 0.5 | | 1.4 ± 0.5 | | 1.4 ± 0.5 | | 0.92 |
| Method of Detection | | | | | | | |
| - Radioactive | 23 | 92 | 9 | 82 | 14 | 100 | 0.18 |
| - Blue | 18 | 72 | 8 | 73 | 10 | 71 | 1.00 |
| - NIR Fluorescent | 25 | 100 | 11 | 100 | 14 | 100 | 1.00 |
| Signal-to-Background Ratio | 10.0 ± 4.4 | | 8.4 ± 3.6 | | 11.3 ± 4.8 | | 0.18 |
| Percutaneous NIR Fluorescent Lymph Drainage Visualization | | | | | | | 0.004 |
| - Yes | 10 | 56 | 1 | 13 | 9 | 90 | |
| - Partially[a] | 3 | 17 | 3 | 38 | 0 | 0 | |
| - No | 5 | 28 | 4 | 50 | 1 | 10 | |
| Average Time between Injection and Skin Incision ± S.D. (minutes) | 15.6 ± 2.2 | | 15.3 ± 1.7 | | 15.9 ± 2.6 | | 0.55 |
| Average Time between Skin Incision and SLN Resection ± S.D. (minutes) | 11.0 ± 4.1 | | 10.6 ± 5.1 | | 11.3 ± 3.3 | | 0.74 |
| Histology | | | | | | | 0.44 |
| - Negative | 24 | 96 | 10 | 91 | 14 | 100 | |
| - Isolated Tumor Cells | 1 | 4 | 1 | 9 | 0 | 0 | |
| - Macrometastases | 0 | 0 | 0 | 0 | 0 | 0 | |
| Axillary Lymph Node Dissection | | | | | | | 1.00 |
| - No | 18 | 100 | 8 | 100 | 10 | 100 | |
| - Yes | 0 | 0 | 0 | 0 | 0 | 0 | |

Abbreviations: ICG:HSA = indocyanine green adsorbed to human serum albumin; S.D. = standard deviation; SLN = sentinel lymph node.
[a] Partial percutaneous visualization was noted when lymphatic channels could be visualized percutaneously from the injection site, but did not reach the axilla.

study and demonstrated that the optimal concentration of ICG:HSA for NIR-based SLN mapping in breast cancer patients lies between 400 μM and 800 μM.[14] Indeed, above 800 μM ICG:HSA, the fluorescent intensity dropped due to quenching. Based on these results a concentration of 500 μM ICG:HSA, which requires minimal manipulation of albumin volumes and uses only one vial of ICG, was chosen for further studies to identify whether premixing with albumin indeed increases the fluorescent intensity of the node in a clinical setting. In the current study, SLN mapping after ICG or ICG:HSA injection was successful in all patients. ICG showed a comparable or even slightly increased (though not significantly) brightness than ICG:HSA while identifying an equal average number of SLNs. Although no macrometastases in the SLNs were

observed in the current study, our previous study showed that tumor-positive SLNs were also detected by NIR fluorescence, signifying ICG uptake.[14] However, lymph node macrometastases continue to be a contraindication for SLN mapping and preoperative staging of the axilla remains pivotal to minimize false negatives.

The results of our study are discordant with preclinical work in intestine, which suggested an improvement in fluorescent brightness and retention in the SLN by premixing ICG with HSA.[15] Although the current study was powered to determine non-inferiority in SBR of ICG alone when compared to ICG:HSA, it was not formally powered to assess the secondary endpoint, average number of SLNs identified. However, power analysis using data from our previous study[14] demonstrated that a difference of at least one additional SLN identified per patient could be detected with 90% power with the current sample size. The discrepancy between the current clinical results and these preclinical experiments could be caused by the increased distance that the injected dye has to travel, as the preclinical studies were performed in the bowel of healthy pigs.[15] Lymph fluid contains a high concentration of albumin, among other proteins; therefore, a longer traveling distance could aid ICG in adsorbing to albumin or other proteins, as it would after intravenous injection,[18] diminishing the need for premixing ICG with HSA. This observation implies that premixing might prove to be useful in other cancer types (such as colon cancer, for example), where ICG is less likely to completely adsorb to proteins before the SLN is reached. Therefore, the use of ICG:HSA or ICG alone should be tested for every anatomical site.

Although the fluorescent brightness did not differ significantly between both groups, ICG alone showed significantly improved percutaneous visibility of lymphatic channels when compared to ICG:HSA (Figure 1). It has been shown that in plasma, ICG preferably binds to $\alpha_1$-lipoprotein and γ-globulin, despite the higher concentration of albumin.[19] Previous experiments have shown a higher increase in quantum yield when ICG is mixed with serum, in comparison to HSA.[15] Therefore, the observed differences in visualization of lymphatics could likely be attributable to the protein constitution of lymph fluid. The high albumin content (20%) of ICG:HSA could also be a contributing factor, as the increased hydrodynamic diameter and higher viscosity could diminish ICG uptake in lymphatic channels. It should be noted that the anatomical variation (amount of tissue overlying the lymphatic channels) is also a major influencing factor and may be primarily responsible for the observed difference.

An optimal lymphatic tracer is non-toxic, has a high quantum yield (i.e., brightness), migrates quickly to the SLN, and does not migrate to higher tier nodes. If a tracer migrates to higher tier nodes, non-sentinel lymph nodes could incorrectly be identified as SLNs, causing more nodes than necessary to be resected. ICG is far from optimal; in aqueous solution the quantum yield is relatively low and due to its small hydrodynamic diameter, it can flow to higher tier nodes, as is the case with blue dyes. The synthesis and clinical introduction of an optimal probe will be the subject of

future studies and will greatly help to confirm the clinical benefit of NIR fluorescence imaging in the SLN procedure.[15, 20]

In the current study, NIR fluorescence after ICG injection could consistently be visualized before the blue dye could be observed, which is consistent with earlier findings.[14] Therefore, NIR fluorescence imaging has the potential to replace blue dyes in SLN mapping of breast cancer patients. Furthermore, as NIR fluorescence light penetrates relatively deep into tissue, it can potentially replace radiocolloids in SLN mapping in a selected group of patients, for example those with a low body mass index. A clinical trial on omitting blue dyes and using NIR fluorescence without the need for radiocolloids is currently ongoing (NTR2674).

In conclusion, this double-blind, randomized trial showed no advantage of ICG:HSA in comparison to ICG alone for the SLN procedure. To reduce the cost and complexity of the procedure, a dose of 500 μM ICG alone (1.6 ml) is recommended for NIR fluorescence SLN mapping in breast cancer patients. Therefore, this study has determined the optimal parameters that can be used to validate this technique in a larger series in order to investigate patient benefit.

## ACKNOWLEDGEMENTS

We thank the following individuals for the contribution to this study: Gemma Ranke, Elly Krol-Warmerdam, Annemarie Voet-van den Brink, Gerlinda van Gent-de Bruijn (Breast Cancer Unit) and Linda van der Hulst (Central Pharmacy). We thank Lindsey Gendall for editing. This work was supported in part by NIH grants R01-CA-115296 and R21-CA-130297, the Dutch Cancer Society grant UL2010-4732, the Nuts Ohra Fund, the "Maurits and Anna de Kock" Foundation and the American Women's Club of The Hague. J.S.D. Mieog is a MD-medical research trainee funded by The Netherlands Organisation for Health Research and Development (grant nr. 92003526).

## REFERENCES


1. Cox CE, Pendas S, Cox JM, et al. Guidelines for sentinel node biopsy and lymphatic mapping of patients with breast cancer. Ann Surg 1998; 227:645-651.
2. Goyal A, Newcombe RG, Chhabra A, et al. Factors affecting failed localisation and false-negative rates of sentinel node biopsy in breast cancer--results of the ALMANAC validation phase. Breast Cancer Res Treat 2006; 99:203-208.
3. Krag DN, Anderson SJ, Julian TB, et al. Technical outcomes of sentinel-lymph-node resection and conventional axillary-lymph-node dissection in patients with clinically node-negative breast cancer: results from the NSABP B-32 randomised phase III trial. Lancet Oncol. 2007; 8:881-888.
4. Zavagno G, De Salvo GL, Scalco G, et al. A Randomized clinical trial on sentinel lymph node biopsy versus axillary lymph node dissection in breast cancer: results of the Sentinella/GIVOM trial. Ann Surg 2008; 247:207-213.
5. Straver ME, Meijnen P, van Tienhoven G, et al. Sentinel Node Identification Rate and Nodal Involvement in the EORTC 10981-22023 AMAROS Trial. Ann Surg Oncol 2010.
6. Kitai T, Inomoto T, Miwa M, et al. Fluorescence navigation with indocyanine green for detecting sentinel lymph nodes in breast cancer. Breast Cancer 2005; 12:211-215.
7. Murawa D, Hirche C, Dresel S, et al. Sentinel lymph node biopsy in breast cancer guided by indocyanine green fluorescence. Br J Surg 2009; 96:1289-1294.
8. Tagaya N, Yamazaki R, Nakagawa A, et al. Intraoperative identification of sentinel lymph nodes by near-infrared fluorescence imaging in patients with breast cancer. Am J Surg 2008; 195:850-853.
9. Hirche C, Murawa D, Mohr Z, et al. ICG fluorescence-guided sentinel node biopsy for axillary nodal staging in breast cancer. Breast Cancer Res Treat 2010.
10. Hojo T, Nagao T, Kikuyama M, et al. Evaluation of sentinel node biopsy by combined fluorescent and dye method and lymph flow for breast cancer. Breast 2010.
11. Troyan SL, Kianzad V, Gibbs-Strauss SL, et al. The FLARE intraoperative near-infrared fluorescence imaging system: a first-in-human clinical trial in breast cancer sentinel lymph node mapping. Ann Surg Oncol 2009; 16:2943-2952.
12. Sevick-Muraca EM, Sharma R, Rasmussen JC, et al. Imaging of lymph flow in breast cancer patients after microdose administration of a near-infrared fluorophore: feasibility study. Radiology 2008; 246:734-741.
13. Tanaka E, Choi HS, Fujii H, et al. Image-guided oncologic surgery using invisible light: completed pre-clinical development for sentinel lymph node mapping. Ann Surg Oncol 2006; 13:1671-1681.
14. Mieog JS, Troyan SL, Hutteman M, et al. Towards Optimization of Imaging System and Lymphatic Tracer for Near-Infrared Fluorescent Sentinel Lymph Node Mapping in Breast Cancer. Ann Surg Oncol 2011.
15. Ohnishi S, Lomnes SJ, Laurence RG, et al. Organic alternatives to quantum dots for intraoperative near-infrared fluorescent sentinel lymph node mapping. Mol.Imaging 2005; 4:172-181.
16. Cherrick GR, Stein SW, Leevy CM, et al. Indocyanine green: observations on its physical properties, plasma decay, and hepatic extraction. J.Clin.Invest 1960; 39:592-600.
17. Fogh-Andersen N, Altura BM, Altura BT, et al. Composition of interstitial fluid. Clin Chem 1995; 41:1522-1525.
18. Moody ED, Viskari PJ, Colyer CL. Non-covalent labeling of human serum albumin with indocyanine green: a study by capillary electrophoresis with diode laser-induced fluorescence detection. J.Chromatogr.B Biomed.Sci.Appl. 1999; 729:55-64.
19. Sauda K, Imasaka T, Ishibashi N. Determination of protein in human serum by high-performance liquid chromatography with semiconductor laser fluorometric detection. Anal Chem 1986; 58:2649-2653.
20. Hutteman M, Choi HS, Mieog JS, et al. Clinical Translation of Ex Vivo Sentinel Lymph Node Mapping for Colorectal Cancer Using Invisible Near-Infrared Fluorescence Light. Ann Surg Oncol 2010.

# Chapter 8

# Optimization of near-infrared fluorescent sentinel lymph node mapping in cervical cancer patients

van der Vorst JR[1], Hutteman M[1], Gaarenstroom KN, Peters AAW, Mieog JSD, Schaafsma BE, Kuppen PJK, Frangioni JV, van de Velde CJH, Vahrmeijer AL

[1] Shared first authorship

*Int J Gynecol Cancer 2011; In press.*

# ABSTRACT

## Objective

In early cervical cancer, a total pelvic lymphadenectomy is the standard of care even though most patients have negative nodes and thus undergo lymphadenectomy unnecessarily. Although the value of sentinel lymph node mapping in early stage cervical cancer has not yet been established, near-infrared (NIR) fluorescence imaging is a promising technique to perform this procedure. NIR fluorescence imaging is based on invisible NIR light and can provide high sensitivity, high-resolution, and real-time image-guidance during surgery.

## Methods/materials

Clinical trial subjects were 9 consecutive cervical cancer patients undergoing total pelvic lymphadenectomy. Prior to surgery, 1.6 mL of indocyanine green adsorbed to human serum albumin (ICG:HSA) was injected transvaginally and submucosally in 4 quadrants around the tumor. Patients were allocated to 500, 750, or 1,000 μM ICG:HSA concentration groups. The Mini-FLARE™ imaging system was used for NIR fluorescence detection and quantitation.

## Results

Sentinel lymph nodes were identified in all 9 patients. An average of 3.4 ± 1.2 sentinel lymph nodes was identified per patient. No differences in signal to background of the sentinel lymph nodes between the 500, 750, and 1,000 μM dose groups were found ($P = 0.73$). In 2 patients, tumor-positive lymph nodes were found. In both patients, tumor-positive lymph nodes confirmed by pathology were also NIR fluorescent.

## Conclusions

This study demonstrated preliminary feasibility to successfully detect sentinel lymph nodes in cervical cancer patients using ICG:HSA and the Mini-FLARE™ imaging system. When considering safety, cost-effectiveness, and pharmacy preferences, an ICG:HSA concentration of 500 μM was optimal for sentinel lymph node mapping in cervical cancer patients.

## INTRODUCTION

Approximately 11,000 women are diagnosed with cervical cancer annually in the United States, resulting in over 4,000 deaths per year.[1] Cervical cancer is also the most common cause of cancer-related death in women in developing countries.[2] The prognosis of cervical cancer patients depends on tumor stage and tumor size, but nodal status remains the single most important prognostic factor. The surgical treatment of invasive cervical cancer depends upon the FIGO stage of the patient at time of diagnosis.[3] In early stage cervical cancer, a radical hysterectomy is performed in combination with a bilateral pelvic lymphadenectomy to detect lymphatic spread. Nodal tumor involvement occurs in up to 27% of early stage cervical cancer patients[4] and in these patients, radiotherapy or chemoradiation is the primary treatment of choice.[5] Therefore, a total lymphadenectomy is performed unnecessarily in a substantial fraction of patients, exposing them to the risk of lymphedema and surgical injuries.

SLN mapping and biopsy is an accepted procedure for vulvar cancer, cutaneous melanomas, and breast cancer; however, its reliability for clinical use in the treatment of early stage cervical cancer has not yet been established.[6, 7] Research on the use of the SLN procedure in early stage cervical cancer patients has been extensively described using a blue dye, a radiocolloid such as $^{99m}$Technetium ($^{99m}$Tc), or a combination of both with various results.[8, 9] Van de Lande et al. published a literature review involving over 800 patients with cervical cancer in which they described detection rates of 84%, 88%, and 97% when using blue dye alone, $^{99m}$Tc alone, or a combination of both, respectively.[10] Regarding the sensitivity to detect the SLNs, $^{99m}$Tc, alone or in combination with blue dye, yielded the highest pooled sensitivity (92%, range 79%-98%); however, this was not significantly higher than the pooled sensitivity of blue dye alone (82%, range 67%-92%).

Due to the midline position of the cervix, it often has a bilateral multifarious drainage pattern, which makes the SLN procedure in cervical cancer patients more challenging than in breast cancer patients, for example. The main lymphatic drainage patterns have been described previously,[11] and several studies have shown that satisfactory SLN detection in cervical cancer is established when SLNs are detected on both sides of the pelvis. Of note, status of a SLN on one side of the pelvis does not predict the nodal status of the other side.[12]

NIR fluorescence imaging is a technique that can be used in real time during surgery. This technique uses invisible near-infrared light that can be visualized using specialized camera systems.[13] NIR fluorescence imaging has several advantages, such as relatively high tissue penetration (up to 5 millimeters without special techniques), low autofluorescence, and the lack of ionizing radiation.[14] Recent preclinical and clinical studies have demonstrated that near-infrared (NIR) fluorescence imaging using the NIR fluorescence agent indocyanine green (ICG) enables real-time intraoperative visualization of lymphatic channels and detection of the SLNs in various forms of

cancer without the need for radioactivity.[15] Furthermore, previous preclinical work has demonstrated that adsorption of ICG to human serum albumin (HSA, complex is ICG:HSA) increases the fluorescence intensity and the hydrodynamic diameter, thereby providing improved detection and better retention in the SLN.[16]

Crane et al. recently described that the use of NIR fluorescence imaging in cervical cancer patients is technically feasible.[17] ICG was injected after laparotomy. In this pilot study, a detection rate of 60% was reached, bilateral SLNs were detected in 30% of patients and 1 of 2 patients who had nodal involvement was false-negative.

The aim of the current study was to assess the intraoperative use of NIR fluorescence imaging using ICG:HSA and the Mini-FLARE™ imaging system in SLN biopsy in cervical cancer patients. A secondary goal was to optimize the dose of the ICG:HSA NIR fluorescent lymphatic tracer.

## MATERIALS AND METHODS

### Preparation of Indocyanine Green Adsorbed to Human Serum Albumin

ICG (25 mg vials) was purchased from Pulsion Medical Systems (Munich, Germany) and was resuspended in 10 cc of sterile water for injection to yield a 2.5-mg/ml (3.2 mM) stock solution for the 500-μM concentration group. Of this solution, 7.8 cc was transferred to a 50- cc vial of Cealb (20% human serum albumin (HSA) solution; Sanquin, Amsterdam, The Netherlands) to yield ICG in HSA (ICG:HSA) at a final concentration of 500 μM. ICG (25 mg vials) was resuspended in 5 cc of sterile water for injection to yield a 5.0 mg/ml (6.4 mM) for the 750-μM and 1,000-μM concentration groups. Of this solution, 5.8 cc or 7.8 cc was transferred to a 50-cc vial of Cealb (20% human serum albumin (HSA) solution to yield ICG in HSA (ICG:HSA) at a final concentration of 750 μM or 1,000 μM, respectively.

### Intraoperative NIR Imaging System (Mini-FLARE™)

SLN mapping was performed using the Mini-FLARE™ image-guided surgery system as described in Chapter 6. Briefly, the system consists of 2 wavelength-isolated light sources: a "white" light source, generating 26,600 lx of 400-650 nm light and a "near-infrared" light source, generating 7.7 mW/cm$^2$ of 760 nm light. Color video and NIR fluorescence images are simultaneously acquired and displayed in real time using custom optics and software that separate the color video and NIR fluorescence images. A pseudo-colored (lime green) merged image of the color video and NIR fluorescence images is also displayed. The imaging head is attached to a flexible gooseneck arm, which permits positioning of the imaging head virtually anywhere over the surgical field, and at extreme angles. For intraoperative use, the imaging head and imaging

system pole stand are wrapped in a sterile shield and drape (Medical Technique Inc., Tucson, USA).

### Clinical Trial

The single-institution clinical trial was approved by the Medical Ethics Committee of the Leiden University Medical Center and was performed in accordance with the ethical standards of the Helsinki Declaration of 1975. A total of 9 consecutive patients with cervical cancer that planned to undergo a radical abdominal trachelectomy or a radical hysterectomy and a total pelvic lymphadenectomy were included. All patients provided informed consent and were anonymized. Exclusion criteria were pregnancy, lactation or an allergy to iodine, shellfish, or indocyanine green. All procedures were performed by 2 gynecologists who were assisted by experienced researchers. Before the start of surgery, 1.6 mL ICG:HSA (concentration: 500, 750 or 1,000 μM) was transvaginally injected submucosally in 4 quadrants around the cervical tumor using a 21G, 1½ inch needle. Directly after the ICG:HSA injection, surgical scrub and sterile covering of the operation field commenced, and a laparotomy was performed. Before the systematic pelvic lymphadenectomy was performed, all standard locations (along the external iliac vessels and the hypogastric artery, along the common iliac artery, the obturator fossa and the lateral parametrium) were examined for NIR fluorescence using the Mini-FLARE™ imaging system. Fluorescent hotspots exhibiting a signal-to-background ratio (SBR) ≥ 1.1 *in vivo* were considered positive by NIR fluorescence. All fluorescent hotspots were denominated as SLNs and were subsequently resected and measured for fluorescence *ex vivo*. Then, the systemic pelvic lymphadenectomy was performed and all resected LNs were also measured for fluorescence *ex vivo.* Lymphadenectomy consisted of removal of all lymph node-bearing fatty tissue along the external iliac vessels, the common iliac artery, the hypogastric artery, and from the obturator fossa.[18] Also, the area lateral to and underneath the superior vesical arteries (lateral parametrium) was cleared from the lymphatic tissue. The radical hysterectomy and abdominal trachelectomy were performed according to the standard procedure. In case of a radical trachelectomy, histopathological frozen analysis was performed and when nodes were found to contain metastases, a hysterectomy was performed in addition. Afterwards, all resected lymph nodes were examined by routine histopathological analysis, and lymph nodes were fixed in formalin and embedded in paraffin for routine hematoxylin and eosin staining. SLNs and non-SLNs were examined separately.

### Statistical Analysis

For statistical analysis and to generate graphs, GraphPad Prism Software (Version 5.01, La Jolla, USA) was used. Differences in SBR between concentration groups were tested

with a one-way analysis of variance (ANOVA) with subsequent pairwise comparisons corrected according to the Bonferroni correction. Assumption of equal variances was confirmed using Levene's test. All statistical tests were two-tailed and $P < 0.05$ was considered significant.

## RESULTS

### Patient and Tumor Characteristics

Patient and tumor characteristics are described in Table 1. Nine patients with stage Ib cervical cancer undergoing primary surgery were included in the study. Of these patients, median BMI was 21 (range 18-35), median age was 40 years (range 29-77 years), and median tumor size was 3.05 cm (range 0.7-11 cm). One patient presented with an exophytic cervical tumor measuring 11 cm in length and 4 cm in width protruding into the vagina. Five patients underwent a radical hysterectomy and 3 patients underwent a radical trachelectomy. In one patient, extensive endometriosis precluded radical hysterectomy. In this patient, the uterus was left in situ, but a pelvic lymphadenectomy was performed.

### Intraoperative NIR Fluorescence Imaging

In all patients (N = 9), NIR fluorescence imaging enabled identification of 1 or more fluorescent hotspots. An example of the NIR fluorescence images of the procedure in cervical cancer is shown in Figure 1. Average time between injection of ICG:HSA and NIR fluorescence imaging was 51 ± 18 min. A total of 31 fluorescent hotspots were detected. On average, 3.4 ± 1.2 (range 1-5) fluorescent hotspots per patient were identified by NIR fluorescence (Table 2). Within these hotspots, a total of 41 lymph nodes were found after histopathological examination, yielding an average of 4.6 ± 2.1 true lymph nodes per patient . In 3 fluorescent hotspots, adipose tissue only, with

**Table 1.** Patient and Tumor Characteristics

| Patient no. | ICG:HSA Dose (μM) | Age (Years) | BMI | FIGO Stage | Type of Surgery | Tumor Type | Tumor Size (cm) |
|---|---|---|---|---|---|---|---|
| 1 | 500 | 35 | 35 | IB1 | Trachelectomy | Adenosquamous | 2.5 |
| 2 | 500 | 43 | 26 | IB2 | Hysterectomy | Squamous | 4.5 |
| 3 | 500 | 77 | 21 | IB2 | Hysterectomy | Squamous | 11.0 |
| 4 | 750 | 46 | 30 | IB1 | No resection | Squamous | n/a |
| 5 | 750 | 59 | 21 | IB1 | Hysterectomy | Squamous | 4.2 |
| 6 | 750 | 29 | 22 | IB1 | Trachelectomy | Squamous | 2.5 |
| 7 | 1000 | 30 | 18 | IB1 | Trachelectomy | Squamous | 1.0 |
| 8 | 1000 | 40 | 20 | IB1 | Hysterectomy | Squamous | 0.7 |
| 9 | 1000 | 34 | 21 | IB1 | Hysterectomy | Squamous | 3.6 |

no lymph tissue present, was found after histopathological examination. An average of 25.1 lymph nodes (range 10-39) per patient were harvested. Histological analysis showed that 2 of 9 patients had metastases in a total of 3 SLNs. No other lymph node metastases were observed.

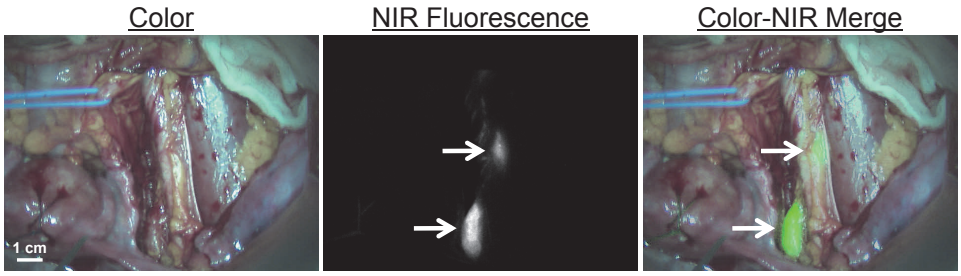


**Figure 1. NIR Fluorescence-Based SLN mapping using ICG:HSA and Mini-FLARE™:** Identification of two SLNs (arrows), located along the left iliac vessels, with NIR fluorescence imaging is demonstrated in a cervical cancer patient, 45 min after administration of 750 μM ICG:HSA. Camera exposure time was 100 msec. Scale bar represents 1 cm.

### Localization of Sentinel Lymph Nodes

A total of 31 fluorescent hotspots were confirmed to be SLNs. All SLNs were pelvic nodes and were identified along the left (n = 8) and right (n = 6) external iliac vessels, the right common iliac vessels (n = 4), the left (n = 5) and right (n = 4) obturator fossa, and the left (n = 2) and right (n = 2) lateral parametrium. Table 2 provides exact locations for all SLNs. In 8 of 9 patients, bilateral SLNs were found. After histological confirmation, 3 positive SLNs were found in 2 patients. In the first patient, the positive SLNs were located in the left lateral parametrium and along the right external iliac vessels. In the second patient, the positive SLN was located along the left external iliac vessels.

### *Ex vivo* imaging of lymph nodes

All lymph nodes were examined for fluorescence *ex vivo* using the Mini-FLARE™ imaging system. In 4 of 9 patients additional fluorescent hotspots (N=10) were identified, which were not identified during *in vivo* NIR fluorescence imaging (Table 2). Within 8 of these 10 hotspots, a total of 10 lymph nodes were found after histopathological examination and within 2 of 10 these hotspots, adipose tissue only, with no lymph node tissue present, was found after histopathological examination. The hotspots that contained lymph nodes were harvested along the left (n = 1) and the right (n = 1) external iliac vessels, and the left (n = 1) and the right (n = 5) obturator fossa. The hotspots that contained only adipose tissue were harvested along the left (n

= 1) and the right (n = 1) external iliac vessels. No additional metastases were found during *ex vivo* analysis.

### Optimization of ICG:HSA Dose

In all dose groups (500, 750, and 1,000 μM), fluorescence intensity of the SLN was significantly higher than the fluorescence intensity of surrounding tissue ($P<0.001$). Mean SBRs of the SLNs were 10.1 ± 1.2, 10.3 ± 1.2 and 12.0 ± 5.7 for the 500 μM, 750 μM, and 1,000 μM dose groups, respectively (Figure 2). A one-way ANOVA test showed no significant differences in SBRs of SLNs between the different dose groups ($P = 0.76$).

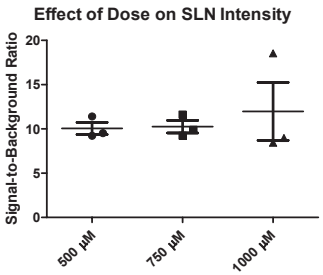


**Figure 2. Brightness of SLNs as a Function of ICG:HSA Dose:** Signal-to-background ratio (mean ± S.D) of the SLNs (ordinate) as a function of injected dose of ICG:HSA (abscissa). Statistical comparisons are as follows: The SBRs of the 500, 750, and 1,000 μM concentration groups were not significantly different.

## DISCUSSION

The current study showed the feasibility of the SLN procedure in early stage cervical cancer patients using ICG:HSA and the Mini-FLARE™ imaging system. The Mini-FLARE™ imaging system that was used in the current study displays NIR fluorescence signal, color signal, and a merge of both and illuminates the surgical field with white light. This enabled the gynecologist to perform the SLN detection and resection under direct image guidance. The imaging head of the Mini-FLARE™ system is attached to a flexible gooseneck arm, which permitted flexible positioning of the imaging head at extreme angles over the surgical field. This is of particular importance in large abdominal surgery. During all procedures, intraoperative imaging using this imaging system was successful and uneventful.

No differences in SBR of the SLNs between the 500, 750, and 1,000 μM dose groups were found. The location of the NIR fluorescent SLNs was in concordance with formerly published drainage patterns.[11] Furthermore, bilateral SLNs were found in 8 of 9 patients. The 3 tumor-positive SLNs (in 2 patients) were located along the left external iliac vessels (n = 1), the right external iliac vessels (n = 1), and in the left lateral

**Table 2.** Results from In Vivo and Ex Vivo SLN Imaging

| Patient no. | NIR Hotspots In Vivo | Additional NIR Hotspots Ex Vivo | Total LNs Harvested | Tumor-Positive SLNs From Pathology | Tumor-Positive SLNs that were NIR Fluorescent | False-Negatives | Location of NIR Fluorescent SLNs | Injection-Imaging Interval (min) | Bilateral SLNs Identified |
|---|---|---|---|---|---|---|---|---|---|
| 1 | 3 | 3 | 15 | 0 | 0 | n/a | Left (1) and right (1) external iliac, left obturator (1) | 94 | Yes |
| 2 | 4 | 0 | 36 | 2 | 2 | 0 | Left (1) and right (1) parametrium, right external iliac (1), right common iliac (1) | 35 | Yes |
| 3 | 3 | 0 | 17 | 0 | 0 | n/a | Left external iliac (1) left obturator (2) | 43 | Yes |
| 4 | 3 | 1 | 23 | 0 | 0 | n/a | Left (1) and right (1) external iliac, left obturator (1) | 44 | Yes |
| 5 | 4 | 0 | 39 | 0 | 0 | n/a | Left (1) and right (1) external iliac, right parametrium (1), right common iliac (1) | 40 | Yes |
| 6 | 5 | 0 | 33 | 0 | 0 | n/a | Left (1) and right (1) external iliac, right common iliac (1), left obturator (1), left parametrium (1) | 44 | Yes |
| 7 | 1 | 0 | 16 | 0 | 0 | n/a | Right obturator (1) | 41 | No |
| 8 | 5 | 2 | 37 | 0 | 0 | n/a | Left (1) and right (1) external iliac, right common iliac (1) obturator right (2) | 62 | Yes |
| 9 | 3 | 4 | 10 | 1 | 1 | 0 | Left (2) and right (1) external iliac | 58 | Yes |
| | 31 | 10 | 226 | 3 | 3 | 0 | Average = 51 ± 18 | | |

parametrium (n = 1). Identification of a parametrial SLN is rather remarkable because there is presently no consensus on removal of parametrial lymph nodes during total pelvic lymphadenectomy.[19-22] Although larger clinical trials will be required to answer this question, from this study we can at least conclude that parametrial lymph nodes are identifiable using ICG:HSA and Mini-FLARE™.

The detection rate of SLNs in our pilot-study was 100% and this detection rate is in concordance with a prospective, multicenter cohort study of 590 patients that examined SLN mapping in cervical cancer patients and observed a detection rate of 93.5% when a combination of patent blue and radiocolloids was used.[23] In the current study, on average, a total of 3.4 SLNs were identified per patient intraoperatively, which is also consistent with previously published data.[8, 9] In the recently published study by Crane et al.[17] on NIR fluorescence SLN mapping in cervical cancer patients, ICG was injected after laparotomy and NIR fluorescence measurements were made directly after injection. Furthermore, ICG was diluted in patent blue prior to injection. These differences in study design along with the use of a different imaging system hinder a direct comparison of the results.

The optimal time interval between injection of ICG:HSA and NIR fluorescence imaging is still unknown. Nevertheless, timing of imaging could be of great importance in terms of detection rate, sensitivity, and SBRs of SLNs. The mean interval between administration of ICG:HSA and NIR fluorescence measurements in the current study was 51 min. This time interval was relatively long because the ICG:HSA injection was performed prior to surgery, followed by surgical scrub and operation time to expose the iliac vessels. During surgery, no more than several minutes were needed for SLN detection and resection.

*Ex vivo* NIR fluorescence imaging of total lymphadenectomy specimens detected 10 additional fluorescent hotspots in 4 of 9 patients. Detection of these additional fluorescent hotspots during *ex vivo* imaging could possibly be explained by the relatively long time interval between ICG:HSA administration and performance of the total lymphadenectomy. Although ICG:HSA has an improved hydrodynamic diameter compared to ICG alone, passage through the SLN to second tier nodes can still possibly occur if the time interval is long enough. An alternative explanation for the additional *ex vivo* detected fluorescent hotspots is that these hotspots were missed *in vivo* due to technical limitations, as for example, the limited penetration depth (millimeters) for NIR fluorescent light. Future larger studies are needed to optimize timing and to evaluate the importance of additional fluorescent hotspots that are missed *in vivo* and are detected in the resection specimen. Nevertheless, to bypass this pitfall, the development of new lymphatic tracers that are retained in the SLN without flowing through to higher tier nodes is imperative to optimize NIR fluorescence SLN mapping in cervical cancer.

In the current study, fluorescent hotspots were found *in vivo* (n = 3) and *ex vivo* (n = 2) that did not contain lymphatic tissue but consisted of adipose tissue, which is not an uncommon observation in the SLN procedure. A plausible explanation for these fluorescent hotspots is that fluorescent lymph fluid can exit the lymphatic channel, due to extensive manipulation during surgery or anatomical aberrations, for example. If detection of a relatively small number of these hotspots does not obfuscate the identification of the true SLNs, this phenomenon does not negatively influence the SLN procedure.

In a recently published dose-finding clinical study performed by our group using NIR fluorescence SLN mapping in breast cancer patients, an optimal ICG:HSA dose range between 400 and 800 μM was found.[15] In the 1,000 μM ICG:HSA dose group, the fluorescent intensity and the SBR of the SLNs decreased, most probably caused by an effect known as fluorescence quenching.[24] In the current study, no differences were found in SBRs between the 500, 750, and 1,000 μM dose groups. This lack of difference combined with pharmacy preferences, safety, previous results, and costs make a dose of 500 μM most convenient to perform the SLN procedure in cervical cancer patients.

As in other areas of surgery, the use of laparoscopy is expanding in cancer surgery. Lymphadenectomies are being performed laparoscopically as standard of care in several centers. NIR fluorescence may also be of great value in laparoscopic surgery because palpation is not possible and the surgeon can only rely on visual inspection and preoperative imaging. To implement NIR fluorescence in laparoscopic surgery, laparoscopic NIR fluorescence camera systems are currently being developed and tested.[25]

In conclusion, we assessed the potential value of NIR fluorescence imaging in SLN mapping in early stage cervical cancer patients. Although sample size was small, this study showed a high SLN detection rate (100%) and no false-negative lymph nodes. However, to prove actual patient benefit and to assess sensitivity more precisely, larger clinical trials will be necessary.

## REFERENCES


1. Jemal A, Siegel R, Ward E, et al. Cancer statistics, 2009. CA Cancer JClin 2009; 59:225-249.
2. Ferlay J, Bray F, Pisani P, et al. GLOBOCAN: Cancer Incidence, Mortality and Prevalence Worldwide. Vol. 1st. Lyon: IARCPress, 2001.
3. Hacker NF. Revised FIGO staging for carcinoma of the vulva. Int J Gynaecol Obstet 2009; 105:105-106.
4. Horn LC, Hentschel B, Fischer U, et al. Detection of micrometastases in pelvic lymph nodes in patients with carcinoma of the cervix uteri using step sectioning: Frequency, topographic distribution and prognostic impact. Gynecol Oncol 2008; 111:276-281.
5. Green J, Kirwan J, Tierney J, et al. Concomitant chemotherapy and radiation therapy for cancer of the uterine cervix. CochraneDatabaseSystRev 2005:CD002225.
6. Van Der Zee AG, Oonk MH, De Hullu JA, et al. Sentinel node dissection is safe in the treatment of early-stage vulvar cancer. J Clin Oncol 2008; 26:884-889.
7. Morton DL, Wen DR, Wong JH, et al. Technical details of intraoperative lymphatic mapping for early stage melanoma. Arch Surg 1992; 127:392-399.
8. Levenback C, Coleman RL, Burke TW, et al. Lymphatic mapping and sentinel node identification in patients with cervix cancer undergoing radical hysterectomy and pelvic lymphadenectomy. J Clin Oncol 2002; 20:688-693.
9. Marchiole P, Buenerd A, Scoazec JY, et al. Sentinel lymph node biopsy is not accurate in predicting lymph node status for patients with cervical carcinoma. Cancer 2004; 100:2154-2159.
10. van de Lande J, Torrenga B, Raijmakers PG, et al. Sentinel lymph node detection in early stage uterine cervix carcinoma: a systematic review. Gynecol Oncol 2007; 106:604-613.
11. Ercoli A, Delmas V, Iannone V, et al. The lymphatic drainage of the uterine cervix in adult fresh cadavers: anatomy and surgical implications. Eur J Surg Oncol 2010; 36:298-303.
12. Silva LB, Silva-Filho AL, Traiman P, et al. Sentinel node detection in cervical cancer with (99m) Tc-phytate. Gynecol Oncol 2005; 97:588-595.
13. Vahrmeijer AL, Frangioni JV. Seeing the invisible during surgery. Br J Surg 2011; 98:749-50.
14. Frangioni JV. In vivo near-infrared fluorescence imaging. Curr Opin Chem Biol 2003; 7:626-634.
15. Mieog JS, Troyan SL, Hutteman M, et al. Towards Optimization of Imaging System and Lymphatic Tracer for Near-Infrared Fluorescent Sentinel Lymph Node Mapping in Breast Cancer. Ann Surg Oncol 2011.
16. Ohnishi S, Lomnes SJ, Laurence RG, et al. Organic alternatives to quantum dots for intraoperative near-infrared fluorescent sentinel lymph node mapping. Mol Imaging 2005; 4:172-181.
17. Crane LM, Themelis G, Pleijhuis RG, et al. Intraoperative Multispectral Fluorescence Imaging for the Detection of the Sentinel Lymph Node in Cervical Cancer: A Novel Concept. Mol Imaging Biol 2010.
18. Pieterse QD, Kenter GG, Gaarenstroom KN, et al. The number of pelvic lymph nodes in the quality control and prognosis of radical hysterectomy for the treatment of cervical cancer. Eur J Surg Oncol 2007; 33:216-221.
19. Bader AA, Winter R, Haas J, et al. Where to look for the sentinel lymph node in cervical cancer. Am J Obstet Gynecol 2007; 197:678-7.
20. Steed H, Capstick V, Schepansky A, et al. Early cervical cancer and parametrial involvement: is it significant? Gynecol Oncol 2006; 103:53-57.
21. Winter R, Haas J, Reich O, et al. Parametrial spread of cervical cancer in patients with negative pelvic lymph nodes. Gynecol Oncol 2002; 84:252-257.
22. Photopulos GJ, Zwaag RV. Class II radical hysterectomy shows less morbidity and good treatment efficacy compared to class III. Gynecol Oncol 1991; 40:21-24.
23. Altgassen C, Hertel H, Brandstadt A, et al. Multicenter validation study of the sentinel lymph node concept in cervical cancer: AGO Study Group. Journal of clinical oncology : official journal of the American Society of Clinical Oncology 2008; 26:2943-51.
24. Gioux S, Choi HS, Frangioni JV. Image-guided surgery using invisible near-infrared light: fundamentals of clinical translation. Mol Imaging 2010; 9:237-255.

25. van der Poel HG, Buckle T, Brouwer OR, et al. Intraoperative Laparoscopic Fluorescence Guidance to the Sentinel Lymph Node in Prostate Cancer Patients: Clinical Proof of Concept of an Integrated Functional Imaging Approach Using a Multimodal Tracer. Eur Urol 2011.

# Chapter 9

# Optimization of near-infrared fluorescent sentinel lymph node mapping for vulvar cancer

Hutteman M[1], van der Vorst JR[1], Gaarenstroom KN, Peters AAW, Mieog JSD, Schaafsma BE, Löwik CWGM, Frangioni JV, van de Velde CJH, Vahrmeijer AL

[1] Shared first authorship

*Amer J Obstet Gynecol; In press.*

## ABSTRACT

### Background

Near-infrared (NIR) fluorescence imaging has the potential to improve sentinel lymph node (SLN) mapping in vulvar cancer, which was assessed in the current study. Furthermore, dose optimization of indocyanine green adsorbed to human serum albumin (ICG:HSA) was performed.

### Methods

Nine vulvar cancer patients underwent the standard SLN procedure using $99^{m}$technetium-nancolloid and patent blue. In addition, intraoperative imaging was performed after peritumoral injection of 1.6 mL of 500, 750 or 1000 μM of ICG:HSA.

### Results

NIR fluorescence SLN mapping was successful in all patients. A total of 14 SLNs (average 1.6, range 1-4) were detected: 14 radioactive (100%), 11 blue (79%), and 14 NIR fluorescent (100%).

### Conclusions

This study demonstrates feasibility and accuracy of SLN mapping using ICG:HSA. Considering safety, cost, and pharmacy preferences, an ICG:HSA concentration of 500 M appears optimal for SLN mapping in vulvar cancer.

## INTRODUCTION

Vulvar cancer is a relatively rare disease with an annual incidence of approximately 4000 cases in the United States, resulting in 900 deaths per year.[1] Tumor size and invasion into adjacent tissues are important factors for staging vulvar cancers, but nodal status remains the single most important prognosticator.[2] Radical vulvectomy with en bloc inguinofemoral lymphadenectomy has been replaced in the surgical treatment of vulvar cancer by radical wide local excision or radical vulvectomy with inguinofemoral lymphadenectomy using separate groin incisions.[3] The latter modification has significantly decreased surgery-related morbidity.[3] However, 30% to 70% of patients treated with full inguinofemoral lymphadenectomy still suffer from lymphedema.[4-6] Only 27% of patients with clinically stage I or II vulvar cancer have tumor positive lymph nodes; therefore, approximately 70% of patients undergo unnecessary lymphadenectomy.[6]

The sentinel lymph node (SLN) biopsy, as introduced in the management of cutaneous melanoma by Morton,[7] was first described in vulvar cancer by Levenback in 1994.[8] The SLN procedure in vulvar cancer patients has been validated in multicenter trials and its introduction in regular clinical practice has marked a significant reduction in lymphedema, wound infection, and wound dehiscence.[9, 10] Currently, the procedure usually involves a combination of a radioactive colloid and a blue dye. However, the use of radiotracers requires complex logistics including the involvement of a nuclear medicine physician and the transport of radioactivity, and is therefore not available in all clinics. Moreover, blue dyes cannot be visualized when the lymph nodes and lymphatic channels are covered by tissue, such as skin or fat.

The use of invisible near-infrared (NIR) light (700-900 nm) has several characteristics that can be advantageous in the SLN procedure, which include relatively high penetration into living tissue (millimeters to centimeters), when compared to blue dyes, and the lack of ionizing radiation.[11] Indocyanine green (ICG) is one of only 2 clinically available NIR fluorescent agents and is currently the most optimal agent for SLN mapping.[12] In several studies, intraoperative imaging systems in combination with ICG have been used for the SLN procedure for various types of cancer.[13-18] The lymphatic channels and SLNs in vulvar cancer are often located in a relatively superficial location in the groin when compared to other tumors; therefore, NIR fluorescence imaging could be particularly useful for this indication. Indeed, Crane et al. reported the successful use of ICG alone at a concentration of 645 μM, in conjunction with an intraoperative imaging system for the SLN procedure in vulvar cancer.[19] In that study involving 10 patients, 26 of 29 SLNs (90%) were detected *in vivo* by NIR fluorescence. Furthermore, lymphatic channels could be visualized in 5 of 16 groins (31%) containing SLNs.

Preclinical evidence demonstrated that premixing of ICG with human serum albumin (HSA, complex is ICG:HSA) increases the fluorescence intensity and

hydrodynamic diameter of ICG, resulting in better retention in the SLN.[20] The aims of the current study were to assess the use of NIR fluorescence imaging using ICG:HSA and the Mini-FLARE intraoperative imaging system for the SLN procedure in vulvar cancer and to optimize ICG:HSA dose.

## MATERIALS AND METHODS

### Preparation of Indocyanine Green Adsorbed to Human Serum Albumin

ICG (25 mg vials) was purchased from Pulsion Medical Systems (Munich, Germany) and resuspended in 10 mL of sterile water for injection for the 500 μM group, or in 5 mL of sterile water for injection for the 750 μM and 1000 μM groups, to yield stock solutions of 3.2 mM and 6.4 mM, respectively. Various amounts of this stock solution were transferred to a 50 cc vial of Cealb (20% human serum albumin [HSA] solution; Sanquin, Amsterdam, The Netherlands) to yield ICG in HSA (ICG:HSA) at a final concentration of 500 μM, 750 μM, or 1000 μM.

### Intraoperative NIR Fluorescence Imaging

SLN mapping was performed using the Mini-FLARE image-guided surgery system as described in detail previously.[14] Briefly, the system consists of 2 wavelength separated light sources: a "white" LED light source, generating 26,600 lx of 400 to 650 nm light to illuminate the surgical field and an NIR LED light source, generating 7.7 mW / $cm^2$ of fluorescence excitation light. White light and NIR fluorescence images are acquired simultaneously and displayed in real time, using custom designed optics and software. A pseudo-colored (lime green) image of NIR fluorescence superimposed over the white light image is also displayed, to provide the NIR fluorescence signal in proper anatomical context.

### Clinical Trial

The current dose escalation clinical trial was approved by the Medical Ethics Committee of the Leiden University Medical Center and was performed in concordance with the ethical standards of the Helsinki Declaration of 1975. Nine consecutive patients that planned to undergo a SLN procedure for squamous cell vulvar carcinoma were included in this study between June 2010 and January 2011. All patients had clinically FIGO stage I vulvar cancer with a unifocal carcinoma measuring less than 4 cm in diameter, not encroaching the vagina, anus or urethra and with negative inguinofemoral nodes as determined by palpation and ultrasonography. Exclusion criteria were pregnancy, lactation or an allergy to iodine, shellfish, or indocyanine green.

All patients gave informed consent and were anonymized. Patients received the standard-of-care SLN procedure.[9] For our institution, this implies peritumoral injections of 60-100 MBq $^{99m}$technetium-nanocolloid on the afternoon of the day before, or the morning prior to surgery. Before the start of the operation, 1 mL total of patent blue V (Guerbet, France) was injected at 4 sites peritumorally. Immediately after injection of patent blue, 1.6 mL total of ICG:HSA was injected as 4 injections at the same location as the patent blue injections. After surgical scrub, the Mini-FLARE imaging head was positioned at approximately 30 cm above the surgical field. The NIR fluorescence signal was measured percutaneously, prior to skin incision, and continuously during the surgical procedure. Throughout the procedure, the surgeon was continuously provided with real-time NIR fluorescence image guidance. When the SLN could not be found easily by NIR fluorescence, the handheld gamma probe could be used for the localization of SLNs. Relative brightness of the SLNs was determined by measuring signal-to-background ratios (SBR), that is the NIR fluorescence signal of the SLN divided by a directly adjacent region. Excised sentinel lymph nodes were analyzed *ex vivo* for NIR fluorescence and radioactivity and were routinely analyzed by histopathological frozen section analysis. SLNs were fixed in formalin and embedded in paraffin for hematoxylin, eosin, and immunohistopathological staining for AE1/AE3 at multiple levels, with an interval of 250 μm, according to the GROningen INternational Study on Sentinel nodes in Vulvar cancer (GROINSS-V) study protocol.[9]

### Statistical Analysis

For statistical analysis, SPSS statistical software package (Version 17.0, Chicago, USA) was used. Graphs were generated using GraphPad Prism Software (Version 5.01, La Jolla, USA). To compare the SBR between concentration groups, a one-way analysis of variance (ANOVA) was performed with pairwise comparison with least square difference (LSD) adjustment for multiple comparisons. Assumption of homogeneity of variances was assessed using Levene's test. All statistical tests were two-tailed and $P < 0.05$ was considered significant.

## RESULTS

### Patient and Tumor Characteristics

Nine consecutive patients with vulvar cancer undergoing SLN mapping were included in this study. Patients and tumor characteristics are described in Table 1. Median body mass index (BMI) was 27 (range 23-45), median age was 50 years (range 30-72 years), and median tumor size was 13 mm (range 4-22 mm). In 6 patients, the tumor was laterally located and in 3 patients the tumor was located on, or near, the midline.

**Table 1.** Patient and Tumor Characteristics

| Patient | Dose (μM) | Age (Years) | BMI | Tumor Localization | Tumor Type | Tumor Size (mm) |
|---|---|---|---|---|---|---|
| 1 | 500 | 72 | 33 | Right | Squamous | 22 |
| 2 | 500 | 30 | 22 | Right | Squamous | 10 |
| 3 | 500 | 67 | 26 | Left | Squamous | 10 |
| 4 | 750 | 37 | 29 | Midline | Squamous | 17 |
| 5 | 750 | 42 | 45 | Left | Squamous | 22 |
| 6 | 750 | 37 | 23 | Right | Squamous | 20 |
| 7 | 1000 | 72 | 27 | Midline | Squamous | 6 |
| 8 | 1000 | 50 | 26 | Midline | Squamous | 4 |
| 9 | 1000 | 74 | 32 | Left | Squamous | 13 |

Abbreviation: BMI = body mass index

## Intraoperative NIR Fluorescence Imaging

Average time between ICG:HSA injection and skin incision was 19 ± 4 minutes. In all patients (N = 9), NIR fluorescence imaging using the Mini-FLARE system enabled visualization of one or more SLNs (Figure 1). Average time between skin incision and resection of the first SLN was 13 ± 5 minutes. A total of 14 SLNs were detected, all of which were radioactive and fluorescent (Table 2). Four SLNs from 3 patients did not have blue staining from patent blue. After all NIR fluorescent nodes were resected, the surgical field was systematically inspected for remaining radioactivity or blue nodes. No additional nodes were found that were not detected by NIR fluorescence. No adverse reactions associated with the use of ICG:HSA or the Mini-FLARE imaging system were observed.

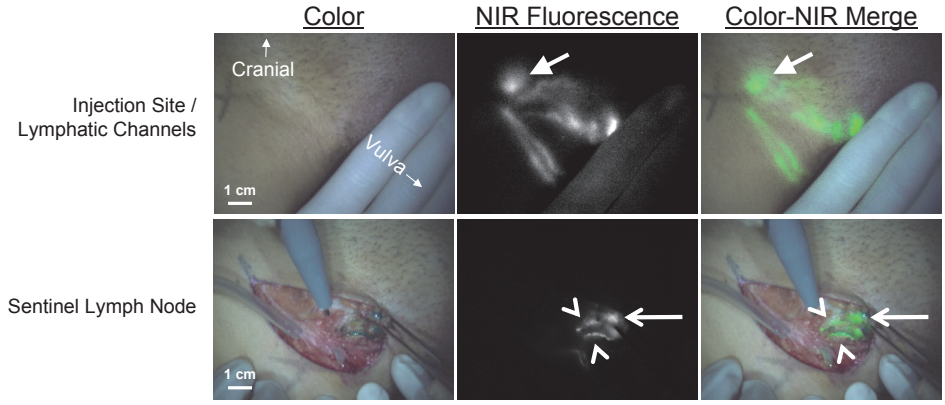


**Figure 1. Sentinel lymph node mapping using NIR fluorescence imaging in vulvar cancer:** Peritumoral injection of 1.6 mL of 500 μM ICG:HSA (injection site covered by hand) identifies lymphatic channels, which converge in a SLN (arrow) that can be seen percutaneously (top row). Identification of the SLN (arrow) and two afferent lymphatic channels (arrowheads) is demonstrated using NIR fluorescence imaging 17 min after injection of ICG:HSA (bottom row). Camera exposure times were 100 msec (top row) and 45 msec (bottom row). Scale bars represent 1 cm.

**Table 2.** SLN Identification Results

| Patient | Number of SLN detected | Radiocolloid | Blue | NIR Fluorescence | SLN+ | Percutaneous Visualization |
|---|---|---|---|---|---|---|
| 1 | 2 (1 left, 1 right) | 2 | 2 | 2 | 0 | Unilateral |
| 2 | 1 (right) | 1 | 1 | 1 | 0 | Yes |
| 3 | 1 (left) | 1 | 1 | 1 | 1 | Yes |
| 4 | 2 (1 right, 1 left) | 2 | 1 | 2 | 0 | Unilateral |
| 5 | 1 (left) | 1 | 1 | 1 | 0 | No |
| 6 | 1 (right) | 1 | 1 | 1 | 0 | Yes |
| 7 | 1 (left) | 1 | 0 | 1 | 0 | Yes |
| 8 | 4 (2 left, 2 right) | 4 | 3 | 4 | 0 | Yes |
| 9 | 1 (left) | 1 | 1 | 1 | 1 | No |
| **Total** | **14** | **14 (100%)** | **11 (79%)** | **14 (100%)** | **2** | **8 of 12 groins** |

Abbreviation: SLN+ = number of SLNs containing tumor cells

## The Effect of Lymphatic Tracer Dose on SLN Brightness

The effect of injected lymphatic tracer dose on fluorescence brightness was determined by comparing SBRs between concentration groups. Mean SBRs of the SLNs were 12.3 ± 2.9, 16.6 ± 4.3, and 9.5 ± 4.3 for the 500, 750 and 1000 μM concentration groups, respectively (Figure 2). A one-way ANOVA showed no significant effect of concentration on SBR ($P = 0.16$), and pairwise comparison with LSD adjustment for multiple comparison showed no difference between the individual concentration and SBR, although a trend was found for a decreased SBR of the 1000 μM group when compared to the 750 μM group ($P = 0.07$). However, due to the small sample size, the current pilot study may not have sufficient power to detect significant differences in dose groups.

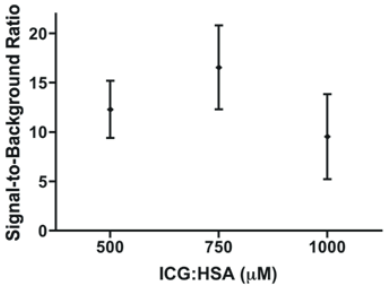


**Figure 2. Optimization of ICG:HSA dose:** Signal-to-background ratio (mean ± S.D.) of vulvar SLNs (ordinate) is plotted as a function of injected dose of ICG:HSA (abscissa). The SBRs of the 500, 750, and 100 μM concentration groups were not significantly different, although a trend was found favoring 750 μM over 1000 μM (P = 0.07).

## Percutaneous Visualization of Lymphatic Channels

The mean BMI of patients in which lymphatic channels were visualized percutaneously to all SLN containing groins (N = 5 patients) was 24.8 ± 2.2. In patients with bilateral SLNs in which percutaneous visualization was possible for the groin (N = 2 patients),

the mean BMI was 31.0 ± 2.8, and in patients where percutaneous visualization of lymphatic channels was not possible (N = 2 patients), the mean BMI was 38.5 ± 9.2. A one-way ANOVA showed a significant difference in the BMIs between these 3 groups ($P$ = 0.024). A pairwise comparison with LSD adjustment for multiple comparison showed a significantly higher BMI for the group in which percutaneous visualization of lymphatic channels was not possible, when compared to the group in which percutaneous visualization of lymphatic channels was possible ($P$ = 0.009).

## DISCUSSION

The current study showed feasibility and accuracy of SLN mapping in vulvar cancer using ICG:HSA and the Mini-FLARE imaging system. In all 9 cases, the Mini-FLARE permitted the gynecologist to perform SLN mapping under direct image-guidance after skin incision. The flexible gooseneck of the Mini-FLARE could be used to position the system at any required location over the surgical field, which ensured no interference with the procedure. Indeed, no additional time was needed to complete the procedure, with an average time between skin incision and resection of the first SLN of 13 ± 5 minutes.

All radioactive SLNs could also be detected by NIR fluorescence. This higher detectability compared to the study by Crane et al. that utilized ICG alone[19] may be due to improved brightness of ICG:HSA over ICG, better retention in the SLN, better imaging system performance, an optimized tradeoff between injection concentration and tracer dilution within lymphatic channels, or a combination thereof.[14] In contrast, 4 out of 14 SLNs could not be detected by patent blue, which is comparable to previous findings.[10, 19, 21] Lymphatic channels could be visualized in the majority of patients prior to skin incision. This aided the gynecologist in determining the location of the incision and facilitated a more efficient identification of SLNs. In the patients where percutaneous visualization of lymphatic channels was not possible, a higher BMI was observed when compared to patients where the lymphatic channels could be visualized percutaneously. Crane et al. observed similar findings.[19] Future studies will have to determine whether NIR fluorescence imaging can replace radiocolloids in the SLN procedure in vulvar cancer, which could potentially be feasible only in non-obese patients. This could be particularly beneficial in clinics where radiotracers are not available. Furthermore, as the patient population in Western societies tends to suffer from increasingly higher BMIs, the penetration depth has to be increased for NIR fluorescence imaging to be a generally usable imaging modality. To accomplish this, current research is focusing on improved fluorophores (some of which are currently in the process of clinical approval[22]) and improved camera systems using optimized detection techniques to maximize the depth at which a fluorophore can be detected.[23, 24]

In the current study, no significant differences in NIR fluorescence signal were observed between the different concentrations that were administered. However, a trend was observed showing a decline of signal in the 1000 μM group, which is in line with previously reported results in breast cancer.[14] A decrease of fluorescence signal with an increase in concentration can be explained by an effect in fluorescence quenching.[12] Fluorescence quenching occurs when the concentration of a fluorophore is too high, causing molecules to absorb the emitted light of other nearby molecules, thereby effectively attenuating the fluorescence signal. In the current study, ICG was adsorbed to HSA prior to injection. Preclinical work has shown premixing to increase the fluorescence brightness of ICG and improve retention in the SLN.[20] Flow to higher tier nodes seemed to have been avoided, as no additional NIR fluorescent nodes were identified that were not radioactive. An ongoing study is investigating whether the albumin is actually needed for optimal SLN mapping in vulvar cancer. When the optimal imaging parameters have been determined, larger trials can be performed to assess patient benefit.

In conclusion, the current study demonstrates the feasibility of SLN mapping in vulvar cancer patients using ICG:HSA and the Mini-FLARE image-guided surgery system. The preferred dose can be determined by local preparation preferences because no differences between tested doses were observed. In general, a dose of 500 μM seemed to be optimal, as it requires minimal manipulation of ICG and albumin volumes.

## ACKNOWLEDGEMENTS

The authors like to thank Dorien M.A. Berends-van der Meer and Margriet J.G. Löwik for their assistance with inclusion of patients, and Lindsey Gendall for editing. This work was supported in part by the Dutch Cancer Society grant UL2010-4732 and National Institutes of Health grant R01-CA-115296. This research was performed within the framework of CTMM, the Center for Translational Molecular Medicine, project MUSIS (grant 03O-202).

## REFERENCES


1. Jemal A, Siegel R, Xu J, et al. Cancer statistics, 2010. CA Cancer J Clin 2010; 60:277-300.
2. Hacker NF. Revised FIGO staging for carcinoma of the vulva. Int J Gynaecol Obstet 2009; 105:105-106.
3. Ansink A, van der Velden J. Surgical interventions for early squamous cell carcinoma of the vulva. Cochrane database of systematic reviews (Online) 2000:CD002036.
4. Gaarenstroom KN, Kenter GG, Trimbos JB, et al. Postoperative complications after vulvectomy and inguinofemoral lymphadenectomy using separate groin incisions. Int J Gynecol Cancer 2003; 13:522-527.
5. Rouzier R, Haddad B, Dubernard G, et al. Inguinofemoral dissection for carcinoma of the vulva: effect of modifications of extent and technique on morbidity and survival. J Am Coll Surg 2003; 196:442-450.
6. de Hullu JA, van der Zee AG. Surgery and radiotherapy in vulvar cancer. Crit Rev Oncol Hematol 2006; 60:38-58.
7. Morton DL, Wen DR, Wong JH, et al. Technical details of intraoperative lymphatic mapping for early stage melanoma. Arch Surg 1992; 127:392-399.
8. Levenback C, Burke TW, Gershenson DM, et al. Intraoperative lymphatic mapping for vulvar cancer. Obstet Gynecol 1994; 84:163-167.
9. Van Der Zee AG, Oonk MH, De Hullu JA, et al. Sentinel node dissection is safe in the treatment of early-stage vulvar cancer. J Clin Oncol 2008; 26:884-889.
10. Hampl M, Hantschmann P, Michels W, et al. Validation of the accuracy of the sentinel lymph node procedure in patients with vulvar cancer: results of a multicenter study in Germany. Gynecol Oncol 2008; 111:282-288.
11. Frangioni JV. In vivo near-infrared fluorescence imaging. Curr Opin Chem Biol 2003; 7:626-634.
12. Gioux S, Choi HS, Frangioni JV. Image-guided surgery using invisible near-infrared light: fundamentals of clinical translation. Mol Imaging 2010; 9:237-255.
13. Hojo T, Nagao T, Kikuyama M, et al. Evaluation of sentinel node biopsy by combined fluorescent and dye method and lymph flow for breast cancer. Breast 2010.
14. Mieog JS, Troyan SL, Hutteman M, et al. Towards Optimization of Imaging System and Lymphatic Tracer for Near-Infrared Fluorescent Sentinel Lymph Node Mapping in Breast Cancer. Ann Surg Oncol 2011.
15. Troyan SL, Kianzad V, Gibbs-Strauss SL, et al. The FLARE intraoperative near-infrared fluorescence imaging system: a first-in-human clinical trial in breast cancer sentinel lymph node mapping. Ann Surg Oncol 2009; 16:2943-2952.
16. Murawa D, Hirche C, Dresel S, et al. Sentinel lymph node biopsy in breast cancer guided by indocyanine green fluorescence. Br J Surg 2009; 96:1289-1294.
17. Crane LM, Themelis G, Pleijhuis RG, et al. Intraoperative Multispectral Fluorescence Imaging for the Detection of the Sentinel Lymph Node in Cervical Cancer: A Novel Concept. Mol Imaging Biol 2010.
18. Fujiwara M, Mizukami T, Suzuki A, et al. Sentinel lymph node detection in skin cancer patients using real-time fluorescence navigation with indocyanine green: preliminary experience. J Plast Reconstr Aesthet Surg 2009; 62:e373-e378.
19. Crane LM, Themelis G, Arts HJ, et al. Intraoperative near-infrared fluorescence imaging for sentinel lymph node detection in vulvar cancer: First clinical results. Gynecol Oncol 2010.
20. Ohnishi S, Lomnes SJ, Laurence RG, et al. Organic alternatives to quantum dots for intraoperative near-infrared fluorescent sentinel lymph node mapping. Mol Imaging 2005; 4:172-181.
21. Rob L, Robova H, Pluta M, et al. Further data on sentinel lymph node mapping in vulvar cancer by blue dye and radiocolloid Tc99. Int J Gynecol Cancer 2007; 17:147-53.
22. Marshall MV, Draney D, Sevick-Muraca EM, et al. Single-dose intravenous toxicity study of IRDye 800CW in Sprague-Dawley rats. Mol Imaging Biol 2010; 12:583-594.
23. Gioux S, Mazhar A, Cuccia DJ, et al. Three-dimensional surface profile intensity correction for spatially modulated imaging. J Biomed Opt 2009; 14:034045.
24. Kumar AT, Raymond SB, Bacskai BJ, et al. Comparison of frequency-domain and time-domain fluorescence lifetime tomography. Opt Lett 2008; 33:470-472.

# Chapter 10

# The FLARE™ intraoperative near-infrared fluorescence imaging system: a first-in-human clinical trial in perforator flap breast reconstruction

Lee BT, Hutteman M, Gioux S, Stockdale A, Lin SJ, Ngo LH, Frangioni JV

*Plast Reconstr Surg 2010; 126:1472-1481.*

## ABSTRACT

### Background

The ability to determine flap perfusion in reconstructive surgery is still primarily based on clinical examination. In this study, we demonstrate the use of an intraoperative, near infrared (NIR) fluorescence imaging system for evaluation of perforator location and flap perfusion.

### Methods

Indocyanine green (ICG) was injected intravenously in six breast cancer patients undergoing a deep inferior epigastric perforator (DIEP) flap breast reconstruction after mastectomy. Three dose levels of ICG were assessed using the Fluorescence-Assisted Resection and Exploration (FLARE™) imaging system. This system uses light emitting diodes (LED) for fluorescence excitation; different from current commercially available systems. In this pilot study, the operating surgeons were blinded to the imaging results.

### Results

Use of the FLARE™ system was successful in all six study subjects with no complications or sequelae. Among the three dose levels, 4-mg per injection resulted in the highest observed contrast-to-background ratio (CBR), signal-to-background ratio, and signal-to-noise ratio. However, due to small sample size, we did not have sufficient power to detect statistical significance for these pairwise comparisons at the multiple-comparison adjusted type-I error of 0.017. Six mg per injection provided a similar CBR, but also a higher residual background signal.

### Conclusions

Based on this pilot study, we conclude that NIR assessment of perforator flap breast reconstruction is feasible with an LED based system, and that a dose of 4 mg of ICG per injection yields the best observed CBR compared to a dose of 2 or 6 mg for assessment of flap perfusion.

## INTRODUCTION

The use of imaging as an adjunct is becoming increasingly popular in perforator flap reconstruction. As perforating vessels demonstrate a high degree of variability in size and location, identification of target vessels can decrease operative time and increase reliability. The currently used techniques for imaging include duplex ultrasound, CT, and MRI.[1-8] With improvements in technology and resolution, reconstructive surgeons are able to visualize small perforating vessels.

The current imaging modalities, however, rely on a static preoperative assessment. Ideally, the use of an intraoperative imaging adjunct would be most beneficial in order to provide a dynamic assessment. Changes in flap physiology and microsurgical flap transfer could be assessed more accurately if imaging was performed during surgery.

Our laboratory has previously described the use of a real time, near-infrared (NIR) Fluorescence-Assisted Resection and Exploration (FLARE™) imaging system in large animal surgery.[9-11] This system uses light-emitting diodes (LEDs) for fluorescence excitation and requires an intravenous injection of indocyanine green (ICG), an FDA-approved fluorophore. Because NIR light is invisible, the surgical field is unaltered. Our current system simultaneously displays real-time color video, up to two NIR fluorescence images, and merged images of all. Rapid recall of images is also available as needed.

We have described previously the ability of NIR imaging to identify suitable perforators during large animal surgery.[12] In addition, we validated the number of perforators identified with conventional x-ray angiography.[13] The identification of perforators can be performed reliably at multiple anatomic sites, including abdominal and submental flaps.[14] Finally, we were able to describe quantitative metrics to assess arterial and venous compromise.[15]

During an extensive pre-clinical laboratory experience with NIR fluorescence angiography using the FLARE™ imaging system, we have demonstrated safety in use in over 200 rodent and 100 large animal surgeries. This study describes the successful clinical translation of this technology for use in a six-subject pilot trial in patients undergoing microsurgical perforator flap breast reconstruction with a deep inferior epigastric perforator (DIEP) flap. In addition, determination of ideal ICG dosage was performed based on a quantitative assessment.

## MATERIALS AND METHODS

### Preparation of NIR Fluorophore

Indocyanine green (ICG) USP (25-mg vials) was purchased from Akorn (Decatur, USA) and resuspended in 10 mL of supplied diluent to yield a 2.5 mg/mL (3.2 mM)

stock solution. For each participant, four syringes were loaded with either 0.8 mL, 1.6 mL, or 2.4 mL of the ICG stock solution, equivalent to 2 mg, 4 mg, or 6 mg per injection.

### FLARE™ Intraoperative Imaging System

The FLARE™ imaging system and its use in a clinical setting have been described previously for sentinel lymph node resection.[9] Briefly, the imaging system consists of an imaging head mounted on an articulated arm and a cart containing control equipment, computer, and monitors (Figure 1). The imaging head has a 43" to 70" reach relative to the floor and a 50.7" reach from the cart, and can be positioned anywhere in 3-D space with six degrees of freedom. The system is engineered to meet all relevant subsections of the Association for the Advancement of Medical Instrumentation (AAMI)/International Electrotechnical Commission (IEC) standard #60601. A customized software system enables the real-time display of color video and two NIR fluorescence channels at up to 15 frames-per-sec. The software is capable of displaying the NIR fluorescence signal as a pseudo-colored overlay on the color video, thereby providing anatomical guidance to the surgeon. For intraoperative use, the entire system is wrapped in a sterile shield and drape (Medical Technique Inc., Tucson, USA). Additional details can be found in [10] and at www.frangionilab.org.

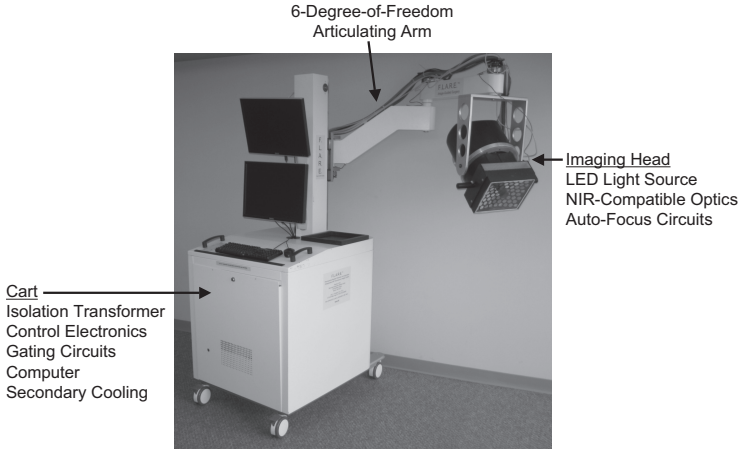


**Figure 1. The FLARE™ Imaging System:** The cart-based imaging system is shown with major parts identified. A satellite monitor and footswitch are also available to the surgeon (not shown).

### Clinical Trial during Breast Reconstruction Surgery

The clinical trial was approved by the Institutional Review Board (IRB) of the Beth Israel Deaconess Medical Center and performed in concordance with the ethical standards of the Helsinki Declaration of 1975. The IRB deemed the FLARE™ imaging system a "non-significant risk" device. All subjects gave written informed consent

and identifying information was anonymized. Clinical trial participants were women undergoing unilateral mastectomy and reconstruction with a microsurgical deep inferior epigastric perforator (DIEP) flap. Subjects received four injections of either 2 mg, 4 mg, or 6 mg ICG each. Two patients received each dose level. Before flap elevation, the camera was positioned 18" over one side of the abdomen and NIR imaging was performed using the FLARE™ system after an intravenous injection of ICG. Imaging system settings included 14 mW/cm$^2$ of 760-nm NIR fluorescence excitation light and a 67-msec camera exposure time. After ICG was cleared from the body and fluorescence levels restored to pre-injection levels, the contralateral side of the abdomen was imaged in an identical fashion. In this feasibility and dose-finding study, the operating surgeons were blinded to the FLARE™ images, thereby not changing the standard-of-care that patients were receiving during surgery.

After dissection of the vessels through the intramuscular course and isolation of the selected perforator vessels and vascular pedicle, the flap was imaged at the abdomen with a third ICG injection prior to transfer. The flap was then transferred to the chest and a microsurgical anastomosis was performed of the deep inferior epigastric artery and vein to the internal mammary vessels. A final assessment was performed with a fourth ICG injection. Subjects were evaluated for complications at one week and six weeks after surgery as part of regular postoperative follow-up.

**Analysis of Near-Infrared Fluorescence Data**

After each injection, NIR fluorescence data were acquired using the FLARE™ system continuously preceding the vascular signal; acquisition continued until two minutes after onset of vascular fill. Contrast-to-background ratio (CBR) was defined as the mean fluorescence intensity of the region of interest (ROI) minus the mean fluorescence intensity of a background ROI on the flap, divided by the mean camera noise. Signal-to-background ratio (SBR) was defined as the mean fluorescence intensity of the ROI, divided by the mean fluorescent intensity of a background ROI on the flap. Signal-to-noise ratio (SNR) was defined as the mean fluorescence signal of the ROI divided by the mean camera noise.

CBR, SBR, and SNR were calculated and recorded for each injection and compared among the three dose groups. Since this is a repeated-measures analysis with each subject receiving multiple injections, we used a modeling method to account for within-subject measurements correlation. We first examined the distribution of CBR, SBR, and SNR via the use of the Shapiro-Wilks test to check for normality of each variable. The assumption of normality was satisfied for CBR, and SNR, but not for SBR. The variability was also heterogeneous with the standard deviation for dose 4 mg and 6 mg higher than that of dose 2 mg. Thus the modeling would also need to take into account the difference in dose-specific variability of these three variables. For CBR and SNR, with the normality assumption satisfied, we made use of the linear

mixed-effects model,[16, 17] which allows the modeling of the variance-covariance matrix of the within-subject measurements. We used the compound symmetry structure to model the within- and between-subject variance components, which was assumed to be heterogeneous among the three different dose levels (the variances for dose 4 mg and 6 mg were estimated higher than that of the dose 2 mg, and these variances were used in the linear mixed-effects model). For SBR, due to the non-normality of the distribution, we used a generalized estimating equation (GEE),[18] which could model the within-subject correlation via the exchangeable working correlation structure. We used linear contrasts to obtain the pairwise comparisons among the three dose levels. We set the adjusted level of significance (type-I error) to 0.017 (0.05 divided by 3 comparisons) when we made inference on the pairwise comparisons. We used the SAS/STAT (SAS/STAT Software, Version 8, SAS Institute, Cary, USA) procedure MIXED and GENMOD for our statistical modeling.

## RESULTS

### Deployment of the FLARE™ System in the Operating Room

The preparation and ergonomics of the FLARE™ system in the operating room are similar to our previous description.[9] The system was draped in a sterile fashion using a shield/drape combination that could be applied by a single person (scrub nurse). After draping, the imaging head enters the sterile field and is positioned at a fixed distance and position before each injection. Including positioning of the system, each injection and subsequent FLARE™ measurement required less than three minutes, thereby not significantly affecting the normal operative course.

The FLARE™ system is housed in a portable cart for easy transfer into the operating room. The cart houses two monitors for the technologist operating the system; one monitor displays the control software while the other displays a duplicate of the surgeon's monitor. The surgeon's monitor is on a satellite pole that can be positioned up to 16 feet away from the cart. The articulating head is specifically designed with six degree-of-freedom movements. Depression of a brake release button on the handle permits smooth and precise positioning over the field. Release of the button engages the brakes, thereby fixing the head in three-dimensional space. The maximum reach of the articulating head is 50.7 inches from the cart.

### Intraoperative NIR Imaging of Perforator Vessels during Reconstructive Surgery

After IRB approval, six subjects participated in a first-in-human clinical trial using the FLARE™ system in reconstructive breast surgery after mastectomy. Precautions were taken to maintain the standard-of-care by blinding the surgeons to the results

of NIR imaging. Subjects were assigned to three dose groups (n = 2 subjects per dose group) of 2 mg, 4 mg, or 6 mg per injection. Clinical study subject characteristics are displayed in Table 1.

Subjects received an intravenous bolus injection of ICG that was administered by the anesthesiologist at four separate, fixed moments during surgery, as described above. Representative FLARE™ images of each dose group are shown in Figure 2. CBR, SBR, and SNR were quantified using the ROI as displayed in Figure 1 and are summarized in Table 2 and Figure 3. Observed mean and median values of all three variables were higher in the 4-mg group when compared to the 2-mg and 6-mg group. The variability of all three variables was also higher in the 4-mg and 6-mg dose. For CBR, the only comparison statistically significant at the multiple-comparison adjusted type-I error of 0.017 was between 2-mg and 6-mg (p-value: 0.0007) (see footnote Table 2). No statistically significant differences at the level of 0.017 were found for SBR and SNR among the 3 dose levels.

The average time intervals between injections 1 and 2, 2 and 3, and 3 and 4 were 19 min/36 sec, 3 h/16 min/41 sec, and 2 h/12 min/42 sec, respectively. The effect of dose on mean background fluorescence intensity between injections 1 and 2 was significant (ANOVA, $F(2, 20) = 5.761$, $p = .011$). Notably, the background fluorescence intensity was higher in the 6-mg group, when compared to both the 2-mg ($p = .009$) and 4-mg groups ($p = .008$), indicating residual ICG fluorescence.

In two cases, the surgeon selected and dissected perforator vessels that, by NIR imaging, were not the dominant vessels (example in Figure 3). CBR was measured for the NIR-dominant perforator vessel and the selected perforator vessel (Figure 4A) after all injections. As is displayed, the CBR of the previously NIR-dominant perforator vessel decreases after ligation and the CBR of the selected perforator vessel increases. These findings are consistent with the visual display seen during NIR imaging (Figure 4B).

### Postoperative Complications

None of the subjects developed any adverse reactions to the injected ICG. Minor complications were reported in three cases: a small area of fat necrosis, a breast seroma, and a small area of mastectomy skin loss. All complications were within normal range and resolved uneventfully. No partial or total flap loss occurred.

## DISCUSSION

This study demonstrates the successful translation of NIR angiography with the FLARE™ imaging system for use in microsurgical perforator-flap breast reconstruction. The design of our optical imaging system incorporated the ergonomic needs for use by surgeons in the operating room environment. The system is portable and

**Table 1.** Study Subject Characteristics

| Subject | ICG dose (mg) | Age (yr) | Weight (kg) | Height (cm) | Body mass index | ADA Skin type | Pre-operative radiotherapy | Post-operative complications |
|---|---|---|---|---|---|---|---|---|
| 1 | 2 | 29 | 84 | 173 | 28.1 | II | No | Minor fat necrosis |
| 2 | 2 | 47 | 66 | 163 | 24.8 | III | No | None |
| 3 | 4 | 64 | 77 | 168 | 27.3 | II | No | None |
| 4 | 4 | 56 | 70 | 160 | 27.3 | II | No | Breast seroma |
| 5 | 6 | 47 | 66 | 160 | 25.8 | II | Yes | None |
| 6 | 6 | 45 | 59 | 163 | 22.2 | II | No | Minor skin loss |
| Mean | | 48.0 ± 11.8 | 70.3 ± 8.9 | 164.5 ± 5.1 | 25.9 ± 2.2 | | | |

Skin Type = American Academy of Dermatology Skin Types I-VI:

I. Pale white skin: Always burns easily; never tans (Celtic, Scandinavian, and infants)
II. White: Usually burns easily; tans minimally (Northern European)
III. White (average): Sometimes burns; tans gradually to light brown (Central European)
IV. Beige or lightly tanned: Burns minimally; always tans to moderately brown (Mediterranean, Asian)
V. Moderate brown or tanned: Rarely burns; tans well (South American, Indian, Native American)
VI. Dark brown or black: Never burns; deeply pigmented (African, African-American, Aborigine)

**Table 2.** Contrast per Dose Group (Mean ± SD; Median)

| Dose | Contrast-to-Background Ratio (CBR) | Signal-to-Background Ratio (SBR) | Signal-to-Noise Ratio (SNR) |
|---|---|---|---|
| 2 mg | 1.5 ± 0.3; 1.6 | 2.1 ± 0.2; 2.2 | 3.0 ± 0.3; 3.0 |
| 4 mg | 4.2 ± 1.8; 3.9 | 3.6 ± 1.0; 3.5 | 6.0 ± 1.8; 5.7 |
| 6 mg | 3.7 ± 1.7; 3.7 | 3.3 ± 1.2; 3.0 | 5.5 ± 1.7; 5.7 |

P-value from linear mixed-effects and GEE models: CBR (2 mg vs. 4 mg: 0.053, 2 mg vs. 6 mg: 0.0007, 4 mg vs. 6 mg: 0.604); SBR (2 mg vs. 4 mg: 0.084, 2 mg vs. 6 mg: 0.068, 4 mg vs. 6 mg: 0.539); SNR (2 mg vs. 4 mg: 0.028, 2 mg vs. 6 mg: 0.024, 4 mg vs. 6 mg: 0.628).

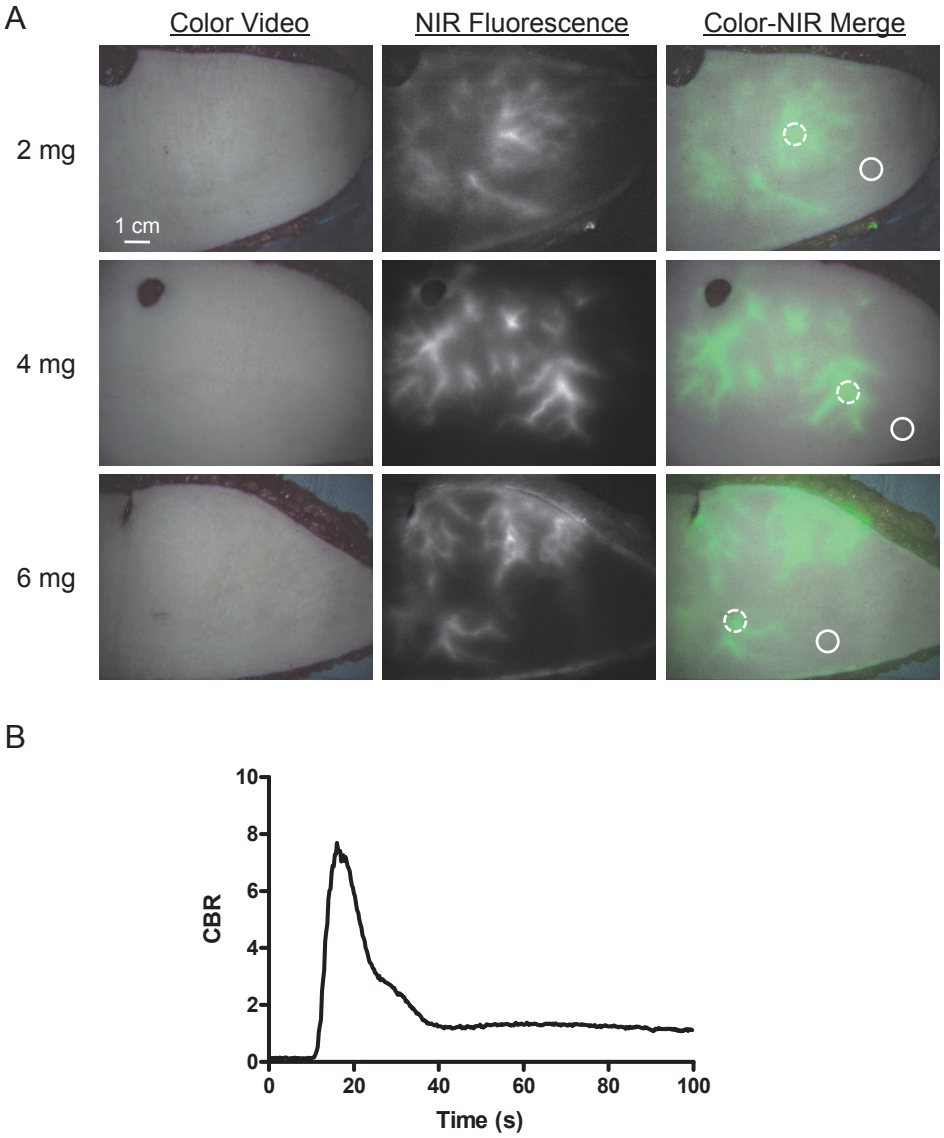


**Figure 2. NIR Fluorescence Imaging after ICG Injection: A.** Identification of perforating vessel (dashed circle) after injection of 2 mg (top), 4 mg (middle), or 6 mg (bottom) ICG on transferred skin flaps. Contrast was quantified using fluorescence intensity of the perforating vessel and background (solid circle). **B.** Typical CBR curve after ICG injection. Signal peaks shortly after injection and gradually declines.

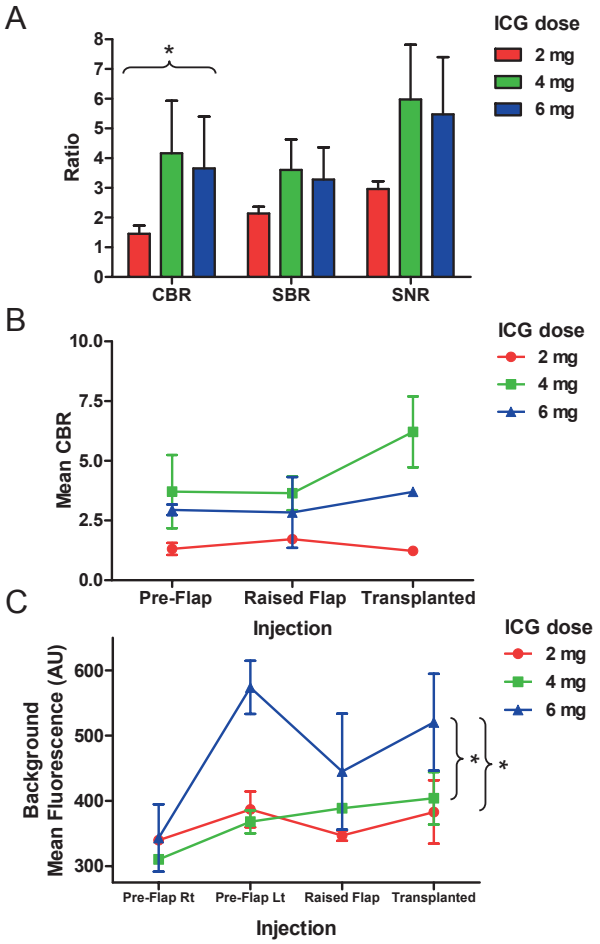


**Figure 3. Near-infrared fluorescence contrast per dose of indocyanine green (ICG): A.** Contrast-to-background ratio (CBR), signal-to-background ratio (SBR), and signal-to-noise ratio (SNR) in each dose group. Contrast-to-background ratio was defined as $(I_{perforator} - I_{background})/I_{noise}$, where I is fluorescence intensity. Observed mean and median values of all three variables were higher in the 4-mg group compared with those in the 2-mg and 6-mg groups, though the only statistically significant difference was contrast-to-background ratio of the 2-mg group compared to the 6-mg group. The p values for 2 mg versus 4 mg were as follows: contrast-to-background ratio, p = 0.053; signal-to-background ratio, p = 0.084; and signal-to-noise ratio, p = 0.028. The p values for 2 mg versus 6 mg were as follows: contrast-to-background ratio, p = 0.0007; signal-to- background ratio, p = 0.068; and signal-to-noise ratio, p = 0.024. **B.** Effect of indocyanine green dose on contrast after repeated injections. **C.** Effect of indocyanine green dose on background intensity after injection 2. After repeated injection of 6 mg of indocyanine green, the background intensity remains increased in comparison with the 2-mg (p = 0.009) and 4-mg (p = 0.008) groups.

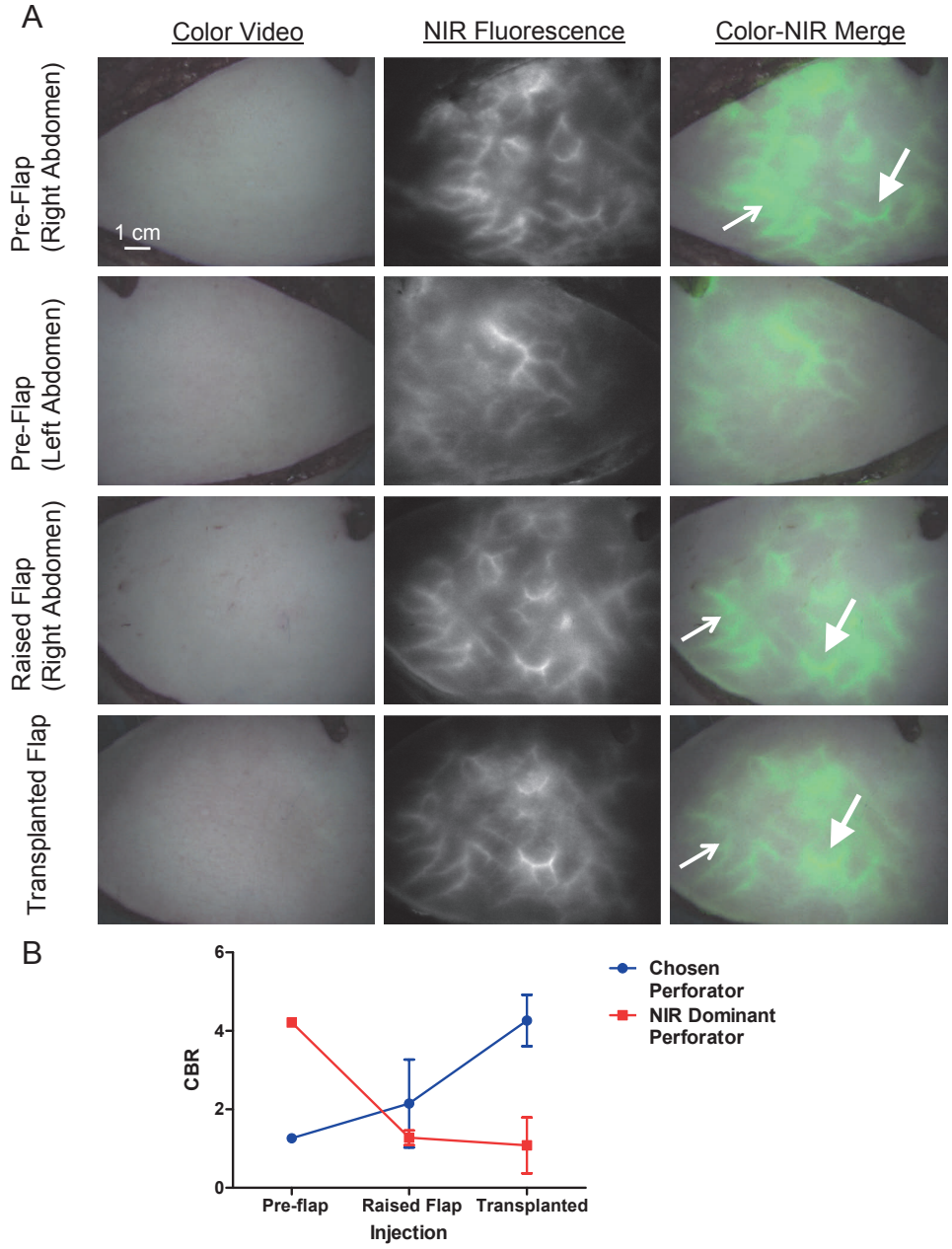


**Figure 4 – Selected perforator is not the NIR fluorescence dominant perforator: A.** Quantification of the signal confirms the increase in fluorescence intensity of the selected perforator and decrease in intensity of the perforator that was not chosen. **B.** Left and right sides of the abdomen are assessed before perforator dissection (two top rows) and the right side is chosen. Since the surgeon was blinded, NIR fluorescence information was not available for perforator selection. The perforator with the highest intensity (small arrow) was not selected in favor of a less fluorescent perforator (large arrow). After perforator dissection (third row) and subsequent transfer (bottom row) the chosen perforator appears to gain intensity.

completely self-contained; it can easily be transferred into the operating room and deployed rapidly. The ability to visualize the operative field simultaneously with NIR fluorescence is particularly advantageous. As the reconstructive surgeon is able to recall stored video and images, the findings can be correlated with surgical findings without any distortion.

NIR fluorescence imaging has the potential to find widespread use in plastic and reconstructive surgery, as well as general and oncologic surgery. It provides real-time guidance for tumor resection,[19], rapid identification of sentinel lymph nodes,[9] real-time avoidance of critical structures, such as nerves and blood vessels,[20] and quantitation of tissue metrics.[15]

By altering the intravenous dose of the fluorophore ICG we determined that 4 mg of ICG per injection had the highest observed CBR for clinical NIR angiography, although a larger study with more statistical power will be needed to better define the optimal dose. In addition, at a time interval of ≈ 20 min between injections, 4 mg resulted in significantly less residual background fluorescence intensity compared to 6 mg. Use of a higher dose would require a longer time interval, i.e., a longer clearance period, between doses to avoid dose stacking. It should be noted that even with repeat dosing at 6 mg, the total dose (24 mg) was below the standard package size (25 mg).

The use of a real-time, intraoperative imaging system is particularly advantageous in microsurgical perforator flap reconstruction in order to provide a dynamic assessment of flap perfusion. In this study, we performed four assessments: both sides of the abdominal flap prior to elevation, the selected abdominal flap after isolation on the perforators prior to transfer, and the same flap after microsurgery. This permitted a comparison of perforator vessel selection and identification, analysis of flap perfusion after isolation on the perforating vessels, and differences after flap harvest and microsurgical transfer. Flap physiology changes with vessel isolation, harvest, and transfer, so that obtaining real-time NIR imaging at multiple points becomes a dynamic process. This is in contrast to preoperative imaging modalities such as duplex ultrasound, CT, or MRI, where identification of the dominant perforator is a static one-time assessment. In the future, we plan to use NIR imaging to assist directly in vessel selection and isolation, as well as to apply quantitative metrics previously validated in large animal model systems,[15] to determine arterial or venous insufficiency.

In two cases, the dominant perforator identified by NIR imaging was not the perforator selected by the operating surgeon. This occurred as the surgeon was blinded to the results of the FLARE™ system. Of note, the CBR at the dominant perforator decreased after ligation, and the CBR at the selected perforator increased to the previous level of the dominant perforator (Figure 3A). This further demonstrates that flap physiology is often altered during surgery and the results will differ from preoperative imaging. The changes in flap physiology from perforator vessel isolation can only be seen with a real-time, intraoperative system.

The early clinical use of NIR imaging has been described previously.[21-29] The imaging systems used in these studies were limited to a handheld camcorder device. These systems provide subjective, qualitative results with low resolution. In addition, the outputs from previous generation devices were single grayscale images. As these systems used laser-induced fluorescence, the ICG dose was also higher at 0.5 mg/kg,[29] so that an average 70-kg patient would require a 35-mg dose.

Newer commercially available NIR imaging systems, such as the SPY system (Novadaq Technologies Inc., Toronto, Canada), have been used recently in reconstructive surgery.[30, 31] These early clinical experiences mirror the results seen in our study. There are major differences between the two imaging systems, however. The SPY system is laser-based while the FLARE™ system is LED-based; this may pose differences in eye safety in the operating room. More importantly, the FLARE™ imaging system acquires color video and NIR fluorescence images simultaneously and is capable of real-time overlay of the invisible NIR light images onto the color video images. This provides the surgeon with unambiguous surgical landmarks for image-guided surgery. The FLARE™ system also has the ability to quantify perforator perfusion metrics, as previously shown by our laboratory.[14, 15, 32] The cost of parts in quantity 1 for the FLARE™ imaging system is ≈ $120,000 USD. A miniaturized version of FLARE™, termed Mini-FLARE™, costs ≈ $40,000 USD (Chapter 6).

Although this is the first successful clinical pilot study with the FLARE™ system in reconstructive surgery, there are many areas that will need to be evaluated. Larger-scale studies need to be performed to assess clinical benefits. Each NIR angiography evaluation takes only two minutes, and a more effective decision-making process for perforator selection could potentially decrease overall operative times. Other benefits include the potential ability to prevent complications associated with poor perfusion. The costs associated with the additional use of this type of technology also need to be assessed. One limitation of the FLARE™ system is its 15-cm field of view: it is possible that flaps larger than this size would not be completely captured. For example, imaging was performed on each side of the abdomen, as the entire abdominal flap could not be captured with one scan. Finally, the surgeons in this study were blinded to the results of NIR imaging; in future studies we plan to have the surgeons directly apply the imaging results in perforator choice and flap design.

## CONCLUSION

This is the first-in-human study demonstrating use of the FLARE™ system for NIR angiography in microsurgical perforator-flap breast reconstruction. It represents the successful translation of the technology from pre-clinical to clinical use. In this pilot study, an ICG dose of 4 mg per injection resulted in the highest observed CBR,

SBR, and SNR relative to 2-mg and 6-mg dose; however, a larger study with sufficient statistical power is needed to confirm this result.

## ACKNOWLEDGEMENTS

We thank Lorissa A. Moffitt and Mary McCarthy for editing, and Eugenia Trabucchi for administrative assistance. This work was funded by the National Institutes of Health grants R01-EB-005805 and R01-CA-115296 to JVF.

## REFERENCES


1. Giunta RE, Geisweid A, Feller AM. The value of preoperative Doppler sonography for planning free perforator flaps. Plast Reconstr Surg 2000; 105:2381-6.
2. Masia J, Clavero JA, Larranaga JR, et al. Multidetector-row computed tomography in the planning of abdominal perforator flaps. J Plast Reconstr Aesthet Surg 2006; 59:594-9.
3. Rozen WM, Stella DL, Phillips TJ, et al. Magnetic resonance angiography in the preoperative planning of DIEA perforator flaps. Plast Reconstr Surg 2008; 122:222e-223e.
4. Saint-Cyr M, Schaverien M, Arbique G, et al. Three- and four-dimensional computed tomographic angiography and venography for the investigation of the vascular anatomy and perfusion of perforator flaps. Plast Reconstr Surg 2008; 121:772-80.
5. Mathes DW, Neligan PC. Current techniques in preoperative imaging for abdomen-based perforator flap microsurgical breast reconstruction. J Reconstr Microsurg 2010; 26:3-10.
6. Chernyak V, Rozenblit AM, Greenspun DT, et al. Breast reconstruction with deep inferior epigastric artery perforator flap: 3.0-T gadolinium-enhanced MR imaging for preoperative localization of abdominal wall perforators. Radiology 2009; 250:417-24.
7. Uppal RS, Casaer B, Van Landuyt K, et al. The efficacy of preoperative mapping of perforators in reducing operative times and complications in perforator flap breast reconstruction. J Plast Reconstr Aesthet Surg 2009; 62:859-64.
8. Rosson GD, Williams CG, Fishman EK, et al. 3D CT angiography of abdominal wall vascular perforators to plan DIEAP flaps. Microsurgery 2007; 27:641-6.
9. Troyan SL, Kianzad V, Gibbs-Strauss SL, et al. The FLARE intraoperative near-infrared fluorescence imaging system: a first-in-human clinical trial in breast cancer sentinel lymph node mapping. Ann Surg Oncol 2009; 16:2943-2952.
10. Gioux S, Kianzad V, Ciocan R, et al. High-power, computer-controlled, light-emitting diode-based light sources for fluorescence imaging and image-guided surgery. Mol Imaging 2009; 8:156-65.
11. Lee BT, Matsui A, Hutteman M, et al. Intraoperative near-infrared fluorescence imaging in perforator flap reconstruction: current research and early clinical experience. J Reconstr Microsurg 2010; 26:59-65.
12. Matsui A, Lee BT, Winer JH, et al. Real-time intraoperative near-infrared fluorescence angiography for perforator identification and flap design. Plast Reconstr Surg 2009; 123:125e-7e.
13. Matsui A, Lee BT, Winer JH, et al. Image-guided perforator flap design using invisible near-infrared light and validation with x-ray angiography. Ann Plast Surg 2009; 63:327-330.
14. Matsui A, Lee BT, Winer JH, et al. Submental perforator flap design with a near-infrared fluorescence imaging system: the relationship among number of perforators, flap perfusion, and venous drainage. Plast Reconstr Surg 2009; 124:1098-104.
15. Matsui A, Lee BT, Winer JH, et al. Quantitative assessment of perfusion and vascular compromise in perforator flaps using a near-infrared fluorescence-guided imaging system. Plast Reconstr Surg 2009; 124:451-60.
16. Laird NM, Ware JH. Random-effects models for longitudinal data. Biometrics 1982; 38:963-74.
17. Littell RC, Milliken GA, Stroup WW, et al. SAS for Mixed Models, Second Edition. Cary, NC: SAS Institute, Inc., 2006.
18. Liang KY, Zeger SL. Longitudinal data analysis using generalized linear models. Biometrika 1986; 73:13-22.
19. Winer JH, Choi HS, Gibbs-Strauss SL, et al. Intraoperative localization of insulinoma and normal pancreas using invisible near-infrared fluorescent light. Ann Surg Oncol 2010; 17:1094-100.
20. Gibbs-Strauss SL, Vooght C, Fish KM, et al. Molecular imaging agents specific for the annulus fibrosus of the intervertebral disk. Mol Imaging 2010; 9:128-40.
21. Still J, Law E, Dawson J, et al. Evaluation of the circulation of reconstructive flaps using laser-induced fluorescence of indocyanine green. Ann Plast Surg 1999; 42:266-74.
22. Holm C, Mayr M, Hofter E, et al. Intraoperative evaluation of skin-flap viability using laser-induced fluorescence of indocyanine green. Br J Plast Surg 2002; 55:635-44.

23. Holm C, Tegeler J, Mayr M, et al. Monitoring free flaps using laser-induced fluorescence of indocyanine green: a preliminary experience. Microsurgery 2002; 22:278-87.
24. Mothes H, Donicke T, Friedel R, et al. Indocyanine-green fluorescence video angiography used clinically to evaluate tissue perfusion in microsurgery. J Trauma 2004; 57:1018-24.
25. Krishnan KG, Schackert G, Steinmeier R. The role of near-infrared angiography in the assessment of post-operative venous congestion in random pattern, pedicled island and free flaps. Br J Plast Surg 2005; 58:330-8.
26. Krishnan KG, Schackert G, Steinmeier R. Near-infrared angiography and prediction of postoperative complications in various types of integumentary flaps. Plast Reconstr Surg 2004; 114:1361-2.
27. Yamaguchi S, De Lorenzi F, Petit JY, et al. The "perfusion map" of the unipedicled TRAM flap to reduce postoperative partial necrosis. Ann Plast Surg 2004; 53:205-9.
28. Holm C, Mayr M, Hofter E, et al. Perfusion zones of the DIEP flap revisited: a clinical study. Plast Reconstr Surg 2006; 117:37-43.
29. Holm C, Mayr M, Hofter E, et al. Interindividual variability of the SIEA Angiosome: effects on operative strategies in breast reconstruction. Plast Reconstr Surg 2008; 122:1612-20.
30. Newman MI, Samson MC. The application of laser-assisted indocyanine green fluorescent dye angiography in microsurgical breast reconstruction. J Reconstr Microsurg 2009; 25:21-6.
31. Pestana IA, Coan B, Erdmann D, et al. Early experience with fluorescent angiography in free-tissue transfer reconstruction. Plast Reconstr Surg 2009; 123:1239-44.
32. Matsui A, Lee BT, Winer JH, et al. Predictive capability of near-infrared fluorescence angiography in submental perforator flap survival. Plast Reconstr Surg 2010; 126:1518-1527.

# Chapter 11

# Near-infrared fluorescence imaging in patients undergoing pancreaticoduodenectomy

Hutteman M[1], van der Vorst JR[1], Mieog JSD, Bonsing BA, Hartgrink HH, Kuppen PJK, Löwik CWGM, Frangioni JV, van de Velde CJH, Vahrmeijer AL

[1] Shared first authorship

*Eur Surg Res 2011; 47:90-97.*

## ABSTRACT

### Background

Intraoperative visualization of pancreatic tumors has the potential to improve radical resection rates. Intraoperative visualization of the common bile duct and bile duct anastomoses could be of added value. In this study, we explored the use of indocyanine green (ICG) for these applications, and attempted to optimize injection timing and dose.

### Methods

Eight patients undergoing a pancreaticoduodenectomy were injected intravenously with 5 or 10 mg ICG. During and after injection, the pancreas, tumor, common bile duct, and surrounding organs were imaged in real-time using the Mini-FLARE™ near-infrared (NIR) imaging system.

### Results

No clear tumor-to-pancreas contrast was observed, except for incidental contrast in one patient. The common bile duct was clearly visualized using NIR fluorescence, within 10 minutes after injection, with a maximal contrast between 30 to 90 min after injection. Patency of biliary anastomoses could be visualized due to biliary excretion of ICG.

### Conclusion

No useful tumor demarcation could be visualized in pancreatic cancer patients after intravenous injection of ICG. However, the common bile duct and biliary anastomoses were clearly visualized during the observation period. Therefore, these imaging strategies could be beneficial during biliary surgery in cases where the surgical anatomy is aberrant or difficult to identify.

## INTRODUCTION

Pancreatic cancer is the fourth leading cause of cancer-related mortality in the United States, with an incidence of approximately 38,000 cases and an estimated 34,000 deaths. The overall 5-year survival rate is very low (< 5%).[1] Approximately 10% to 15% of patients are eligible for surgical resection, which is presently the only potentially curative treatment option. Even after curative resection, the reported 5-year survival rates are disappointing and vary from 10% to 17 %.[2-5] Several factors, such as tumor size, lymph node status, tumor grade, and blood vessel invasion are correlated with prognosis. Involvement of tumor margins is an important prognostic factor, as reported survival for R0 (radical) resections (20.3 months) is twice that of R1 resections (10.3 months).[6] For preoperative staging and determination of resectability, the imaging procedure of choice is a multiphase, multidetector helical computed tomography (CT) with intravenous administration of a contrast agent combined with an endoscopic ultrasonography.[7]

During pancreatic surgery, assessment of the extent of the pancreatic tumor is made based on visual inspection and palpation, sometimes in conjunction with intraoperative ultrasonography.[8, 9] Intraoperative tumor identification remains challenging, partly because the surrounding pancreatic tissue is frequently inflamed. Local recurrence rates of 72% to 86% are reported,[10-12] which in part could be caused by inadequate intraoperative evaluation of the location and extent of the tumor.

Near-infrared (NIR) fluorescence imaging is a promising technique to facilitate intraoperative, real-time, visual information.[13-15] In order to detect tumors using NIR fluorescence, contrast agents that target tumor-specific characteristics can be used to selectively label tumor cells.[16-19] Novel NIR fluorescent agents have been developed that target tumor-specific cell surface markers,[16, 20] enzymatic activity,[17, 19, 21] or increased glucose metabolism.[22] However, these tumor-specific agents are not yet available for clinical use. The only NIR fluorescent contrast agents currently available, methylene blue and indocyanine green (ICG), are not tumor-specific. However, the enhanced permeability and retention (EPR) effect can potentially be used to obtain accumulation of non-targeted contrast agents in tumors.[23, 24] Due to newly formed, more porous blood vessels, molecules can passively accumulate into the surrounding tissue. Furthermore, poorly developed lymphatics in the tumor result in an increased retention. Previous studies showed breast carcinomas and liver tumors could be identified noninvasively with NIR fluorescence using ICG based on the EPR effect.[25-28] The aim of our study was to assess the applicability of NIR fluorescence imaging using ICG to provide a clear tumor-to-background contrast in oncologic pancreatic surgery.

Because ICG is almost exclusively excreted into the bile, it can also be used for intraoperative NIR fluorescence exploration of the biliary anatomy.[29-31] This can be useful in patients with a difficult laparoscopic cholecystectomy, due to an aberrant biliary anatomy or an acute cholecystitis, for example. Furthermore, ICG can potentially

be used to assess anastomosis patency in patients undergoing bile duct reconstruction. This is a well-suited setting to study both biliary anatomy and anastomosis patency intraoperatively, as the common bile duct can be visualized for a long time during pancreaticoduodenectomy.

## MATERIALS AND METHODS

### Intraoperative Near-Infrared Imaging System (Mini-FLARE™)

Intraoperative imaging was performed using the hand-held Fluorescence-Assisted Resection and Exploration (Mini-FLARE™) image-guided surgery system as described in Chapter 6.[32] This system consists of two wavelength isolated light sources: a "white" light source, generating 26,600 lx of 400-650 nm light and a NIR light source, generating 7.7 mW/cm$^2$ of 760 nm light. Color video and NIR fluorescence images are simultaneously acquired and displayed in real-time using custom optics and software that separate the color video and NIR fluorescence images. A pseudo-colored (lime green) merged image of the color video and NIR fluorescence images is also displayed. The imaging head is attached to a flexible gooseneck arm, which permits positioning of the imaging head virtually anywhere over the surgical field, even at extreme angles. For intraoperative use, the imaging head and imaging system pole stand are wrapped in a sterile shield and drape (Medical Technique Inc., Tucson, USA).

### Preparation and Administration of Indocyanine Green

ICG (25 mg vials) was purchased from Pulsion Medical Systems (Munich, Germany) and resuspended in 10 cc of sterile water for injection to yield a 2.5 mg/ml (3.2 mM) stock solution. Of this stock solution 2 or 4 mL, corresponding with doses of 5 or 10 mg, was administered.

### Clinical Trial

The study was approved by the Local Medical Ethics Committee of the Leiden University Medical Center and was performed in accordance with the ethical standards of the Helsinki Declaration of 1975. A total of 8 consecutive patients with suspected ampullary or pancreatic head carcinoma planned to undergo curative resection were included. All patients provided informed consent. Exclusion criteria included pregnancy, lactation or an allergy to iodine, shellfish, or indocyanine green. The surgical technique used in our center implies a standard pancreaticoduodenectomy with resection of peripancreatic tissues and lymph nodes. Following resection, reconstruction is performed with pancreaticojejunostomy, choledochojejunostomy,

and pylorojejunostomy for pylorus preserving pancreaticoduodenectomy or a gastrojejunostomy as part of Whipple's procedure. After opening the omental bursa, performing the Kocher maneuver, and exploration of the hepatoduodenal ligament, the pancreatic tumor was fully exposed. The Mini-FLARE imaging system was positioned 30 centimeters above the surgical field. Next, 4 patients were intravenously administrated 5 mg ICG diluted in 2 mL sterile water as a bolus and 4 patients were intravenously administrated 10 mg ICG diluted in 4 mL sterile water as a bolus. All operating room lights, with the exception of the white light and NIR light of the Mini-FLARE imaging system, were dimmed. The NIR fluorescence measurements of the pancreatic tumor, pancreas, duodenum, stomach, liver, gall bladder, and common bile duct were recorded at the time of injection (T=0), 45 seconds and 3-, 10-, 30-, 60-, 90-, 120-, 180- min post-injection. At each measurement, camera exposure times were set appropriately to prevent the NIR fluorescence signal from reaching saturation. Bile duct imaging ended at 90 min because the bile duct was resected at this time as part of the pancreaticoduodenectomy. Furthermore, imaging of the choledochojejunostomy was performed to assess leakage and patency. Fluorescent intensity of these structures was quantified using the custom Mini-FLARE software. To calculate tumor-to-pancreas ratios, tumor and healthy pancreas regions of interest were manually drawn, guided by palpation. Signal-to-background ratios (SBR) for the common bile duct were manually drawn, and a background region of interest was drawn on direct surrounding tissue.

### Statistical Analysis

For statistical analysis and graph design, GraphPad Prism Software (Version 5.01, La Jolla, USA) and SPSS (Version 17.0, Chicago, USA) were used. All data were reported as mean ± standard deviation or median and range. To compare the signal-to-background ratios between the two concentration groups, T-tests were used. Repeated-measures ANOVAs were used to test differences between time points. All statistical tests were two-tailed and $P < 0.05$ was considered significant.

## RESULTS

Patient and tumor characteristics are listed in Table 1. Eight patients undergoing surgery for a suspected ampullary or pancreatic head carcinoma were included in the study. In one patient, the common bile duct was cut several minutes after ICG administration and therefore measurements beyond 3 min were excluded from the analysis. Four patients underwent a complete Whipple procedure, three patients underwent a pylorus preserving pancreaticoduodenectomy, and one patient had an irresectable tumor, resulting in a biopsy without further resection.

**Table 1.** Patient Characteristics

| Pt | Age (y) | Sex | Weight (kg) | Length (cm) | BMI | AF (U/L) | gGT (U/L) | ASAT (U/L) | ALAT (U/L) | Tumor size (cm) | Tumor location | Surgery | T | N | M | R | Vasc inv | Perin inv | Pathology |
|---|---|---|---|---|---|---|---|---|---|---|---|---|---|---|---|---|---|---|---|
| 1 | 39 | M | 90 | 186 | 26 | 261 | 86 | 92 | 155 | n/a | Head | Bypass | 3 | + | - | n/a | n/a | n/a | Poorly diff. adenoca. |
| 2 | 76 | V | 64 | 164 | 24 | 97 | 72 | 21 | 16 | 4.7 | Ampulla | Whipple | 3 | - | - | R0 | - | + | Poorly diff. adenoca. |
| 3 | 45 | M | 65 | 179 | 20 | 118 | 274 | 20 | 19 | 4 | Head | PPPD | 3 | + | - | R1 | - | + | Well diff. adenoca. |
| 4 | 32 | M | 88 | 188 | 25 | 114 | 66 | 48 | 78 | - | - | Whipple | | - | - | | | | No malignancy |
| 5 | 74 | V | 75 | 169 | 26 | 72 | 46 | 69 | 40 | 6 | Head | Whipple | 2 | + | - | R1 | - | - | Adenoca. |
| 6 | 61 | V | 73 | 176 | 24 | 674 | 1472 | 280 | 292 | 1.7 | Head | PPPD | 3 | + | - | R0 | - | + | Adenoca. |
| 7 | 46 | V | 89 | 170 | 31 | 42 | 11 | 59 | 39 | 1.8 | Head | Whipple | 1 | + | - | R1 | - | - | Neuroendocrine |
| 8 | 62 | M | 68 | 180 | 21 | 71 | 64 | 21 | 23 | 2.3 | Duodenum | PPPD | | - | - | R0 | - | - | Adenomatous polyp |

AF, alkaline phosphatase; gGT, gamma-glutamyltransferase; ASAT, aspartate transaminase, ALAT, alanine transaminase, Vasc inv, vascular invasion; Perin inv, perineural invasion; n/a, not available due to irresectable tumor; PPPD, pylorus-preservaring pancreaticoduodenectomy.

## Tumor Imaging

Directly after injection, superficial arterial flow of ICG was identified by NIR fluorescence on the surface of the pancreas followed by venous drainage. In the 5- mg patient group (N = 4), a mean tumor-to-pancreas ratio of 0.89 ± 0.25 was observed. In the 10-mg patient group (N = 4), a mean tumor-to-pancreas ratio of 1.22 ± 0.39 was observed (Figure 1a). Time had no significant effect on tumor-to-pancreas ratio ($P$ = 0.899). Tumor-to-pancreas ratios were significantly higher in the 10-mg group, when compared to 5-mg group ($P$ = 0.002). In one patient (patient 5, 10-mg dose group), a clear NIR fluorescent hotspot was observed on the pancreas (Figure 1b). Histological analyses confirmed that the signal corresponded to tumor tissue surrounding the pancreatic duct. Other than this incidental finding, no contrast was observed.

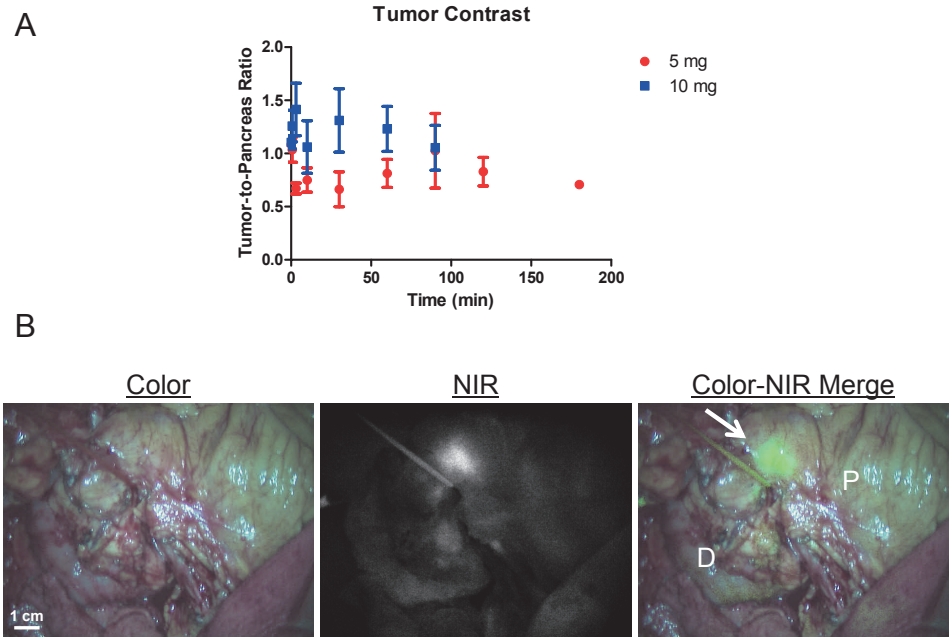


**Figure 1. Tumor-to-Pancreas Contrast using NIR Fluorescence and ICG: A.** Tumor-to-pancreas ratios (mean ± SD) of the pancreatic tumors over time, per dose group. **B.** Color video (left panel), NIR fluorescence (middle panel) and a color-NIR overlay (right panel) of intraoperative imaging of the pancreas. In this example, clear contrast (arrow) is shown between pancreatic tumor and normal pancreatic tissue (P), 20 min after administration of 10 mg of ICG. However, this was an incidental finding in one patient. The duodenum is marked with the letter D.

## Imaging of the Common Bile Duct using NIR Fluorescence

Within 10 min after administration of ICG, the common bile duct, cystic duct, and common hepatic duct could clearly be identified by NIR fluorescence (Figure 2a and b) in all patients. The NIR fluorescence signal of the liver outshined the left and

right hepatic ducts and therefore prevented a clear visualization. The fluorescent signal of the bile ducts lasted until 90 min postinjection, at which point the bile duct was resected, along with the head of the pancreas and the duodenum, as part of the pancreaticoduodenectomy. No difference was observed between the 5-mg and 10-mg groups ($P$ = 0.849). Time significantly influenced signal-to-background ratio ($P$ = 0.002). An optimum was found between 30 and 90 min postinjection, with a maximum mean signal-to-background ratio of 6.24 ± 1.32 at 60 min postinjection. After completion of the choledochojejunostomy, anastomotic patency could be confirmed by visualizing the NIR fluorescence signal passing the anastomosis into the jejunum (Figure 2c).

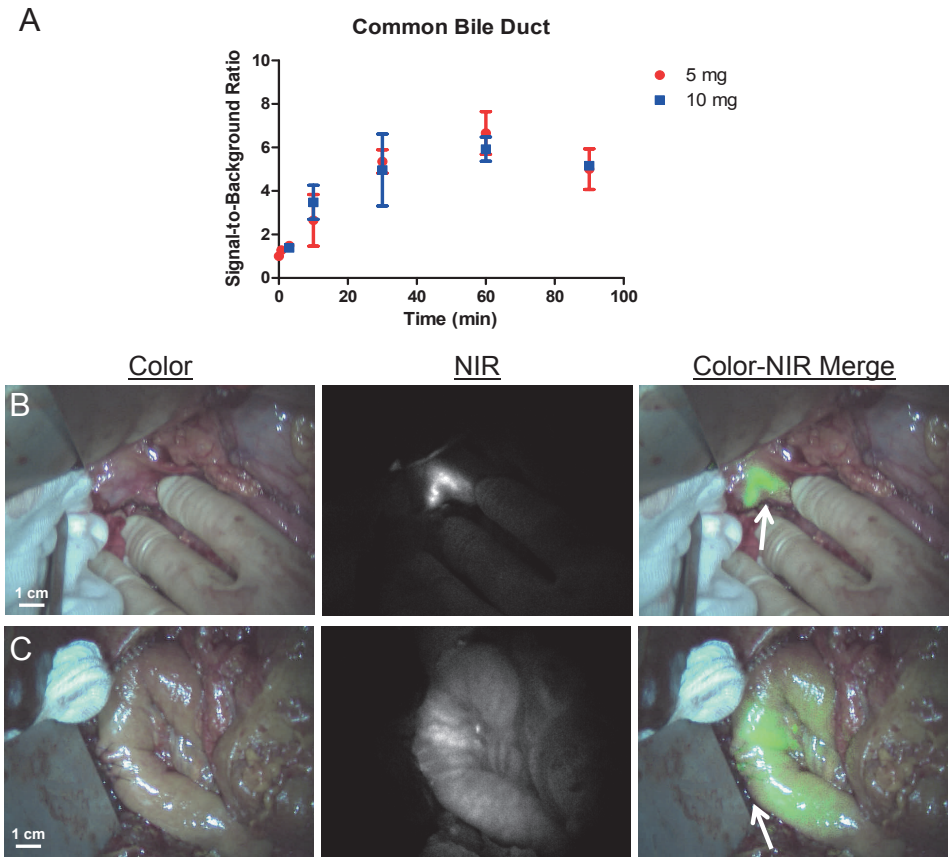


**Figure 2. Intraoperative Imaging of the Common Bile Duct using NIR Fluorescence and ICG: A.** Signal-to-background ratios (mean ± SD) of the common bile duct over time, per dose group. Signal-to-background ratios (SBR) for the common bile duct were calculated. A background region-of-interest was drawn on direct surrounding tissue. **B.** Color video (left panel), NIR fluorescence (middle panel) and a color-NIR overlay (right panel) of intraoperative imaging of the common bile duct in a patient who underwent a cholecystectomy during previous surgery, 30 min after administration of 5 mg ICG. A clear contrast is shown between common bile duct (arrow) and surrounding tissue. **C.** Color video (left panel), NIR fluorescence (middle panel) and a color-NIR overlay (right panel) of a choledochojejunostomy (arrow), 30 min after completion of the anastomosis. NIR fluorescence signal of excreted ICG is visualized intraluminally in the jejunum, indicating anastomotic patency and absence of leakage.

### Biodistribution of ICG

The NIR fluorescence signal of the pancreas, stomach, liver, duodenum and common bile duct was measured at fixed time intervals (Figure 3). As reported in preclinical studies [30], within the first 2 min vascular signal (an arterial phase followed by a venous phase) could be visualized. The pancreas, stomach and duodenum showed comparable washout patterns. As ICG is cleared by the liver, the liver and common bile duct exhibited high levels of NIR fluorescence, indicating hepatic uptake and clearance in bile.

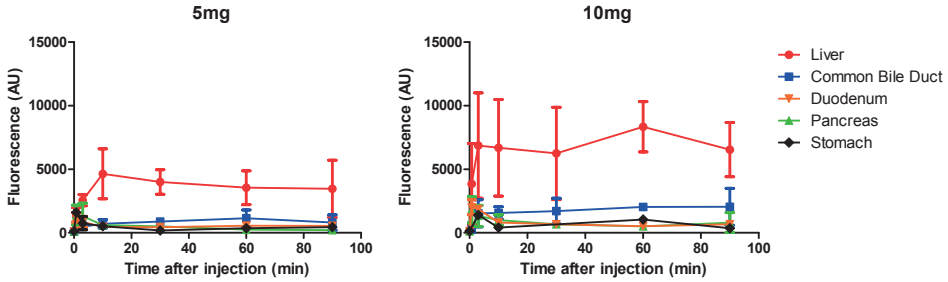


**Figure 3. Biodistribution of ICG in Organs Exposed During Pancreaticoduodenectomy**: Shown are NIR fluorescence intensities of organs exposed during pancreaticoduodenectomy. Measurements of the duodenum were taken over an area not containing bile. Intensities are shown over time for both 5 mg (left panel) and 10 mg (right panel) groups.

## DISCUSSION

The first objective of this study was to exploit the EPR effect[23, 24] to induce retention of the non-targeted probe ICG in pancreatic tumors. However, in all but one patient, no useful intraoperative tumor-to-pancreas ratios in pancreatic cancer patients were observed using NIR fluorescence and ICG. In one patient, a clear hotspot was observed on the pancreas, which corresponded with the resected adenocarcinoma. No specific pathological characteristics were observed that could account for this phenomenon. Several factors might explain the observed lack of contrast in all other patients. Healthy pancreas tissue showed a relatively high uptake of ICG, whereas tumor tissue showed similar uptake. As washout of NIR fluorescence signal was comparable in both healthy pancreas tissue and tumor tissue, no EPR effect could be visualized. This is possibly the result of different tumor biology of pancreatic cancer when compared to breast cancer, in which the EPR effect has been observed in previous studies. Several earlier studies reported a lower perfusion of tumor tissue in comparison with healthy pancreas tissue,[33, 34] which might decrease availability of ICG for a potential EPR effect of the tumor. Furthermore, previous studies that reported an EPR effect of ICG in breast tumors used detection methods (laser scanning or optical tomography), that

may detect lower concentrations of ICG but require post-processing, and are therefore not applicable for real-time intraoperative imaging.[26, 27]

Novel NIR fluorescent probes are being developed to increase signal penetration depth and decrease background uptake. For multiple applications within cancer surgery, it is imperative to design improved tumor targeting probes. Tumor targeting can be accomplished by conjugating a fluorophore to a targeting ligand such as antibodies or peptides, for example.[16, 19, 21, 22] It is expected that several of those tumor targeted probes will be available for first-in-human trials within the coming years.

The second objective of this study was to evaluate the biodistribution of ICG and its clearance by the liver into the bile. Patients undergoing a pancreaticoduodenectomy are well suited for this study, as the bile ducts and abdominal organs can be studied for a relatively long time. As stated before, iatrogenic common bile duct injury occurs in patients undergoing cholecystectomy. A non-invasive imaging modality that can visualize the common bile duct intraoperatively could potentially reduce the incidence of common bile duct injury in these patients. For example, this technique can help the surgeon identify vital structures during difficult laparoscopic cholecystectomies in patients with acute cholecystitis or aberrant biliary anatomy. This technique could potentially prevent the need to convert to an open procedure.

In this study, the common bile duct was identified using NIR fluorescence imaging after ICG administration in all patients. This is in concordance with preclinical data, described by Matsui et al.[30] and in clinical studies of patients undergoing cholecystectomy.[29, 31] A useful contrast between the common bile duct and surrounding tissue was observed starting at 10 min postinjection. The optimal timing of ICG administration prior to imaging lies between 30 and 90 min. In this interval, mean SBRs of 5 to 6 were observed. Ideally, background fluorescence levels of all surrounding organs should be minimal. In this study, the liver signal remained high throughout the imaging interval. Although this did not prevent a contrast being observed between common bile duct and surrounding tissues, future studies should focus on optimal timing to minimize background fluorescence, especially when studying the liver. Indeed, in a separate study, in which patients with colorectal liver metastases were injected intravenously with 10 mg ICG at 24 hours prior to liver surgery, liver fluorescence decreased to background levels, while bile duct imaging was still possible. However, compared to the fluorescent intensity observed in the present study, the bile duct signal was significantly decreased by 88 % (van der Vorst et al., manuscript in preparation). Therefore, novel NIR fluorescent agents should be developed that are excreted into bile, with minimal liver uptake, thereby reducing background fluorescence and increasing the ability to visualize bile ducts. In contrast to most other imaging systems, the Mini-FLARE imaging system used in this study can display the NIR fluorescence signal in relation to the surgical anatomy, by simultaneously displaying color video and NIR fluorescence. This feature is of added

benefit in performing true image-guided surgery. The Mini-FLARE can only be used during open surgery. However, most cholecystectomies are performed by laparoscopy. In order to enable intraoperative NIR fluorescence imaging during laparoscopic surgery, laparoscopic camera systems are currently being developed and tested.[30, 31, 35] Furthermore, as with all novel techniques, large clinical studies are necessary to prove the added value of NIR fluorescence imaging in patients undergoing a cholecystectomy. These trials can use the data presented in this study to select the optimal time of imaging after ICG administration.

This study showed that no useful tumor demarcation could be visualized in pancreatic cancer patients using intraoperative NIR fluorescence imaging after ICG administration. Furthermore, our study showed the ability to visualize the common bile duct after ICG administration and demonstrated the influence of time on signal-to-background ratio. Moreover, patency of the jejunal-biliary anastomosis could be visualized. For a translation to clinical practice, larger trials should be executed. This is dependent on broad availability of commercial intraoperative NIR fluorescence imaging systems. When these imaging systems become available for use in the clinic in the coming years, the true value of this technique can be assessed.

## ACKNOWLEDGEMENTS

We thank Lindsey Gendall for editing. This work was supported in part by the Nuts Ohra Fund, the Foundation "Maurits and Anna de Kock", and NIH grant #R01-CA-115296.

## REFERENCES


1. Jemal A, Siegel R, Ward E, et al. Cancer statistics, 2008. CA Cancer J Clin 2008; 58:71-96.
2. Yeo CJ, Sohn TA, Cameron JL, et al. Periampullary adenocarcinoma: analysis of 5-year survivors. Ann Surg 1998; 227:821-831.
3. Sohn TA, Yeo CJ, Cameron JL, et al. Resected adenocarcinoma of the pancreas-616 patients: results, outcomes, and prognostic indicators. J Gastrointest Surg 2000; 4:567-579.
4. Cleary SP, Gryfe R, Guindi M, et al. Prognostic factors in resected pancreatic adenocarcinoma: analysis of actual 5-year survivors. J Am Coll Surg 2004; 198:722-731.
5. Conlon KC, Klimstra DS, Brennan MF. Long-term survival after curative resection for pancreatic ductal adenocarcinoma. Clinicopathologic analysis of 5-year survivors. Ann Surg 1996; 223:273-279.
6. Garcea G, Dennison AR, Pattenden CJ, et al. Survival following curative resection for pancreatic ductal adenocarcinoma. A systematic review of the literature. JOP 2008; 9:99-132.
7. Miura F, Takada T, Amano H, et al. Diagnosis of pancreatic cancer. HPB (Oxford) 2006; 8:337-342.
8. Shin LK, Brant-Zawadzki G, Kamaya A, et al. Intraoperative ultrasound of the pancreas. Ultrasound Q 2009; 25:39-48.
9. Sun MR, Brennan DD, Kruskal JB, et al. Intraoperative ultrasonography of the pancreas. Radiographics 2010; 30:1935-1953.
10. Griffin JF, Smalley SR, Jewell W, et al. Patterns of failure after curative resection of pancreatic carcinoma. Cancer 1990; 66:56-61.
11. Sperti C, Pasquali C, Piccoli A, et al. Recurrence after resection for ductal adenocarcinoma of the pancreas. World J Surg 1997; 21:195-200.
12. Westerdahl J, Andren-Sandberg A, Ihse I. Recurrence of exocrine pancreatic cancer--local or hepatic? Hepatogastroenterology 1993; 40:384-387.
13. Keereweer S, Kerrebijn JD, van Driel PB, et al. Optical Image-guided Surgery-Where Do We Stand? Mol Imaging Biol 2010.
14. Frangioni JV. New technologies for human cancer imaging. J Clin Oncol 2008; 26:4012-4021.
15. Gioux S, Choi HS, Frangioni JV. Image-guided surgery using invisible near-infrared light: fundamentals of clinical translation. Mol Imaging 2010; 9:237-255.
16. Lee SB, Hassan M, Fisher R, et al. Affibody molecules for in vivo characterization of HER2-positive tumors by near-infrared imaging. Clin Cancer Res 2008; 14:3840-3849.
17. Jiang T, Olson ES, Nguyen QT, et al. Tumor imaging by means of proteolytic activation of cell-penetrating peptides. Proc Natl Acad Sci U S A 2004; 101:17867-17872.
18. Hutteman M, Mieog JS, van der Vorst JR, et al. Intraoperative near-infrared fluorescence imaging of colorectal metastases targeting integrin alpha(v)beta(3) expression in a syngeneic rat model. Eur J Surg Oncol 2011.
19. Mieog JS, Hutteman M, van der Vorst JR, et al. Image-guided tumor resection using real-time near-infrared fluorescence in a syngeneic rat model of primary breast cancer. Breast Cancer Res Treat 2010.
20. Gleysteen JP, Newman JR, Chhieng D, et al. Fluorescent labeled anti-EGFR antibody for identification of regional and distant metastasis in a preclinical xenograft model. Head Neck 2008; 30:782-789.
21. Weissleder R, Tung CH, Mahmood U, et al. In vivo imaging of tumors with protease-activated near-infrared fluorescent probes. Nat Biotechnol 1999; 17:375-378.
22. Zhou H, Luby-Phelps K, Mickey BE, et al. Dynamic near-infrared optical imaging of 2-deoxyglucose uptake by intracranial glioma of athymic mice. PLoS ONE 2009; 4:e8051.
23. Matsumura Y, Maeda H. A new concept for macromolecular therapeutics in cancer chemotherapy: mechanism of tumoritropic accumulation of proteins and the antitumor agent smancs. Cancer Res 1986; 46:6387-6392.
24. Maeda H, Wu J, Sawa T, et al. Tumor vascular permeability and the EPR effect in macromolecular therapeutics: a review. JControl Release 2000; 65:271-284.
25. Hagen A, Grosenick D, Macdonald R, et al. Late-fluorescence mammography assesses tumor capillary permeability and differentiates malignant from benign lesions. Opt Express 2009; 17:17016-17033.

26. Intes X, Ripoll J, Chen Y, et al. In vivo continuous-wave optical breast imaging enhanced with Indocyanine Green. Med Phys 2003; 30:1039-1047.
27. Alacam B, Yazici B, Intes X, et al. Pharmacokinetic-rate images of indocyanine green for breast tumors using near-infrared optical methods. Phys Med Biol 2008; 53:837-859.
28. Ishizawa T, Fukushima N, Shibahara J, et al. Real-time identification of liver cancers by using indocyanine green fluorescent imaging. Cancer 2009; 115:2491-2504.
29. Tagaya N, Shimoda M, Kato M, et al. Intraoperative exploration of biliary anatomy using fluorescence imaging of indocyanine green in experimental and clinical cholecystectomies. J Hepatobiliary Pancreat Surg 2009; 17:595-600.
30. Matsui A, Tanaka E, Choi HS, et al. Real-time intra-operative near-infrared fluorescence identification of the extrahepatic bile ducts using clinically available contrast agents. Surgery 2010; 148:87-95.
31. Ishizawa T, Bandai Y, Ijichi M, et al. Fluorescent cholangiography illuminating the biliary tree during laparoscopic cholecystectomy. Br J Surg 2010; 97:1369-1377.
32. Mieog JS, Troyan SL, Hutteman M, et al. Towards Optimization of Imaging System and Lymphatic Tracer for Near-Infrared Fluorescent Sentinel Lymph Node Mapping in Breast Cancer. Ann Surg Oncol 2011.
33. Reuter SR, Redman HC, Bookstein JJ. Differential problems in the angiographic diagnosis of carcinoma of the pancreas. Radiology 1970; 96:93-99.
34. Komar G, Kauhanen S, Liukko K, et al. Decreased blood flow with increased metabolic activity: a novel sign of pancreatic tumor aggressiveness. Clin Cancer Res 2009; 15:5511-5517.
35. Aoki T, Murakami M, Yasuda D, et al. Intraoperative fluorescent imaging using indocyanine green for liver mapping and cholangiography. J Hepatobiliary Pancreat Surg 2009; 17:590-594.

# Chapter 12

# Identification and image-guided resection of occult superficial liver metastases using indocyanine green and near-infrared fluorescence imaging

van der Vorst JR[1], Hutteman M[1], Schaafsma BE, Mieog JSD, Verbeek FPR, Liefers GJ, Hartgrink HH, Löwik CWGM, Kuppen PJK, Smit VTHBM, Frangioni JV, van de Velde CJH, Vahrmeijer AL

[1] Shared first authorship

*Submitted.*

## ABSTRACT

### Background

Near-infrared (NIR) fluorescence imaging using indocyanine green (ICG) is a promising technique for identifying and resecting colorectal liver metastases, however, optimal dosage and timing is not known. The current study was performed to assess feasibility of NIR fluorescence in liver surgery and to assess the optimal dose of ICG and timing of ICG administration.

### Methods

The Mini-FLARE™ imaging system was used for real-time identification of colorectal liver metastases in 22 patients undergoing liver resection. NIR fluorescence imaging was performed 24 or 48 h after systemic administration of 10 or 20 mg ICG. Resected specimens were prepared for *ex vivo* macroscopic and microscopic evaluation of fluorescent patterns.

### Results

A total of 40 superficially located colorectal liver metastases were identified and resected using NIR fluorescence imaging and ICG. In all patients, ICG fluorescence was seen as a rim around the tumor, located microscopically in the transition zone between tumor and normal liver tissue. Median tumor-to-liver ratio (TLR) was 7.4 (range 1.9 – 18.7) and no significant differences between time-points or doses were found. Four metastases detected using NIR fluorescence were occult and not visible using preoperative CT, palpation, or intraoperative ultrasound (IOUS). NIR fluorescence also distinguished benign liver lesions from metastases. Preoperative CT, IOUS, and/or palpation, however, found seven lesions, all deeper than 8 mm, which were not seen using NIR fluorescence.

### Conclusions

This study suggests that NIR fluorescence imaging is complementary to conventional imaging for liver metastasectomies, and has the potential to improve surgical care.

# INTRODUCTION

Prognosis and survival of colorectal cancer patients depends primarily on the occurrence of distance metastases, which occur most frequently in the liver.[1] A resection with curative intent can offer patients with colorectal liver metastases a 5-year survival rate of 36% to 60%.[2-5] Despite improvements in preoperative imaging modalities, surgical techniques, and chemotherapy regimens, intrahepatic recurrence rates vary from 11% to 37.5%, and 65% to 85% of these recurrences appear within 2 years after resection.[2, 6-9] A possible explanation for this high intrahepatic recurrence rate is that some hepatic metastases are already present at time of liver resection, but were undetected by preoperative imaging, intraoperative ultrasound (IOUS), and inspection by the surgeon. It is known that small and superficially located liver metastases are difficult to identify using conventional imaging modalities such as preoperative computed tomography (CT) and IOUS.[10-12]

Near-infrared (NIR) fluorescence imaging using indocyanine green (ICG) is a promising technique to intraoperatively visualize the contrast between liver metastases and normal liver tissue in real time.[13, 14] ICG is excreted exclusively into the bile after intravenous injection. It has been hypothesized that colorectal liver metastases can be visualized due to passive accumulation of ICG caused by hampered biliary excretion, which results in a fluorescent rim around the metastasis. Recently, Ishizawa et al.[13] described the intraoperative detection of colorectal liver metastasis using NIR fluorescence imaging after intravenous ICG injection 1 to 14 days prior to surgery. The interval between ICG injection and surgery is one of the key determinants of the remaining background fluorescence signal of the liver and the fluorescent rim surrounding the tumor. In a preclinical study in rats, performed by our group, the influence of injection time prior to surgery and dose of ICG on the contrast between the fluorescent rim around the hepatic metastases and normal liver tissue (tumor-to-liver ratio) was examined.[15] In this preclinical study, the highest tumor-to-liver ratio was reached when ICG was injected 72 hours prior to surgery. Furthermore, this study demonstrated that even small liver metastases (1 mm) could be identified using NIR fluorescence. In the current study, these preclinical results were translated to a clinical trial in colorectal cancer liver metastases patients in order to optimize intraoperative identification of liver metastases using ICG.

# MATERIALS AND METHODS

### Intraoperative Near-Infrared Imaging System

Intraoperative NIR fluorescence imaging of the liver was performed using the Mini-FLARE™ image-guided surgery system as described in Chapter 6.[16] Briefly, the system

consists of 2 wavelength isolated light sources: a "white" light source, generating 26,600 lx of 400 to 650 nm light and a "near-infrared" light source, generating 7.7 mW/cm$^2$ of 760 nm light. Color video and NIR fluorescence images are simultaneously acquired and displayed in real-time using custom optics and software that separate the color video and 800 nm NIR fluorescence images. A pseudo-colored (lime green) merged image of the color video and NIR fluorescence images is also displayed. The imaging head is attached to a flexible gooseneck arm, which permits positioning of the imaging head virtually anywhere over the surgical field, and at extreme angles. For intraoperative use, the imaging head and imaging system pole stand are wrapped in a sterile shield and drape (Medical Technique Inc., Tucson, USA).

**Preparation and administration of Indocyanine Green**

ICG (25 mg vials) was purchased from Pulsion Medical Systems (Munich, Germany) and resuspended in 10 cc of sterile water for injection to yield a 2.5-mg/ml (3.2 mM) stock solution. Of this stock solution 4 or 8 mL, corresponding to doses of 10 or 20 mg, was administered intravenously.

**Clinical trial**

The study was approved by the Local Medical Ethics Committee of the Leiden University Medical Center and was performed in accordance with the ethical standards of the Helsinki Declaration of 1975. A total of 22 consecutive patients with suspected colorectal liver metastases who were planning to undergo curative intended liver resection were included. All patients provided informed consent. Exclusion criteria were pregnancy, lactation or an allergy to iodine, shellfish or indocyanine green.

Patients received 10 mg or 20 mg of ICG diluted in a total volume of 4 mL and 8 mL, respectively, as an intravenous bolus at 24 or 48 hours prior to surgery on an inpatient base. This resulted in 4 groups of 4 patients per group (N = 16 patients). Subsequently, six patients were included at the optimal combination of ICG dose and injection time. During surgery and after mobilization of the liver, NIR fluorescence signal of metastases and normal liver were measured using the Mini-FLARE™ imaging system. Directly following liver resection, liver resection specimens were immediately delivered to the Department of Pathology, where the specimens were sliced into 5 to 7 mm thick slices and examined for NIR fluorescence using the Mini-FLARE™ imaging system.

**Fluorescence Microscopy**

Based on macroscopic evaluation and *ex vivo* fluorescence imaging, the transition area between tumor and normal liver tissue was identified whereupon these areas were snap-frozen on dry ice. Frozen tissue sections of 20 μm were measured for fluorescence

using the Nuance multispectral imager (CRi, Woburn, USA) mounted on a Leica DM IRE2 inverted microscope (Leica, Wetzlar, Germany) and subsequently stained with hematoxylin and eosin. White light images where created using the same microscope and subsequently merged with fluorescence images.

### Statistical Analysis

For statistical analysis, SPSS statistical software package (Version 17.0, Chicago, USA) was used. Graphs were generated using GraphPad Prism Software (Version 5.01, La Jolla, USA). Tumor-to-liver (TLR) signal, rim fluorescence, and background fluorescence were reported as median and range. Tumor size was reported as mean and standard deviation. To test differences between groups, the Kruskal-Wallis one-way analysis of variance test and the Dunn's Multiple Comparison Test were used to test for differences between time and dose groups. Statistical tests were two-tailed and $P < 0.05$ was considered significant.

## RESULTS

### Study Subjects

Patient and tumor characteristics of the 22 patients included are listed in Table 1. In five patients, no liver resection was performed due to invasion of tumor into the portal vein (N = 3), the presence of additional irresectable liver metastases (N = 1), or the appearance of lymph node metastases (N = 1). These patients were included for TLR, rim fluorescence and background fluorescence analysis.

### Intraoperative detection of colorectal liver metastases

Results of liver metastases detection are summarized in Table 1. Using a combination of preoperative CT scanning, IOUS, visual inspection, and/or palpation, a total of 49 lesions were identified as suspected colorectal liver metastases. After resection, six of these lesions were histologically proven to be benign, for a net detection of 43 metastatic lesions by conventional imaging. NIR fluorescence imaging (Fig. 1) detected a total of 40 lesions proven histologically to be metastases (Table 1), all of which were ≤ 6.2 mm from the surface of the liver capsule.

However, only 36 of the 40 lesions identified using NIR fluorescence overlapped with conventional imaging. In four patients, superficially located, occult liver metastases were detected using NIR fluorescence but not by conventional imaging (Fig 2). After resection, these lesions were found to be 2, 4, 6, and 9 mm in diameter. Histopathological examination confirmed these lesions to be colorectal liver

**Table 1.** Patient Characteristics

| Characteristic | Median (Range) / N (%) |
|---|---|
| Age | 63 (49 - 77) |
| BMI | 25 (19 - 38) |
| Sex (M / F) | 10 (45%) / 12 (55%) |
| Primary tumor location | |
| - Colon | 11 (50) |
| - Sigmoid | 5 (22.7) |
| - Rectum | 5 (22.7) |
| - Anus | 1 (4.5) |
| Primary Tumor type | |
| - Adenocarcinoma | 14 (63.6) |
| - No vital tumor cells | 2 (9.1) |
| - No resection | 6 (27.3) |
| Primary Tumor size (mm) | 20 (1.7 - 70) |
| Type of resection | |
| - Right hemihepatectomy | 1 (4.5) |
| - Left hemihepatectomy | 1 (4.5) |
| - Left lateral hepatic resection + metastasectomy | 3 (13.6) |
| - Metastasectomy | 9 (40.9) |
| - Metastasectomy + Radiofrequency ablation | 1 (4.5) |
| - Radiofrequency ablation | 1 (4.5) |
| - No resection | 6 (27.3) |
| Number of liver metastases identified A | |
| - Preoperative CT scan, IOUS, and/or palpation | 43 [B] |
| - Intraoperative (NIR fluorescence) | 40 [C] |

[A] Liver metastases were confirmed by histology or in the case of non-resected lesions by clinical appearance, IOUS, and CT.
[B] 7 of these lesions were not seen by NIR fluorescence imaging.
[C] 4 of these lesions were not seen by preoperative CT scan, IOUS, and/or palpation.

metastases. One of these 4 occult lesions was labeled as a complicated cyst based on IOUS and CT, whereas the clear NIR fluorescent ring around the lesion suggested that it was a liver metastasis. Seven liver metastases identified by conventional imaging could not be identified using NIR fluorescence and were located 8, 13, 13, 16, 24, 30, and 32 mm beneath the liver surface.

In addition to liver metastases, a total of four hemangiomas and four cysts were identified in four patients. These hemangiomas and cysts did not show a NIR fluorescent signal or rim (Fig. 2). Thus, NIR fluorescence imaging appeared to differentiate benign from malignant lesions.

### Optimization of ICG dose and injection timing

To determine the effect of ICG dosage and post-injection imaging time, patients were allocated to two dose groups and imaged at two time-points after ICG administration, resulting in four groups containing four patients per group. Subsequently six more patients were included at the most favorable combination of ICG dose and time of

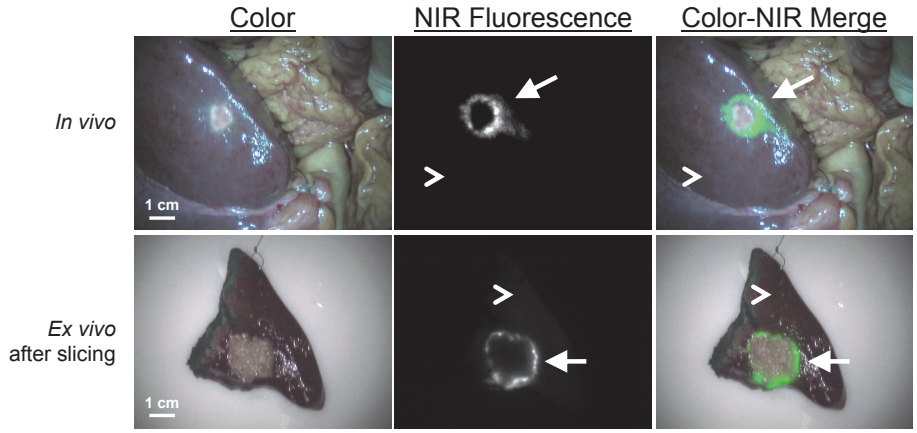


**Figure 1 – NIR fluorescence imaging of colorectal liver metastases:** A colorectal liver metastasis (arrow) is clearly identified by a rim around the tumor *in vivo* (top row), 24 h after injection of 10 mg ICG. Normal liver tissue (arrowhead) shows minimal background uptake of ICG. After resection and slicing of the specimen, the rim around the tumor can be visualized *ex vivo* (bottom row).

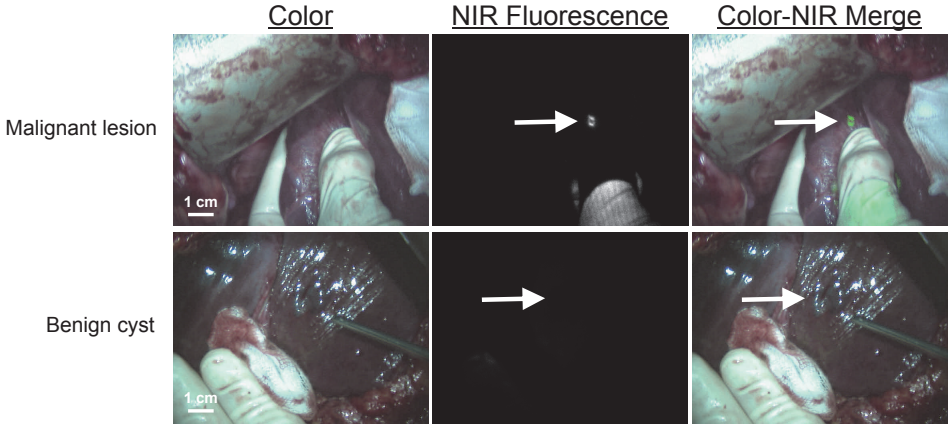


**Figure 2 – Identification of occult metastases and differentiation from benign lesions:** In 4 patients, small superficial metastases (top row, arrow) were identified by NIR fluorescence imaging that were otherwise occult. Benign lesions (bottom row, arrow) could be differentiated from malignant lesions by a lack of a fluorescent rim around the lesion.

injection. Fluorescence intensity of the rim around the liver metastases was significantly higher than the fluorescent signal in the liver ($P < 0.001$). Median tumor-to-liver ratio (TLR) in all patients was 7.4 (range: 1.9 – 18.7). Median TLRs were 6.4 (range: 2.2 – 15.4), 6.7 (range: 2.7 – 9.2), 10.5 (range: 1.9 – 18.7), 8.0 (range: 7.0 – 9.3) for the 10 mg at 24 hr, 20 mg at 24 hr, 10 mg at 48 hr and 20 mg at 48 hr patient group, respectively (Fig. 4). Median rim fluorescence (normalized pixel value) was 700.1 (range: 220.7 – 1144.5), 938.4 (range: 902.3 – 1239.1), 648.6 (range: 137.1 – 1929.36), 608.5 (range: 507.6 – 688.1) for the 10 mg at 24 hr, 20 mg at 24 hr, 10 mg at 48 hr and 20 mg at 48 hr patient group, respectively (Fig. 4). Median background fluorescence (normalized pixel value) was 97.9 (range: 53.6 – 165.9), 209.1 (range: 96.1 – 356.5), 64.6 (range: 53.4

– 112.4), and 77.4 (range: 67.5 – 96.2) for the 10 mg at 24 hr, 20 mg at 24 hr, 10 mg at 48 hr, and 20 mg at 48 hr patient group, respectively (Fig. 4). Using the independent samples Kruskal-Wallis Test no significant differences in signal-to-background ratios ($P$ = 0.72) and rim fluorescence ($P$ = 0.38) were observed. Using the independent samples Kruskal-Wallis Test, a significant difference in background fluorescence was observed ($P$ = 0.038). Post tests using Dunn's Multiple Comparison Test showed a significant difference between the 20 mg at 24 hr and the 10 mg at 48 hr groups. No differences were observed between other separate groups. Because no differences in TLRs were observed between the various groups, the optimal dose was determined by clinical and logistical preferences (the minimal dose of 10 mg of ICG administered 24 h prior to surgery).

**Ex vivo detection of colorectal liver metastases and fluorescence microscopy**

Liver resection specimens were sliced in 5-7 mm slices and subsequently the slices were imaged with the Mini-FLARE imaging system. In all patients for whom a liver resection was performed (N = 17), *ex vivo* NIR fluorescence imaging was performed. All known metastases were identified *ex vivo* by a clear fluorescent ring around the lesion. A tissue section containing both tumor tissue and normal liver tissue was then snap frozen and sectioned at 20 μm for fluorescence microscopy. After fluorescence microscopy, tissue sections were stained with hematoxylin and eosin and overlay images of NIR fluorescence were created (Fig. 3). Fluorescence signal was located in liver transition tissue surrounding the tumor and appeared to be located in the vicinity of blood vessels.

## DISCUSSION

The current study investigated the use of intraoperative NIR fluorescence imaging in patients undergoing liver surgery for colorectal cancer liver metastases. The aim of this study was to assess the effect of timing of ICG administration and dose of ICG. Furthermore, *ex vivo* imaging of the liver resection specimen was performed. All superficially located (< 6.2 mm beneath the liver surface) metastases were identified using NIR fluorescence. Additionally, in four patients occult metastases were detected using NIR fluorescence, which were missed by conventional detection methods.

A major problem with NIR fluorescence imaging, though, is the limited penetration depth of ≈ 6 - 8 mm. Indeed, in the current study, seven metastases that were located 8 mm or more beneath the liver capsule could not be identified using NIR fluorescence. Preoperative CT scanning and IOUS are more appropriate for deeper located lesions and did successfully identify these seven lesions. However, superficially located, small occult metastases are known to be difficult to detect using IOUS, inspection and palpation. Indeed, in the current study, four superficially located,

malignant lesions were detected by NIR fluorescence that were otherwise missed and would not have been resected. Although IOUS is still required to identify deep (≥ 6 mm) metastases in the liver, our results suggest that NIR fluorescence imaging is complementary and helps find small, superficially located liver metastases. However, to prove clinical outcome and patient benefit, larger clinical trials must be performed.

The use of NIR fluorescence imaging to detect liver metastases is dependent on the clearance of ICG by the liver. To optimize the use of this technique, it is necessary to examine the influence of ICG dose and timing of ICG administration prior to surgery. In the current study, differences in dose and timing did not significantly influence the TLR. A previously performed study in rats by our group showed an optimal TLR in the group where ICG was administered at 72 hours prior to surgery.[15] In the current clinical study, liver signal was comparable to pre-injection baseline level (data from Hutteman and van der Vorst et al, manuscript submitted) at 24 to 48 hours post-injection of 10 mg ICG, eliminating the need to test other time-points. Therefore, NIR fluorescence imaging at 72 hours after ICG administration was not performed. Other clinical work performed by Ishizawa et al. suggested an interval between administration of ICG and liver surgery of at least 2 days to lower background fluorescence and to obtain adequate TLRs.[13] However, in that study a substantially higher dose of ICG (0.5 mg/kg; ≈ 35 mg per subject) was administered. In the current study, a relatively low dose of ICG (0.13 – 0.26 mg/kg) was used and it was therefore possible to reach acceptable TLRs and sufficiently low background liver fluorescence at 24 hours after administration of 10 mg ICG, which is safe and desirable from a logistical point of view.

The liver can be a challenging organ for optical imaging, as liver tissue has a relatively high light absorptivity and scatter, and many fluorescent probes show hepatic accumulation.[17, 18] In a previously reported preclinical study by our group, using a tumor-targeted NIR fluorescent probe in a rat model of colorectal liver metastases, TLRs of approximately 2 were observed.[19] Preclinical work using ICG for NIR fluorescence imaging in the same tumor model showed TLRs of approximately 4,[15] whereas in the current clinical study, a median TLR of 7.4 was observed. These results demonstrate excellent performance of ICG as a non-targeted NIR fluorescent probe for intraoperative imaging of colorectal metastases. The development of novel, tumor-targeted probes with minimal background uptake is, however, essential to be able to detect other tumor types or extrahepatic colorectal tumors.[20]

Liver function, and in particular liver clearance capacity, affects the clearance rate of ICG and its biliary secretion and thereby retention of ICG fluorescence in the liver. However, the liver has a large reserve capacity, as has been shown in patients with cirrhosis and patients undergoing hepatic resection, potentially enabling the use of NIR fluorescence imaging after ICG administration even in patients with reduced liver function.[21] In these patients, however, the optimal time interval between ICG

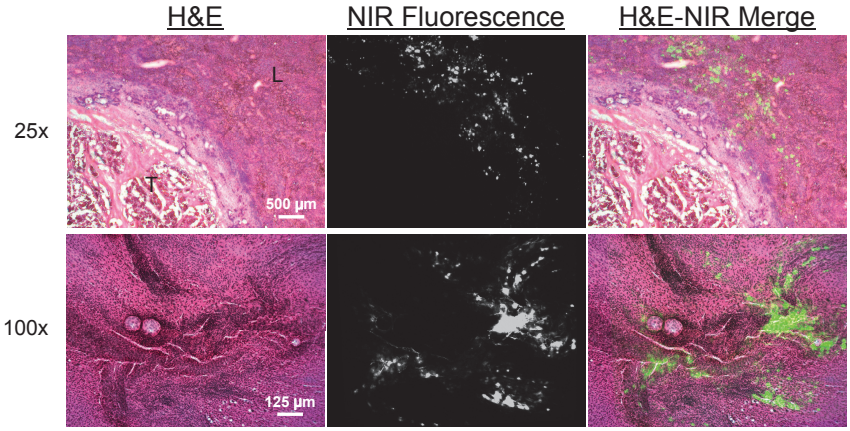


**Figure 3 – Microscopic analysis of the tumor border:** Shown are hematoxylin and eosin staining (left), NIR fluorescence images (middle), and a pseudo-colored green merge of the two (right) of a 20 µm frozen tissue section of a colorectal liver metastasis using a 2.5 X objective (top row) and 10 X objective (bottom row). The fluorescent rim in stromal tissue appears in the border between tumor (T) and normal liver tissue (L).

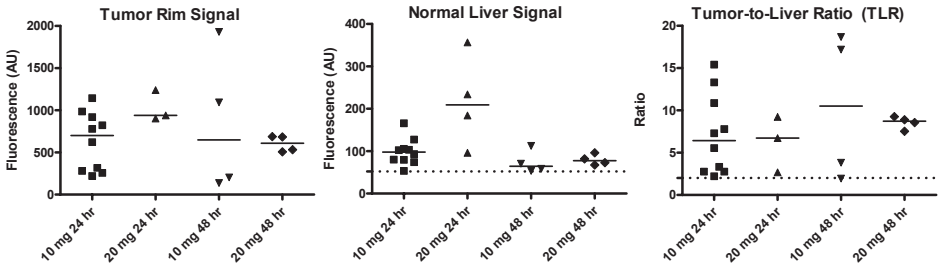


**Figure 4 – Influence of ICG dose and injection time on NIR fluorescence signal:** Fluorescence intensity of the rim around the tumor (left panel), normal liver (middle panel), and the ratio between the two (right panel) is plotted for the various dose and time groups as indicated. No differences were observed between the groups. Liver signal approaches baseline fluorescence of the liver (middle panel, dotted line) in all groups except 20 mg, 24 h. All ratios observed were above the clinically relevant ratio of 2 (right panel, dotted line).

administration and imaging could differ from patients with a normal liver function. Future clinical studies must clarify this issue.

In addition to tumor detection, NIR fluorescence imaging appears capable of differentiating between benign and malignant tumors. In three patients, additional benign liver lesions were intraoperatively identified. These lesions could be clearly differentiated from malignant lesions due to the lack of fluorescent signal in the lesion and the lack of a fluorescent rim around them. Using fluorescence microscopy, we observed accumulation ICG in the transition area between tumor and normal liver tissue, in the vicinity of blood vessels. This phenomenon of rim enhancement is observed in arterial phase CT-scans of patients with liver metastases.[22] This peripheral enhancement seen in metastases may be caused by disrupted vasculature surrounding the tumor tissue, causing delayed drainage of ICG from the tumor surroundings.

As in other areas of surgery, the use of laparoscopy is expanding to liver surgery. Minor liver resections such as the left lateral hepatic resections are being performed laparoscopically as standard-of-care in several centers.[23] NIR fluorescence may also be of great value in laparoscopic surgery because palpation of the liver is not possible and the surgeon can only rely on visual inspection, IOUS, and preoperative imaging. To implement NIR fluorescence in laparoscopic liver surgery, laparoscopic NIR fluorescence camera systems are currently being developed and tested.[24, 25] In conclusion, this study suggests that NIR fluorescence imaging is complementary to conventional imaging for liver metastasectomies, and has the potential to improve surgical care.

## ACKNOWLEDGEMENTS

This study was performed within the framework of CTMM, the Center for Translational Molecular Medicine (DeCoDe project, grant 03O-101). This work was supported in part by the Dutch Association for Gastroenterology, the Dutch Cancer Society grant UL2010-4732 and NIH grant R01-CA-115296.

## REFERENCES


1. Manfredi S, Lepage C, Hatem C, et al. Epidemiology and management of liver metastases from colorectal cancer. Ann Surg 2006; 244:254-259.
2. Abdalla EK, Vauthey JN, Ellis LM, et al. Recurrence and outcomes following hepatic resection, radiofrequency ablation, and combined resection/ablation for colorectal liver metastases. Ann Surg 2004; 239:818-825.
3. Choti MA, Sitzmann JV, Tiburi MF, et al. Trends in long-term survival following liver resection for hepatic colorectal metastases. Ann Surg 2002; 235:759-766.
4. Pawlik TM, Izzo F, Cohen DS, et al. Combined resection and radiofrequency ablation for advanced hepatic malignancies: results in 172 patients. Ann Surg Oncol 2003; 10:1059-1069.
5. Rees M, Tekkis PP, Welsh FK, et al. Evaluation of long-term survival after hepatic resection for metastatic colorectal cancer: a multifactorial model of 929 patients. Ann Surg 2008; 247:125-135.
6. Wei AC, Greig PD, Grant D, et al. Survival after hepatic resection for colorectal metastases: a 10-year experience. Ann Surg Oncol 2006; 13:668-676.
7. Pawlik TM, Scoggins CR, Zorzi D, et al. Effect of surgical margin status on survival and site of recurrence after hepatic resection for colorectal metastases. Ann Surg 2005; 241:715-22, discussion.
8. Karanjia ND, Lordan JT, Fawcett WJ, et al. Survival and recurrence after neo-adjuvant chemotherapy and liver resection for colorectal metastases: a ten year study. Eur J Surg Oncol 2009; 35:838-843.
9. Fong Y, Cohen AM, Fortner JG, et al. Liver resection for colorectal metastases. J Clin Oncol 1997; 15:938-946.
10. Leen E, Ceccotti P, Moug SJ, et al. Potential value of contrast-enhanced intraoperative ultrasonography during partial hepatectomy for metastases: an essential investigation before resection? Ann Surg 2006; 243:236-240.
11. Sahani DV, Kalva SP, Tanabe KK, et al. Intraoperative US in patients undergoing surgery for liver neoplasms: comparison with MR imaging. Radiology 2004; 232:810-814.
12. Nomura K, Kadoya M, Ueda K, et al. Detection of hepatic metastases from colorectal carcinoma: comparison of histopathologic features of anatomically resected liver with results of preoperative imaging. J Clin Gastroenterol 2007; 41:789-795.
13. Ishizawa T, Fukushima N, Shibahara J, et al. Real-time identification of liver cancers by using indocyanine green fluorescent imaging. Cancer 2009; 115:2491-2504.
14. Gotoh K, Yamada T, Ishikawa O, et al. A novel image-guided surgery of hepatocellular carcinoma by indocyanine green fluorescence imaging navigation. J Surg Oncol 2009.
15. van der Vorst JR, Hutteman M, Mieog JS, et al. Near-Infrared Fluorescence Imaging of Liver Metastases in Rats using Indocyanine Green. The Journal of surgical research 2011.
16. Mieog JS, Troyan SL, Hutteman M, et al. Towards Optimization of Imaging System and Lymphatic Tracer for Near-Infrared Fluorescent Sentinel Lymph Node Mapping in Breast Cancer. Ann Surg Oncol 2011.
17. Blum G, Weimer RM, Edgington LE, et al. Comparative assessment of substrates and activity based probes as tools for non-invasive optical imaging of cysteine protease activity. PLoS ONE 2009; 4:e6374.
18. Frangioni JV. The problem is background, not signal. Mol Imaging 2009; 8:303-304.
19. Hutteman M, Mieog JS, van der Vorst JR, et al. Intraoperative near-infrared fluorescence imaging of colorectal metastases targeting integrin alpha(v)beta(3) expression in a syngeneic rat model. Eur J Surg Oncol 2011.
20. Choi HS, Liu W, Liu F, et al. Design considerations for tumour-targeted nanoparticles. NatNanotechnol 2010; 5:42-47.
21. Bloemen JG, Olde Damink SW, Venema K, et al. Short chain fatty acids exchange: Is the cirrhotic, dysfunctional liver still able to clear them? Clin Nutr 2010; 29:365-369.
22. Nino-Murcia M, Olcott EW, Jeffrey RB, Jr., et al. Focal liver lesions: pattern-based classification scheme for enhancement at arterial phase CT. Radiology 2000; 215:746-51.
23. Chang S, Laurent A, Tayar C, et al. Laparoscopy as a routine approach for left lateral sectionectomy. The British journal of surgery 2007; 94:58-63.

24. Matsui A, Tanaka E, Choi HS, et al. Real-time intra-operative near-infrared fluorescence identification of the extrahepatic bile ducts using clinically available contrast agents. Surgery 2010; 148:87-95.
25. van der Pas MH, van Dongen GA, Cailler F, et al. Sentinel node procedure of the sigmoid using indocyanine green: feasibility study in a goat model. Surg Endosc 2010; 24:2182-2187.

# Chapter 13

## Summary and future perspectives

## SUMMARY

Intraoperative imaging using NIR fluorescence has the potential to be of major impact on surgical practice, and cancer surgery in particular.[1] The ability to visualize tumors and lymph nodes that need to be resected, simultaneously with nerves, bile ducts and other structures that need to be spared, can improve outcomes and reduce complications in a wide variety of surgical procedures (**chapter 1**). Since NIR fluorescence imaging involves no ionizing radiation, requires only relatively low-cost camera systems and can be used for real-time visualization during surgery, the technique can be disseminated all around the world, potentially also to areas were less healthcare budget is available.

Multiple NIR fluorescence imaging systems have recently become available,[2] two NIR fluorescent probes are already clinically available (indocyanine green, ICG, and methylene blue, MB) and many novel probes are being developed. This thesis focuses on preclinical validation of this technique for intraoperative tumor identification and image-guided resection (**Part I**), and a clinical translation of this technique using clinically available probes (**Part II**).

**Part I, chapter 2** describes the use of an integrin $\alpha_v\beta_3$-targeted NIR fluorescent probe for the intraoperative detection of colorectal liver metastases in a syngeneic rat tumor model. In this study, all of the induced colorectal liver metastases could be identified intraoperatively using a NIR fluorescent imaging system. Furthermore, several intra-abdominal metastases, were detected by NIR fluorescence. The study shows proof-of-principle of the application of novel tumor-targeted probes and NIR fluorescence for intraoperative tumor detection.

Positive resection margins are a major problem in the treatment of breast cancer, with reported rates of up to 40 percent. The possibility of visualizing breast tumors during surgery could reduce the number of irradical resections and therefore be of great impact on patient care. In **chapter 3**, a protease-activatable NIR fluorescent probe was used to intraoperatively detect breast tumors in a syngeneic rat model of breast cancer. Subsequently, tumors were resected under direct image-guidance, with minimal excision of healthy tissue. NIR fluorescent image-guidance allowed for radical resection of all tumors, with minimal margins of healthy tissue (mean minimum and a mean maximum tumor-free margin of 0.2 ± 0.2 mm and 1.3 ± 0.6 mm, respectively). When these tumor specific probes become clinically available, patient benefit and the effect on the number of radical resections can be assessed.

The clinically available probe ICG is cleared by the liver and has been shown to passively accumulate around colorectal liver metastases. **Chapter 4** focuses on preclinical optimization of the use of indocyanine green for intraoperative detection of colorectal liver metastases, in a syngeneic rat model. All liver metastases could be

identified intraoperatively after ICG injection. The optimal interval between ICG injection and intraoperative imaging was 72 h.

In **part II**, focus lies on clinical translation of intraoperative NIR fluorescence imaging. Analysis of the sentinel lymph node (SLN), the first node that drains from a tumor, is an important procedure in the staging and treatment of breast cancer, cutaneous melanoma and vulvar cancer. This procedure has been studied extensively in colorectal cancer patients, but it has yet to show clear patient benefit. This could be caused by a suboptimal technical procedure for SLN mapping in colorectal cancer. As an oncologic resection involves the *en bloc* resection of regional lymph nodes, *ex vivo* tracer injection and SLN mapping are possible. In **chapter 5**, the use of NIR fluorescence imaging for *ex vivo* SLN mapping in combination with an experimental, more optimized probe are studied in colorectal cancer patients. This technique was optimized in a swine model and subsequently tested in a pilot series of colorectal cancer patients. NIR fluorescence imaging enabled the detection of SLNs in all cases. In one case, a mesenteric metastasis was encountered that was not NIR fluorescent, however, this was a tumor mass without any remaining lymph node tissue, preventing lymphatic flow.

SLN mapping in breast cancer typically involves the use of a radiotracer and a blue dye. NIR fluorescence imaging has the potential to improve SLN mapping in breast cancer, by possibly replacing one of the current modalities, or even both, or functioning as an adjunct. In **chapter 6**, optimization of imaging system and injected ICG dose are performed. In this study, ICG is premixed with human serum albumin (HSA), to increase the retention in the SLN and increase fluorescence brightness of ICG. SLN mapping using NIR fluorescence was uneventful in all patients and allowed the detection of on average 1.45 SLNs. Optimal ICG:HSA dose was between 400 and 800 μM.

In previous preclinical studies, premixing of ICG with HSA showed clear advantages: it improved the retention of the dye in the SLN and increased the fluorescence brightness.[3] **Chapter 7** aims to test this advantage in a clinical, randomized setting, as injection into a human breast might induce coupling with the physiologically available albumin and eliminate the need of premixing. Patient groups injected with or without premixed ICG showed no difference in fluorescence contrast ($P = 0.18$), or in number of identified nodes ($P = 0.74$), indicating that premixing of ICG with HSA can be omitted in case of breast cancer. This simplifies the clinical procedure and can facilitate the introduction of this technique in clinical practice.

**Chapter 8** describes the use of NIR fluorescence for the intraoperative detection of SLNs in cervical cancer patients. Shortly prior to surgical scrub, patients received peritumoral injections of ICG:HSA. After exposure of lymph node basins, NIR fluorescence imaging enabled successful detection of SLNs in all patients. No false negatives were observed. In **chapter 9**, the use of NIR fluorescence imaging was

described in SLN mapping in vulvar cancer patients, who also received standard-of-care injections of radiotracer and patent blue dye. In all patients, SLNs (N = 11) could be detected by NIR fluorescence and radiotracer, 3 nodes, however, were not blue. These pilot studies show the successful use of NIR fluorescence imaging in the detection of SLNs in gynecologic malignancies.

Nowadays, the majority of breast cancer resections are breast-conserving surgeries, where only the tumor itself and a safety margin around it are resected. When a mastectomy is performed, several reconstructive techniques are available. The use of free skin flaps is associated with good cosmetic results and high patient satisfaction. The surgical procedure, however, can be challenging and creation of skin flaps for autotransplantation requires careful planning to select the right blood vessels for optimal flap perfusion. In **chapter 10**, the use of NIR fluorescence imaging for visualizing flap vascularization is assessed in a clinical trial of breast cancer patients undergoing deep inferior epigastric perforator flap reconstructive surgery after mastectomy. ICG was injected at 3 dose levels and NIR fluorescent angiography was performed at fixed moments during surgery. NIR fluorescence permitted visualization of flap vascularization in all patients and a dose of 4 mg ICG was found to be optimal.

Intraoperative visualization of pancreatic tumors could help reduce the number of irradical resections. As no tumor specific probes are clinically available, in the study described in **chapter 11**, ICG was injected in order to test if tumors could be identified by passive accumulation (the enhanced permeability and retention effect). Furthermore, as ICG is excreted into bile, it was evaluated if bile ducts could be visualized intraoperatively. Unfortunately, no useful tumor contrast could be observed in all but one patient. NIR fluorescence did, however, enable the identification of extrahepatic bile ducts during surgery. **Chapter 12** then describes a study in which patients suffering from colorectal liver metastases were injected intravenously with ICG, prior to surgery. During surgery, superficially located metastases could clearly be identified by a fluorescent rim around the tumor. This could be caused by hampered excretion of ICG into bile, by compression of liver tissue by the expanding tumor. Importantly, other than tumors identified preoperatively by CT or MRI, and intraoperatively by visual inspection and palpation, NIR fluorescence enabled the detection of 4 hotspots that were not found by other modalities. These were histologically confirmed to be metastases. Tumor-to-liver ratios of 7.4 (range 1.9 – 18.7) were observed, which is higher than any of the preclinically tested tumor-targeted probes.

# FUTURE PERSPECTIVES

## Future perspectives

The availability of already clinically approved NIR fluorescent probes has been essential for the first clinical trials. However, these probes, indocyanine green and methylene blue were not designed as contrast agents for image-guided surgery and are not optimal, but can be used off-label for imaging applications. When the first intraoperative imaging systems became available in the course of the last decade, research groups all around the world have used these probes for many applications.[4-9] For NIR fluorescence imaging to perform up to its full potential and have a significant impact on patient care, several new developments are necessary.

*Probe development*

The ability to selectively visualize tumor cells and nerves can be a game changer in cancer surgery, and can potentially result in higher radical resection rates and lower complication rates. However, for this to be a reality, tumor and nerve specific probes need to be approved for clinical application.[10, 11] In general, these targeted probes consist of a fluorophore and a targeting ligand. Currently clinically available fluorophores have suboptimal properties and cannot be conjugated to targeting ligands, necessitating the development of novel fluorophores. These fluorophores should be non-toxic, highly fluorescent (high quantum yield) and have the possibility of conjugation to a targeting ligand. IRDye 800CW (LI-COR Biosciences, United States) is a fluorophore that matches these requirements and has recently completed its toxicity tests in rodents.[12] Choi et al. have shown that quantum dots can be cleared rapidly from the body, if the hydrodynamic diameter is smaller than 5.5 nm and the surface charge is balanced of the molecule.[13] Following these observations, the Frangioni Lab (Harvard Medical School, United States) has developed a novel organic fluorophore that is zwitterionic (ZW800-1).[14] Both IRDye 800CW and ZW800-1 are currently manufactured following cGMP guidelines and it is expected that the first clinical studies can start within the next months to years. Future research should be focused on maximizing the fluorescent properties of probes, optimizing rapid excretion and further reduction background uptake.[15]

To selectively label tumor cells, various distinguishing hallmarks of cancer, as described by Hanahan and Weinberg, can be used as targets.[16] An optimal target is exclusively and abundantly expressed by tumor cells and can be targeted without causing toxicity. Novel NIR fluorescent probes have been developed that target growth factor receptors,[17-20] glucose metabolism,[21] angiogenesis,[22-24] and enzymatic activity,[25, 26] and these probes have been studied in preclinical tumor models. First-in-human

results of intraoperative fluorescence imaging in debulking surgery for metastatic ovarian cancer have been reported with a folate-receptor targeted probe (van Dam et al., manuscript accepted for publication). Although the probe used in these studies was based on fluorescein, which fluoresces in the non-optimal visible light spectrum, these results are highly promising for clinical application of targeted NIR fluorescent probes in image-guided surgery.

Iatrogenic nerve damage is a major complication in oncologic surgery, which could potentially be avoided by NIR fluorescence imaging. Small molecule, nerve specific agents BMB and its derivative GE3082 pass the blood-nerve-barrier and selectively target nerves (although background uptake in adipose tissue is also observed).[10] These probes, however, do not fluoresce in the NIR spectrum and have therefore limited tissue penetration. Furthermore, these probes show *in vivo* toxicity. Further research is currently focused on reducing toxicity and shifting the fluorescence excitation and emission wavelengths to the NIR window. Whitney et al. developed a nerve-specific probe by using phage display to select a peptide specific for peripheral nerves and conjugating to a NIR fluorophore.[11] Although the chemical properties of this probe prevent it from penetrating the blood-nerve-barrier, nerve staining was observed *in vivo*. Future research will have to show what strategy is most optimal to selectively target nerves.

*Intraoperative imaging systems*

Currently available imaging systems all have their drawbacks, some only show NIR fluorescence signal without displaying anatomical context, others are relatively large and most are not yet unobtrusive and sufficiently user friendly to be used outside of a research setting.[5, 7, 9, 27] Furthermore, laparoscopic systems are not widely available, and currently available systems do not provide anatomical context.[6] Depth penetration of NIR light is limited and novel camera system designs are focused on increasing the depth at which a fluorophore can be detected. Various strategies can be followed to achieve higher detection depth. Detection of tissue autofluorescence will minimize background noise and increase the maximal depth at which a fluorophore can be detected. For this purpose, fluorescence lifetime imaging (FLIM, which measures the decay of fluorescence intensity of a fluorophore) can be utilized.[28] Temporal and spatial frequency domain modulation of the light source can be used to determine depth information of the fluorescent signal (as reviewed by Gioux et al.[2]). Optimized camera systems are being developed by various groups and companies and research is focused on improving performance, and improving the ease of use in the operating room. When these optimized imaging systems become available, NIR fluorescence imaging has a chance to leap from the research setting into general clinical practice.

## Conclusions

Intraoperative imaging using NIR fluorescence is a highly promising imaging modality that has the potential to revolutionize cancer surgery. The studies described in this thesis show proof of principle that it is possible to use NIR fluorescence imaging in surgical practice. When targeted contrast agents and optimized camera systems become available, this technique has the opportunity to prove its true benefit to patient care.

## REFERENCES


1. Frangioni JV. New technologies for human cancer imaging. J Clin Oncol 2008; 26:4012-4021.
2. Gioux S, Choi HS, Frangioni JV. Image-guided surgery using invisible near-infrared light: fundamentals of clinical translation. Mol Imaging 2010; 9:237-255.
3. Ohnishi S, Lomnes SJ, Laurence RG, et al. Organic alternatives to quantum dots for intraoperative near-infrared fluorescent sentinel lymph node mapping. Mol Imaging 2005; 4:172-181.
4. Mieog JS, Troyan SL, Hutteman M, et al. Towards Optimization of Imaging System and Lymphatic Tracer for Near-Infrared Fluorescent Sentinel Lymph Node Mapping in Breast Cancer. Ann Surg Oncol 2011.
5. Troyan SL, Kianzad V, Gibbs-Strauss SL, et al. The FLARE intraoperative near-infrared fluorescence imaging system: a first-in-human clinical trial in breast cancer sentinel lymph node mapping. Ann Surg Oncol 2009; 16:2943-2952.
6. Ishizawa T, Bandai Y, Ijichi M, et al. Fluorescent cholangiography illuminating the biliary tree during laparoscopic cholecystectomy. Br J Surg 2010; 97:1369-1377.
7. Ishizawa T, Fukushima N, Shibahara J, et al. Real-time identification of liver cancers by using indocyanine green fluorescent imaging. Cancer 2009; 115:2491-2504.
8. Lee BT, Hutteman M, Gioux S, et al. The FLARE intraoperative near-infrared fluorescence imaging system: a first-in-human clinical trial in perforator flap breast reconstruction. Plast Reconstr Surg 2010; 126:1472-1481.
9. Crane LM, Themelis G, Arts HJ, et al. Intraoperative near-infrared fluorescence imaging for sentinel lymph node detection in vulvar cancer: First clinical results. Gynecol Oncol 2010.
10. Gibbs-Strauss SL, Nasr K, Fish KM, et al. Nerve-Highlighting Fluorescent Contrast Agents for Image-Guided Surgery. Mol Imaging 2011; 10:91-101.
11. Whitney MA, Crisp JL, Nguyen LT, et al. Fluorescent peptides highlight peripheral nerves during surgery in mice. Nat Biotechnol 2011.
12. Marshall MV, Draney D, Sevick-Muraca EM, et al. Single-dose intravenous toxicity study of IRDye 800CW in Sprague-Dawley rats. Mol Imaging Biol 2010; 12:583-594.
13. Choi HS, Liu W, Misra P, et al. Renal clearance of quantum dots. Nat Biotechnol 2007; 25:1165-1170.
14. Choi HS, Nasr K, Alyabyev S, et al. Synthesis and In Vivo Fate of Zwitterionic Near-Infrared Fluorophores. Angewandte Chemie 2011.
15. Frangioni JV. The problem is background, not signal. Mol Imaging 2009; 8:303-304.
16. Hanahan D, Weinberg RA. Hallmarks of cancer: the next generation. Cell 2011; 144:646-74.
17. Gleysteen JP, Duncan RD, Magnuson JS, et al. Fluorescently labeled cetuximab to evaluate head and neck cancer response to treatment. Cancer Biol Ther 2007; 6:1181-1185.
18. Lee SB, Hassan M, Fisher R, et al. Affibody molecules for in vivo characterization of HER2-positive tumors by near-infrared imaging. Clin Cancer Res 2008; 14:3840-3849.
19. Withrow KP, Newman JR, Skipper JB, et al. Assessment of bevacizumab conjugated to Cy5.5 for detection of head and neck cancer xenografts. Technol Cancer Res Treat 2008; 7:61-66.
20. Ogawa M, Kosaka N, Longmire MR, et al. Fluorophore-Quencher Based Activatable Targeted Optical Probes for Detecting in Vivo Cancer Metastases. Mol Pharm 2009.
21. Zhou H, Luby-Phelps K, Mickey BE, et al. Dynamic near-infrared optical imaging of 2-deoxyglucose uptake by intracranial glioma of athymic mice. PLoS ONE 2009; 4:e8051.
22. Chen K, Xie J, Chen X. RGD-human serum albumin conjugates as efficient tumor targeting probes. Mol Imaging 2009; 8:65-73.
23. Jin ZH, Razkin J, Josserand V, et al. In vivo noninvasive optical imaging of receptor-mediated RGD internalization using self-quenched Cy5-labeled RAFT-c(-RGDfK-)(4). Mol Imaging 2007; 6:43-55.
24. Kossodo S, Pickarski M, Lin SA, et al. Dual In Vivo Quantification of Integrin-targeted and Protease-activated Agents in Cancer Using Fluorescence Molecular Tomography (FMT). Mol Imaging Biol 2009.
25. Weissleder R, Tung CH, Mahmood U, et al. In vivo imaging of tumors with protease-activated near-infrared fluorescent probes. Nat Biotechnol 1999; 17:375-378.
26. Jiang T, Olson ES, Nguyen QT, et al. Tumor imaging by means of proteolytic activation of cell-penetrating peptides. Proc Natl Acad Sci U S A 2004; 101:17867-17872.

27. Pestana IA, Coan B, Erdmann D, et al. Early experience with fluorescent angiography in free-tissue transfer reconstruction. Plast Reconstr Surg 2009; 123:1239-44.
28. Gioux S, Lomnes SJ, Choi HS, et al. Low-frequency wide-field fluorescence lifetime imaging using a high-power near-infrared light-emitting diode light source. J Biomed Opt 2010; 15:026005.

# Chapter 14

## Nederlandse samenvatting

# NEDERLANDSE SAMENVATTING

Ondanks vele verbeteringen bij niet-chirurgische behandelvormen van kanker (bijvoorbeeld chemotherapie, immunotherapie, bestraling), blijft chirurgische verwijdering van een gezwel in bijna alle vormen van kanker de belangrijkste curatieve behandeloptie. Voor een curatieve verwijdering van een gezwel is het van groot belang dat alle tumorcellen verwijderd worden, om het ontstaan van een recidief te voorkomen. Het is evenzeer van groot belang om vitale structuren (zenuwen, urinewegen, galwegen) te sparen. Preoperatieve beeldvorming zoals CT, PET, SPECT en MRI maken het mogelijk om voorafgaand aan de operatie inzicht te krijgen in de tumorgrootte, locatie en positie ten opzichte van vitale structuren. Tijdens de operatie is de chirurg echter voornamelijk aangewezen op zicht en gevoel om te bepalen welk weefsel verwijderd en welk weefsel gespaard moet worden. Helaas is het onderscheid tussen tumorweefsel en gezond weefsel vaak lastig te maken op zicht en gevoel, waardoor onvolledige (irradicale) resecties regelmatig voorkomen. Daardoor bestaat de behoefte aan een beeldvormende modaliteit, die de chirurg tijdens de operatie helpt te beslissen welk weefsel verwijderd dient te worden en welk niet.

Het onderzoek beschreven in dit proefschrift betreft een dergelijke beeldvormende modaliteit, 'nabij-infrarode fluorescentie imaging', die de potentie heeft deze structuren in real-time, tijdens de operatie zichtbaar te maken (**hoofdstuk 1**). Nabij-infrarood (NIR) licht heeft een golflengte tussen de 700 en 900 nm en is voor het menselijk oog niet zichtbaar. Dit licht heeft als voordeel dat het minder door weefsel geabsorbeerd wordt, waardoor het dieper door weefsel penetreert in vergelijking met zichtbaar licht. Doordat het niet zichtbaar is voor het menselijk oog, heeft het gebruik van deze techniek daarnaast als voordeel dat het operatieveld niet wordt verkleurd. Om tijdens de operatie tumoren zichtbaar te maken zijn tumorspecifieke, NIR fluorescente contrastmiddelen (probes) nodig en gespecialiseerde camerasystemen om deze stoffen zichtbaar te maken.

Dit proefschrift is verdeeld in 2 delen: in **deel I** wordt het gebruik van nabij-infrarode fluorescentie imaging gevalideerd in preklinische tumormodellen. In **deel II** worden klinische trials beschreven met deze techniek, gebruikmakend van contrastmiddelen die reeds klinisch beschikbaar zijn.

**Deel I, hoofdstuk 2** beschrijft het gebruik van een tumorspecifieke NIR fluorescente probe, gericht op het integrine $\alpha_v\beta_3$ eiwit, voor de detectie van uitzaaiingen van dikkedarmkanker in een syngeen ratmodel. In deze studie konden alle geïnduceerde leveruitzaaiingen intraoperatief worden geïdentificeerd door middel van NIR fluorescentie. Daarnaast konden ook enkele intra-abdominale metastasen worden gedetecteerd door middel van NIR fluorescentie. Hiermee toonde deze studie "proof of

principle" voor het gebruik van nieuwe, tumorspecifieke stoffen en NIR fluorescentie voor de intraoperatieve detectie van tumoren.

Tumorpositieve snijvlakken vormen een groot probleem bij de behandeling van borstkanker. Percentages oplopend tot 40% aan irradicale operaties worden gerapporteerd. De mogelijkheid om borsttumoren tijdens de operatie te visualiseren zou het aantal irradicale resecties kunnen verlagen en daardoor een grote impact hebben op de uitkomst voor patiënten. In **hoofdstuk 3** werd een protease-geactiveerde NIR fluorescente stof gebruikt om borsttumoren intraoperatief te detecteren in een syngeen ratmodel voor borstkanker. Vervolgens werden deze tumoren op geleide van het NIR fluorescentiebeeld gereseceerd, met verwijdering van een minimale hoeveelheid gezond weefsel. NIR fluorescentie maakte het mogelijk alle tumoren geheel te verwijderen, met een minimale marge van gezond weefsel (gemiddelde minimale en maximale tumorvrije marge van respectievelijk 0.2 ± 0.2 mm en 1.3 ± 0.6 mm). Zodra deze tumorspecifieke stoffen beschikbaar komen voor toepassing bij patiënten kan het effect op het aantal volledige tumorresecties en bijkomend voordeel voor de patiënt worden onderzocht.

De al klinisch beschikbare fluorescente stof indocyanine groen (ICG) wordt na intraveneuze injectie geklaard door de lever en kan daardoor passief ophopen rondom colorectale levermetastasen. In **hoofdstuk 4** wordt het gebruik van ICG voor de intraoperatieve detectie van colorectale levermetastasen geoptimaliseerd in een syngeen ratmodel. Alle levermetastasen konden intraoperatief worden geïdentificeerd na injectie van ICG. Het optimale interval tussen ICG injectie en intraoperatieve tumorbeeldvorming was 72 uur.

In **deel II** wordt het gebruik van intraoperatieve NIR fluorescentie imaging beschreven in een klinische setting. Analyse van de schildwachtklier, de lymfklier die direct draineert van een tumor en dus de grootste kans heeft om tumorcellen te bevatten in het geval van uitzaaiing naar lymfklieren, is een belangrijke procedure bij de behandeling van borstkanker, melanomen en vulvakanker. Hierbij worden een kleurstof en/of een radioactieve tracer geïnjecteerd rondom de tumor, waarna de lymfklieren, die verkleuren of radioactief worden, verwijderd worden en onderzocht op aanwezigheid van tumorcellen. De procedure is ook uitgebreid bestudeerd bij dikkedarmkanker, maar heeft daar nog geen duidelijke meerwaarde laten zien. De oorzaak hiervan zou kunnen zijn dat de huidige technieken minder geschikt zijn voor de schildwachtklierprocedure bij dikkedarmkanker. Doordat bij een oncologische resectie van dikkedarmkanker de regionale lymfklieren *en bloc* worden verwijderd met de primaire tumor, is het mogelijk om *ex vivo* de tracer te injecteren voor de schildwachtklierprocedure. In **hoofdstuk 5** werd het gebruik van NIR fluorescentie imaging voor de *ex vivo* schildwachtklierprocedure met een experimentele, geoptimaliseerde probe bestudeerd bij dikkedarmkankerpatiënten. De techniek werd

eerst geoptimaliseerd in een varkenmodel en vervolgens getest in een pilotstudie bij dikkedarmkankerpatiënten. Het was in alle gevallen mogelijk met behulp van NIR fluorescentie imaging de schildwachtklier te identificeren. In één geval werd een uitzaaiing gevonden in het mestenterium, die niet fluorescent was. Er was hier echter sprake van een tumormassa zonder residu van lymfklierweefsel, waardoor er geen lymfdrainage meer was.

De schildwachtklierprocedure bij borstkankerpatiënten omvat normaliter een injectie van een radioactieve tracer en een blauwe kleurstof. NIR fluorescentie imaging heeft de potentie om de schildwachtklierprocedure bij borstkankerpatiënten te verbeteren, mogelijk door het vervangen van een van de huidige modaliteiten, of als aanvulling. In **hoofdstuk 6** werden een intraoperatief camerasysteem en de geïnjecteerde dosis ICG geoptimaliseerd bij borstkankerpatiënten. In deze studie werd ICG gekoppeld aan humaan serum albumine (HSA), om hierdoor de eigenschappen als lymftracer te verbeteren. Er ontstonden bij patiënten geen complicaties en in alle gevallen werd de schildwachtklier succesvol geïdentificeerd (gemiddeld 1,45 klieren per patiënt). De optimale dosis ICG:HSA lag tussen 400 en 800 μM.

In eerder beschreven preklinische studies liet het koppelen van ICG aan HSA duidelijke voordelen zien: de retentie in de schildwachtklier werd verbeterd en er was sprake van een verhoogde fluorescente helderheid. In **hoofdstuk 7** werd dit voordeel in een gerandomiseerde klinische studie bestudeerd, daar injectie in borstweefsel zou kunnen betekenen dat ICG zich bindt aan daar aanwezige eiwitten, waardoor vooraf koppelen overbodig kan zijn. Er werd geen verschil gevonden tussen patiënten waarbij ICG wel of niet gekoppeld werd met HSA: niet in fluorescent contrast (P = 0.18), of het aantal klieren dat werd gevonden (P= 0.74). Hierdoor werd duidelijk dat koppelen met HSA niet nodig is, waardoor deze techniek gemakkelijker breed kan worden toegepast in een klinische setting.

**Hoofdstuk 8** beschrijft het gebruik van NIR fluorescentie voor de intraoperatieve detectie van de schilwachtklier in baarmoederhalskankerpatiënten. Kort voor de operatie werd bij deze patiënten ICG:HSA rondom de tumor geïnjecteerd. Na vrij leggen van de lymfklierstations kon door middel van NIR fluorescentie imaging de schildwachtklier gevonden worden in alle patiënten, waarbij geen fout-negatieven werden gevonden (een fout-negatief ontstaat als de geïdentificeerde schildwachtklieren tumornegatief zijn, terwijl andere klieren tumorcellen bevatten). In **hoofdstuk 9** wordt het gebruik van NIR fluorescentie imaging beschreven bij de schildwachtklierprocedure bij vulvakankerpatiënten, die daarnaast ook de standaard schildwachtklierprocedure met blauw en een radioactieve tracer ondergingen. Bij alle 9 patiënten werden lymfklieren gevonden (in totaal 11 klieren) met zowel NIR fluorescentie als de radioactieve tracer; 3 klieren waren echter niet blauw. In deze pilotstudies werd met succes het gebruik van NIR fluorescentie imaging voor de detectie van schildwachtklieren bij gynaecologische tumoren getoond.

De meerderheid van de operaties bij borstkanker kan borstsparend worden uitgevoerd, waarbij alleen de tumor zelf en een veiligheidsmarge hier omheen worden verwijderd. Wanneer toch de gehele borst moet worden verwijderd, zijn diverse reconstructieve operaties mogelijk. Het gebruik van vrije huidflappen van het eigen lichaam wordt geassocieerd met een goede cosmetische uitkomst en hoge patiënttevredenheid. De chirurgische procedure kan echter lastig zijn en voor het creëren van een vrije flap voor autotransplantatie moet met nauwkeurigheid bepaald worden welke bloedvaten gebruikt gaan worden. **Hoofdstuk 10** beschrijft het gebruik van NIR fluorescentie imaging voor het visualiseren van flapvascularisatie in een pilot trial bij borstkankerpatiënten, waarbij een "deep inferior epigastric perforator flapreconstructie" wordt uitgevoerd na een borstamputatie. ICG werd geïnjecteerd op 3 dosisniveaus en de doorbloeding werd geanalyseerd door NIR fluorescentie imaging op vaste momenten. NIR fluorescentie imaging toonde de flapvascularisatie in alle patiënten, waarbij een dosis van 4 mg ICG optimaal was.

Intraoperatieve visualisatie van alvleeskliertumoren zou kunnen helpen het aantal irradicale resecties te verkleinen. Daar nog geen tumorspecifieke stoffen klinisch toegepast kunnen worden, werd in de studie, beschreven in **hoofdstuk 11,** ICG geïnjecteerd, om een contrast te verkrijgen door passieve accumulatie (het "enhanced permeability and retention" effect). Voorts werd bekeken of door uitscheiding in de gal, de galwegen intraoperatief zichtbaar konden worden gemaakt. Helaas werd geen bruikbaar tumorcontrast gezien, bij alle behalve 1 patiënt. De extrahepatische galwegen werden echter bij alle patiënten geïdentificeerd door NIR fluorescentie.

**Hoofdstuk 12** beschrijft een studie, waarbij bij patiënten met een uitzaaiing in de lever van dikkedarmkanker, ICG werd geïnjecteerd voorafgaand aan de operatie. Tijdens de operatie konden de oppervlakkige uitzaaiingen duidelijk worden geïdentificeerd door een fluorescente rand rondom de tumor. Dit wordt mogelijk veroorzaakt door verstoorde galuitscheiding, door compressie van gezond leverweefsel door de tumor. Daarnaast werden behalve de reeds bekende uitzaaiingen, extra laesies gevonden, die niet vooraf op CT of MRI en intraoperatief door inspectie en palpatie waren geïdentificeerd. Deze extra laesies waren histologisch bewezen uitzaaiingen. Deze studie toonde tumor-tot-lever fluorescentieratio's van gemiddeld 7.4 (bereik 1.9 – 18.7), wat beduidend hoger is dan alle preklinisch geteste tumorspecifieke probes.

## CONCLUSIE

Intraoperatieve imaging met gebruik van NIR fluorescentie is een veelbelovende beeldvormende modaliteit, die de potentie heeft oncologische chirurgie te verbeteren. De studies beschreven in dit proefschrift tonen 'proof of principle', niet alleen preklinisch, in diermodellen, maar ook klinisch bij diverse typen tumoren. Zowel specifieke contrastmiddelen als camerasystemen kunnen nog verder verbeterd

worden. Zodra deze beschikbaar komen, heeft de techniek de kans zijn meerwaarde voor patiënten te laten zien.

# LIST OF PUBLICATIONS

**Hutteman M**, van der Vorst JR, Gaarenstroom KN, Peters AAW, Mieog JSD, Schaafsma BE, Löwik CWGM, Frangioni JV, van de Velde CJH, Vahrmeijer AL. Optimization of near-infrared fluorescent sentinel lymph node mapping for vulvar cancer. Amer J Obstet Gynecol 2011; In press.

van der Vorst JR, **Hutteman M**, Gaarenstroom KN, Peters AAW, Mieog JSD, Schaafsma BE, Kuppen PJK, Frangioni JV, van de Velde CJH, Vahrmeijer AL. Optimization of near-infrared fluorescent sentinel lymph node mapping in cervical cancer patients. Int J Gynecol Cancer 2011; In press.

**Hutteman M**, van der Vorst JR, Mieog JSD, Bonsing BA, Hartgrink HH, Kuppen PJK, Löwik CWGM, Frangioni JV, van de Velde CJH, Vahrmeijer AL. Near-infrared fluorescence imaging in patients undergoing pancreaticoduodenectomy. Eur Surg Res 2011;47:90-97.

Schaafsma BE, Mieog JS, **Hutteman M**, van der Vorst JR, Kuppen PJ, Löwik CW, Frangioni JV, van de Velde CJ, Vahrmeijer AL. The clinical use of indocyanine green as a near-infrared fluorescent contrast agent for image-guided oncologic surgery. J Surg Oncol 2011; In press.

van der Vorst JR, **Hutteman M**, Mieog JS, de Rooij KE, Kaijzel EL, Löwik CW, Putter H, Kuppen PJ, Frangioni JV, van de Velde CJ, Vahrmeijer AL. Near-infrared fluorescence imaging of liver metastases in rats using indocyanine green. J Surg Res 2011; In press.

**Hutteman M**, Mieog JS, van der Vorst JR, Liefers GJ, Putter H, Löwik CW, Frangioni JV, van de Velde CJ, Vahrmeijer AL. Randomized, double-blind comparison of indocyanine green with or without albumin premixing for near-infrared fluorescence imaging of sentinel lymph nodes in breast cancer patients. Breast Cancer Res Treat 2011;127:163-70.

Mieog JS, Troyan SL, **Hutteman M**, Donohoe KJ, van der Vorst JR, Stockdale A, Liefers GJ, Choi HS, Gibbs-Strauss SL, Putter H, Gioux S, Kuppen PJ, Ashitate Y, Löwik CW, Smit VT, Oketokoun R, Ngo LH, van de Velde CJ, Frangioni JV, Vahrmeijer AL. Towards Optimization of Imaging System and Lymphatic Tracer for Near-Infrared Fluorescent Sentinel Lymph Node Mapping in Breast Cancer. Ann Surg Oncol 2011; In press.

**Hutteman M**, Mieog JS, van der Vorst JR, Dijkstra J, Kuppen PJ, van der Laan AM, Tanke HJ, Kaijzel EL, Que I, van de Velde CJ, Löwik CW, Vahrmeijer AL. Intraoperative near-infrared fluorescence imaging of colorectal metastases targeting integrin α(v) β(3) expression in a syngeneic rat model. Eur J Surg Oncol 2011; 37:252-7.

**Hutteman M**, Choi HS, Mieog JS, van der Vorst JR, Ashitate Y, Kuppen PJ, van Groningen MC, Löwik CW, Smit VT, van de Velde CJ, Frangioni JV, Vahrmeijer AL. Clinical Translation of Ex Vivo Sentinel Lymph Node Mapping for Colorectal Cancer Using Invisible Near-Infrared Fluorescence Light. Ann Surg Oncol 2011; 18:1006-14.

Keereweer S, Kerrebijn JD, van Driel PB, Xie B, Kaijzel EL, Snoeks TJ, Que I, **Hutteman M**, van der Vorst JR, Mieog JS, Vahrmeijer AL, van de Velde CJ, Baatenburg de Jong RJ, Löwik CW. Optical Image-guided Surgery-Where Do We Stand? Mol Imaging Biol 2011; 13:199-207.

Lee BT, **Hutteman M**, Gioux S, Stockdale A, Lin SJ, Ngo LH, Frangioni JV. The FLARE intraoperative near-infrared fluorescence imaging system: a first-in-human clinical trial in perforator flap breast reconstruction. Plast Reconstr Surg 2010; 126:1472-81.

Mieog JS, **Hutteman M**, van der Vorst JR, Kuppen PJ, Que I, Dijkstra J, Kaijzel EL, Prins F, Löwik CW, Smit VT, van de Velde CJ, Vahrmeijer AL. Image-guided tumor resection using real-time near-infrared fluorescence in a syngeneic rat model of primary breast cancer. Breast Cancer Res Treat 2010; Epub ahead of print

Mieog JS, Vahrmeijer AL, **Hutteman M**, van der Vorst JR, Drijfhout van Hooff M, Dijkstra J, Kuppen PJ, Keijzer R, Kaijzel EL, Que I, van de Velde CJ, Lowik CW. Novel intraoperative near-infrared fluorescence camera system for optical image-guided cancer surgery. Mol Imaging 2010; 9:223-31.

Lee BT, Matsui A, **Hutteman M**, Lin SJ, Winer JH, Laurence RG, Frangioni JV. Intraoperative near-infrared fluorescence imaging in perforator flap reconstruction: current research and early clinical experience. J Reconstr Microsurg. 2010; 26:59-65.

Gioux S, Ashitate Y, **Hutteman M**, Frangioni JV. Motion-gated acquisition for in vivo optical imaging. J Biomed Opt 2009; 14:064038.

**Hutteman M**, Van der Ende J, Schweizer JJ. Presence and functioning of scales and stadiometers in paediatric units. Clin Nutr 2008; 27:171-2.

# CURRICULUM VITAE

Merlijn Hutteman was born in Rotterdam on 18 June 1983. After graduating high school at the Erasmiaans Gymnasium in Rotterdam, he started the study Cognitive Artificial Intelligence at Utrecht University in 2001. He performed research for his master's thesis at the department of psychopharmacology at Utrecht University, under supervision of dr. K.B.E. Böcker and prof. dr. J.L. Kenemans. After graduating in 2006, he started medical school at Leiden University. In 2008, he performed a student research project on image-guided surgery, under supervision of dr. A.L. Vahrmeijer and prof. dr. C.J.H. van de Velde. This led to the start of his PhD research at the same group, in 2009.

During his PhD research, he has worked as a visiting research fellow at the lab of prof. dr. J.V. Frangioni, at Beth Israel Medical Center, Harvard Medical School, Boston, United States.

In 2011, Merlijn is continuing his medical training at Leiden University Medical Center.

# ACKNOWLEDGEMENTS

The research performed for this thesis has been a team effort from start to finish, for which I would like to thank all the people who have contributed.

Dr. Vahrmeijer, dear Alex, your guidance has been essential, whether I was in Leiden, Boston, or anywhere in between. You have helped me focus on what is important and were always there for me whenever things did not go as planned.

Prof. van de Velde, thank you for giving me the opportunity to start working in your group, when I had little to no experience. Meetings with you always gave rise to new ideas.

Prof. Frangioni, dear John, under your guidance, I have learned what translational research truly means. From performing experiments in the lab, to clinical trials and traveling around the world to discuss them, you have opened a world for me.

Dr. Kuppen, dear Peter, your enormous experience has been of great help with all our endeavors in the lab. Prof. Löwik, Vincent Smit, prof. Tanke, prof. Lelieveldt and prof. Reiber, thank you for all your help.

The 'Green Team' a.k.a. J3-104: Sven, you were there from the beginning, helping me set my first steps in the lab when we did not even have our own camera system. I will never forget those long nights of experimenting whenever we could borrow a camera for a week or two (with an inspirational 'talk to me, Hut' every once in a while at 2 am). It all paid off, we're defending our theses within weeks of each other. The both of us will still be involved in all the great research that our successors are performing, and I'm sure we will keep in touch, inside the hospital, and definitely outside of the hospital.

Joost, your never-ending motivation and impatience have brought us to where we are: our protocols were written and approved in no time and before we knew it, we were in the OR almost on a daily basis, with the Mini-FLARE. Even though our working hours were long at times, there was always a balance, whether it was during the day with some fine arts to get our minds off work (what should we do without Entourage?), or after hours in the sun, whether it was in Leiden or Warsaw. I can only hope we end up working in the same hospital, but we will definitely meet outside,

Bob, your extensive knowledge of ICG is invaluable for our group and it's great to have you on board. All eyes are on you now! Floris, you knew from the beginning that you wanted to join our team, and were always there, working hard, whenever we needed help. Kees, Mark, Sanne, the list of great people is ever expanding, thanks!

Frangioni Lab: Hak Soo, thank you for teaching me everything about fluorophores, helping me set my first steps in chemistry, and even how to snowboard. I hope to keep on learning from you in the future. Khaled, your chemical knowledge and eternal love for the Red Sox have kept me sane. Rafiou, there are not enough stroopwafels on this planet to repay you for everything you did! Sylvain and Alan, without your technical

guidance, I would have been nowhere. Aya and Yoshi, performing surgery under your guidance was phenomenal. Linda, Lori, Dina, Kelly, Jenn, Kazu, Tejas, Summer, Jeong Heon, Eugenia, Soon Hee, Hoon, Conor, Kyle, Lanee, Allison, Nick, Fangbing, Lindsey, Rita, Onkar: thank you for everything.

Surgical lab Leiden: Rob, Geeske, Connie, Frank, Eliane, Esther, Gabi, Ronald, Anouck, Anita, molecular endocrinology lab: Isabel, Karien, Eric; experimental radiology: Jouke, Martijn, thank you!

All surgeons, urologists and gynecologists participating in our studies: Henk Hartgrink, Gerrit-Jan Liefers, Bert Bonsing, Wobbe de Steur, prof. Tollenaar, prof. Kievit, Henk Elzevier, prof. Pelger, Cor de Kroon, Katja Gaarenstroom, prof. Peters, prof. Trimbos, and all residents (surgery, pathology, gynecology, urology), thank you for all your patience and enthusiasm.

Nurses Annemarie, Graziella, Gemma, Elly, Dorien, Margriet, thank you for all your help and all the patients you've included. My gratitude goes out to all patients who participated in our studies.

Finally, I would like to thank my family and friends, for tolerating my ramblings about research. Roos, Mom, Dad, your support means everything.